International Symposium on Sustainable Aviation 2018

ISSA 2018

9 - 11 July 2018 Rome, Italy

Proceeding Book

Editors:

Prof. Dr. T. Hikmet Karakoc

Prof. Dr. Claudio Scarponi

Prof. Dr. Fabrizio Sarasini

Asst. Prof. Dr. Yasin Sohret

ISBN

978-605-68640-2-5

Republic of Turkey Ministry of Culture and Tourism Department of Libraries and Publication ISBN Turkey Agency Publication Data

Proceedings Book of International Symposium on Sustainable Aviation 2018.
Edited by T. Hikmet Karakoc, Claudio Scarponi, Fabrizio Sarasini, Yasin Şöhret
Printed by Çetemenler Baskı ve Kopyalama Merkezi on July 8, 2018.
ISBN: 978-605-68640-2-5

This book includes full papers presented at International Symposium on Sustainable Aviation 2018.

MESSAGE FROM THE SYMPOSIUM CHAIR

Prof.Dr.T. Hikmet Karakoc

Symposium Founding Chair
On Behalf of the Organizing Committee

It is my great pleasure to see you at the International Symposium on Sustainable Aviation 2018 (ISSA- 2018) in Rome, Italy.

Environmental problems, especially global warming, has gain importance because of its increasing effects like climate change and drought. It is big part of the sustainability and the sustainable development. Other big part of the sustainable development is the economical concerns. These two parameters are connected closely with the energy consumption. Fossil fuels meet the most of the World's energy need. However, these fuels not only expensive but only very harmful to environment, in addition, they are going to be depleted in near future. According to the reasons referred above, alternative and renewable energy sources must be searched and used instead of fossil fuels.

As it well known, aviation is the one of the biggest industry. Therefore, it consumes very significant amount energy. Result of these, aviation industry is important part of the sustainable development and the environmental damages that are caused by fossil fuels which is used as main energy source. Hence, aviation should be handled in detail respect to new technologies, environmental, economical and sustainability effects.

We are very keen on making this conference a great success with its technical program and social events, which could be possible with your kind participation. We wish you a fruitful symposium.

Best wishes,
T. Hikmet Karakoc

MESSAGE FROM THE SYMPOSIUM CO CHAIR
Prof. Dr. Cloudio Scarponi
Symposium Co-Chair

Astst. Prof. Dr. Fabrizio Sarasini
Symposium Co-Chair

It is my great pleausere to have so many researchers, professionals, experts, have in Rome at the Fourth International Symposium on Sustainable Avation, ISSA 2018.

We arrived interesting studies from many coutries all over the World, I mean Euorupe, Asia, North and South America, Australia. This is the best demonstration to underline how relevant is the common interest to protect our Planet from the pollution.

Aviation field can have a very important role, in consideration of the fact that flights all over the World will become the double in only 15 years if you consider the amount of fuel, the incredible number of CO2 tons in our atmosphere, the economy related to this development, it is clear tgat such a care is well justified.

The Symposium consists of oral presecntions, poster sessions and presentations of keynote and intived speakers, delegates from Clean Sky European Project and from İtalian National Civil Authority (ENAC).

I do hope you will enjoy Rome, in my opinion one of the most beautiful city of the World, Capital of one o the beautiful Country in the World. Welcome to Rome.

Best Wishes,

Prof. Dr. Claudio Scarponi, Asst. Prof. Dr. Fabrizio Sarasini

Honory Chair

Eugenio Gaudio
University of Rome ‘’La Sapienza’’, Italy

Symposium Founding Chair

T. Hikmet Karakoc
Eskisehir Technical University
Faculty of Aeronautics and Astronautics – Department of Airframe and Powerplant Maintenance

Symposium Chairs

Claudio Scarponi
University of Rome ‘’La Sapienza’’, Italy

Fabrizio Sarasini
University of Rome ‘’La Sapienza’’, Italy

Technical Chairs

Yasin Sohret
Suleyman Demirel University

Organising Committee

- Akbulut, Ugur, Recep Tayyip Erdogan University, Turkey
- Karakoc, T. Hikmet, Eskisehir Technical University, Turkey
- Sarasini, Fabrizio, Sapienza Universita di Roma, Italy
- Scacia, Rosita, Sapienza Universita di Roma, Italy
- Scarponi, Claudio, Sapienza Universita di Roma, Italy
- Sohret, Yasin, Suleyman Demirel University, Turkey
- Synylo, Kateryna, National Aviation University, Ukraine
- Valente, Marco, Sapienza Universita di Roma, Italy
- Yakin, Evren Yilmaz, Eskisehir Osmangazi University, Turkey

Symposium Secretariat

- Scacia, Rosita, Sapienza Universita di Roma, Italy
- Yakin, Evren Yilmaz, Eskisehir Osmangazi University, Turkey

Executive Committee

- Acikkalp, Emin, Bilecik S.E. University, Turkey
- Altuntas, Onder, Anadolu University, Turkey
- Agarwal, Ramesh K., Washington University in St. Louis, USA
- Azami, Ahadollah, Eastern Mediterranean University, Northern Cyprus
- Celikel, Ayce, Envisa, France
- Colpan, C. Ozgur, Dokuz Eylul University, Turkey
- Dupoirieux, Francis, ONERA, France
- Hajiyev, Chingiz, Istanbul Technical University, Turkey
- Hepbasli, Arif, Yasar University, Turkey
- Jagadeesh, Gopalan, Indian Institute of Science, India

CONTENTS

Proceedings

ISSA-2018-001

RISK METHODOLOGY FOR AIRCRAFT NOISE ASSESSMENT AND CONTROL

Oleksandr Zaporozhets
[1]*National Aviation University, 1 avenue Cosmonaut Komarov, Kiev 03058, Ukraine*
zap@nau.edu.ua

- *Aircraft noise is one of the subjects of environmental or community noise, which is a kind of physical stressor on environment/community, which may produce a number of negative effects, including health impacts, as for humans as for environmental systems/objects (nonhuman impacts on environment). Among them are the following mostly recognized outcomes for humans: annoyance by noise (noise annoyance), sleep disturbance, direct health impacts, hearing loss (more important for occupational health protection), etc.*

Keywords: aircraft noise annoyance, balanced approach, aircraft noise assessment and management

INTRODUCTION

Noise pollution around airports is a major problem with regards to environment in modern societies, generating significant negative effects on the surrounding communities (health and performance effects, health care costs, properties depreciation, loss of operation by airports, etc.). Among other noise effects, noise annoyance is the most documented subjective response to noise, and the great reason of complaints in airports, and, therefore, of concern for airport authorities. The combination of continuous airport development and public concern about aircraft noise disturbance and annoyance continues to grow, has led to considerable mitigation efforts by governmental administrations and the civil aviation industry as a whole. The aircraft noise is the single or somewhere one of the most important local impact arising from airport operations which, unless managed effectively, has the potential to constrain the ability of airports to grow in response to demand and hence limit the social and economic benefits that future growth could bring. Together with these and various other social, flight safety and economic problems, including a number of specific environmental issues, aircraft noise has the potential to multiplying constrain the operation and growth of the airports and air traffic.

In particular, the optimisation can be used to search for cost-minimal balances of controls of all the factors under consideration over the various scenarios in aviation sector that simultaneously try to achieve user-specified targets for human health impacts (for example, expressed in terms of reduced life expectancy in accordance with WHO guidelines for these factors), ecosystems protection, and maximum allowed violations of WHO guideline values [Berglund, B. et al., 1999], etc. (Fig. 1).

Traditional taken approaches to aircraft noise management include reducing aircraft noise at source, to devise operational procedures and restrictions, routes, and other forms of mitigation, etc., to minimize individual residential exposure via ICAO Balanced Approach (BA) to aircraft noise control around the airports [ICAO Doc 9829, 2004], and to keep the public fully informed about noise management and noise control [Woodward J.M. et al., 2009]. The main objective is that noise problems can be addressed in an environmentally and economically responsible manner within the system, while preserving potential benefits gained from aircraft-related measures.

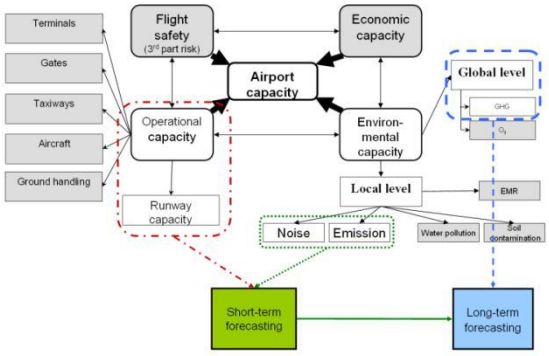

Fig. 1. Airport interdependency capacity analysis scheme [Zaporozhets O., et al., 2014]

Even current ACARE SRA and SRIA noise targets use both technology and operational mechanism to reach them [ACARE, 2012]. For example, if the Goal 2020 to reduce the noise levels for the aircraft up to 10 EPNdB, the 2-3 decibels is considered to be reached with noise abatement operational procedures (NAOP), Fig. 2. An important aspect needs to be taken into account – the efficiency of NAOP for noise reduction is less for quieter aircraft, it is less for aircraft with acoustic performances in accordance with more stringent noise standards.

One more important consideration that ICAO and ACARE targets and goals are not only to reduce the noise levels, the novel and more real approach is based on the idea that noise level reduction at receiver point is not a final result for society, but it is just a tool to achieve the real final goal, which is the reduction of the noise effects. By ICAO this effect is defined currently as a reduction of number of people affected by aircraft noise – or simply a number of exposed people by noise over the protection guide value (Fig. 3), or predefined number of highly annoyed people. In this case even for quiet aircraft in a fleet the high intensity flight traffic in airport under consideration

may provide total number of annoyed people by noise of unacceptable value.

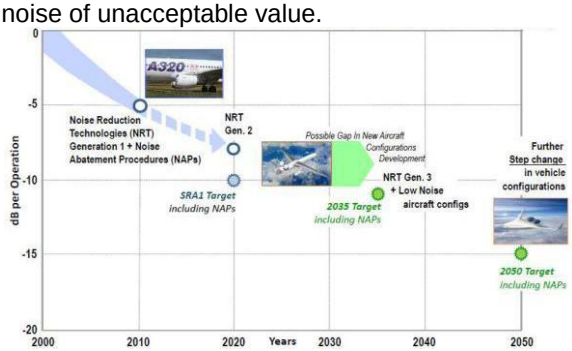

Fig.2. Current ACARE SRA and SRIA noise targets for fixed wing aircraft [Collin D., 2014]

It should be a primary objective of future research into environmental noise impact to investigate the interplay of sound level control and perceived control. New and additional (political) measures to mitigate noise impact may result from the redirection of attention from sound to noise and to noise annoyance. Strategies that reduce noise annoyance, as opposed to noise, may be more effective in terms of protecting public health from the adverse impacts of noise and its interdependency with other environmental, operational, economic and organizational issues of airport and airlines operation and maintenance.

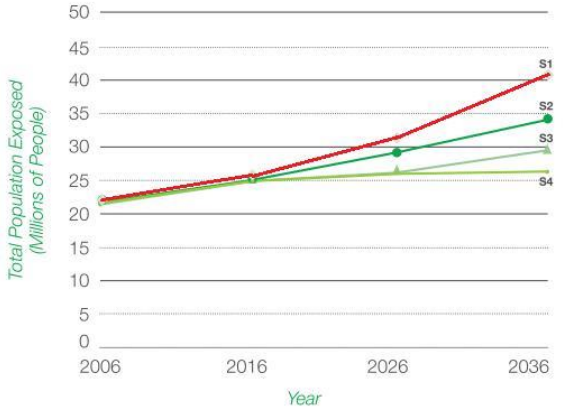

Fig. 3. Total global population exposed to aircraft noise above 55 DNL: CAEP forecasting for noise reduction in preparation to new ICAO standard (Chapter 14 of Annex 16, vol. 1) for aircraft noise control [Fleming G.G., Ziegler U.R.F., 2013]

This is the reason for a number of current concept, approaches and efforts to reduce aviation noise annoyance, keeping the produced noise levels the same. This objective is expected to be achieved by bringing information closer to the people living in airport surroundings. For example, there is some previous assumption that shared unattended noise monitoring results can improve airport noise acceptance, as general public can check the compliance with noise limits in their proximity, raising people awareness [O.Zaporozhets, 2011].

The reviewed and proposed models provide a good model fit and support to the toolboxes of noise annoyance management, currently under the design. It can be concluded that the concern about the negative health effects of noise and pollution, other environmental issues, are still the subjects of scientific and societal attention, their newish deliverables may improve the approach to build the fifth element of ICAO balanced approach to aircraft noise control around the airports, which cover the measures to reach the final goal of aircraft noise management – to reduce the number of people loving in vicinity of the airports and affected by noise.

ICAO BALANCED APPROACH TO AIRCRAFT NOISE CONTROL

With this context it is appropriate to begin with new vision on ICAO BA to aircraft noise control, namely to add to the existing elements of noise reduction: at source, by noise zoning and land use planning, with operational procedure and mitigation measures, the newish element – the reduction of the noise effects via novel concept, approaches and efforts to reduce aviation noise annoyance.

Till now all the existing BA elements are subjects to identify and assess the noise exposure, mostly via noise contour modelling, in some cases via monitoring, which allows to evaluate noise control measures and to determine the most cost effective and efficient for environment protection set of them [ICAO Doc 9829, 2004]. In best known solutions the process is continuing with public notification and consultation procedures and even being a mechanism for dispute resolution. This important approach is implemented in the European Environmental Noise Directive [Directive 2002/49/EC]. According to it, noise action plans will be developed with the participation of the public. The claim of the citizens in participation has steadily grown, especially if their residential area or essential environmental aspects are concerned.

There is important to differentiate between noise exposure and the resulting noise nuisance in different communities, and manage each appropriately. The type of information collected and the way in which it is analyzed and reported will differ according to the objective of the program of noise control. Usual option of quantifying overall noise exposure - through noise contour modelling and quantifying the number of people inside the contour with specified noise level (predefined by rules for noise zoning around airports or by general noise control rules like Environmental Noise Directive or CAEP documents, see Fig. 3).

Acoustic modeling around airports currently is intended to satisfy the needs of many users and ranges between sophisticated noise spectrum modeling and noise environment assessment in terms of cumulative noise exposure or even, by means of dose-response relationships, in terms of the size of the noise-annoyed population in the

area of concern. It must be noted that the form and structure of noise indices, which we must assess and investigate around the airport or under the particular flight path have the predominant role on the method we have to use for their assessment. Methods for modeling noise radiation, propagation and attenuation, include both analytical and semi-empirical results. The current tendency is towards less empirical and more analytical techniques. In general prediction schemes are based on three basic components:

- a noise radiation model corresponding to an aircraft noise emission model;
- a model of sound transmission from source to control point in the form of an aircraft noise propagation model;
- a noise impact model at the control point in the form of an aircraft noise imission model.

The imission model, as a component of the overall noise modeling scheme, is a subject of current deeper consideration, with psychological phenomenon of annoyance inside.

People are driven to complain when some nuisance factor (or stressor) in the environment gives rise to annoyance and when this stressor reaches a threshold of tolerance. In this context the stressor is an aircraft noise, which is described by exposure metrics usually. The actual situation is rather more complex. Exposure can lead to more than one effect, and community impacts depend on multiple effects (Fig. 4). While sleep disturbance during night time and annoyance during composite day time are the primary recognized health consequences of community noise exposure, cardiovascular disease and cognitive impairment in children also contribute [Berglund, B. et al., 1999].

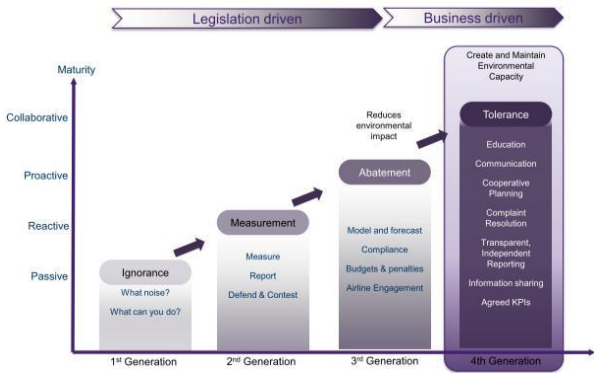

Fig. 4. An airports noise management typically evolves over time

WHO indicates also that positive wellbeing and quality of life can be compromised by noise annoyance and sleep disturbance first of all. Both of them are estimated for grounding the noise zoning and land use planning around the airports, using Critical Limits, Protection Guides and Threshold Values for sleep disturbance and annoyance [Griefahn and Scheuch, 2004] to control the aircraft noise impact in usual way. Among diversity of acoustical metrics describing air traffic noise the L_{eq} based indices like *DNL* and *DENL* (during appropriate estimation time) show the closest connection to annoyance and disturbance judgments. It was found also that the data were not strong enough to establish criteria for annoyance or threshold values for chronic disease from separate event value in form of maximum level L_{Amax}. At the same moment the probability values of night sleep disturbance among population depends from maximum noise level of the noise events, while its definition in annual approach requires more detailed specification and statistical understanding. Even they are not appropriate for the evaluation of distinct (intermittent) noise events as a whole [Jagnatinskas A., Fiks B., Zaporozhets O., 2011].

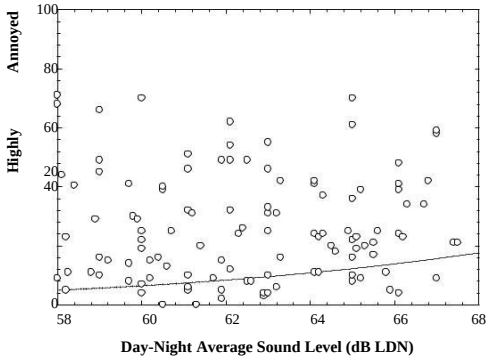

Fig. 5. Percentage highly annoyed at aircraft noise plotted as a function of noise level. The solid curve is a portion of that presented in Fig. 5, while the scattered points represent real measurements [Fidell, S., 2003]

Scrutiny of Fig. 5 reveals that annoyance reactions to noise vary substantially and do not appear to be correlated with noise level. What is more difficult to describe and measure – there are many factors that give rise to annoyance and are the non-auditory effects of noise dealing with nuisance. There is no agreed method to combine everything into an overall response, even if this were meaningful when taken out of the context of the many and varied social and economic factors that often have much greater health impacts.

AIRCRAFT NOISE ANNOYANCE

Noise is an environmental nuisance that has the potential to degrade health and negatively impact the relationship between humans and their environment. Aircraft noise annoyance is a still increasing problem, especially in the densely-populated areas and without reducing population's annoyance, it will become more and more difficult to increase the number of aircraft movements, or to build new runways or other airport infrastructure.

There is also evidence that environmental noise can be considered like in occupational noise case as a risk-factor for health. From this point airport capacity will be limited huge from this noise annoyance acceptability level. In general the aviation noise (as any kind of environmental

noise) effects include [Shaw E.A.G. 1996]: psycho-social effects such as annoyance and other subjective assessments of general well-being and quality of life; effects on mental health; effects on sleep which can be both psychological and physical effects; effects on physical health such as hearing loss; and stress-related health effects which can be psychological, behavioural, somatic and physical. According to the WHO, an outdoor noise level exceeding 55 dB L_{DN} is considered to be 'seriously annoying' [Berglund B. et al., 1999].

A significant increase over the years was observed in annoyance at a given level of aircraft noise exposure. Crucial evidence that annoyance measured last decade in European airports (the more recent studies in airports of Manchester, Paris, Amsterdam, Frankfurt) is much higher dependent from the noise indices [Flindell I. et al., 2013], the clear difference equivalent to around 5-6 dBA between the average trend of all of these more recent studies and the much older data, it means that high number of annoyed people observed in acoustic conditions which were considered not so serious decades before, Fig. 6. The results are of highest importance to the applicability of current exposure-annoyance relationships for aircraft noise and provide a basis for decisions on whether these need to be updated.

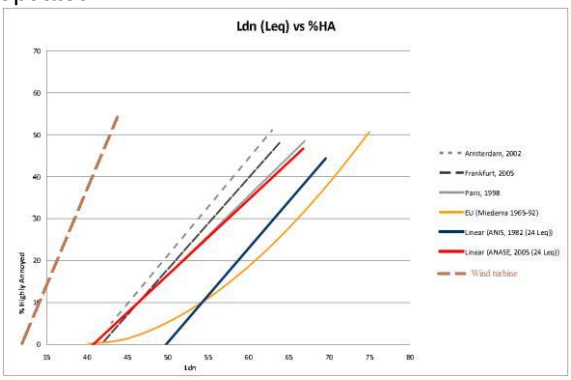

Fig. 6. Aircraft noise annoyance curves for a number of studies in EU

In any case, if doing nothing with annoyance management, the future scenarios for air transportation are looking unsatisfactorily, because existing results of the studies of noise annoyance in other sectors, different from aviation and having the same or quite similar acoustical properties (Fig. 7), for example, wind turbine noise, show the much higher annoyance than existing aircraft noise studies (Fig. 6).

From one point of view the existing exposure-response curve, used in any studies for impact assessments, has to be updated. From other point of view all the non-acoustical factors, influencing on annoyance, at any specific case need to be managed correctly, providing less annoyance if it should be possible.

The extent of noise annoyance is clearly influenced by numerous non-acoustic factors such as personal, attitudinal, and situational factors in addition to the amount of noise per se [Scheuch et al., 2003]. Any possible interpretations of the various relationships between noise and reported annoyance, which usually may vary from one study to another, show both direct and indirect routes from stimulus to effect. Approximately one-third of the variation (even only 18% by some results!) in noise annoyance can be explained by acoustical factors e.g., the sound level, peak levels, sound spectrum, and number of noise events and a second third by non-acoustical factors [Guski,1999]. While individual responses to noise vary considerably amongst the population, the social context in which the noise exposure occurs has also been found to be important [Job R.F.S., 1988].

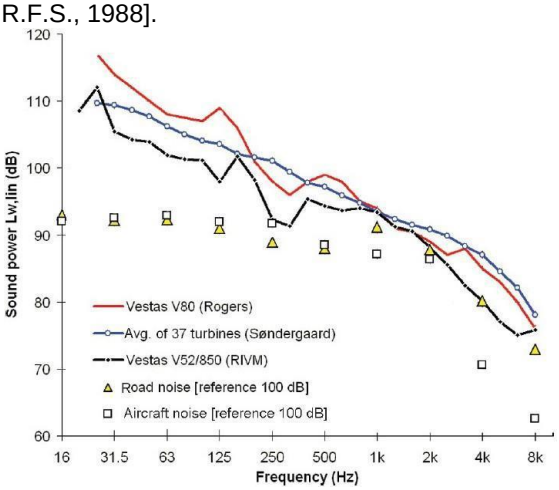

Fig. 7. Comparison of generalized sound spectra for different environmental acoustic sources: transportation noise via wind turbine noise

Different models have been developed that aim to provide insight into the processes that result in noise annoyance [Taylor, 1984; Job, 1988; Guski, 1999]. However, all these models are developed based on empirical evidence related to previously found results of correlation analysis or multiple regression analysis between noise annoyance and other variables. Both these methods have severe deficiencies in modeling noise annoyance, even the direction of causation may remain uncertain. The results of correlation analysis can be misinterpreted since the effect of the factor under investigation is not controlled for noise exposure or other factors [Alexandre, 1976]. Also, in [Taylor, 1984] it was noted, that "many of the models which are tested by using path analysis are exploratory. As such, they probably do not adequately represent the processes leading to the outcome in question e.g., noise annoyance".

RESULT AND DISCUSSION

To control annoyance the effective adequate model should be designed. In a same manner as the appropriate models were designed to control all other elements of BA to aircraft noise

management, for example like US models ANOPP and INM are used for that, or their Ukrainian analogues: BELTRA (combines two large modules: BELTAS - for noise assessment at points of interest around the source and hence derivation of the directivity pattern of a noise event, and TRANOI - which indicates the need for noise control under the flight paths) and IsoBella (full analogue of INM) soft tools, both used for decision-making procedures concerning aircraft noise problems. Models and methods used for assessing environmental noise problems must be based on measured or/and calculated noise exposure indices, which are used by relevant national and international noise control regulations and standards [Zaporozhets O., 2011].

Comparing with traditional BA elements, which are defined by physical effects of sound generation and propagation, an annoyance is a psychological phenomenon (in nature of effect on humans the noise is a psychological phenomenon too!). Acoustical factors of environment noise events like sound intensity, peak levels, duration of time in-between sound events, number of events, etc., were focused for explanation of annoyance mainly [Janssen S.A., 2011]. The non-acoustical factors ('moderators' and/or 'modifiers' of the effect) have still received an empirical attention, without deep theoretical approach, never mind that various comparative studies reveal that they play a major role in defining the impact on people [Job, 1988].

Noise annoyance is defined as a form of psychological stress, which is determined by the perceived impact of a stressor and the perceived resources to cope with this stressor. From the point of view of psychological stress theory, the generation of noise-induced annoyance is essentially a dynamic process. In [Guski, 1999] it is also emphasized that noise annoyance is not just reflecting acoustic characteristics: "noise annoyance describes a situation between an acoustic situation and a person who is forced by noise to do things he or she does not want to do, who cognitively and emotionally evaluates this situation and feels partly helpless."

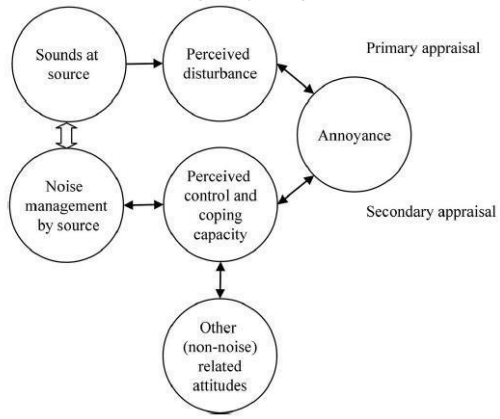

Fig. 8. The conceptual model used to explain noise annoyance [Stallen, 1999]

Acoustical and non-acoustical factors are appraised and re-appraised by the individuals on the basis of their needs and the resources available to satisfy them. Here a primary appraisal is the level of perceived disturbance, which is evaluated by any person for the impact of the threat or harm in relation to their well being. After a threat or harm is recognized, a process of secondary appraisal is triggered. The nature of annoyance is rooted in the fact that the exposure to noise makes it difficult or impossible to attain something valued, – that is the nature of disturbance, and two factors determine the deepness of the disturbance [Stallen, 1999].

In other words noise annoyance as a form of psychological stress is determined by the extent to which a person perceives a threat, i.e. perceived disturbance and the possibilities or resources that a person has with which to face this threat, i.e. perceived control [Stallen, 1999]. Based on the model it was argued [Stallen, 1999] that noise annoyance will arise if the perceived threat, i.e. noise, is larger than the perceived resources to face and to cope the threat, i.e. perceived control and coping capacity. In addition, even though the perceived disturbance may be very high, no noise annoyance will arise if there are sufficient coping resources.

The structure in Fig. 9 represents this popular noise annoyance model [Stallen, 1999]: non-acoustical factors are regarded as affecting the relationship between sound exposure and noise annoyance. The double arrows in Fig. 9 show the capacity of permanently reconsidering appraisals of noise. The protection of the residents is understood as a dynamic process, meaning that the evaluation criteria must be repeatedly tested and - if necessary - adapted to new scientific findings [Zaporozhets O., 2014]. The only significant determinant of perceived disturbance is the level of noise exposure. Thus through the effective management and control of aircraft noise, best practice – through ICAO BA, it must be possible to minimize adverse impacts of aircraft noise on health and quality of life.

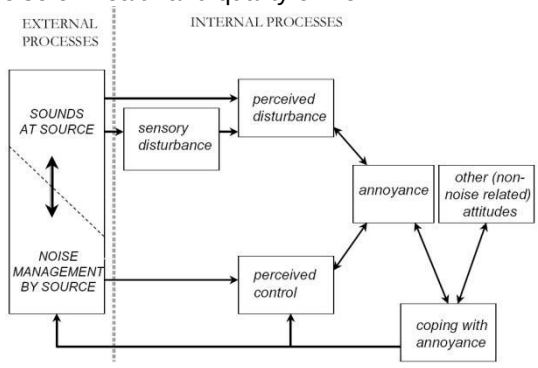

Fig. 9. Noise annoyance modeled as a stress-response to the external stimuli 'sounds' and 'noise management' [Stallen, 1999]

Besides noise level, non-acoustical factors are associated with current aircraft noise annoyance:

e.g. individual noise sensitivity (Pearson correlation r = 0.324 for relation of the sensitivity to annoyance, from [Job, 1988] it is varying between 0.15 and 0.48); in [Guski, 1999] it is cited the found correlations between source evaluation and noise annoyance in the order of (-0.25), this covariation is higher with annoyance by private airplanes; trust in authorities responsible for noise level reduction (-0.307), expected changes in residential situation due to airport extension. The effects of noise annoyance on perceived disturbance and perceived control and coping capacity are equal to 0.90 and 0.94 respectively.

The significant determinants of the perceived level of control and coping capacity (Tab. 1 [Kroesen M., Molin E.J.E., van Wee B., 2008]) are the negative attitude toward noise source authorities and the noise policy −0.22, the negative expectations related to noise development −0.42, the concern about negative health effects of noise and pollution −1.15, and the concern about property devaluation −0.15. Especially, the concern about negative health effects has a large effect on the capacity of people to handle the noise situation. The most important determinant of this factor is the positive social evaluation of noise source −0.40 and the belief that noise can be prevented 0.24.

Table 1. Standardized total effects of each variable on noise annoyance [Kroesen M., Molin E.J.E., van Wee B., 2008]

Variable	Effect
Concern about negative health effects of noise and pollution	0.59
Perceived disturbance	0.56
Perceived control and coping capacity	−0.51
Negative expectations toward noise development	0.26
Negative attitude toward source authorities	0.11
Concern about property devaluation	0.08
Positive social evaluation of the noise source	−0.05
Belief noise can be prevented	0.03
Noise annoyance	0.02
Noise exposure *DENL*	0.02
Annoyance non-noise effects	0.01

Under the standard [ISO 31000:2009] the definition of "risk" is no longer "chance or probability of loss", but "effect of uncertainty on objectives". The purpose of risk assessment is to provide evidence-based information and analysis to make informed decisions on how to treat particular risks and how to select between options. Principal benefits of a performing risk assessment includes a wide set of positive outcomes for person, group or/and community.

Risk is defined as the probability of harmful consequences, or expected losses (deaths, injuries, property, livelihoods, economic activity disrupted or environment damaged) resulting from interactions between natural or human-induced hazards and vulnerable conditions [UN-ISDR, 2009].

Risk can presented conceptually in relation to **H**azard, **V**ulnerability and **A**mount of elements-at-risk with the following basic equation:

$$\mathbf{R = H * V * A}_{\text{elements-at-risk}}$$

or taking into account the **C**apacity (opposite characteristic to vulnerability) to cope the hazard consequences [Blyukher B., Zaporozhets O.I., 2016]:

$$\mathbf{R = H * V / C}$$

The equations given above are not only a conceptual one, but can also be actually calculated (for example, with spatial data in a GIS to quantify risk from geo-distributed hazards).

Mathematically **R**isk is proportional to a measure for the **P**robability of an event (frequency, likelihood) and the **C**onsequences of an event (impact, effect on objectives):

$$\mathbf{R = P*C}.$$

For individual risk this basic condition may be expressed by the formula [Zaporozhets O.I., Khaidar H.A., 2001]:

$$\mathbf{R = P_f * P_{d/f}},$$

where P_f – the probability of harmful event (eg, aircraft accident); $P_{d/f}$ – the likelihood of the consequences (effect or damage), particularly the fatal consequences caused to individuals in the absence of protection from (or resistance to) a danger.

In more general form probability of accident P_f may be divided to the probability of scenario p_{Sc} and the probability of hazard exposure p_{Ex}:

$$\mathbf{P_f} = p_{Sc}\, p_{Ex}.$$

The effects are usually described in terms of various type damage k (eg, fatality, injury, physical damage, environmental losses, loss of income, etc. depending what are the elements-at-risk) and their vulnerability v_k (for example, a person's vulnerability can be defined as mortality):

$$\mathbf{P_{d/f} = k*}v_k$$

Vulnerability is determined by physical, social, economic and environmental factors (or simply conditions or processes), which increase the susceptibility of a community to the impact of hazards. Vulnerability can be classified as shown in Tab. 2. Risk assessment is concerned with determining those factors which are especially dangerous and determining the likelihood of unacceptable harmful exposure. Among vulnerability properties of the population under the risk of noise impact is a number of acoustic

factors (fleet composition, their respective distribution over given time period of observation) and non-acoustic factors (personal noise sensitivity, attitude towards the noise source, performed activities at the moment, etc.).

Table 2. General classification of vulnerability [van Westen C.J.,2017]

	Human - social	Physical	Economic	Cultural Environmental
Direct losses	• Fatalities • Injuries • Loss of income or employment • Homelessness	• Structural damage or collapse to buildings • Non-structural damage and damage to contents • Structural damage infrastructure	• Interruption of business due to damage to buildings and infrastructure • Loss of productive workforce through fatalities, injuries and relief efforts • Capital costs of response and relief	• Sedimentation • Pollution • Endangered species • Destruction of ecological zones • Destruction of cultural heritage
Indirect losses	• Diseases • Permanent disability • Psychological impact • Loss of social cohesion due to disruption of community • Political unrest	• Progressive deterioration of damaged buildings and infrastructure which are not repaired	• Economic losses due to short term disruption of activities • Long term economic losses • Insurance losses weaken-ing the insurance market • Less investments • Capital costs of repair • Reduction in tourism	• Loss of biodiversity • Loss of cultural diversity

Risk assessment needs to be used in framework of its regulation (Fig. 10) [10]. To investigate the effects of hazards there are important factors of vulnerability - physical, social, economic and environmental conditions and processes that tend to increase the damage from the effects of the hazards impact on the person or society as a whole. There is necessary a covering *capacity* - capabilities of a human, system, society, nature to confront the consequences of dangers and threats, ie resources are needed that may reduce the negative effects.

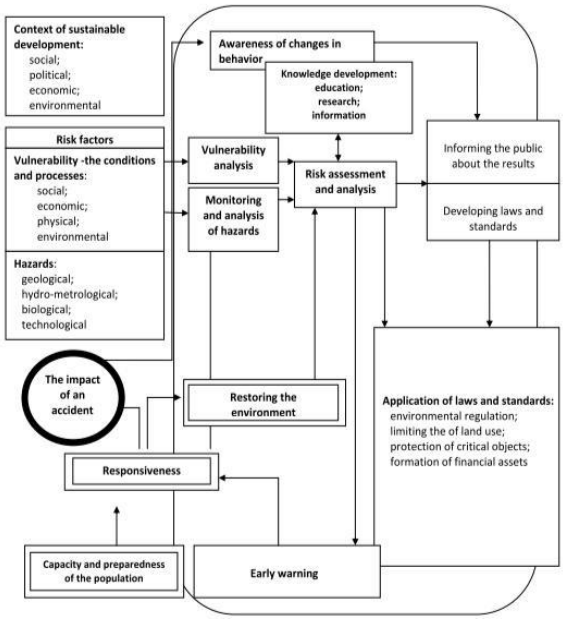

Fig. 10. Framework for risk assessment and reduction [ACS GUIDE, 1998]

CONCLUSIONS

It should be a primary objective of future research into environmental noise impact to investigate the interplay of sound level control and perceived control. New and additional (political) measures to mitigate noise impact may result from the redirection of attention from sound to noise and to noise annoyance. Strategies that reduce noise annoyance, as opposed to noise, may be more effective in terms of protecting public health from the adverse impacts of noise and its interdependency with other environmental, operational, economic and organizational issues of airport and airlines operation and maintenance.

Noise annoyance as a form of psychological stress is determined by the extent to which a person perceives a threat, i.e. perceived disturbance and the possibilities or resources that a person has with which to face this threat. New communication technologies must provide better understanding of the problem to the community, to every individual living around the airports, providing their more positive response to aircraft operation and noise in consequence.

Risk assessment and management methodology is proposed to be used for noise impact assessment and management. It provides necessary tools to include in consideration *vulnerability & capacity* values, both very important for management of the impact first of all.

The reviewed and proposed models provide a good model fit and support to the toolboxes of noise annoyance management, currently under the design. It can be concluded that the concern about the negative health effects of noise and pollution, other environmental issues, are still the subjects of scientific and societal attention, their newish deliverables may improve the approach to build the fifth element of ICAO balanced approach to aircraft noise control around the airports, which cover the measures to reach the final goal of aircraft noise management – to reduce the number of people loving in vicinity of the airports and affected by noise.

ACKNOWLEDGEMENTS

Paper is prepared in accordance with EC Grant Agreement No:769627, 2017-2020 “Aviation Noise Impact Management through novel Approaches”.

REFERENCES

ACARE, 2012. Realising Europe’s vision for aviation. Strategic Research & Innovation Agenda. Vol. 1.

ACS Guide, 1998. Understanding Risk Analysis. A Short Guide For Health, Safety, And Environmental Policy Making. Internet Edition, American Chemical Society, WASHINGTON, DC 20036,1998.

Alexandre, A., 1976. An assessment of certain causal models used in surveys on aircraft noise annoyance. J. Sound Vib., vol. 44.

Berglund, B. et al., 1999. Guidelines for Community Noise. World Health Organization, revised version.

Blyukher B., Zaporozhets O.I., 2016. Hazard Analysis And Risk Assessment Methodology: Generalized Model. Encyclopedia of Energy Engineering and Technology, 2nd Ed.2016. – p. 1-15.

Collin, D., 2014. Aircraft Noise research at national and international levels. X-noise EV Workshop on Future Trends in Aviation Noise Research, Brussels.

Directive 2002/49/EC of the European Parliament and of the Council of 25 June 2002 relating to the assessment and management of environmental noise, OJ L 189, 18.7.2002.

Fidell, S., Piersons, K.S. ,1997. Community response to environmental noise, in: M. J. Crocker (ed.) Encyclopaedia of acoustics, New York: Wiley.

Fidell, S. 2003. The Schultz curve 25 years later: a research perspective. Journal of the Acoustical Society of America, 114 (6).

Fields J. M., 1996. Effect of personal and situational variables on noise annoyance in residential areas. J. Acoust. Soc. Am., 46.

Fleming,G.G., Ziegler,U.R.F., 2013. Environmental Trends in Aviation to 2050. ICAO 2013 Environmental Report.

Flindell, I. et al., 2013. Understanding UK Community Annoyance with Aircraft Noise. ANASE Update Study Report for 2M Group, Ian Flindell & Associates.

Griefahn and Scheuch, 2004. Protection goals for residents in the vicinity of civil airports. Noise Health, vol. 6(24).

Guski, R., 1999. Personal and social variables as co-determinants of noise annoyance. Noise Health, vol. 1(4).

Jagnatinskas A., Fiks B., Zaporozhets O., Kartyshev, O. 2011. Aircraft noise assessment in the vicinity of airports with different descriptors. INTER-NOISE-2011, Osaka, Japan, 4-7 September, 2011.

Janssen, S.A., Vos, H., van Kempen, E.E., Breugelmans, O.R., Miedema, H.M., 2011. Trends in aircraft noise annoyance: the role of study and sample characteristics. J. Acoust. Soc. Am., 129(4).

Job, R.F.S. , 1988. Community response to noise: A review of factors influencing the relationship between noise exposure and reaction // J. Acoust. Soc. Am., vol. 83.

ICAO, 2004. Guidance on the Balanced Approach to Aircraft Noise Management. ICAO Doc 9829, AN/451, Montreal.

ISO 31000:2009. Risk management -- Principles and guidelines. 2009. URL: http://www.iso.org/iso/home/standards/iso31000.htm

Kroesen, M., Molin, E.J.E., van Wee, B., 2008. Testing a theory of aircraft noise annoyance: A structural equation analysis // J. Acoust. Soc. Am. 123 (6).

Scheuch, K., Griefahn, B., Jansen, G., Spreng, M., 2003. Evaluation criteria for aircraft noise // Rev Environ Health, vol. 18(3).

Shaw, E.A.G., 1996. Noise environments outdoors and the effects of community noise exposure. Noise Control Engineering, vol. 44 (3).

Stallen, P. J. M., 1999.A theoretical framework for environmental noise annoyance // Noise Health, 1.

Taylor, S. M., 1984. A path model of aircraft noise annoyance? J. Sound Vib., vol. 96.

UN-ISDR, 2009. Terminology on Disaster risk Reduction. URL: https://www.unisdr.org/we/inform/terminology

van Westen C.J.,2017. Introduction to Exposure, Vulnerability and risk assessment http://www.charim.net/methodology/51

Woodward, J.M., Lassman Briscoe, L., Dunholter, P., 2009. Aircraft Noise: A Toolkit for Managing Community Expectations. ACRP Report 15, Washington, D.C.

Zaporozhets O.I., Khaidar H.A. , 2001. Instruments and procedures for management of aviation safety provision // Visnyk of the National Aviation University, Kyiv, Iss. 6, No 1, 2001. - pp. 186-189.

Zaporozhets O., Tokarev V., Attenborough K., 2011. AIRCRAFT NOISE: assessment, prediction and control. Glyph International, Taylor and Francis.

Zaporozhets O., 2014. Criteria for aircraft noise control around airports and their role in reaching the strategic goals in environmental protection from aviation impact. Acoustic Climate Inside and Outside Buildings, International Conference, 23-26 September, 2014, Vilnius, Lithuania, abstract Number: Acoustic.09.

Zaporozhets O., et al., 2014. Interdependency analysis of current and future criteria and their limits for aircraft noise control in urban areas. Acoustic Climate Inside and Outside Buildings, International Conference, 23-26 September, 2014, Vilnius, Lithuania, abstract Number: Acoustic.14.

International Symposium on Sustainable Aviation 2018
9 – 11 July 2018
Rome, Italy

ISSA-2018-002

DESIGN OF A SHORT TO MEDIUM RANGE HYBRID TRANSPORT AIRCRAFT

Sarah M. Ortega & Nikos J. Mourtos
Aerospace Engineering
San Jose State University
One Washington Square, San Jose, CA 95192, USA
sarah.bass44@yahoo.com
nikos.mourtos@sjsu.edu

SUMMARY

Small, electric, unmanned aircraft have been in use for s ome time. However, it is the recent advances in the capabilities of batteries and electric motors, which have allowed electric manned flight to become a reality . Most electric, manned aircraft are current ly small, general aviation airplanes with minimal payload capacity and modes t range, as batteries are not yet capable for fully powering larger, long range aircraft . This paper explores the possibility of a hybrid jet transport with a size and mission spe cification similar to the Boeing 737 - 100. The paper presents the preliminary sizing and design of a 96 -passenger, medium range hybrid jet transport . The results indicate that such an aircraft is indeed feasible, promising reduced fossil fuel emissions , a greener form of air transportation , comparable takeoff weight, and competitive direct operating costs .

Keywords: Hybrid aircraft, electric aircraft, green transportation, lithium ion batteries

INTRODUCTION

With transportation innovations and the widespread availability of aviation to nearly half the global population, environmental protection and stability are motivating factors for exploring hybrid and electric aircraft. This has resulted in imposed constraints monitoring air and water cleanliness, noise impacts, and climate change. The Federal Aviation Administration (FAA) published the "Aviation Environmental and Energy Policy Statement" in 2012, emphasizing the commitment to both aviation growth and environmental protection (Federal Aviation Administration, 2015). To achieve this commitment, the FAA's Next Generation Air Transportation System will be responsible for establishing programs to develop new technologies, operations, and systems, while minimizing aviation's environmental impact.

Both aircraft and aviation infrastructure contribute to emissions of pollutants. Aircraft emissions consist of carbon dioxide (CO_2), water vapor (H_2O), nitrogen oxides, sulfur oxides, carbon monoxide, partially burned or unburned hydrocarbons, particulate matter, and other trace compounds. CO_2 and H_2O emissions constitute about 70% and 30%, respectively, with the remainder of pollutants comprising less than 1%. From 1970-2014, the number of general aviation aircraft increased by approximately 1% per year. (Davis, Williams, & Boundy, 2016) Emissions from aviation activity and fossil fuel usage are projected to increase due to the rise in aircraft and demand for air transportation. Electric aircraft would remove that dependence and hybrid vehicles would alleviate oil dependence.

Electric aircraft are currently limited by the energy storage capabilities of batteries. These limits impose weight penalties due to low energy-to-mass and energy-to-volume densities. Thus, battery weight and power plays a significant role in electric power selection. Lithium ion batteries have the highest energy density offered, which means they are the smallest in both volume and weight for the amount of energy stored. With cost, weight, and volume being critical factors in aircraft design, lithium ion batteries demonstrate good promise statistically and have illustrated their capabilities through their use in small aircraft.

Current lithium ion battery specific energy is 250 Wh/kg, and battery specific power is at 320 W/kg (Hepperle). These values are expected to rise to 750 Wh/kg and 950 W/kg, respectively, as studies show that lithium ion battery energy densities are increasing at a rate of 8-10% per year (Ullman).

Using lithium ion batteries and jet fuel to power the aircraft, the following paper presents the preliminary design of a hybrid transport aircraft. This aircraft is designed with the following requirements: a payload of 96 passengers, including luggage, a crew of two, a range of 3,185 km, and a cruise speed of 805 km/hr at a maximum cruise altitude of 12,192 m. The required takeoff field length is 1,676 m and the required landing distance is 1,125 m.

METHODOLOGY

This hybrid aircraft has been designed and sized through a combination of techniques that account for both fuel and battery usage. The Roskam (2003) approach is used to perform a Class I preliminary sizing and design. The battery weight is considered to be constant and has been determined using electric and hybrid aircraft databases, such as those in Riboldi and Gualdoni (2016) and the Subsonic Ultra Green Aircraft Research (SUGAR) (Bradley & Droney, 2015). Trade studies are performed to assess the best combination of fuel and battery usage during each flight phase.

Once the takeoff weight required for the mission was determined, performance sizing yielded the gross wing area, thrust, and energy required to carry

out the mission. Finally, the preliminary design yielded the geometric characteristics of the fuselage, the wing, the empennage, and the landing gear, following a weight and balance and a stability and control analysis to ensure appropriate center-of-gravity travel and adequate longitudinal, directional, and lateral stability and control characteristics. Finally, a drag polar estimation confirmed that the aircraft performance will meet the requirements set in the mission specification.

Performance limits were also explored using a V-n diagram, and a Class II weight and balance analysis. Finally, a cost analysis determined the operating cost of the proposed hybrid aircraft.

RESULTS AND DISCUSSION

The proposed hybrid transport aircraft features a conventional configuration with two hFan engines suspended below the low, cantilever wings, a single vertical tail mounted on the fuselage, and a conventional, tricycle landing gear. The interior of the fuselage holds 96 passengers, with 6 abreast seating. Two battery pods are suspended below the wings, allowing for easy exchange of batteries, potentially sized specifically for the mission range. This would allow the use of smaller batteries for shorter trips, to achieve additional weight savings.

The hFan engine is a hybrid electric system, which allows the aircraft to use a gas turbine for some stages of the mission and batteries for other stages of the mission, while providing sufficient thrust for all flight stages with the added battery weight. The 1,015 kW produced is equivalent to 93.4 kN of Boeing thrust. A schematic of the hFan propulsion system is illustrated in the figure below (Bradley & Droney, 2011).

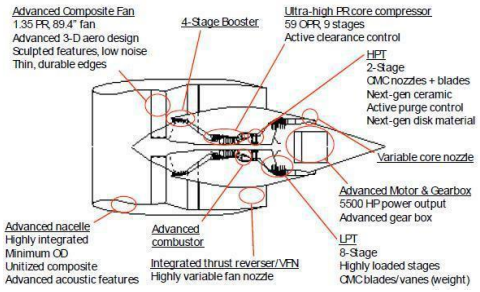

Fig. 1. hFan engine overview.

Using fuel for engine start-up, taxi, takeoff, and climb, and batteries for cruise, loiter, descent, and landing, the Class I estimate of the takeoff weight is 35,200 kg, consisting of an empty weight of 21,944 kg, a payload of 8,927 kg, a crew weight of 372 kg, a fuel weight of 1,946 kg, and a battery weight of 4,672 kg.

Using these estimates, trade studies were performed and the performance constraints of the aircraft analyzed. Both of these were computed manually, as well as using Advanced Aircraft Analysis (AAA) (Advanced Aircraft Analysis, 2016).

Trade studies illustrate the airplane growth factor due to payload, and sensitivity studies illustrate the sensitivity of takeoff weight to range and empty weight. For each 1 kg increase in payload,

increases by 1.59 kg. For a change in range, decreases by 7.56 kg/km, and increases 1.89 kg per 1 kg increase in .

The performance requirements are plotted in Figure 2, as functions of wing loading and thrust-to-weight ratio. A design point with W/S =6,145 N/m^2 and T/W=0.31 is selected, resulting in a required takeoff thrust of 107 kN and a gross wing area of 57.06 m^2, with batteries used during the cruise, loiter, descent, and landing phases.

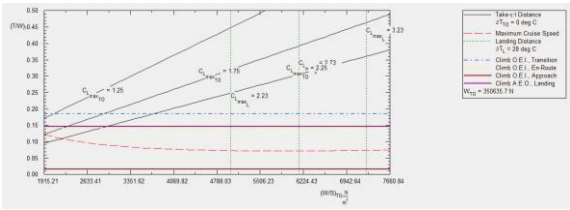

Fig. 2. Performance sizing plot.

The aircraft also features Fowler flaps to provide adequate lift during takeoff, climb, and landing. The landing gear is of the conventional, tricycle type.

The V-n diagram, below, depicts the velocity vs. load factor, illustrating the aircraft performance limits. These limits include the design ultimate load factor and speed, to which the airplane structure will be designed (Roskam, 2003).

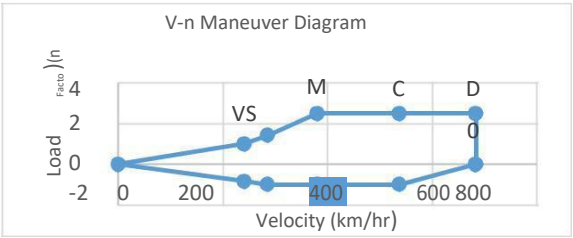

Fig. 3. V-n maneuver diagram.

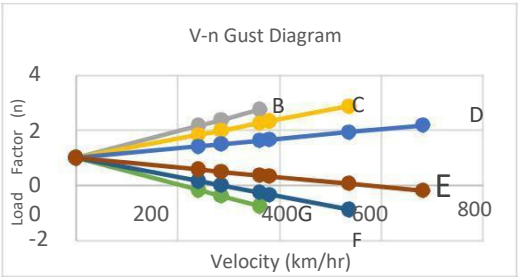

Fig. 4. V-n gust diagram.

According to these diagrams, the highest positive load factor permitted during flight is 2.5, while the negative load factor is limited to -1. Any velocity and load factor combination that lies outside of the envelope in Figure 3 would result in stall or structural failure. These diagrams were constructed assuming symmetrical loading and an altitude of 12.2 km but can also be plotted at other

altitudes to determine the allowable load factors for various flight conditions. The gust lines fall within the maneuvering V-n diagram.

The Class II weight sizing yields more accurate estimates for the empty weight and the takeoff weight. The empty weight is the sum of the structural weight, powerplant weight, and fixed equipment weight.

The Class II structure weight estimate was equations provided by Roskam (2003), General Dynamics, Torenbeek, and Nikolai (1984), as well as data from the 737-200, and the SUGAR aircraft.

The powerplant weight estimate is

9,870 kg from manufacturer's data for the hFan propulsion system, while the fixed equipment weight is = 1,946 kg from the Class I fuel fraction method (Roskam, 2003). Thus, the Class II empty weight estimate is = 23,786 kg.

To perform the Class II estimate of the takeoff weight, the known weights from the Class I estimate were used, along with the empty weight. The takeoff weight can be broken down as follows:

(2)

The Class II estimate is found to be = 39,703 kg. This is approximately 11% higher than the Class I estimate.

The life cycle cost consists of the research and development costs, production and construction costs, operations and maintenance costs, and retirement and disposal costs. For typical aircraft, the operating cost composes nearly 94% of the life cycle cost (Ploetner, Schmidt, Baranowski, Isikveren, & Hornung, 2013). Thus, the preliminary cost analysis for the hybrid aircraft will consider the operating cost (Roskam, 2011).

The direct operating cost (DOC) for the proposed hybrid transport is 4.56 USD/km, calculated as the sum of the cost of flying, maintenance, depreciation, landing fees, and financing.

The breakdown of a typical jet transport DOC is shown in Figure 5, while Figures 6 and 7 show the DOC of the proposed hybrid aircraft and a fuel powered version of the same aircraft. As one can see through a comparison of Figures 6 and 7, there is a significant decrease in flight cost due to reduced fuel usage, but also a higher maintenance cost due to the batteries. Additionally, there is an increase in the depreciation of the batteries due to the life cycles. For a hybrid aircraft, the DOC decreases faster over time, due to much lower fuel usage. Many of these calculations were performed assuming a 10 year life cycle for the airplane. However, many aircraft last longer than 10 years, resulting in further increases in profit.

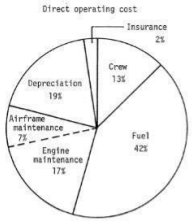

Fig. 5. DOC for a jet transport.

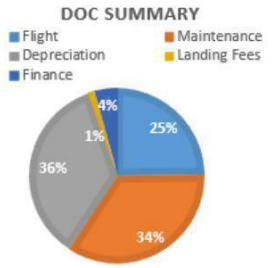

Fig. 6. DOC for a hybrid transport.

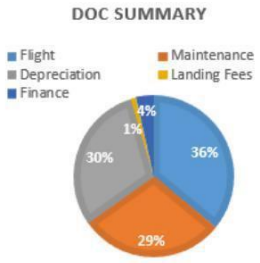

Fig. 7. DOC for an all-fuel transport.

Sensitivity studies on a fully electric jet transport demonstrate that fuel price and electricity price have the strongest impact on the DOC. The study shows that with a 10% increase in fuel costs, there is a 3% increase in DOC. Additionally, a reduction in the number of cycles of battery use, less than the typical 2000 cycles, combined with battery installation costs also produces higher DOCs (Ploetner, Schmidt, Baranowski, Isikveren, & Hornung, 2013).

The indirect operating cost (IOC) is estimated at 2.28 USD/km and consists of the cost for passenger services, maintaining depreciating ground equipment and facilities, airplane and traffic servicing, promotions sales and entertainment, and general administrative expenses.

The program operating cost depends on the indirect program operating costs, the direct program operating costs, and the number of aircraft acquired. Due to the fact that operating costs vary between customers, the program operating cost depends on the number of customers. For the purposes of these calculations, 1,200 aircraft will be assumed to be in acquisition (Sales, 2018). As of January 1, 2018, Boeing has orders for more than 4,300 737- MAX aircraft. Hence, this is a very conservative estimate since the hybrid has similar mission specification to the 737. (Roskam, 2015). Assuming the aircraft will be in use for 10 years, the operating cost will be 191 billion USD. As always, the preliminary design has a significant impact on the ultimate cost of the aircraft.

Although the price of jet fuel fluctuates, the general trend illustrates an increase in fuel costs and an increase in the number of general aviation aircraft, as discussed in the introduction. The price of electricity to recharge the batteries is significantly cheaper than jet fuel and has the added benefit of drastically reducing carbon dioxide and other harmful pollutants. Electricity costs approximately 8.5 cents per kW-hr. For a fully-fuel powered version of the hybrid aircraft, which requires 8,114 kg or 10,107 liters of jet fuel, this would reduce the cost of the total fuel per flight from 5,874 USD to 1,129 USD, along with the cost of the electricity, and the one time battery cost.

CONCLUSION

The preliminary sizing and design of the narrow-body, short to medium range transport aircraft demonstrates the feasibility of a hybrid propulsion system fueled by lithium ion batteries and jet fuel.

This vehicle provides an environmentally friendly form of air transportation, reducing emissions and dependence on oil. As the number of general aviation aircraft increases and FAA standards call for reduced emissions, aircraft designs that depend less on oil and fuel is necessary. While current state-of-the-art batteries can only provide sufficient power for small, general aviation aircraft, a hybrid propulsion system can power much larger air transports, hopefully providing for an acceptable transition to greener aircraft in the near future.

Compared to the Boeing 737-100 model, the aircraft has comparable weights, and possibly a lower takeoff weight. Additionally, with the research behind the SUGAR aircraft, the availability of hybrid engines would make the transition of power between fuel and electricity significantly simpler to integrate.

As battery technology continues to develop, resulting in higher specific energy densities, battery weight will eventually decrease to much lower levels allowing better payload fractions in future aircraft.

Additionally, more studies could be performed on the benefits of using fuel and battery power during different phases of the flight. Trade studies could show the advantages and disadvantages of each power source during the phase of flight. The direct operating cost, although preliminary, demonstrates that the batteries, as a power source, are competitive from a cost perspective. Finally, trade studies could be performed on the number of years in service and the number of aircraft acquired per year to determine the effect on the operating cost.

Overall, the hybrid transport aircraft demonstrates strong potential as a preliminary design to meet FAA standards, reduce emissions, and utilize future battery technology to pave the way toward new-age transport jets.

NOMENCALTURE

AAA	Advanced Aircraft Analysis
DOC	Direct Operating Cost
FAA	Federal Aviation Administration
IOC	Indirect Operating Cost
SUGAR	Subsonic Ultra Green Aircraft Research
USD	United States Dollars
W	weight

Subscripts

bat	battery
crew	crew
e	empty
f	fuel
feq	fixed equipment
pwr	power
struct	structure
tfo	trapped fuel and oil
TO	takeoff

REFERENCES

Advanced Aircraft Analysis. 2016, DARcorporation.

Bradley, M. K., & Droney, C. K., 2015, Subsonic Ultra Green Aircraft Research: Phase II- Volume II- Hybrid Electric Design Exploration. NASA. Huntington Beach: Boeing Research and Technology.

Davis, S. C., Williams, S. E., & Boundy, R. G. (2016). *Transportation Energy Data Book* (35 ed.). Oak Ridge, Tennessee: Oak Ridge National Laboratory.

Federal Aviation Administration. 2015. *Aviation Emissions, Impacts, and Mitigation: A Primer.* Office of Environment and Energy.

Hepperle, M. (n.d.). Electric Flight- Potential and Limitations. *NATO OTAN*.

Nicolai, L.M. (1984). *Fundamentals of Aircraft Design*. METS, Inc. 6520 Kingsland Court, San Jose, CA 95120.

Ploetner, K. O., Schmidt, M., Baranowski, D., Isikveren, A. T., & Hornung, M. (2013). Operating Cost Estimation for Electric-Powered Transport Aircraft. *American Institute of Aeronautics and Astronautics*.

Riboldi, C., & Gualdoni, F. (2016). An integrated approach to the preliminary weight sizing of small aircraft. *Aerospace Science and Technology, 58*, 134-149.

Roskam, J. (2003). *Airplane Design Part V: Component Weight Estimation.* Lawrence: DARcorporation.

Roskam, J. (2011). *Airplane Design Part II: Preliminary Configuration Design and Integration of the Propulsion System.* Lawrence: DARcorporation .

Roskam, J. (2015). *Airplane Design Part VIII: Airplane Cost Estimation: Design, Development, Manufacturing, and Operating.* Lawrence: DARcorporation.

Ullman, D. (n.d.). The Electric Powered Aircraft: Technical Challenge

An Experimental Study on the Reduction of Airfoil Trailing-edge Noise Using a Single-Leg Spiral Array in an Anechoic Wind Tunnel

QIAO Weiyang[1], CHEN Weijie[2], WANG Liangfeng[3], TONG Fan[4], and CHENG Haoyi[5]
School of Power and Energy, Northwestern Polytechnical University, Xi'an, 710072, China

Acoustic beamforming with phased microphone array is performed in an anechoic wind tunnel to investigate the noise reduction effect of two passive bionic noise reduction modifications: serrated trailing edges and wavy leading edges (denoted as STE and WLE, respectively). The baseline airfoil is NACA 0012 with a chord length of 150 mm and the freestream velocity is 40 m/s with an angle of attack of 0 deg. The Reynolds number based on airfoil chord length and the freestream velocity is 400,000. The deconvolution approach, CLEAN-SC, is used to analyze the array data in the present paper. It is obviously that the designed microphone array can identify the trailing edge sound source. It is also found that both the STE and WLE can reduce the airfoil trailing-edge self-nosie effectively and the WLE with smaller wavelength can achieve larger noise reduction effect.

Nomenclature

A = amplitude of the wavy leading edge
W = wavelength of the wavy leading edge
H = amplitude of the serrated trailing edge
= wavelength of the serrated trailing edge
c = baseline airfoil chord length
L = baseline airfoil span-wise length
= angle of attack
U_0 = free stream velocity
SPL = sound pressure level
CSD = cross spectral density
PSF = point spread function
FFT = fast Fourier transform

Project No. 51776174 and 51476134 supported by National Natural Science Foundation of China.
[1] Professor, Northwestern Polytechnical University, Xi'an, China, 710072, Qiaowy@nwpu.edu.cn
[2] PhD Student, Northwestern Polytechnical University, Xi'an, China, 710072, cwj@mail.nwpu.edu.cn
[3] PhD Student, Northwestern Polytechnical University, Xi'an, China, 710072, wlfzxlgnl@126.com
[4] PhD Student, Northwestern Polytechnical University, Xi'an, China, 710072, nwputongfan@163.com
[5] Graduate Student, Northwestern Polytechnical University, Xi'an, China, 710072, hycheng@mail.nwpu.edu.cn

I. Introduction

Acoustic beamforming with microphone phased-array is a powerful method to investigate the flow noise emission. This technique has been largely used in aeronautics to investigate and characterize aerodynamic noise. The microphone array has become a standard method for localizing the noise sources on aircraft, trains, cars and other machinery. The performance of conventional beamforming depends to a large extend on a good design of the array geometry and on a good beamforming software. The recent developments of inverse methods make it possible for the first time to determine the strengths of the sources.[1-5] To obtain higher resolution acoustic source plots from microphone array measurements, deconvolution techniques are becoming increasingly popular. Deconvolution algorithms aim at identifying Point Spread Functions (PSF) in source plots, and may therefore fall short when actual beam patterns of measured noise sources are not similar to synthetically obtained PSF's. To overcome this, a new version of the classical deconvolution method CLEAN is proposed: CLEAN-SC. By this new method, which is based on spatial source coherence, side lobes can be removed of actually measured beam patterns. Essentially, CLEAN-SC iteratively removes the part of the source plot which is spatially coherent with the peak source. A feature of CLEAN-SC is its ability to extract absolute sound power levels from the source plots.[6]

The reduction of turbulence broadband noise has been a matter of concern since the early days of aircraft manufacturing. The ability to fly silently of most owl species has long been a source of inspiration for finding solutions for quieter aircraft and turbomachinery[7,8]. Since the sharp trailing edge acts as a scattering enhancer, the reduction of broadband trailing edge noise through trailing edge modification appears to be a fruitful strategy in the global goal of reducing aircraft noise. Inspired from the ability to fly silently of the owl species, Howe first proposed the noise reduction concept using a serrated TE design.[9,10] Following Howe's encouraging theoretical work, many numerical and experimental studies assessed the acoustic benefit of serrated TE, and serrations reveal to be a robust noise reduction device since the reduction occurs for all airfoils.[11-15]

Another passive treatment named wavy leading edges were originally bio-inspired from Humpback whale flippers and have been identified as a lift-enhancing and drag-reducing attribute connected with this animal's feeding ecology.[16] After this early morphological investigation, many studies attempted to demonstrate the feasibility of WLE as passive flow control devices for wings to quantify the magnitude of any benefit that they may offer.[17-20] All the studies concerning the effect of WLE on airfoil performance draw a consensus that the WLE can delay the stall occurrence, increase post-stall lift, decrease post-stall drag and reduce the laminar separation bubble. WLE were also adopted to reduce the self-noise generated by boundary layer turbulence scattering at the trailing edge of airfoils. Hansen et al.[21] studied experimentally the aeroacoustics effect (tonal noise) of a sinusoidal modification to the leading edge of a NACA 0021 airfoil and found that the larger amplitude and smaller wavelength serrations are the most effective configurations for eliminating tonal noise. The mechanism of noise reduction is believed to be strongly related to the formation of stream-wise vortices which are generated by serrations. However, most of the attention concerned the WLE was put on the broadband noise due to theinteraction between turbulence and the leading edge of airfoils.[22-30]

The present paper concerns the application of beamforming to the airfoil Trailing-Edge (TE) noise. In this study, phased microphone array with one spiral leg is applied to localize the airfoil TE noise sources with special leading edge and trailing edge modifications. The organization of the paper is as follows. In Section II, the experimental methodology used will be outlined. Then in Section III, the phased microphone array with be discussed in detail. After that, the nosie reduction effect of the STE and WLE will be elaborated in Section IV. Finally, some conclusions will be drawn in Section V.

II. Experimental Set-up

The anechoic wind tunnel with the size of 6 m×4 m×6 m and the test airfoil are shown in figure 1. Test airfoil was put in the open test section of wind tunnel. It could be seen that the test airfoil is located on the center of the wind tunnel exhaust flow, and the airfoil is pressed from both sides using two plexiglass plates. The experimental airfoils include the airfoils with- or without the wavy leading edge and serrated trailing edge which is with the same airfoil. The baseline airfoil as well as the airfoils with serrated trailing edge and wavy leading edge are shown in figure 2. Three types of serrated trailing edge airfoil and nine types of wavy leading edge are experimental investigated. However, only some of the results are shown in the present paper.

The test airfoil is NACA0012 airfoil, and airfoil chord is c=150 mm and their span is L=300 mm, and the flow attack angle $\alpha = 0$ deg. The outlet of the wind tunnel is a 0.24 m×0.3 m rectangular channel.

Air is supplied by wind tunnel at Mach numbers ranging up to 0.30, with the Reynolds numbers based on airfoil chord ranging from 2×10^5 to 8×10^5 at the free-stream turbulence intensity about 1%.

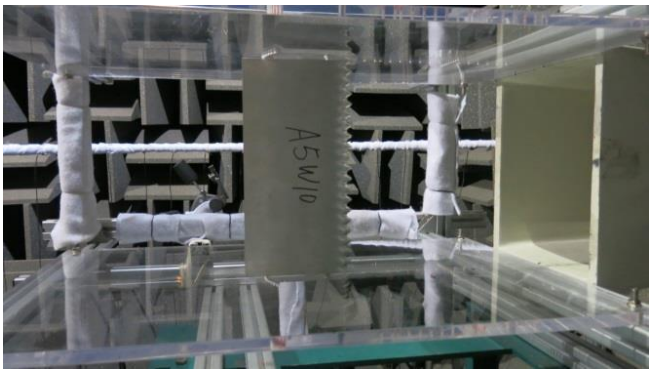

Fig. 1 Picture and sketch of the anechoic wind tunnel and the test airfoil.

(a) Baseline airfoil (b) Serrated trailing edge
(c) Wavy leading edge

Fig. 2 Picture of the test airfoil.

Three serrated trailing edges which are respectively with the sawtooth of λ/H = 0.8, 0.4, and 0.27 (the ratio of wavelength λ to their amplitude H) were tested in present study as show in table 1. Nine wavy leading edges which are respectively with different wavelength and amplitude were tested in present study as shown in table 2.

Table 1. The design parameter of serrated trailing edge.

Configuration	Label	λ/H
NACA0012 baseline	Baseline	---
H=0.05c,λ=0.04c	*H* 5 4	0.8
H =0.1c,λ=0.04c	*H*10 4	0.4
H =0.15c,λ=0.04c	*H*15 4	0.27

Table 2. The design parameter of wavy leading edges.

Configuration	Label	A/W
NACA0012 baseline	Baseline	---
A=0.025c,W=0.1c	A2.5W10	0.25
A=0.025c,W=0.2c	A2.5W20	0.125
A=0.025c,W=0.4c	A2.5W40	0.0625
A=0.05c,W=0.1c	A5W10	0.5
A=0.05c,W=0.2c	A5W20	0.25
A=0.05c,W=0.4c	A5W40	0.125
A=0.1c,W=0.1c	A10W10	1
A=0.1c,W=0.2c	A10W20	0.5
A=0.1c,W=0.4c	A10W40	0.25

III. Phased Microphone Array

A. Microphone Array

A single-leg spiral planar microphone array with 32 microphones (Fig. 3(a)) is designed and is used to localize leading edge and trailing edge noise source. The range of the spiral array was about 0.9 m×0.9 m. As shown in Fig. 3(b), the array is located of 1.2m below the airfoil, some of the mircropnones are shielded by the plexiglass, so that the microphone array could only directly focus on middle part of the airfoil, as shown in Fig. 3(c). Only the sound sourece information in the middle part of the airfoil trailing edge will be used to evaluate the noise reduction effect of the two passive modifications is Section IV.

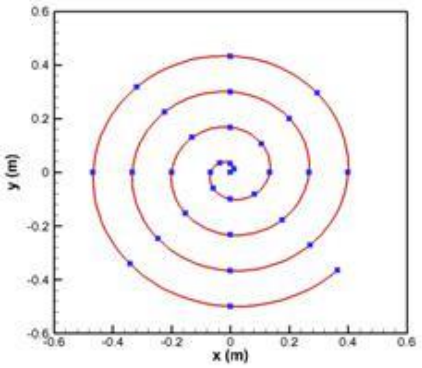

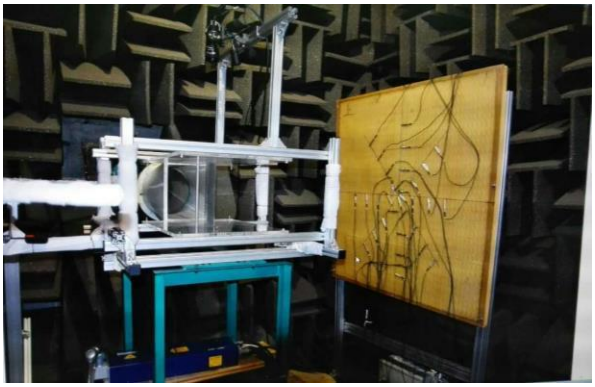

(a) spiral array (b) placement of array

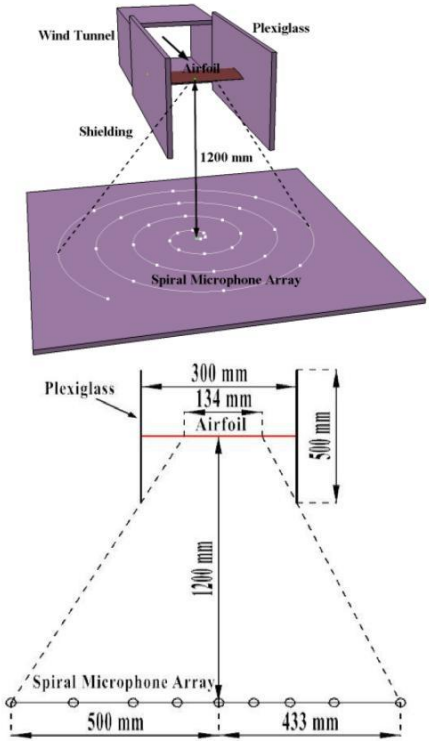

(c) Shielding effect of the plexiglass

Fig. 3 Single leg spiral microphone array and placement in the wind tunnel.

The ¼ inch capacitive microphones produced by BSWA Company are used. They are free-field types with a frequency bandwidth from 20 Hz to 20 kHz, and sound pressure levels up to 168 dB. The sensitivity is 5 mV/Pa. The microphone has an operating temperature range from –50 to +110 degree Celsius, and with a main ambient temperature coefficient of 0.01 dB/K and a main ambient pressure coefficient of -10^{-5} dB/Pa. The ¼ inch measuring microphone preamplifier is a high-impedance transducer for condenser measuring microphone cartridges. It permits a wide-band measurements and sound level measurements with a dynamic range from 17 up to 168 dB. Its frequency range is from 1 Hz to 1 MHz. The microphone preamplifiers were connected to the BBM data acquisition system. The largest sampling rate of the BBM system was 102.4 KHz. All microphone signals were simultaneously sampled with an AD conversion of 16-bit at a sampling frequency of 32768 Hz. The recording time for one measurement was 10 s. The calibration constants of microphones were obtained by using a 1000 Hz single frequency standard sound source directly on each capsule before the measurement started. All microphones were mounted with their preamplifiers lying on top of the plate with a grazing incidence of the microphone diaphragm.

B. The Beamforming of Microphone Array

The array analysis is carried out in the frequency domain. The deconvolution beamforming, **CLEAN-SC** array data reduction method, is used in this study to quantify differences of trailing edge sound source and leading edge noise source. In this study, the cross-spectral density (CSD) matrix was calculated from the measured signals using a Hanning window with a block-size of N = 8192 samples and a 50% overlap. The performance of a microphone array is the beam pattern, and this beam pattern is the spatial response of the array to a mono-pole wave, so it is also called as point-spread function (PSF).

The point-spread function of this spiral microphone array for four different frequencies is shown in Fig. 4, which is for a monopole source at emission angle of 90 deg and the distance of 1.2 m from the array. This function gives the information about the spatial resolution and the main- to side-lobe ratio of the microphone array. It can be seen that the spatial resolution is much higher and is suitable to identify airfoil trailing edge noise source. The scanning distance Δx in Fig. 4 is 0.005 m during the **CLEAN-SC** process.

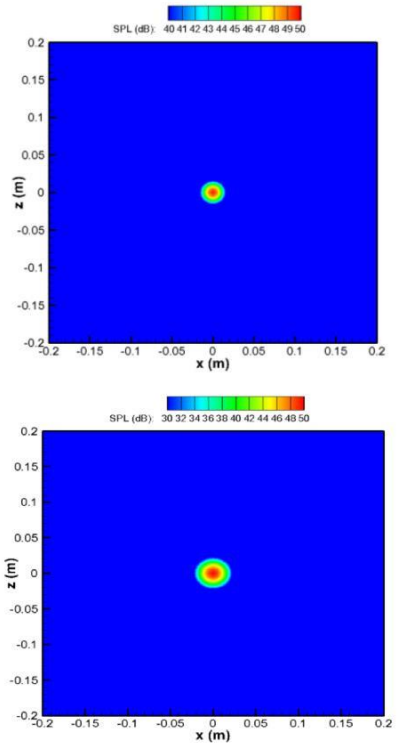

(a) f=2000 Hz (b) f=4000 Hz

(c) f=6300 Hz (d) f=8000 Hz

Fig. 4 Array patterns with a monopole source at a distance of 1.2 m from the array. (a), (b), (c), and (d) are respectively for the 1/3-octave band with center frequency of 2000 Hz, 4000 Hz, 6300 Hz and 8000 Hz.

IV. Experimental results

The following experimental results show that trailing edge noise and leading edge noise could be identified clearly with the using of special designed spiral microphone array in an anechoic wind tunnel. Noise reduction on a broadband frequency range was quantified in sound source levels as a result of trailing edge serration modification or wavy leading edge modification. The experimental results and the analysis of the results will be given as follows.

A. The reduction of airfoil self-noise with serrated trailing edge

Figure 5 shows the beamforming results along scanning plan at center frequency of 4 kHz and 6.3 kHz for the baseline and serrated trailing edge airfoils. The freestream velocity is 40 m/s in Fig. 5. The black square frame is the position of the airfoil. For evaluation of the noise reduction using serrated trailing edge, the level of the sound pressure contour is the same in same frequency. It could firstly be seen that the sound pressure level of trailing edge noise source is obviously larger than that of leading edge noise source. This results state clearly that with the low free-stream turbulence intensity inflow, the trailing-edge noise is the main noise source of the airfoil. It could also be clearly seen from Fig. 5 that the airfoil trailing edge noise could be effectively reduced with the using of serrated trailing edge. The more results have noted that the serrated trailing edge with the sawtooth of $\lambda/H = 0.27$ is more effective to reduce airfoil trailing edge noise than other serrated trailing edge in the flow velocity range of the test.

The noise maps were further processed to obtain airfoil trailing edge noise spectrum. The source plot levels within an integration contour around the mid-span part of the airfoil trailing edge (the red square shown in the top left picture of Fig. 5) are summed to mitigate the influence of extraneous sources at airfoil-end plate junctions. The sum region is the same for baseline and serrated trailing edge airfoils as shown in Fig. 5 (a). The narrow band spectrum and 1/3-octave band spectrum within the integration contour for baseline airfoil and H15λ4 serrated trailing edge airfoil are shown in Fig. 6. It can be seen that the trailing edge noise is reduced obviously within a broad frequency region by the serrated trailing edge and the maximum noise reduction effect can be up to 10 dB.

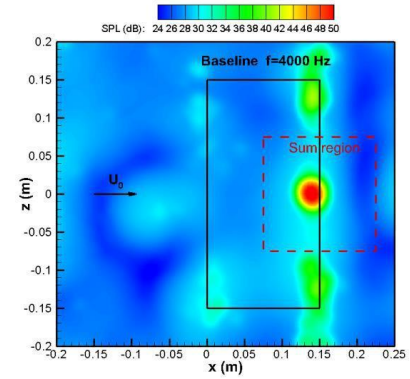

(a) f=4000 Hz

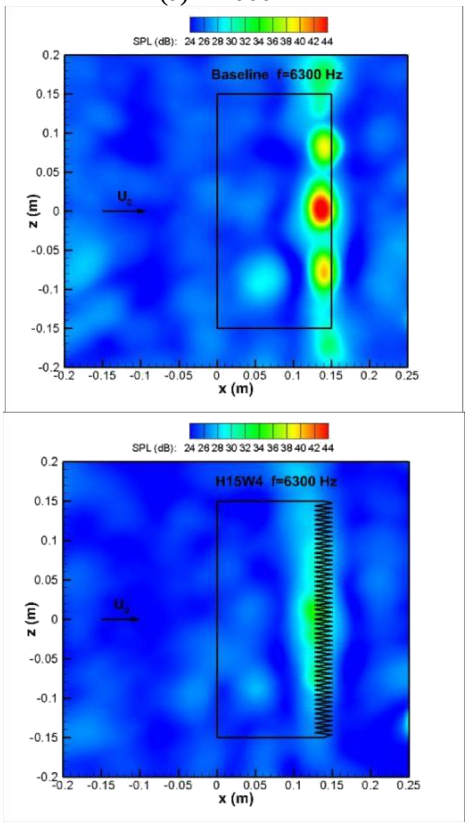

(b) f=6300 Hz

Fig. 5 Source distributions for baseline and serrated trailing edge airfoils.

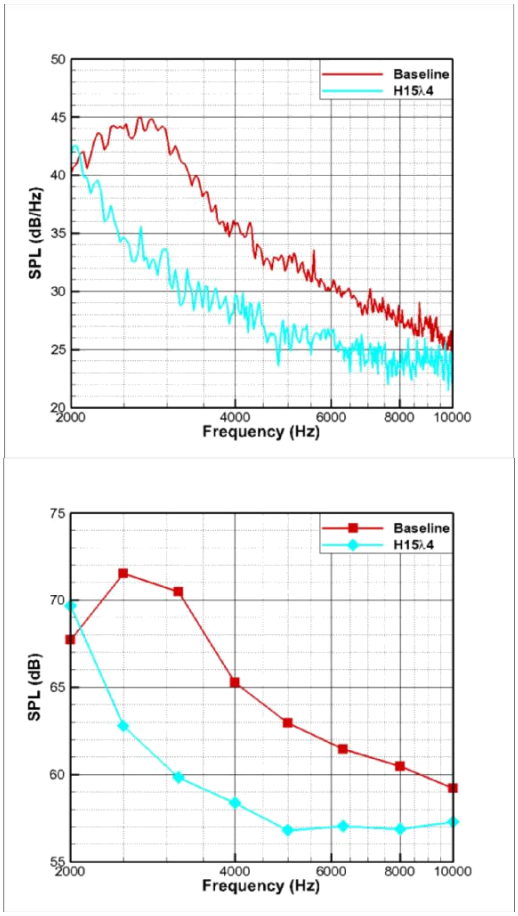

(a) Narrow band spectrum (b) 1/3-octave band spectrum

Fig. 6 Comparison between spectra for the noise source of baseline airfoil and serrated trailing edge airfoil.

B. The reduction of airfoil self-noise with wavy leading edge

Figure 7 shows the beamforming results along scanning plan at center frequency of 4 kHz and 6.3 kHz for the baseline and wavy leading edge airfoils. The freestream velocity is 40 m/s in Fig. 7. The black square frame is the position of the airfoil. For evaluation of the noise reduction using wavy leading edge, the level of the sound pressure contour is the same in same frequency. It could be seen that the appropriate wavy leading edge could obviously reduce airfoil trailing edge noise and the WLE with smaller wavelength can obtain larger noise reduction effect.

As shown in Fig. 7, the noise map within the trailing edge integration contour (the red square

shown in the top left picture of Fig. 7) are summed to obtain trailing edge noise spectrum and to evaluate the noise reduction effect of the wavy leading edges. The integrated narrow band spectrum and 1/3-octave band spectrum for baseline airfoil and wavy leading edge airoil are shown in Fig. 8. The A10W10 wavy airfoil can obtain obviously noise reduction within a broad frequency region and the noise reduction can be up to 10 dB. The A10W40 wavy airfoil has noise reduction at lower frequency but the reduction is negligible at high frequency. The further analysis of the experimental results indicates that wavy leading edge airfoil can reduce airfoil trailing edge noise especially at low frequency and the wavy airfoil with smaller wavelength can obtain larger noise reduction effect.

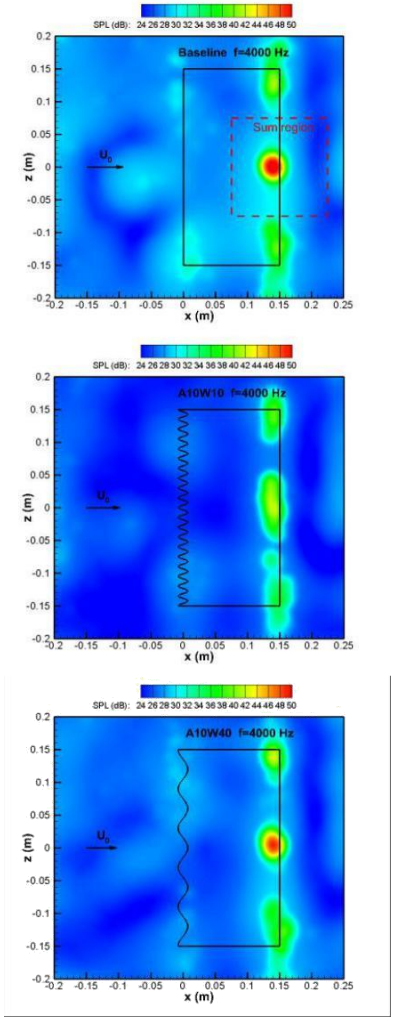

(a) f=4000 Hz

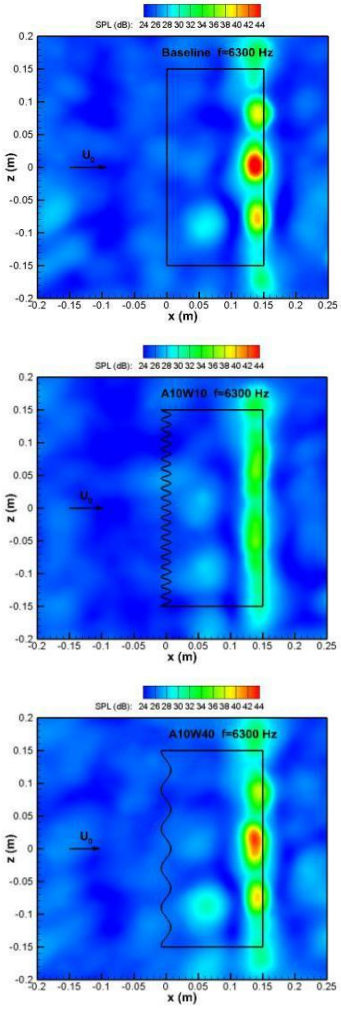

(b) f=6300 Hz

Fig. 7 Source distributions for baseline airfoil and wavy leading edge airfoil.

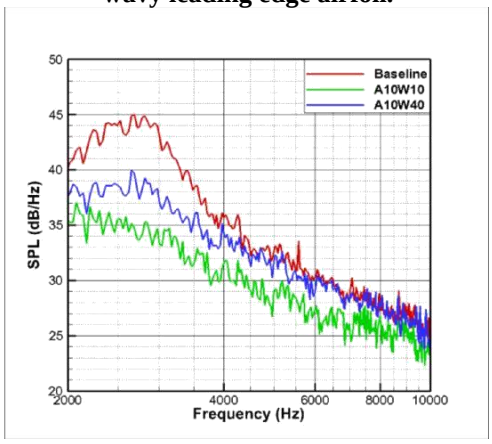

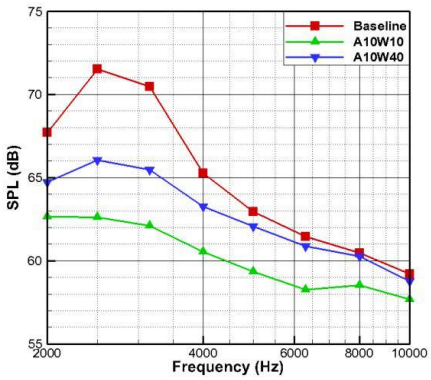

(a) Narrow band spectra
(b) 1/3-octave band spectra

Fig. 8 Comparison between spectra for the noise source of baseline airfoil and wavy leading edge airfoil.

V. Conclusions

A phased microphone array with one spiral-leg has been applied to localize the blade trailing-edge (TE) and leading-edge (LE) noise sources with special leading edge and trailing edge modification in an anechoic wind tunnel. Noise reduction on a broadband frequency range was quantified in sound source levels as a result of trailing edge serration modification or wavy leading edge modification. According to the experimental results, some conclusions can be drawn below.

The present test results show that TE noise and LE noise could be identified clearly with the using of special designed spiral microphone array. With the low free-stream turbulence intensity inflow, the TE noise is obviously louder than the LE noise. The airfoil TE noise could be effectively reduced with the using of serrated trailing edge. It is noted that the serrated trailing edge with the saw-tooth of λ/H = 0.27 is more effective to reduce TE noise than other serrated trailing edge in the flow velocity range of the test. The wavy leading edge could also reduce the airfoil TE noise and the noise reduction effect of A10W10 is better than A10W40 airfoil, which means that the wavy leading edge with smaller wavelength can achieve larger noise reduction effect.

Acknowledgement

The present work is supported by the National Natural Science Foundation of China (Grant No. 51776174 and Grant No.51476134), the European Union and China collaborative project in aviation - IMAGE project (Contract No. 688971-IMAGE-H2020MG-2014-1015688971). The authors also gratefully acknowledge the support of the State Key Laboratory of Aerodynamics (Grant No.SKLA20160201), the Key Laboratory of Aerodynamic Noise Control of China Aerodynamics Research and Development Center (Grant No.ANCL20160102).

References

[1]Michel U., "History of acoustic beamforming", *Berlin Beamforming Conference(BeBeC)*, 21-22, Nov. 2006.

[2]Venkatesh S.R., Polak D.R., and Narayanan S., "Beamforming algorithm for distributed source localization and its application to jet noise", *AIAA Journal*, Vol. 41, NO. 7, 2003, pp. 1238-1246.

[3]Lowis C., and Joseph P., "A focused beamformer technique for separating rotor and stator-based broadband sources", *12th AIAA/CEAS Aeroacoustics Conference*, No. 2006-2710, 2006.

[4]Brooks, T. F., Humphreys, W. M., "A deconvolution approach for the mapping of acoustic sources (DAMAS) determined from phased microphone arrays," *Journal of Sound and Vibration*, Vol. 294, 2006, pp. 856-879.

[5]Brooks, T. F., Humphreys, W. M., Plassman, G. E., "DAMAS processing for a phased array study in the NASA Langley jet noise laboratory," *16th AIAA/CEAS Aeroacoustics Conference*, No. 2010-3780, 2010.

[6]Sijtsma, P., "CLEAN based on spatial source coherence," *International journal of aeroacoustics*, Vol, 6, 2007, pp. 357-374.

[7]Graham, R. R., Lt. Cmdr. R. N., "The silent flight of owls," Roy. Aero. Soc. J, 286, pp.837-843.

[8]Lilley, G. M., "A study of the silent flight of the owl," *4th AIAA/CEAS Aeroacoustics Conference Proceedings*, NO. 1998-2340, 1998.

[9]Howe, M. S., "Aerodynamic noise of a serrated trailing edge," Journal of Fluid and Structures, Vol. 5, 1991, pp. 33–45.

[10]Howe M. S., "Noise produced by a sawtooth trailing edge," *J. Acous. Soc. Am.* , Vol. 90, 1991, pp. 482-487.

[11]Jones, L. E., Sandberg, R. D., "Acoustic and hydrodynamic analysis of the flow around an aerofoil with trailing-edge serrations," *Journal of Fluid Mechanics*, Vol. 706, 2012, pp. 295-322.

[12]Lyu, B., Azarpeyvand, M., and Sinayoko, S., "Prediction of noise from serrated trailing edges," *Journal of Fluid Mechanics*, Vol. 793, 2016, pp. 556-588.

[13]Sanderberg, R. D., Jones, L. E., "Direct numerical simulations of low Reynolds number flow over airfoils with trailing-edge serrations," *Journal of Sound and Vibration*, Vol. 330, 2011, pp. 3818-3831.

[14]Chong, T. P., Joseph, P. F., "An experimental study of airfoil instability tonal noise with trailing edge serrations," *Journal of Sound and Vibration*, Vol. 332, 2013, pp. 6335-6358.

[15]Chong, T. P., Vathylakis, A., "On the aeroacoustic and flow structures developed on a flat plate with a serrated sawtooth trailing edge," *Journal of Sound and Vibration*, Vol. 354, 2015, pp. 65-90.

[16]Fish, F. E., and Battle, J. M., "Hydrodynamic Design

of the Humpback Whale Flipper," *Journal of Morphology*, Vol. 225, July 1995, pp. 51-60.

[17]Miklosovic, D. S., Murray, M. M., Howle, L. E., and Fish, F. E., "Leading Edge Tubercles Delay Stall on Humpback Whale Flippers," *Physics of Fluids*, Vol. 16, No. 5, 2004, pp. L39-L42.

[18]Miklosovic, D. S., Murray, M. M., and Howle, L. E., "Experimental Evaluation of Sinusoidal Leading Edges," *Journal of Aircraft*, Vol. 44, No. 4, 2007, pp. 1404–1408.

[19]Johari, H., Henoch, C., Custodio, D., and Levshin, A., "Effects of Leading-Edge Protuberances on Airfoil Performance," *AIAA Journal*,Vol. 45, No. 11, 2007, pp. 2634–2642.

[20]Stanway, M. J., "Hydrodynamic Effects of Leading-Edge Tubercles on Control Surfaces and in Flapping Foil Propulsion," Ph.D. Dissertation, Massachusetts Institute of Technology, Cambridge, MA, 2008.

[21]Hansen, K. L., Kelso, R. M., and Doolan, C. J., "Reduction of Flow Induced Tonal Noise Through Leading Edge Tubercle Modifications," *16th AIAA/CEAS Aeroacoustics Conference*, 2010.

[22]Polacsek, C., Reboul, G., Clair, V., Le Garrec, T., and Deniau, H., "Turbulence-Airfoil Interaction Noise Reduction Using Wavy Leading Edge: An Experimental and Numerical Study," *Internoise*, 2011.

[23]Gruber, M., Joseph, P., Polacsek, C., and Chong, T. P., "Noise Reduction Using Combined Trailing Edge and Leading Edge Serrations in a Tandem Airfoil Experiment," *18th AIAA/CEAS Aeroacoustics Conference*, 2012.

[24]Clair, V., Polacsek, C., Garrec, T. L., Reboul, G., Gruber, M., and Joseph, P., "Experimental and Numerical Investigation of Turbulence-Airfoil Noise Reduction Using Leading Edge Serrations," *18th AIAA/CEAS Aeroacoustics Conference*, 2012.

[25]Clair, V., Polacsek, C., Garrec, T. L., Reboul, G., Gruber, M., and Joseph, P., "Experimental and Numerical Investigation of Turbulence-Airfoil Noise Reduction Using Wavy Edges," *AIAA Journal*, Vol. 51, September 2013, pp. 2695-2713.

[26]Roger, M., Schram, C., and De Santana, L., "Reduction of Airfoil Turbulence-Impingement Noise by Means of Leading-Edge Serrations and/or Porous Materials," *19th AIAA/CEAS Aeroacoustics Conference*, 2013.

[27]Lau, A. S. H., Haeri, S., and Kim, J. W., "The Effect of Wavy Leading Edges on Aerofoil-Gust Interaction Noise," *Journal of Sound and Vibration* , Vol. 25, August 2013, pp. 6234-6253.

[28]Lau, A. S. H., Haeri, S., and Kim, J. W., "The Effect of Wavy Leading Edges on Aerofoil-Gust Interaction Noise," *19th AIAA/CEAS Aeroacoustics Conference*, 2013.

[29]Narayanan, S., Joseph, P., Haeri, S., Kim, J. W., Chaitanya, P., and Polacsek, C. "Noise Reduction Studies from the Leading Edge of Serrated Flat Plates," *20th AIAA/CEAS Aeroacoustics Conference*, 2014.

[30]Haeri, S., Kim, J. W., Narayanan, S., and Joseph, P., "3D Calculations of Aerofoil-Turbulence Interaction Noise and the Effect of Wavy Leading Edges," *20th AIAA/CEAS Aeroacoustics Conference*, 2014.

ISSA-2018-004

FLIGHT TEST OPERATIONS SUSTAINABLE MANAGEMENT

Vieira, Darli R.; Quattrocchi, Paulo
University of Quebec at Trois-Rivières, C.P. 500
Research Chair in Management of Aeronautical Projects
darli.vieira@uqtr.ca; paulo.quattrocchi@uqtr.ca

SUMMARY

This article takes Flight Test Operations as a time consuming, fuel burning, expensive, unwanted, complicated requirement for aircraft that is not a natural sustainable aviation activity and separates "Sustainable Environment" from the "Sustainable Testing" for this specific study. Using current management and engineering tools that individually have its own gains, but if gathered into one sustainable effort, result in a greatly improved test activity, while reducing fossil fuel burn, cost, time and workforce, as expected today for a sustainable flight operation.

Keywords: *Management Tools; Flight Tests; Engineering Tools, Test Readiness, Sustainable*.

SUSTAINABLE FLIGHTS

Sustainability has been used as a tool to push the scientific research and development of any solution that may, in some way, improve energy use, energy storage and energy transformation, towards a perpetual reutilization of goods (Agarwal, 2009).

Most of these recent solutions are not of easy implementation, not even cheaper than the current means, often demand a long period for industrialization (desired maturity) and even longer time for market (customer) trust and acceptance (Mohan Das Gandhi, Selladurai, & Santhi, 2006) .

One of the challenges for future sustainable aviation, is to safely transpose technologies and experimental laboratory solutions to a flightworthy, profit-making transport, for revenue passengers and cargo, within existing certification requirements.

The most important part of the development of new aviation product, after the conception idea itself, is the test and qualification of those technology changes. Tests are needed to prove already available project data, gather complemental complex performance information and prove compliance with safety and market requirements (Ward, 1998).

This article deals with "sustainable solution" and "sustainable environment". Two test operation procedures definitions created to identify the contribution, in different levels to the ecological use and transformation of energy. The first, is the need to test in flight, a whole new, 100% sustainable airborne system. The second, is the activity to provide a sustainable test environment for aviation-based proposals: current product development, qualification and certification under the actual ruling.

SPECIFIC PROBLEM

Aircraft Tests are needed to prove already available project data, gather complemental complex performance information, prove compliance with safety and market requirements, as well as make sure that integration of production and maintenance activities are functional and safe (Stoliker, 2005)

Test Flights figures (flight hours) are different from one operator to other and their aircraft size results in different operation fuel burn quantities (figure #1). It is an operation that takes nothing to nowhere for many times, and it is often blamed for holding the aircraft out of the profit schedule (ICAO, 2003). Therefore, Flight Tests are not revenue flights as they are not natural sustainable activities either.

ICAO Circular 303-AN-176 (ICAO, 2003) also lists the common operational opportunities to minimize fuel use and reduce emissions: a) fly the most fuel-efficient aircraft type for the sector; b) taxi the most fuel-efficient route; c) fly the most fuel-efficient route; d) fly at the most fuel-efficient speed; e) operate at the most economical altitude; f) maximize the aircraft's load factor; g) minimize the empty mass of the aircraft; h) load the minimum fuel to safely complete the flight; i) minimize the number of non-revenue flights; and j) maintain clean and efficient airframes and engines.

These same procedures are not valid for Development and Certification Flights since its mission relies on supporting the safety of the aircraft, and not transporting goods. These procedures are often used to reduce cost in commercial aviation operations, but this initiative is rarely found in the aviation test and certification environment.

A Sustainable Operation, using the OECD's definition (Organization for Economic Cooperation and Development) may be considered when the use of an energy source is somehow renewable (criteria I), the assimilation rates in pollutant-receiving media are not exceeded (criteria III), as when all gains are close to the expenditures (criteria II), or the other way around (criteria IV) (Organisation for Economic Co-operation Development, 2001), (Upham, 2003).

The remnant means to improve combustion fuel sustainability are to reduce fossil fuel use, reduce carbon gases releases and reduce utilization of non-recyclable or non-renewable materials.

When considering aircraft operation, we may list that all test flights have the subjective and intangible purpose of assuring the safety quality of the product, so the aircraft may reach its final objective of

transporting people/goods safely and securely (Pavlock, 2013).

The problem to be solved is to reduce the total amount of flight test hours that are demanded nowadays by any new aircraft related development, certification or verification flight.

These un-revenue flights become an effort to test and certify an improved solution, consequently reducing carbon footprint, high atmosphere damage and indirectly reaching a new level of sustainability in this activity. They are the means that justify a few steps back, to jump into a cleaner solution.

OBJECTIVES

The direct way to reduce tests, are reducing flight related activities, thus reducing the fossil fuel burn. These measures may be done immediately, as all technology is already available, but unfortunately, they are found into several isolated efforts.

Improved Management and Engineering Tools (ET) are used to reduce costs, but results are often a way to bring the project schedule and budget back into the initial values from the start of the project.

The novelty approach is to gather PM tools and ET in a coordinated manner with test requirements, so the initial schedule and budget are at least maintained, secured (guaranteed), while flight hours and operational costs are reduced.

PERIMETER OF STUDY

Aircraft operations may be divided into: Airliners, Cargo, Air Taxi, Private/busyness, Military and Non-revenue. The ICAO Circular 303-AN-176 (ICAO, 2003), classifies non-revenue flights as: training, positioning, ferry, test flights, development (tests) and engine testing. This study is concerned with aircraft operations for Development and Certification Tests. This specific activity is mainly performed by aircraft manufacturers and MROs (maintenance and repair organization).

ICAO has issued other documents ruling carbon emission reduction for aircraft (ICAO, 2010), (ICAO, 2016) , but they still do not address certification flight tests on its “opportunities” to minimize fuel use and reduce emissions, and mentions that non-revenue flights are “minimum”. Optimization of the test activity is commonly done after program management control variables (schedule, cost, manpower, service quality) are affected and lately noticed (Gardiner & Stewart, 2000).

If we consider “Sustainable Testing” as all flight test activities involving some sort of improvement towards energy use, the “Sustainable Environment” is considered all remaining situations and activities that provide any other amount of sustainability than 100%. All improvements will focus the aircraft test activity, since it is the phase responsible for quality assurance during development and not accounted on earlier studies for fuel expenses.

FLIGHT TEST OPERATIONS

Flight Tests are the most common means to demonstrate the aircraft complies with safety, performance and operational requirements. They may be classified into:

- Functional or Production tests; Maintenance tests; Certification / qualification tests.

All flight tests demand a conformal test article, a test proposal (request guide), a routine (checklist) (USAF, 1996), someone responsible for the test (request and data result interpretation), a trained test crew and finally a test result report.

Flight Tests shall not be done with the primary target to “find out” or to “discover new things”, as it should not be a trial & error procedure (Stoliker, 2005). Even though Flight Tests are still considered an experimental activity, i.e. you may not get the result you want, it is an activity that should be done to prove results you already know and expect. It is a demonstration process. All previous known results, that indicate the test will be successful, must be available as planning, decision and compliance support through other engineering means as: numerical simulation, calculations, ground tests, separate system tests (Rigs), laboratory tests, scaled prototype tests, and their risk analysis (Maggio, 1996).

Test requirements (certification or qualification) usually come through government agencies regulations (FAA, ANAC, EASA, MIL specs, ISO, ABNT) (Regulation-FAR25, 2000) (EASA, 2013), customer contract demands and corporate quality policy.

Flight Tests are done by all aircraft operators: Aircraft manufacturers (Boeing, Airbus, Embraer, Bombardier, Gulfstream, Lockheed-Martin, UTC, Pilatus, Leonardo, Mitsubishi, Kawasaki, Sikorsky, Sukhoi, SAAB, Piper…); OEMs (Honeywell, P&W, RR, GE, Rockwell-Collins, Thales); MROs; Airlines; Commuter providers; Military forces and Private aircraft owners.

Each different type of tests lasts a different time. The larger the aircraft, the more expensive is to fly, so every minute running engine(s) must produce the expected demonstration and results. A perfect fitting of this testing time is of greatest importance to the primary schedule and finally to the overall delivery.

The amount of fuel burned in a flight test campaign is directly proportional with the size of the aircraft (MTOW). A certification Test Campaign of a new type averages 2000 flight hours and about 18 months from the first flight, until the type certification issuance from the certification authority (graph #1). Detailed data for the graph was found directly from each manufacturer media publications, as their own website, specialized periodical magazines and press-releases.

The following factors imply on the duration of the flight test campaign: financing, weather/ seasoning,

corporate know-how, specialized manpower, project complexity / systems integration and new technology / product maturity.

The unavailability of funds for a part 25 certification process that may reach 24 months (or more), even though is included in the business plan, can turn the project infeasible if any of the other five implication factors overwhelms its predictions. Several industries in the past 20 years have given up new projects during certification tests, as financing was underestimated to support project complexity or product maturity. Ex.: Fairchild-Dornier, Eclipse, Bombardier, Cessna, Piper.

A new manufacturer, with recent knowledge on the certification and test procedures, or a new step up technology on the market, may have the test and certification period increased up to 5 years and 4000 f/h. Ex.: Honda, Mitsubishi and COMAC.

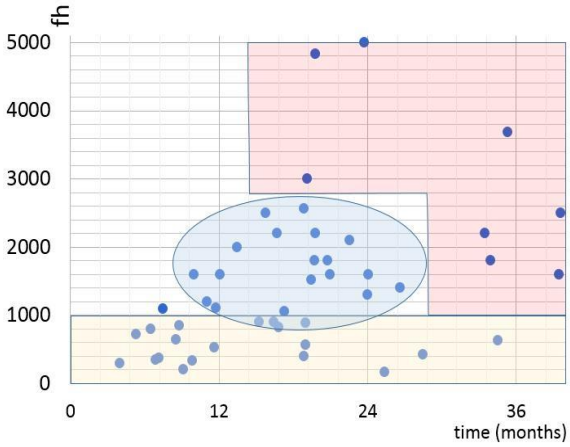

Graph #1 - Dev. & cert.flight test campaigns

The graph #1 plots several development and certification campaigns of new aircraft models, from 6 different aircraft manufacturers. The oval blue area gathers the industry standard flight time and duration time for Flight tests (larger than 1000fh and smaller than 2400fh and lasting less than 25 months). Flight hour values under 1000 (yellow rectangle) represent a partial certification as an STC (supplemental type certificate), that means an aircraft model was developed, based in a previous certified and existing one, thus performing a reduced demonstration.

Most of the values above 2400fh, that lasts more than two years (red polygon), may point out aircraft manufacturers that were not fully prepared for the venue, regarding technology, workforce, or investments at the time of the development and certification demonstration.

FLIGHT TEST MANAGEMENT

Mandatory certification or qualification regulations have become lengthier towards the safety of the users of aircraft, and for the ones who might not even know what's happening overhead: people in the ground.

Reduction on the number of flights are needed, not just because flight testing is expensive, and doesn't seem to add direct value to the product, but because it will be a direct reduction on fossil fuel burning and indirectly reduction over the greenhouse effect by the production of carbon heavy gases (ICAO, 2010).

The flight test operator flies a smaller amount of time, if compared to airline or commuter operators, since the main target is not transport goods, but to complete or fulfill a safety, performance or operational requirement. The useful time of the prototypes correlates directly with the low dependability of new systems, unfinished systems, unconfigured prototypes, unmatched weather conditions, and all variables that determine the "test readiness" and challenge the predictability of the test program.

RESULTS AND DISCUSSION

All solutions must be tested against three criteria: deployability, sustainability and viability. Efficient Solutions are not limited to the production of renewable energy. They encompass products, services, clean technologies and processes that are profitable and sustain economic growth, while protecting the environment and optimizing using natural resources.(Piccard, 2018).

The reduction of the amount of testing aloft, consequently reducing fossil fuel burn into the atmosphere, may be achieved with a more concise, improved test campaign, with less flight hours, challenging the demonstration of requirements by non-flying tests (i.e. analysis, simulations, ground tests, laboratory tests), and a new gathering of current airworthiness requirements,(Kleiner, 2007).

Many of these alternate means to reduce testing, may be achieved through effective Program Management tools tailored to Flight Tests, as a Corporate "Kaisen", Barnes (1996), (Singh & Singh, 2009), 6 Sigma, (Pande, Neuman, & Cavanagh, 2000), Lean Operation (Bergmann & Priebsch, 2011), (Pepper & Spedding, 2010), Supplier Quality and Test Readiness (Sandborn, 2013). Remaining means depend on engineering tools as numerical simulations (Edwards, Lombaerts, & Smaili, 2010), motion simulators, scaled labs (wind tunnel), Rigs and ground tests (Pavlock, 2013).

Project Management (PM) and Engineering Tools (ET), are handled to reduce flight hours (fh), which are a direct improvement on flight tests sustainability. Each flight type has its own possible improvement tool, but the final target is to demand a gathering of all gains (Mrazova, 2014), to benefit tests sustainability process.

System Development Tests may be partially replaced by selected numerical simulations and ground tests (dedicated Rigs and full airplane "iron bird").

System Certification Tests have the flexibility to be done also in a laboratory environment (Rig) and as ground tests (dedicated Rigs and full airplane “iron bird”).

Aircraft Handling development and certification tests may be partially replaced by scaled prototypes, online simulations, motion simulator, and may be scheduled along system tests and system certification, but they are the most difficult to be reduced since the main target, is intrinsically for evaluating the final product control feeling characteristics.

Maintenance Tests and Production Tests improvements are directly proportional with the quality of the service, the existent fault search protocol and parts previously used, instead of the clearance tests for flight.

Recent technologies (Engineering Tools) as GTF engines, eco-fuel blends and reduced approach routes (Şahin & Usanmaz, 2016), are additional features to improve sustainability in test operations, (Mrazova, 2014).

The conclusion procedure that gathers all engineering tools and management tools, to provide an organization and decision-making checkpoint to related aircraft test operations is the “Test Readiness Matrix”. This procedure consists controlling all activities through a “kanban” (Sugimori, Kusunoki, Cho, & Uchikawa, 1977) data bank (test readiness matrix), requiring all preparation steps for each test to be ready (green colored), before next phase schedule for flight. The Lines of the matrix are filled with tasks, milestones and activities. Each column of the matrix is filled with requirements. The “test matrix” lines are prompt to be scheduled on its different time frame calendars: long, medium and short-term schedules, to produce a reduced scope test campaign. This reduces possibility of premature planning over non-complete tasks, thus reducing ineffective flights.

The elaboration of the “Test Readiness Matrix” demands involvement of all areas of product development (management, engineering, test and manufacture) or service areas (management, maintenance, contracts, test and operation).

When running a “test readiness matrix” / checklist, tasks and milestones may be considered for possible execution only if all preparation requirements were previously performed. It may seem a very common and natural organizational process, but if looking at medium to complex project management as aircraft test development and operation during these tests, missing one preparation activity, task or milestone, will result in a no-go (no-flight) situation. The very costly and complex aircraft operations schedule suffers heavily due to schedule foul-outs.

Three aircraft successful manufacturers of high importance and market position were considered (NDA apply), to summarize the possible flight hours (fh) reduction, regarding the cumulated use of tools. Their improvements and leading procedures were listed, compared and plotted.

Table #1

Flight Test Type	Alternate means / tools	Possible fh reduction
System dev.	Rig; numerical sim.; improved supplier quality	25%
Handling dev.	Scaled lab; Online sim.; parallel with system test	25%
System cert.	Lab.; Rig; Reports; Engineer Sim	25%
Handling cert.	Motion Sim.	20%
Maintenance	Ground tests; Test bench; Maturity	10-15%
Production	Assembly quality assurance	50%
All flight tests	Non-fossil fuel blend burn	20%
All flight tests	Low emission / + efficient powerplant	10-20%
All flight tests	Reduced Approach route	5-10%
All flight tests	Test Readiness* (Kanban, Agile, Kaisen)	20%

The table #1 lists possible flight hour % reduction for different project management, engineering novelties and Flight Test Type, as result of the data compilation from the previous mentioned matrix.

CONCLUSION

The key contribution is found after comparing (benchmark) flight test campaigns from many players and conclude that the most productive ones combine management tools and engineering tools, for scheduling, reprogramming and changing means of compliance with regulations. A considerable amount of flights will be eliminated, keeping the same level of product safety and overall operation quality.

The Test Readiness Matrix contribution, which may be detailed also, is used as a corporate management tool to release test flights, so the final certification activity is reduced at the demonstration level, bringing fuel expenses, manpower and resources to an optimum record.

A further incremental study, including implementation details for each tool used, is advised, since improvements and experience with flight test operations may come out often. There should be also detailed statistical and benchmark results from more aircraft manufacturers, especially from China, Japan, Ukraine and Russia.

REFERENCES

Agarwal, R. K. (2009). Sustainable (green) aviation: challenges and opportunities. *SAE International Journal of Aerospace, 2*(2009-01-3085), 1-20.

Barnes, T. (1996). *Kaizen strategies for successful leadership : how to take your organization into the future*. London,: Pitman.

Bergmann, S., & Priebsch, S. (2011). *Real-world solutions for developing high-quality PHP frameworks and applications*. Indianapolis, Ind.: Wiley Pub.

EASA, C. S. (2013). *Acceptable means of compliance for large aeroplanes cs-25*. Retrieved from

Edwards, C., Lombaerts, T., & Smaili, H. (2010). Fault tolerant flight control. *Lecture Notes in Control and Information Sciences, 399*, 1-560.

Gardiner, P. D., & Stewart, K. (2000). Revisiting the golden triangle of cost, time and quality: the role of NPV in project control, success and failure. *International Journal of Project Management, 18*(4), 251-256. doi:10.1016/S0263-7863(99)00022-8

ICAO. (2003). *Operational Opportunities to Minimize Fuel Use and Reduce Emissions, Circular 303-AN/176* (Vol. 303-AN/176). ICAO, Montreal: ICAO.

ICAO. (2010). *ICAO Environmental Report 2010: Aviation Outlook*. Retrieved from Montréal, Québec, Canada:

ICAO. (2016). *On Board a Suatainable Future - ICAO Environmental Report 2016 - Aviation and Climate Change*. Retrieved from Montreal, QC, Canada:

Kleiner, K. (2007). Civil aviation faces green challenge. *Nature, Vol.448(7150),*, p.120.

Maggio, G. (1996). *Space shuttle probabilistic risk assessment: methodology and application.* Paper presented at the Reliability and Maintainability Symposium, 1996 Proceedings. International Symposium on Product Quality and Integrity., Annual.

Mohan Das Gandhi, N., Selladurai, V., & Santhi, P. (2006). Unsustainable development to sustainable development: a conceptual model. *Management of environmental quality: an international journal, 17*(6), 654-672.

Mrazova, M. (2014). Sustainable development - the key for green aviation. *INCAS Bulletin,, Vol.6(1),*, 109-122.

Organisation for Economic Co-operation Development, O. (2001). *OECD Environmental Strategy for the First Decade of the 21st Century: Adopted by OECD Environmental Ministers*. Retrieved from Paris: http://www.oecd.org/env/indicators-modelling-outlooks/1863539.pdf

Pande, P. S., Neuman, R. P., & Cavanagh, R. R. (2000). *The six sigma way: How GE, Motorola, and other top companies are honing their performance*: McGraw-Hill (New York).

Pavlock, K. M. (2013, Sep 19, 2013). *Aerospace Engineering Handbook Chapter 2 - Flight Test Engineering*. (20140010192). Purdue University, NASA Dryden Flight Research Center, Edwards, CA United States.

Pepper, M. P., & Spedding, T. A. (2010). The evolution of lean Six Sigma. *International Journal of Quality & Reliability Management, 27*(2), 138-155.

Piccard, B. (2018). Solar Impulse Foundation World Alliance Solutions. Retrieved from https://solarimpulse.com/world-alliance/solutions

Regulation-FAR25, F. A. (2000). *Title 14 CFR Part 25 including Amendment 25-101*.

Şahin, Ö., & Usanmaz, Ö. (2016). Arrival Traffic Sequence for Converging Runways. In T.H. Karakoc et al. (eds.) (Ed.), *Sustainable Aviation* (pp. 291-296): Springer International Publishing.

Sandborn, P. (2013). *Cost analysis of electronic systems*. Singapore: World Scientific.

Singh, J., & Singh, H. (2009). Kaizen philosophy: a review of literature. *IUP Journal of Operations Management, 8*(2), 51.

Stoliker, F. N. (2005). *RTO AGARDograph 300 - Introduction to Flight Test Engineering (Introduction aux techniques des essais en vol)*. Retrieved from The Flight Test Technical Team (FT3) of the Systems Concepts and Integration Panel (SCI) of the RTO.: www.rta.nato.int

Sugimori, Y., Kusunoki, K., Cho, F., & Uchikawa, S. (1977). Toyota production system and kanban system materialization of just-in-time and respect-for-human system. *The International Journal of Production Research, 15*(6), 553-564.

Upham, P. (2003). *Towards sustainable aviation*. Sterling, VA: Earthscan Publications.

USAF, U. S. A. F. (1996). Acceptance and Functional Check Flight Procedures and Checklist, MIL-PRF-5096F. In *Inspection and Maintenance Requirements;* (Vol. MIL-PRF-5096-F, pp. 84): United States Air Force USAF.

Ward, D. T. S., Thomas W. (1998). *Introduction to Flight Test Engineering* (2nd ed.): Kendall / Hunt Publishing Co., Dubuque, Iowa.

ISSA-2018-005

SYNTHETIC SOLUTIONS FOR TRAINING TASKS TO BE PERFORMED IN THE SHY-147 RECOGNIZED SCHOOLS IN AIRCRAFT MAINTENANCE FIELD

Can URASLI
Marmara University
4722, Kadıköy / İSTANBUL
canurasli@hotmail.com

Emre AKAR
AREL University
34295, K.çekmece / İST.
emreakar@arel.edu.tr

H.Burak AVCI
Marmara University
34722, Kadıköy / İST.
huseyinburakavci@gmail.com

Hayriye KORKMAZ
Marmara University
34722, Kadıköy / İST.
hkorkmaz@marmara.edu.tr

SUMMARY

In this study, a training device which let to perform nine mandatory tasks for "Basic experience" as explained in EASA (or equiv alent regulation of national aviation authority) Part 66. A . 30 is developed. This device is also compatible with synthetic traini ng device specifications of Part 147. A . 115. Feedback was received from 17 specialists from the related field about designed training device. According to these notifications, it was stated that the training device is sufficient to implement recognised scho ol tasks . Here, tasks means actually learning outcomes . In addition, it was observed that this device helped the students for increasing their ability to identfy error cases succesfully .

Keywords: Airworthiness, Synthetic Training Device, Cabin Pressurization.

INTRODUCTION

Accreditation in aviation is essential for continuous airworthiness. Very few of the education institutions in the field of aircraft maintenance technician or aircraft technology have been accredited by the competent authority of the Directorate General of Civil Aviation in Turkey. One of the regulations for becoming a school recognized by the General Directorate of Civil Aviation (SHGM) is that the educational institution possesses the necessary aircraft equipment to carry out the tasks of the Civil Aviation Directive-147 Recognized Schools "Expected Transactions from Staff Members". Depending on the qualification of the tasks, real aircraft parts, whole aircrafts or synthetic training devices can be used as aircraft equipment (SHGM, 2012).

Current synthetic training tools can not satisfy the requirements of modern passenger aircraft systems. Existing devices that were using analogue indicators takes old airplanes as model. On the other hand, when the literature was reviewed, it is understood that there is no graduate thesis or articles focusing on the same objective. Thus, in this study a novel "Cabin Pressurization Training device" in order to complete 9 out of 200 recognized school tasks was developed to overcome the deficiencies mentioned above (SHGM, 2012).

Passenger carrying aircraft are more efficient and economic when operated at high altitudes. In addition, bad weather and turbulence can be avoided by flying at higher altitudes in relatively smooth air. However, while cruising at high altitudes may be suitable for an aircraft and its power units, as essential requirement to be met is the isolation of the aircrafts occupants from the reduced atmospheric pressure encountered at altitude. The limits of the structural strength of the aircraft are also taken into account when providing suitable atmospheric conditions for the passengers. The suitable atmospheric conditions in the aircraft cabin are provided by the cabin pressurization system.

Figure 1 shows a typical cabin pressurization system component. Accordingly, the air from the pressure source is pressurized in a flow control valve and pressed into the cabinet. Excess pressure is discharged to the atmosphere by the outflow valve to keep the cabin pressure at the desired cabin pressure values.

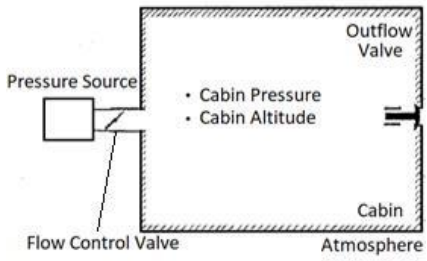

Fig.1. Typical Cabin Pressurization System

The organization of this paper is as follows: In Methodology section, first, minimum requirements for an aircraft cabin pressurizating system was given. Then, the components of the developed training device was introduced. In results and discussion section, inspection reports of the competent authority was given in five sub-titles. In addition, it was stated that besides the tasks examined, three additional tasks can also be conducted by using this training device. Applications in the lab sessions and feedback from the students were also evaluated in this section. In the last section, it has been emphasized that this training device is a useful educational material depending on the positive reviews.

METHODOLOGY

Passenger aircrafts must provide airworthiness conditions as specified by the competent authority. This study is based on EASA CS-25 (European Aviation Safety Agency Certification Specifications Large Aeroplanes) requirements. The following are the basic requirements for cabin pressurization:

The maximum allowed cabin altitude varies for aircraft types having different certifications. For the

aircraft types focused in this study, pressurized cabins and compartments must be equipped to provide a cabin pressure altitude of not more than 8000 feet (ft) under normal operating conditions

A pressurized aircraft cabin must include at least the following valves, controls, and indicators to control cabin pressure:

- Two positive safety relief valves to limit the differential positive pressure automatically. This is defined as the pressure value which is delivered from the pressure source at the maximum flow rate. The capacity of safety relief valves must be large enough, for the failure of any valve to not cause an acceptable rise in the pressure differential. The differential pressure is positive when the cabin pressure is higher than atmosphere pressure.
- Two negative safety relief valves to limit the differential negative pressure automatically. The differential pressure is negative when the cabin pressure is lower than atmosphere pressure. One valve is enough, but, two valves are used. so that in a failure case it keeps the system work. So the differential pressure can be rapidly equalized.
- Intake and exhaust airflow valves to control cabin internal pressure required. They can be controlled by automatically or manually.
- Indicators in the cockpit to show the differential pressure, the cabin pressure altitude, the rate of change of the cabin pressure altitude and aircraft altitude.
- Warning indicators in the cockpit to indicate cases when the safe or pre-set differential pressure and cabin pressure altitude exceed limits.
- Audible and visual warning systems that alert the cockpit crew when the cabin altitude exceeds 10,000 feet.
- A placard to inform the cockpit crew about the maximum permissible differential pressure for the aircraft structure.

Figure 2 shows the developed cabin pressurization training device. This training device includes the following equipment as seen in Figure 2(a): two sealed cabins one for simulating the atmosphere and the other for simulating passenger cabin; a compressor; a vacuum generator; pressure sensors and analogue displays; flow control, outflow and safety valves; Boeing 737 (B737) passenger service unit and a controller interface. The control interface consists of a controller, a user panel, warning indicators and digital displays. The user interface is designed so that it will seem similar to Airbus 320 planes.

Aircraft engine, APU (Auxiliary Power Unit) or ground cart is all used as an air source in aircraft cabin pressurization systems. Instead of those kind of air sources, a compressor was used to represent them in this training device. When the bleed switch is turned on, the compressor activates and air is pumped into the cabin. In the atmosphere cabin, vacuum is provided by a vacuum generator to raise the aircraft altitude. Students can monitor the pressures in each cabin with analog gauges. The pressure data is transmitted to the controller through two sensors of different input ranges. One of them has an input range of 0-1 mbar for aircraft cabin while the other one, for atmosphere, 0-0.1 mbar. Both of them has the same output range of 4-20 mA. By using this data, the pressure for each cabin, the altitude values corresponding to these pressures and differential pressure values are calculated and controlled.

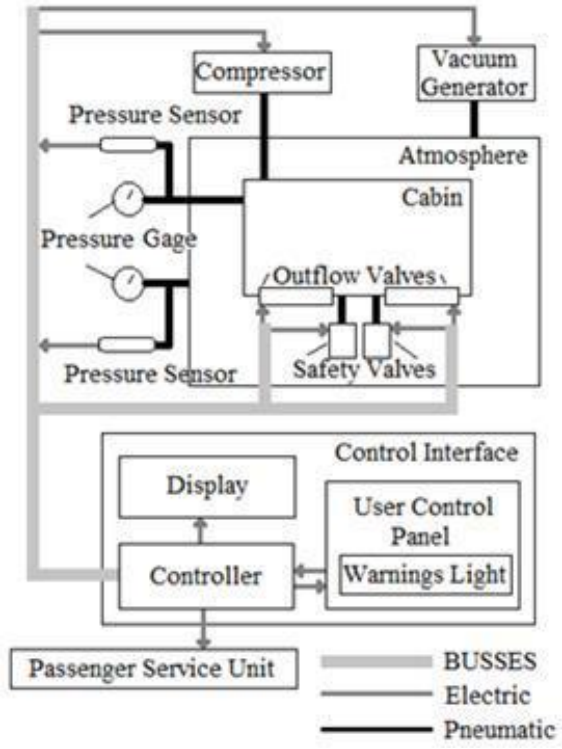

(a)

(b)

Fig.2. Cabin Pressurization Training Device a) Block scheme b) General front view

If there is no error in the system under normal conditions, the cabin altitude increases in direct proportion with the altitude of the aircraft. When the aircraft altitude is 40,000 feet, the cabin altitude reaches 8000 feet. The cabin altitude is fixed at 8000 feet which is the limit of passengers. Increasing the altitude beyond this value can cause serious health problems. This value is monitored on the cabin pressurization system page of ECAM (Electronic Centralized Aircraft Monitor). Cabin pressure, atmospheric pressure, differential pressure, warning flags and other system parameters can also be monitored from the system page.

The amount of air released into the cabin is kept constant. The regular increase of the cabin altitude is provided by two outflow valves located inside the cabin. If the differential pressure exceeds the certain value, a safety relief valve opens to protect the cabin and the pressure is thrown into the atmosphere cabin.

For example, if outflow valves remain open, the cabin altitude may exceed the upper limit of 8000 feet. In this case, the user control panel and PSU warning indicators will light up at different altitudes. According to this, when the cabin altitude reaches 10000 feet, the “Cabin Altitude” indicator lights up and “Master Caution” is activated at the same time. Passenger warning indicator lights up at 11,500 feet. PSU oxygen caps fall at 14000 feet. At 15000 feet, the outflow valves are automatically switched off regardless of pilot intervention.

Arduino Mega was used as the controller of the whole device and programmed in the arduino version 1.8.5 platform. In the development of the control interface, the process steps specified in the relevant aircraft AMMs (Aircraft Maintenance Manuel) of the previously recognized school tasks have been taken into consideration. For these operation steps, the user control panel has been designed by using required switches, warning indicators and system parameters.

On the user control panel, system control switches are grouped in nine sections based on the panel layouts of Airbus aircraft as follows: main supply, master caution, cabin altitude light, air condition, cabin pressurization, air source start, auto flight, circuit breakers and emergency sections.

Another part of the control interface is the 7 inch Nextion LCD display. In the display software, background and screen sembols were created as images. Afterwards, the image file of the images to be displayed on the screen is called up by serial communication with the controller.

General front view of the training device is seen in Figure 2 (b). As seen from the figure, a real B737 aircraft passenger service unit was used and all its functions can be actively used.

RESULTS AND DISCUSSION

A presentation video showing the steps of the SHY-147 Recognized School "Cabin Pressurization Functional Test” and “Control of Emergency Equipment" tasks was recorded (Youtube,2018). This video and training device has been inspected by ten Aircraft Maintenance Area teachers from the Ministry of Education and seven B1.1 Mechanical technicians from THY Technic. The comments of the reviewers were summarized below.

The requirements for the tasks to be carried out in the Cabin Pressure Training Device have been examined. Acceptance of recognized school tasks with passenger service units in the inspections of SHGM proves that these can be fulfilled by using the training device. Pressurization tests, connection of external air source, control of pneumatic systems, lamp and filament replacement tasks can be fulfilled by using this training device. This was also aproved by above mentioned reviewers or authorities.

The videos of the tasks performed in the cabin pressurization training device were presented to THY Technic Project Engineering, Shift Chief and Education Presidency. After presentation, some technical reviews were recorded.

Pressure and vacuum can be created in the cabins used for atmosphere and aircraft cabin. The pressure in these cabins can be monitored instantaneously. The control panel display have the necessary controls for the following tasks. And also LCD display have necessary flags and physical quantities. When the training device is operating, it was observed that corresponding warnings were given for all error cases. In this reviews, the training device is considered to be a useful simulation compatible with the Airbus 320-330 aircraft types. The compatibility of the tasks requested to be reviewed is as follows:

- **Performing pressurization functional tests:**
  The training device includes all the equipment necessary to complete the task on the aircraft. Unlike on the aircraft, auto pilot and air / ground proximity switches were used to increase the cabin altitude. In the implementation of the task, the movement of the outflow and safety valves with the varying altitude, the controls entered from the control panel and the responses of the system, the indicators and the warnings on the control panel have been examined. As a result, it has been pointed out that this task conformed to A320 aircraft.
- **Functional testing of emergency equipment:**
  PSU was used as an emergency equipment in the training device. Performing controls of oxygen caps, oxygen masks, and oxygen generators is suitable for task definition.

- **Replacement of lamp and filament:** The passenger service unit's caution indicators are suitable for replacing the lamp and the filament.
- **Control of pneumatic systems:** There is necessary equipment for the leak test; compressed air source, closed system pipes and indicators.
- **External air sources, connection and use:** GC (ground cart) bleed, power switches and ports for GC connections are available on the system. But GC connection ports do not resemble to the aircraft's. Even if the procedure was the same, it must be supported by real visuals of the ports on the aircrafts.

It was stated that besides the tasks examined above, the following tasks can also be conducted by using this training device by preparing additional task steps:

- Implementation of ESD (electrostatic discharge) procedures,
- Typical maintenance practices in the Electronic Display System,
- Continuity check of cables in a system

With the approval of the above authorities, Bağcılar Vocational and Technical Anatolian High School Aircraft Maintenance Area Students were let to practice on this device.

In normal operation, in the first step, the students complete all the tasks given in the procedures until the end. After that, students restart to perform the same procedures. Unlike the first step, random errors are given to the system by instructor. If the error case can be detected by the student, this task is assumed as successfully completed. If the first step skipped, it was noticed that the students can't detect the error in most cases.

The cabin pressurization functional test has been performed to 60 students who have already learned theoretical knowledge in this regard. The graph of "Success rates of learning with error function" is given in Figure 3.

Three different homogenous groups were tried to form depending on the grades of the students. All grades were ranked from highest to low. First student was picked up to the Group 1, the second student was to the Group 2 and third student was to the Group 3. After that, the fourth one was again picked up to the Group 1 and so on. Each group consists of 20 students with balanced-distributed average grade.

The students in the first group were not let to perform the first step. These students were directed to second step. The operation steps were started with an error case. Only four of students detected the error case correctly. On the other hand, the students in the second group were let to perform the first step. And then, they let to perform process step with random error case. In this case, 12 students could able to identify the error case correctly. In the final case, for the third group's students, an extra step was added between first and second step. Students were allowed to freely practice on the training device before the error detection phase was started. Then they were asked to repeat the functional test with random errors in the system. In this case 19 students out of 20 could able to identify the error case correctly in the system. According to this result, students in the third group has better understanding about the system than the others. With error cases, it became possible to detect permanent learning. Practicing on the system has increased students' ability to detect and identify error cases.

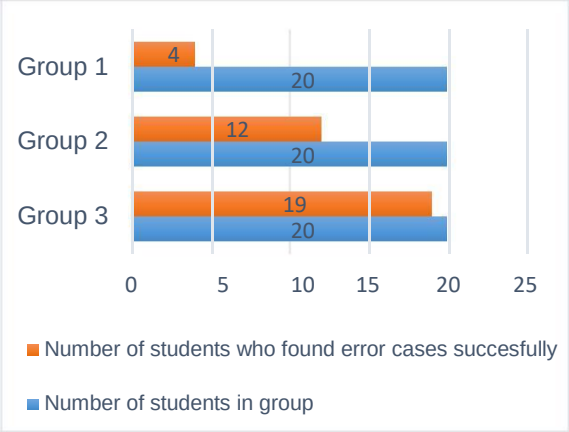

Fig.3. Success Rates of Learning with Error Function

CONCLUSIONS

Training device was presented some of the B1.1 Licensed Mechanic Technicians of Part 147 Maintenance Center, and also to the teachers of the high schools in Istanbul which are already recognized by the competent authority and then asked them to criticize. Depending on the comments, it has been confirmed that the training device is a similitude of modern passenger aircraft systems.

ACKNOWLEDGEMENT

We would like to thank to ADF Engineering for their constructive criticism during the development of the Cabin Pressurization Training device. In addition, we also would like to thank to THY Technic specialists and MEB instructors for their evaluations about the training device in pedagogical manner.

REFERENCES

A320 Aircraft Maintenance Manuel Chapter 21,25,36, Jan 01, 2017

B737 Aircraft Maintenance Manuel Chapter 25 Jan 01, 2017

EASA, Certification Specifications for Large Aeroplanes CS-25, 2010

SHGM, SHY-147 Hava Aracı Bakım Eğitimi Kuruluşları Yönetmeliği, 2012

Youtube, https://www.youtube.com/watch?v=UBTUkIxaAro , 2018

SPRING LOCATING AND TEMPERATURE MONITORING USING UAV: AZMAK SPRINGS, MUGLA, TURKEY

Bedri KURTULUS[1], Cagdas SAGIR[1], Gunseli ERDEM[1], Dilek Funda KURTULUS[2], Ozgur AVSAR[1], Mustafa Can CANOGLU[3], Moumtaz RAZACK[4]
[1]Mugla Sitki Kocman University, Department of Geological Engineering, Mugla, Turkey
[2]Middle East Technical University, Aerospace Engineering Department, Ankara, Turkey
[3]Sinop University, Department of Environmental Engineering, Sinop, Turkey
[4]University of Poitiers, IC2MP Laboratory, Poitiers, France
Authors' e-mails: bkurtulus@mu.edu.tr, cagdassagir@gmail.com, gunselierdem@gmail.com, funda.kurtulus@gmail.com, ozgur.avsar@gmail.com, mccanoglu@sinop.edu.tr, moumtaz.razack@univ-poitiers.fr

SUMMARY

Today, drones are getting more common in every part of human life. Their potential in usage for scientific purposes is encouraging scientists . The data environmental sci entists need are often gathered at the field. Colossal study area may cause trouble by means of time and effort . With intent to speed up and facilitate the field work, drones get into use. In the present study, a thermal camera mounted drone was used with the objective to determine the locations and measure water temperature of a spring grou p that creates a 2 km long river. 3 flights at different altitudes and dates were made. Flights at lower altitudes perfectly revealed the spring locations but had a higher chance to end up with blurred images . However, the measurement accuracy of the thermal camera is n't enough for a study which needs high precision .

Keywords: UAV, temperature, Azmak Spring.

INTRODUCTION

Data collection has an important place in environmental sciences. During the last 5 years, unmanned aerial vehicles (UAVs) has become alluring for rapid collection of high-resolution RGB and thermal images. With the help of UAVs, which are the popular cool gadgets of the innovative technology, researchers can easily access to remote places in order to collect data they need (Marris, 2013; Tang and Shao, 2015; Colomnia and Molina, 2014; McCabe et al., 2017).

Collecting data in environmental sciences becomes complex with the enlargement of the study area. Regarding the work carried out, the data type to be measured and where the measurements should be made are the question marks. In this study, temperature measurements at the springs should be taken. Two questions arise in this context; where are the springs and what are the temperatures of the water that drains from them? It is a time consuming and physically challenging task to determine the locations of about 50 springs along a 2-kilometer river by conventional methods. Hence, it can be tried to use UAVs to gain time and work more efficiently.

The study area is situated in Akyaka district Ula, Muğla (SW Turkey) (Fig. 1). There are numerous springs create a 2 km long river. The springs are the outputs of a large karst system in the area which covers approximately 524 km^2. The present study focuses to determine the practicality of UAVs to locate the springs and measure the water temperature.

METHODOLOGY

A thermal camera mounted drone was used to make flights over the Azmak Springs. *FLIR Vue Pro R 336* radiometric thermal camera was attached to *DJI Phantom 3 Advanced* drone (Fig. 2). *DJI Go* and *PIX4Dcapture* smartphone applications were used to control and fly the drone.

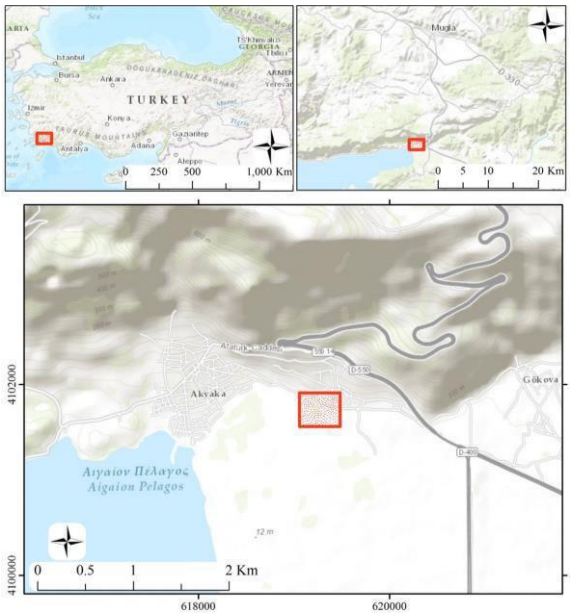

Fig.1. Location map of the study area.

PIX4Dcapture was used to make auto flights on previously determined grids. RGB photos taken by drone's default camera were processed via *PIX4Dmapper* PC software. With the help of this software orthorectified photo and 3D digital surface model of the study area may be created.

The image resolution of the thermal camera is 336x256. It has 13 mm lens with 7.5-13.5 µm spectral band. Its measurement accuracies are +/- 5°C at -25°C to 135°C range and +/-20°C at -40°C to 550°C range. The thermal camera was connected to a smartphone via *Bluetooth* to do the

settings before each flight. For this purpose, *FLIR* provides a smartphone application called *FLIR UAS.* The application lets you record thermal video and take thermal photos. The user could take single or multiple images by setting an interval value. In this study, multiple images with an interval of 2 seconds were used. The user is also allowed to configure radiometry settings. Firstly, the user could choose Celsius or Fahrenheit as temperature unit. Then, studied subject temperature range can be adjusted as -25°C/+135°C or -40°C/+550°C. Subject distance can be set from 0 to 200 m. Sky condition may be selected between the options clear, scattered and cloudy. Humidity and emissivity can be entered as a percentage. Lastly, air temperature can be set. The application also lets the user decide the photo format as 8-bit JPEG, radiometric JPEG or TIFF. In this study, Celsius unit, radiometric JPEG format and -25°C/+135°C subject temperature were chosen. Spring water temperature in the study area is generally between 14-18°C. Drone flights were done at 60, 100 and 150 m of altitude. Varied altitudes were tested to notice the differences. The subject distance was set according to the altitude. Humidity and air temperature were regularly checked and entered before each flight. The subject was water in this study, so 90-95% emissivity value was set. Air temperature and subject distance settings were not very stable due to the software. Occasionally, the entered values were changed to another value. The user must be aware of this inconsistency. Collected thermal images were organized and edited on a PC by using *FLIR Tools+* software. This software allows the user to change the color palette of the image, export it in another format and create a report. Thermal images were checked manually to spot the spring locations. In order to clearly distinguish the temperature anomalies of the springs, the color palettes of the images were edited. Maximum values for images were changed to a lower degree than measured. By doing so, spring locations were made more visible.

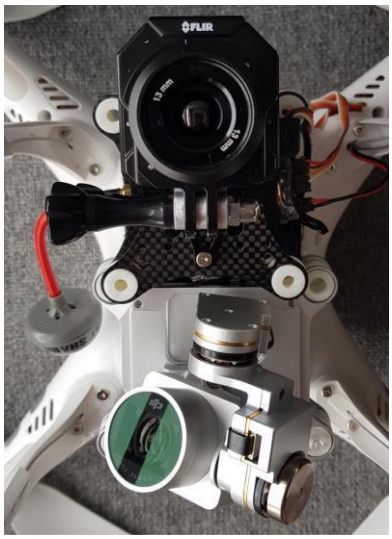

Fig.2. Thermal and RGB cameras at the bottom of the drone.

RESULTS AND DISCUSSION

An orthorectified image of the whole study area was created from the images taken by the RGB camera of the drone (Fig. 3). This high-resolution photo of the area can be used as a base map or a visual material. Its resolution was quite high and it provided higher detail than the satellite images free of charge. The pixel dimension was about 3 cm regarding the 100 m of flight altitude.

Fig.3. Orthorectified image of the study area.

From the images taken by flights made in February 2018 at 100 m of altitude, the locations of the springs were determined quickly and easily. In Fig. 4, dark blue areas were classified as water springs which cannot be seen by the bare eye. However, when flights were made at higher altitudes, the springs couldn't be detected.

Besides locating the springs, temperature measurements of the water were also needed. The temperature measurements were consistent with each other. With the aim of assessing the temporal effects on the thermal camera measurements, two flights were made at the same location on the dates of 30/08/2017 and 28/06/2018 (Fig. 5). First flight's altitude was 60 m while it was 150 m at the second. The measurements yielded coherent results.

Still, it was noticed that there were measurement differences. It can be seen in Fig. 4 that the minimum temperature was 16.89°C on a photo while it was 19.09°C in the other image. At this point, it must be kept in mind that the measurement accuracy of the thermal camera was +/-5°C.

Nevertheless, taking thermal photos while flying poses a problem. Some of the images were blurred because of the motion of the drone. In autopilot mode on a grid, the drone doesn't stop to take photos. This problem may be overcome by

hovering the drone at a certain altitude. Surely, the drone can be controlled manually to take a photo by hovering. But in this case, the drone will drain more battery. Flying at higher altitudes may also solve this problem. The thermal images at 150 m altitude were considerably less blurred.

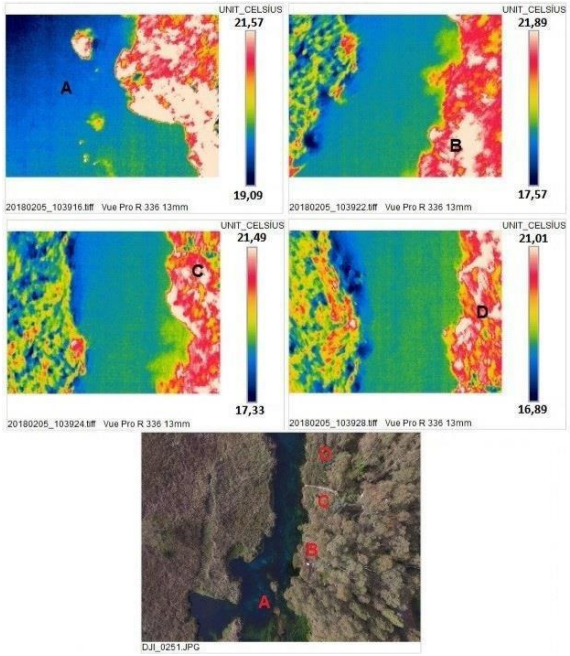

Fig.4. Detected spring locations by thermal UAV on 05/02/2018.

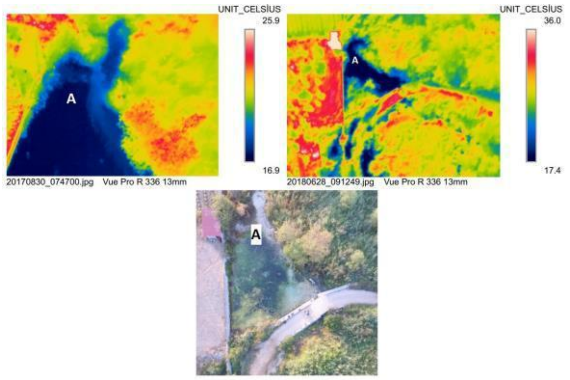

Fig.5. Thermal images of the same location at 60 and 150 m of altitude, on 30/08/2017 and 28/06/2018, respectively.

CONCLUSIONS

In the context of the present study, it has shown that a drone mounted with a thermal camera is quite effective in terms of both time and effort to locate the springs and measure the temperatures of them. Yet, the measurement accuracy of the thermal camera may not let a study that needs the high accuracy of data.

ACKNOWLEDGMENT

This study is a part of an ERANETMED project titled as GRECPIMA (Groundwater Resilience to Climate Change and High Pressure within an IWRM Approach) and funded by TUBITAK, No: 115Y843.

NOMENCLATURE

UAV unmanned aerial vehicle
RGB red-blue-green
SW southwest
PC personal computer
3D 3-dimensional
UAS unmanned aerial system
JPEG joint photographic experts group
TIFF tagged image file format

REFERENCES

Colomina, I. and Molina, P., 2014, Unmanned aerial systems for photogrammetry and remote sensing: A review. *ISPRS Journal of Photogrammetry and Remote Sensing* 92: 79-97.

Marris, E., 2013, Fly, and bring me data. *Nature* 498: 156-158.

McCabe, M. F., Rodell, M., Alsdorf, D. E., Miralles, D. G., Uijlenhoet, R., Wagner, W. et al., 2017, The future of earth observation in hydrology. *Hydrology and Earth System Sciences* 21: 3879-3914.

Tang, L. and Shao, G., 2015, Drone remote sensing for forestry research and practices. *Journal of Forestry Research* 26: 791-797.

SUSTAINABLE SOFTWARE DEVELOPMENT IN THE AIRCRAFT INDUSTRY: AN AGILE PERSPECTIVE

Veira, Darli R.;Silva, M. A.
University of Quebec at Trois-Rivières, C.P. 500
Research Chair in Management of Aeronautical Projects
darli.vieira@uqtr.ca; marcelo.amaral.da.silva@uqtr.ca

SUMMARY

Agile methods have been proven to help the software companies in saving time and money and promoting sustainable development . Despite all the Agile methods principles and good practices in use, making sustainable software projects is not straightfo rward. In particular, applying Agile methods for Aircraft Software Industry has been a challenge as these methods welcome changing requirements, even late in development while the Aircraft development usually demands no late requirement changes . Based on extant literature review the paper integrates Software Sustainability Attributes and Agile Manifesto principles in order to suggest possible solution to this conundrum. A check -list based on the Agile principles is offered to be run during the sprint review ceremony, as a better way of keeping the design the more sustainable as pos sibl e during any development sprint .

Keywords: ISSA, Software development, reuse, sustainability, software testing, automated testing.

Agile Methods have been in use in software companies since 1986 when the word Scrum (Schwaber et al., 2016) was used for the first time in a Harvard Business Review magazine (Takeuchi et al., 1986). Since then, a lot of Agile Methods have been produced until 2001 when a group of seasoned developers have gathered principles underlying these methods, giving birth to the "Agile Manifesto". The manifesto comprised of twelve principles, one of them claiming: "Agile processes promote sustainable development. The sponsors, developers, and users should be able to maintain a constant pace indefinitely." (Beck et al., 2001). Agile methods have been proven to help the company in saving time and money (Baseer et al., 2015).

It is still no clear how to implement sustainability by using Agile methods in software projects, although the Agile Manifesto clearly states that these processes promote sustainability (Beck et al., 2001).

It has been proposed a set of metrics to assess the sustainability of the software projects in more practical ways. (Albertao, 2004).

Agile methods have been preferably used in the software development, in place of traditional methods (waterfall) because it produces results to be delivered to the interested parts in a smaller time frame. Those results can be then reviewed and then the next deliverables can have a better course of action. The cost of changes can be then smaller compared to those of the traditional methods.

SPECIFIC PROBLEM

It is still no clear how to implement sustainability by using Agile methods in software projects, although the Agile Manifesto clearly states that these processes promote sustainability (Beck et al., 2001).

It has been proposed a set of metrics to assess the sustainability of the software projects in more practical ways. (Albertao, 2004).

Agile methods are already present in the Aircraft Production (Presley et al., 1998), and has been a hit in the Software Industry.

Applying Agile methods for Aircraft Software Industry has been a challenge as these methods welcome software requirements changes, even late in development (Beck et al., 2001), but the Aircraft Development usually demands no late software requirements changes.

Scrum methods can still be used in the Aircraft Software Industry leading to higher quality software, and the way to make it sustainable has still to be defined.

The main focus of this study is how we can use a sustainable way of developing software for the aircraft industry, by using the Agile methods. In other words, we can use Agile methods to increase the software development performance in a sustainable approach.

The purpose of this work is to propose a solution to make sustainable software for aircraft by defining a technique to be used in the context of the Scrum framework.

OBJECTIVES

A series of Software Sustainability Attributes have been defined in order to evaluate the sustainability performance of a given software system (Albertao, 2004).

These attributes such as modifiability, reusability, portability, performance, dependability, usability among others, can be used with the Agile Manifesto principles to build a list of aspects to be watched during the software development sprint to build a more sustainable software.

This paper discusses in practical means how this list can be used in the form of a checklist.

The Agile methods are the way of developing software most used lately. This approach of software development is iterative, adaptive, well planned and organized, gives control of improvement, gives early and frequent delivery. It has self organized teams, and this gives the team the responsibility of well using its resources. Everyone in the team knows his responsibilities and they work together not letting any idle resource, so the performance is optimized.

Sustainable Development is a good practice to be used as it is chosen because we need to develop by using the less effort possible. We want to be able to cut costs by using the less energy possible to develop software, and the result is a better development performance.

As there is no study on how we can use the Agile Manifesto to use sustainability to develop software, this work presents how we can do this.

PERIMETER OF STUDY

There are many software development processes, and not all of them deal with the sustainability issue. Speaking of sustainability, one can think of a sustainable software or a sustainable development process.

Agile methods have shown to be a more sustainable development process, contrary to the traditional waterfall method commonly used in the aircraft industry.

This work has the objective of presenting a checklist to assess the sustainability of the software development process in the aircraft industry.

SOFTWARE DEVELOPMENT APPROACHES

Software development process is complex and, even for a small product, involving a single person, some basic steps have to be respected if one wants to have a good product.

Here are some steps to be followed for even the most simple software to be produced:

Conception - the developer defines what is the product he wants to develop, as an answer to a given need.

Specification - in this step, the developer identifies all the features that have to be included in the software, also known as the requirement analysis.

Design - the design is the high level definition of the product, where the features of the same family are organized in blocks or groups.

Implementation - this is the time for writing the code.

Testing - the test is one of the most important steps for writing a quality code. A non tested software may not work as desired in a non controlled environment as the one it was used for production. The way, or the time, the code is tested, depends on the software development process chosen.

Documentation - documentation is important as the code is usually corrected after testing, and it is also usually reused.

Deployment - this step is when the code is installed and run in the costumer environment.

Maintenance - this occurs after the deployment when the software is discovered to have problems in the use. It also happens when the costumer has new needs.

The software development processes can be divided in two different groups: the Classic Model and the Agile Model.

THE CLASSIC WATERFALL DEVELOPMENT MODEL

We cannot start speaking about Agile methods before talking about the methods that have been in use before it. In the waterfall development model, the development process flows in one direction and it is clearly defined in phases like requirements analysis, design, coding, testing and maintenance.

The usual practice of this model claims that it has to have a verification, or a review, at the end of each phase, and a formal approval for passing to the next phase. Once a new phase is attained, is not expected to get back to previous phases.

This plan-driven approach is rigidly defined at the Requirements Analysis phase and forcedly disapproves changes. A problem due to poor work in a given phase found in a later phase can raise the resources use to a level that can become the project not feasible anymore.

SCRUM

Scrum or scrummage is a term that comes from rugby football that means a type of restarting play where the players are gathered closely on attempting to gain the possession of the ball.

Scrum in the software development context is an Agile framework defining how a software product must be developed. The word Scrum was first used in a 1986 Harvard Business Review article, "New New Product Development Game" (Takeuchi et al., 1986), by Hirotaka Takeuchi and Ikujiro Nonaka.

The classic Waterfall Method is an example of how the process is similar to a relay race. The process is sequential, the phases are well divided, are different from each other and the next phase is only started when all the requirements of the preceding phase are fulfilled.

According to the Scrum Guide (Schwaber et al., 2016) Scrum is "A framework within which people can address complex adaptive problems, while productively and creatively delivering products of the highest possible value."

The Scrum process basically has its Product Backlog divided into Sprint Backlog to be developed during the sprint (typically 30 days) delivering a working increment of the software. Each day of this 30 days period has a 15 minutes daily meeting (Daily Scrum) where the development team synchronizes activities and creates plans for the next 24 hours. During this meeting each team member presents an answer for the 3 questions:

1. What I did to help the team meet the Sprint Goal?

2. What will I do to help the team meet the Sprint Goal?

3. Do I see any impediment that prevents me or the team to meet the Sprint Goal?

This three questions creates a kind of mindset, and each team member has to be prepared to answer to them every single day. This mindset makes the team member to check himself all the time he is working on the product. This three questions is a kind of a checklist to be run daily during the daily meeting, and it can be expanded to comply with product requirements or with company requirements.

The Sprint Review is the moment for the team to expose the results of the Sprint, and a checklist is usually run after the sprint results evidences have been shown. This checklist is used to be sure that all company standards were met like checking the test coverage, regression test, if the tests were made over an up to date database, over the master branch and after merging the code to the master branch.

AGILE METHODS

Agile methods have been incorporated in the software industry at many levels, but it was for the first time well defined in the Agile Manifesto.

The Agile Manifesto comprised of twelve principles, one of them claiming: "Agile processes promote sustainable development. The sponsors, developers, and users should be able to maintain a constant pace indefinitely." (Beck et al., 2001).

SUSTAINABILITY

Sustainability is the way of creating and maintaining the conditions under which humans and nature can exist in productive harmony to support present and future generations (EPA, 2011).

One can define sustainable development as a way of developing a product by using less energy, or using the less energy possible. The sustainable product is not the scope of this work. The development must be sustainable as a way of making the development process quicker and using less resources. By using less resources, the cost of the development is the minimum possible.

DEVELOPMENT PERFORMANCE

Performance measurement is a process when information regarding the performance of a system or a component is collected or analyzed (Upadhaya et al., 2014).

Performance measurement can be also viewed as "the process of quantifying the efficiency and effectiveness of past actions" (Neely et al., 2002) or "the process of evaluating how well organizations are managed and the value they deliver for customers and other stakeholders" (Moullin, M. 2002).

A quantitative measurement of the development performance is not in the scope of this work. However, the Scrum team is auto assessed when passing from sprint to sprint by using the checklist, while this helps the team grows into a better performance.

PROPOSITION AND DISCUSSION

Running a checklist during the review ceremony meeting is a usual way of checking the development process requirements and is known to be a very practice. The Scrum team has a mindset built by knowing the checklist beforehand.

Part of the proposed solution lies on the analysis of the Agile methods to extract what can be done about sustainability. Some Agile Manifesto principles will be cited here to understand it in the sustainability context. The result of the principle analysis is a question to be included in the checklist. Additional questions regarding the sustainability of the software development process are included based on the Agile methods good practices.

First principle

"Our highest priority is to satisfy the customer through early and continuous delivery of valuable software."

The sustainability in this principle lies in the words "early" and "valuable software". The maximum sustainability is reached where the less energy is spent to deliver the most possible valuable software at the end of a sprint. The sooner the software is delivered, the less energy is spent to develop it. The Scrum team has to be mature enough to dimension the biggest part of the product backlog to be done during the sprint.

The question to be added to the checklist is: "Was the sprint backlog well quantified, in order to use the most possible team efficiency?"

Second principle

"Welcome changing requirements, even late in development. Agile processes harness change or the customer's competitive advantage"

Agile methods are a great tool when it comes to change requirements. A change in the requirements cannot impair the project milestones neither the schedule.

The question to be added to the checklist is: "Was the project pace, workload or schedule affected by requirements changes?"

Third principle

"Deliver working software frequently, from a couple of weeks to a couple of months, with a preference to the shorter timescale."

Iteration increases sustainability by making smaller software parts easier to be managed.

The question to be added to the checklist is: "Was the software well dimensioned and partitioned in small pieces of size good to be well managed in terms of pace, workload and schedule?"

Fourth principle

"Business people and developers must work together daily throughout the project."

Sustainability is increased by constant stakeholders feedback.

The question to be added to the checklist is: "Were the stakeholders working close to the developers?"

Fifth principle

"Build projects around motivated individuals. Give them the environment and support they need, and trust them to get the job done."

The question to be added to the checklist is: "Was the team sufficiently motivated regarding the environment and the support?"

Eighth principle

"Agile processes promote sustainable development. The sponsors, developers, and users should be able to maintain a constant pace indefinitely. "

The pace is very important for the sustainability of the project. It is known that overtime, night shifts, long periods of work and working on holidays tends to decrease efficiency. Low productivity time translates higher energy consumption.

The question to be added to the checklist is: "The development pace was constant enough to keep the highest possible level of efficiency?"

Checklist

Following is a list of questions to be made during the review ceremony to check the sustainability of the software development process. The team should have knowledge of this list during all the sprints and the process will comply more to the list as the team goes from sprint to sprint. The results of the previous sprints have to be passed along also in case of different teams involved.

1. Was the sprint backlog well quantified, in order to use the most possible team efficiency?

2. Was the project pace, workload or schedule affected by requirements changes?

3. Was the software well dimensioned and partitioned in small pieces of size good to be well managed in terms of pace, workload and schedule?

4. Were the stakeholders working close to the developers?

5. Was the team sufficiently motivated regarding the environment and the support?

6. The development pace was constant enough to keep the highest possible level of efficiency?

7. Was the software development tools well dimensioned the way it doesn't use all the hardware resources available?

8. Was the software development tools available all the time?

9. Is the technical debt kept zero or the lowest possible?

10. Was the code easy to modify the way it is written?

11. Is the code well divided into components that can be readily re-used?

12. Is the software easy configured and maintained?

13. Is the software written to quickly respond to user requests?

14. Is the software ready to function at an given time?

15. Is the software features easy to be used?

16. Was the sprint correctly estimated in terms of effort (time and resources)?

17. Is the software designed taken into account the less use of resources possible?

18. Continuous testing and automated testing are being applied?

CONCLUSION

The checklist is offered as a way of checking the sustainability of the software to be built, and it should be delivered answered during the Sprint Review ceremony.

The way this checklist is built, based on the Aircraft Software development best practices, gives means to provide a more sustainable software development process to the aircraft industry.

Further research will allow to test the proposed checklist, thus additional work have to be done to adjust this checklist. Certain level of customization can be made in order to fit the checklist to different software development processes.

Further research will also allow the quantitative measurement of the development process in order to assess a proper increase of the development process by using the checklist.

REFERENCES

Schwaber K., J. Sutherland, 2016, "The Scrum Guide" https://www.scrum.org/resources/scrum-guide, accessed on March 10, 2018.

Takeuchi H., I. Nonaka, "The New New Product Development Game." In: *Harvard Business Review* 64, no. 1 (January–February 1986).

Beck K., M. Beedle, A. van Bennekum, A. Cockburn, W. Cunningham, M. Fowler,J. Grenning, J. Highsmith, A. Hunt, R. Jeffries, J. Kern, B. Marick, R. C. Martin, S. Mellor, K. Schwaber, J. Sutherland and D. Thomas, 2001, Manifesto for Agile Software Development, http://agilemanifesto.org/principles.html, accessed on March 10, 2018.

Baseer K. K., A. R. M. Reddy and C. S. Bindu, 2015, "A Systematic Survey in Waterfall vs. Agile vs. Lean Process Paradigms" In: *Journal on Software Engineering*. Jan-Mar2015, Vol. 9 Issue 3, p36. 26p.

Albertao F., 2004, "Sustainable Software Engineering", Masters Practicum Paper, Carnegie Mellon University Sillicon Valley, Moffett Field, California, USA.

Presley A., J. Mills and D. Liles, 1995, "Agile Aerospace Manufacturing". Nepcon East, Boston. https://www.researchgate.net/publication/2507288_Presley_A_J_Mills_and_D_Liles_1995_Agile_Aerospace_Manufacturing_Nepcon_East_1995_Boston, accessed on March 10, 2018.

EPA, United States Environmental Protection Agency (2011) " What Exactly Is Sustainability?", http://www.thetomorrowplan.com/exchange/what-exactly-is-sustainability/

Upadhaya, B., Munir, R., & Blount, Y. (2014). Association between Performance Measurement Systems and Organisational Effectiveness. International Journal of Operations & Production Management, 34(7), 2-2

Neely, A.D., Adams, C. and Kennerley, M. (2002), The Performance Prism: The Scorecard for Measuring and Managing Stakeholder Relationships, Financial Times/Prentice Hall, London

Moullin, M. (2002), Delivering Excellence in Health and Social Care, Open University Press,Buckingham

ISSA-2018-008

EXPERIMENTAL INVESTIGATION OF VISCOUS FLOW NORMAL TO NACA 0012 AIRFOIL AT LOW REYNOLDS NUMBERS

Erkan Gunaydinoglu[1,2] and D. Funda Kurtulus[1]
[1] Middle East Technical University, Department of Aerospace Engineering, 06800, Ankara, Turkey [2] Turkish Aerospace Industries, 06520, Ankara, Turkey
gunaydin@ae.metu.edu.tr, dfunda@ae.metu.edu.tr

SUMMARY

The low Reynolds number aerodynamics at high angle of attack is crucial for the design of unmanned aerial vehicles and wind turbine blades . The current study aims to enhance the insight on the near wake of airfoils normal to free stream. The near wake structure on a NACA 0012 airfoil normal to free -stream is measured with particle image velocimetry in the range of Reynolds number 7000 to 20000 . The velocity and vorticity fields of the wake structures are studied and further analysis with Proper Orthogonal Decomposition is employed. The flow - fields are found to be Reynolds number independent

.

Keywords: Vortex dynamics, particle image velocimetry, aerodynamics, wake flow.

INTRODUCTION

Unmanned Aerial Vehicles (UAV) has gained an increasing importance for civilian and military purposes and their designs demand detailed investigation of airfoil characteristics operating at low Reynolds numbers. Most of the studies on low Reynolds number airfoils focus on the laminar separation and the dynamic stall phenomenon. Recent studies on the wake structure of airfoils (Mahbub Alam et al., 2010, Wang et al., 2014) emphasizes on the intrinsic features at low Reynolds numbers and addresses the need for further detailed investigation. The low Reynolds number aerodynamics of blunt bodies does not only broaden our understanding for engineering systems, but also helps us to reveal the dynamics of biological systems (Holden et al., 2014). The studies on two-dimensional flows normal to blunt bodies mainly focus on flat plates since their sharp edges form distinctive wake vortex structures (Dennis 1993). The high angle of attack aerodynamics of airfoils is especially important for the design of wind turbine blades whereas most of those studies focus on the force and moment coefficients (Michos et al., 1983).

The current study aims to experimentally investigate the near wake structure of a NACA 0012 airfoil normal to free stream at low Reynolds numbers ranging from Re=7000 to Re=20000 with particle image velocimetry (PIV) measurements.

EXPERIMENTAL METHODOLOGY

The experiments are performed in a low-speed open type wind tunnel with maximum velocity of 20 m/s and turbulent intensity around Tu =0.5%. An end-to-end acrylic NACA 0012 profile with chord length of 0.06 m is placed into the square test section (0.34 m x 0.34 m). The images are acquired with Phantom v640 camera with 4 megapixels resolution at the mid-plane to ensure the two-dimensionality. The flow is illuminated with New Wave Solo PIV 120 Nd:YAG laser with output energy of 120 mJ. For seeding TSI oil droplet generator model 9307-6 is used where six-jet Laskin nozzle pressurizes the olive oil and generates seed particles with the size of 1 . The image pairs are acquired at 20 Hz and mean flow-fields are achieved by averaging 500 vector fields. The acquired images are processed with Dantec DynamicStudio 5.1 software with adaptive cross-correlations starting from 64x64 pixel windows to 32x32 pixel windows with 50 % overlapping. The resulting field-of-view with these settings is 127x79 mm^2 which results vector spacing around 0.8 mm. The experimental arrangement of the Particle Image Velocimetry measurements is given in Figure 1.

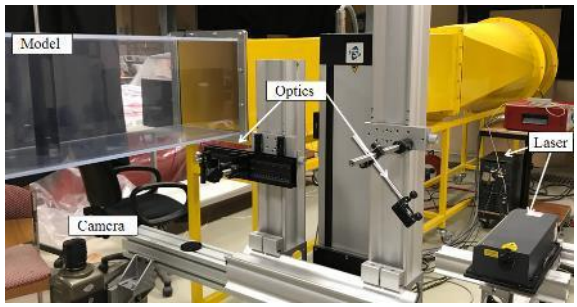

Fig. 1. Particle Image Velocimetry arrangement for the experiments

RESULTS AND DISCUSSION

PIV measurements around a NACA airfoil at four different Reynolds numbers Re=7300, Re=9700, Re=11200 and Re=19500 are studied. The non-dimensional streamwise and lateral velocity components at given Reynolds number range are shown in Figures 2 and 3. The trailing edge of the airfoil is located at point y = 0.2 in all cases and the velocity components are normalized with the free-stream velocity to achieve comparative results. The flow is coming from right to left in all cases.

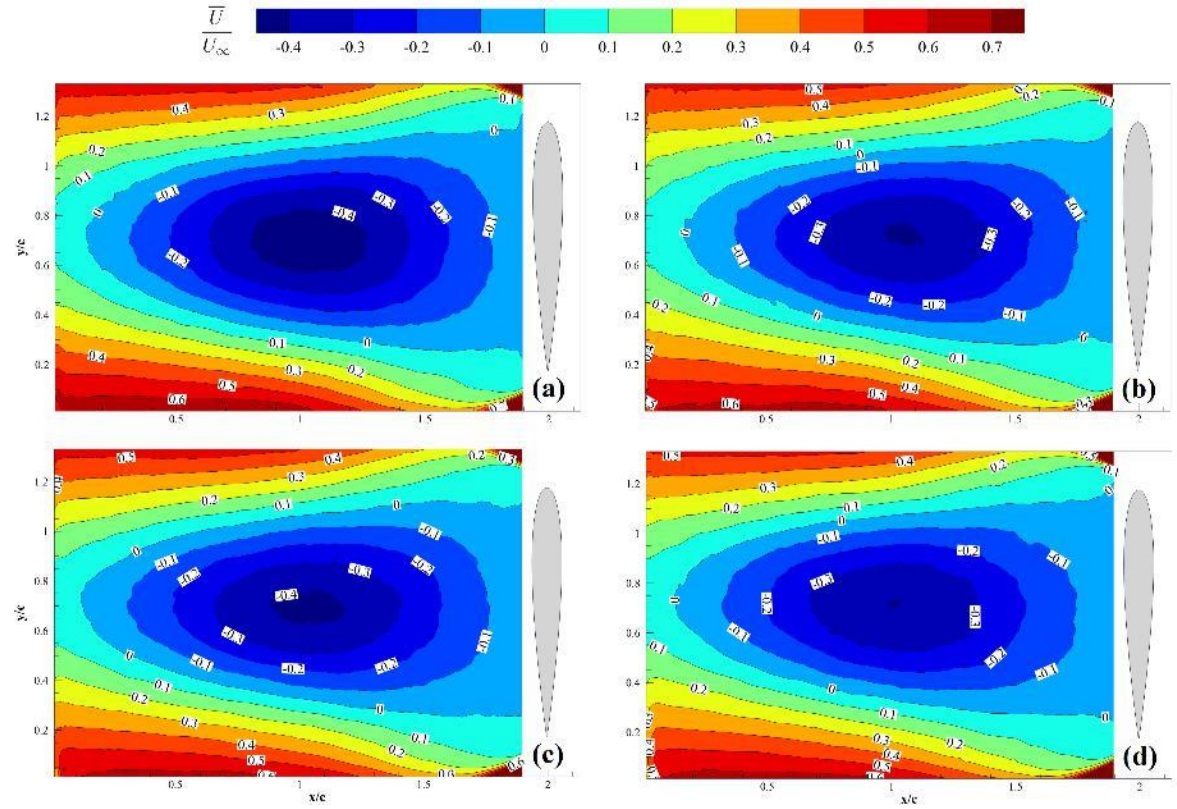

Fig. 2. Normalized mean streamwise velocity contours around NACA 0012 airfoil at (a) Re=7300, (b) Re=9700, (c) Re=11200 and (d) Re=19500

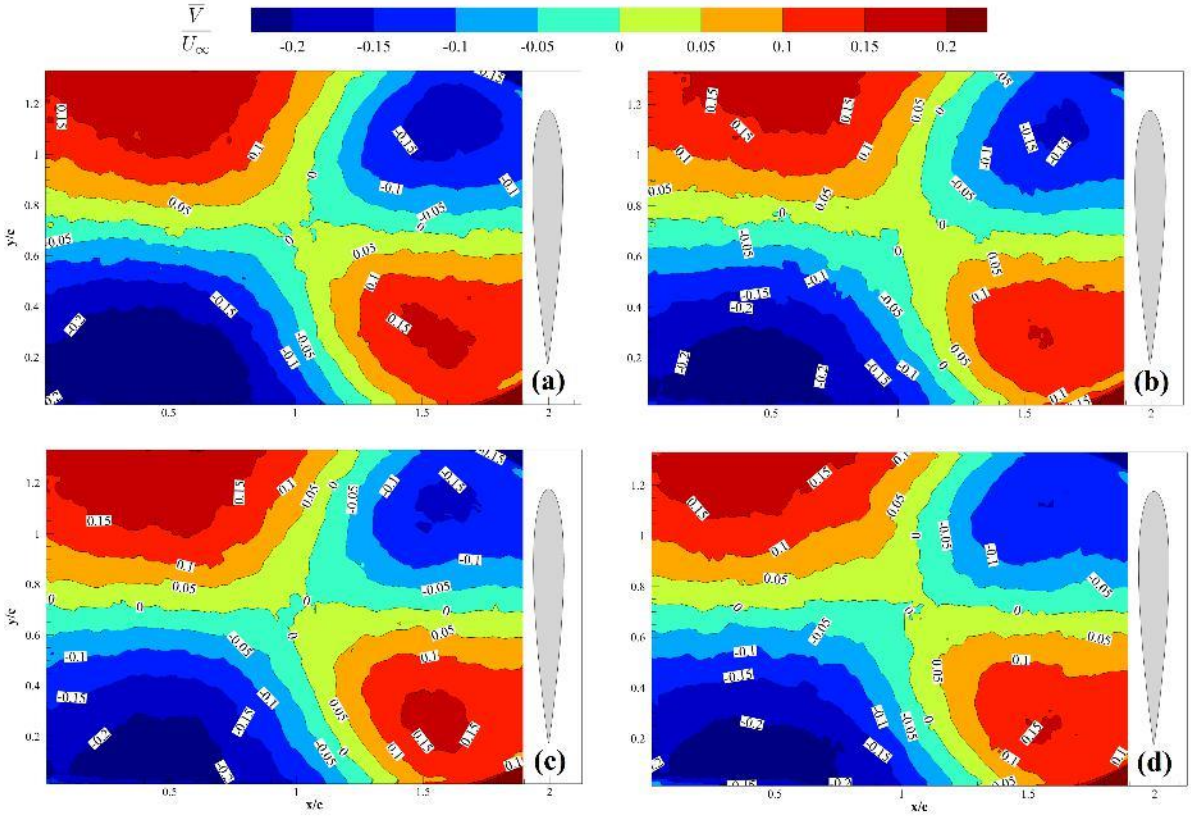

Fig. 3. Normalized mean lateral velocity contours around NACA 0012 airfoil at (a) Re=7300, (b) Re=9700, (c) Re=11200 and (d) Re=19500

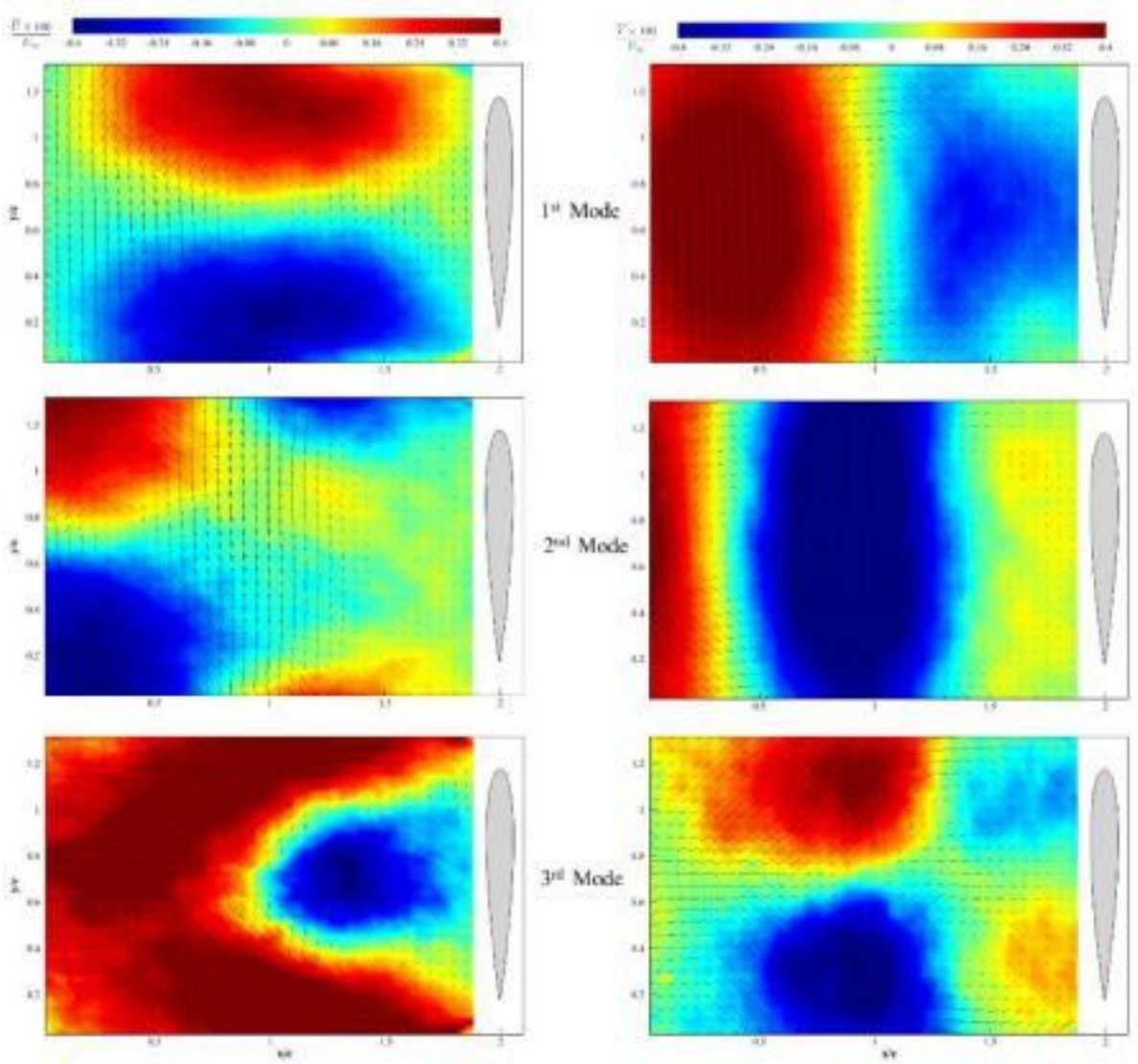

Fig. 4. First three POD modes in x-velocity (left column) and y-velocity (right column). Every second vector is shown.

The near wake structure follows classical bluff body characteristics and the sharp trailing edge does not show a distinctive effect on the wake structures. The wake bubble is found to be symmetric and nearly similar through whole Reynolds number range. The width of the bubble is found to be around 0.8c which agrees with Alam et al. (2010). The area of maximum streamwise velocity is found to be largest at Re=7300 and decreasing with increasing Reynolds number.

The velocity data is also analyzed with Proper Orthogonal Decomposition (POD). The POD provides useful information on identifying the coherent structures. The analysis consists of acquisition of snapshots of the flow and generating a correlation matrix for fluctuations and solving an eigenvalue problem. The detailed information on the theory and application of POD for turbulent flows could be found in Lumley (1967) and Sirovich (1987). Figure 4 shows the first three energetic POD modes for x- and y-velocity components. Figure 5 shows the energy content of the POD modes. The first mode shows a universal vortex structure sitting on the center of the wake bubble.

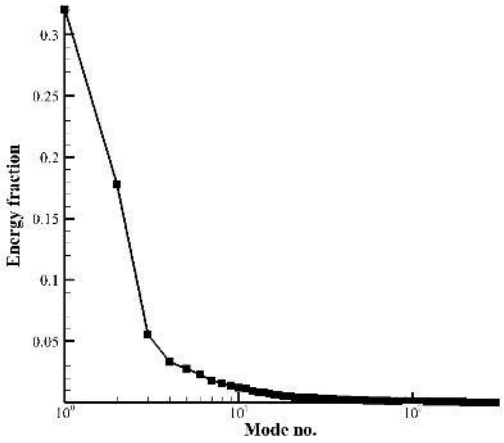

Fig. 5. Modal energy distribution for Re=19500

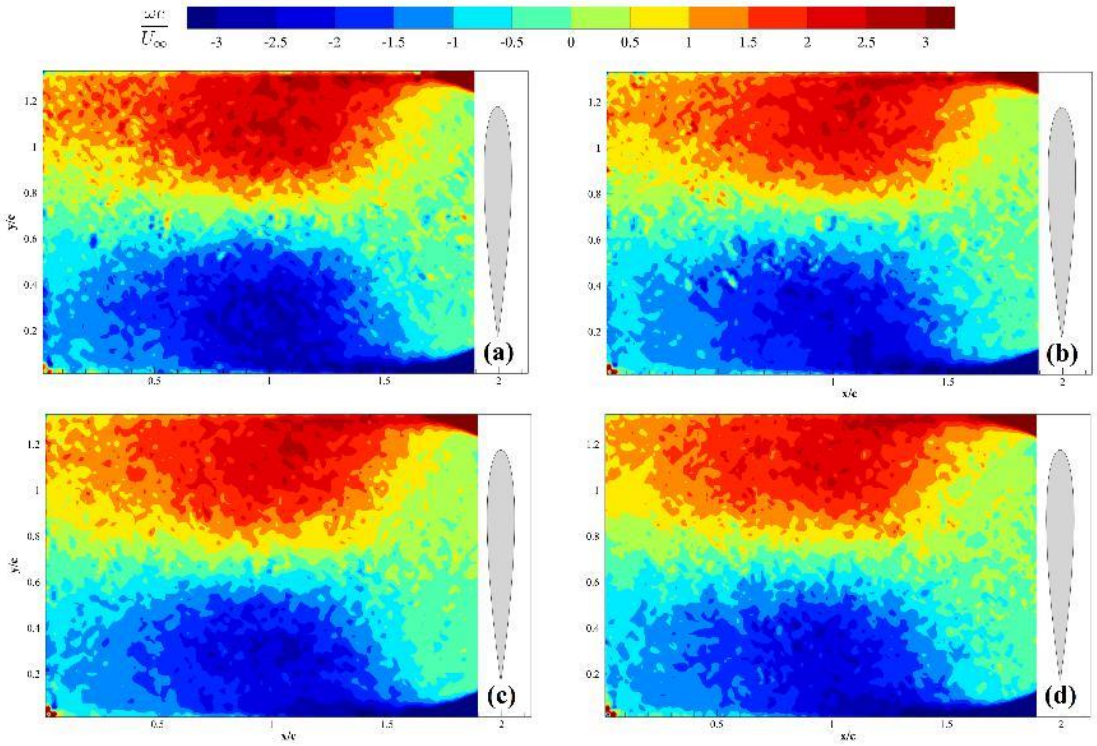

Fig. 6. Normalized mean out-of-plane vorticity contours around NACA 0012 airfoil at (a) Re=7300, (b) Re=9700, (c) Re=11200 and (d) Re=19500

The magnitude of velocities is equal to the turbulence intensity of the wind tunnel flow, so first mode could be related with the in-flow turbulence. The third mode shows similarity with the mean flow as forming a wake bubble but this time with a smaller bubble width.

The non-dimensional mean vorticity contours for the cases are given in Figure 6. At this relatively low Reynolds numbers inertial forces show minor contribution to the wake structures. The streamlines - not shown here- and vorticity contours are also similar for the whole range. Rather than the small variations in flow-fields which is in the order of measurement uncertainty the velocity fields are also found to be similar. The minimum streamwise velocity is found to be -0.48U_∞ in the wake bubble at lowest Reynolds number

The vortex shedding frequency is at the center of the flow-of-interest is measured to be St= 0.15 at Re=7300. Keeping in mind the low resolution of the current methodology the Strouhal number is found to be comparable with available Laser Doppler Anemometry measurements of St=0.144. Due to the reflections around the airfoil, leading and trailing edge velocities could not be measured.

CONCLUSIONS

The viscous flow normal to a NACA 0012 airfoil at Reynolds number range of 7000 to 20000 is

investigated through PIV. The acquired data is further analyzed with POD to characterize the most energetic contents of the flow. The near wake flow in the studied range is found to be Reynolds number independent which agrees with the force and moment measurements in available literature.

REFERENCES

Dennis, S., Qiang, W., Coutanceau, M., & Launay, J., 1993, Viscous flow normal to a flat plate at moderate Reynolds numbers, *Journal of Fluid Mechanics*, 248, 605-635. doi:10.1017/S002211209300093X

Holden, D., Socha, J.J., Cardwell, N.D, Vlachos, P. P., 2014, Aerodynamics of the flying snake Chrysopelea paradisi: how a bluff body cross-sectional shape contributes to gliding performance. *Journal of Experimental Biology* 26:11, 115107

Mahbub Alam, Md., Zhou, Y., Yang, H. X., Guo, H. and Mi, J., 2010, The ultra-low Reynolds number airfoil wake. *Experiments in Fluids* 48:1, pp 81-103

Michos, A., Bergeles, G., & Athanassiadis, N., 1983, Aerodynamic Characteristics of NACA 0012 Airfoil in Relation to Wind Generators, *Wind Engineering*, 7(4), 247-262.

Wang, S., Zhou, Y., Mahbub Alam, Md. and H. Yang, 2014, Turbulent intensity and Reynolds number effects on an airfoil at low Reynolds numbers. *Physics of Fluids* 26:11, 115107

Lumley, L., 1967,The structure of inhomogeneous turbulent flow, -In A. M. Yaglom and V. I. Tatarski, editors: *"Atmospheric Turbulence and Radio Wave Propagation*", pp. 166-178.

Sirovich, L., 1987, Turbulence and the dynamics of coherent structures. Part I: Coherent structures, *Quart. Appl. Math.,* 45(3):561-571.

International Symposium on Sustainable Aviation 2018
9 – 11 July 2018
Rome, Italy

AN ADAPTIVE SAMPLING TECHNIQUE FOR OPTIMIZING THE DESIGN OF AXIAL TURBINE ENDWALLS

Hakim T. Kadhim[a,b] and Aldo Rona [a]
[a]University of Leicester, Leicester, LE1 7RH, U.K.
[b]Al-Dewaniyah Technical Institute, Al-Furat Al-Awsat Technical University, Iraq
Authors' e-mails:hkk10@leicester.ac.uk, ar45@leicester.ac.uk

SUMMARY

C o mp u t e r - based optimi zation is demonstrated for the design of a 1. 5 stage axial turbine casing endwall . It uses a recursive implementation of the Optimal Latin Hypercube technique for sampling the design space and Kriging as the surrogate model for performance. The latter is evaluated by Computational Fluid Dynamics . At design and at off design conditions, reductions in the stage total pressure loss coefficient verify the effectiveness of the optimi zation method.

Keywords: Optimization, CFD, Axial turbine.

INTRODUCTION

Computer-based optimization is an established practice in industrial design to maximize the benefits of a newly introduced design feature. The computer-based optimization of the aerodynamics of axial turbines is typically performed with the objective of maximizing the stage isentropic efficiency. This work uses the stage total pressure loss coefficient, which is closely related to the stage isentropic efficiency, as the objective function to enhance the performance of a representative axial turbine by optimizing the shape of its casing (Kadhim, 2018).

The general process of engineering design with optimization is described by Pahl and Beitz (2013). This design process consists of three main steps. The first step is to create an optimization model in a specific mathematical formation, which is also known as a constrained parametric model. The second step is solving the optimization problem using a chain of appropriate methods. This typically involves the evaluation of a penalty function and locating model parameter combinations that give the lowest penalty. The last step is the *a posteriori* analysis of the optimal solution. Several questions about the optimality, feasibility, sensitivity, and the improvement margin may need to be answered in this step.

The increased accuracy of modern Computational Fluid Dynamics (CFD) simulations enable aerospace engineers nowadays to evaluate the performance of a specific design through virtual prototyping (Forrester and Keane, 2009). This has enabled the progressive reduction of costly experimental tests, such as the ones in wind tunnels. Although the fidelity of computer models has increased, the computing cost has also increased and this has become the main limitation in the design optimization process. This has prompted the replacement of expensive computer simulations with alternative cheaper surrogate models (Søndergaard et al., 2003). Surrogate models approximate key design performance metrics that are otherwise computed from more expensive simulations. A surrogate-based analysis and optimization approach was applied to the design of turbine blade profiles by Madavan et al. (1999), Rai et al. (2000) and Shyy et al. (2001). The key stages in the surrogate-based modelling approach are the Design of Experiment (DoE), the construction of the surrogate model based on CFD simulations performed at selected locations of the design space, and the model validation (Queipo et al., 2005).

Heuristic evolutionary techniques do not provide any basic assumption on the relation between objectives and design variables. A good initial sampling selection, that allows an initial guess on the relations between inputs and outputs, is of great importance for achieving good results and for reducing the optimization effort (Poles et al., 2009). In optimizing a turbine blade, the minimum number of the design samples are usually selected as two to five times the number of design variables (Arabnia, 2012). The number of samples is often severely limited by the computational cost of each sample.

This work uses computer-based optimization to design a guide groove for suppressing endwall secondary flows. An initial set is used to sample the design space using the Optimal Latin Hypercube (OLH) method. From this sample set, a Kriging model of the stage total pressure loss coefficient identifies the region of low total pressure loss coefficient. A local adaptive sample is added to the initial set, which enables to further improve the selection of the design variables and reduce the stage total pressure loss coefficient.

IMPLEMENTATION OF THE OPTIMIZATION PROCESS

The optimization method used in this work is implemented on the Automatic Process Optimization Workflow (APOW), which is software licensed by GE Power. The casing design workflow implemented in APOW is shown in Fig. 1. This is an open loop design workflow in which a black box type optimization approach is implemented. In this context, the black box approach means that no *a priori* topology of the system response is assumed.

The workflow of Fig. 1 is executed in batch mode using APOW, for different values of the design variables (,) and (,). The APOW Design of Experiments (DoE) is used to populate the design space, based on the Optimal Latin Hypercube (OLH) design technique. The optimization analysis of the DoE is performed on a surrogate model. For this purpose, Kriging is selected as the surrogate model type to use.

Different realizations of the turbine passage with a non-axisymmetric casing are then produced based on the values of the design parameters that populate the design space, from the Design of Experiments. As shown in Fig. 1, this is obtained by creating a geometry parametrised on (,) and (,) in Matlab. The computational domain is then discretized in ANSYS ICEM CFD by maintaining similar meshing parameters as for the 1.5 stage turbine model validated in Kadhim et al. (2018), to obtain the same mesh quality as for this validation test case. An unstructured meshing approach is used, as this is the only supported output format accessible through the ANSYS Fluent academic license. The .msh file output is now ready for use by a compatible flow solver.

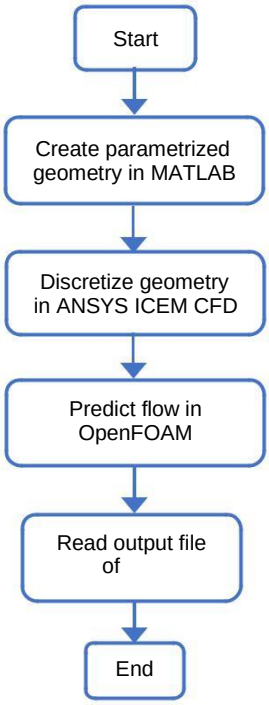

Fig. 1 Workflow for the computer-based assessment of the performance of an axial turbine with non-axisymmetric endwalls.

The next step is to solve the flow field using OpenFOAM to predict the aerodynamic pressure losses. The same boundary conditions are applied as for the validation test case (Kadhim et al., 2018) and the numerical solution is iterated by OpenFOAM to satisfy the same convergence criteria.

The OpenFOAM settings and more details of the above steps are reported in Kadhim (2018). Finally, the stage total pressure loss coefficients are collected as an output file to generate a database which contains the design variables and their associated aerodynamic performance. From this database, a Kriging surrogate model is built.

OPTIMIZATION COST FUNCTIONS

There are many options for the selection of the objective function to be used in the optimization process, which aims to meet some pre-defined design specifications. Panchal et al. (2011) optimised two endwall geometries of an axial turbine cascade. They tested the total pressure loss coefficient and the secondary kinetic energy (SKE) coefficient as the objective functions. They recommend using the total pressure loss coefficient as the objective function, as the SKE reduction was less indicative of the performance of both optimised endwalls.

This work follows the recommendation by Panchal et al. (2011) and uses the total pressure loss coefficient to drive the optimization of the casing. The total pressure loss across the upstream half-stage alters the flow exiting it. The change in the flow exiting the upstream stator passage affects the downstream rotor performance. This change in turns typically alters the stage efficiency. Therefore, the total pressure loss coefficient is used to drive the optimization of the casing by defining the stage total pressure loss coefficient as

where subscript 0 denotes the stator inlet plane, subscript 1 denotes the stator exit plane, subscript 2 denotes the rotor exit plane, and (═) denotes a pitchwise and radially averaged quantity. The objective is to minimise this total pressure loss coefficient.

RESULTS AND DISCUSSION

DESIGN OF EXPERIMENT

In the optimization loop, knowledge is built into the surrogate model by performing numerical experiments by the workflow of Fig. 1. Each numerical experiment samples the parameter space of the endwall and returns a value of the total pressure loss. In this work, each sample requires a full one and half stage CFD simulation. The number of samples is limited by the computational cost of each sample. A set of 10 sampling points is used by the Optimal Latin Hypercube design technique to populate the design space. The bounds in the casing parameters and were set based on the result from an initial feasibility study by Kadhim (2018). Fig. 3 shows the resulting sample spread as red circles, stated in terms of the groove width at the trailing edge and of the axial location of maximum groove depth, . The changes in the response function, which is the stage total pressure loss coefficient, are studied for different combinations of and . As shown in Fig. 2, Kriging provides a continuous response function from the discrete

samples of computational fluid dynamics estimates the stage total pressure loss . It enables to develop an insight of how the design parameters and influence the turbine performance in the parameter space and to identify regions of high performance, with acceptable sensitivity. From the Kriging results of Fig. 2, a region of low was identified over the range 0.025 radians ≤ ≤ 0.05 radians and 0.4 ≤ ≤ 0.8. The optimized (,) values identified by using the minimum in Fig. 2 are (0.05 radians, 0.72). It will be seen in the next section that the ( ) optimum value differs slightly from the one obtained by using the adaptive technique.

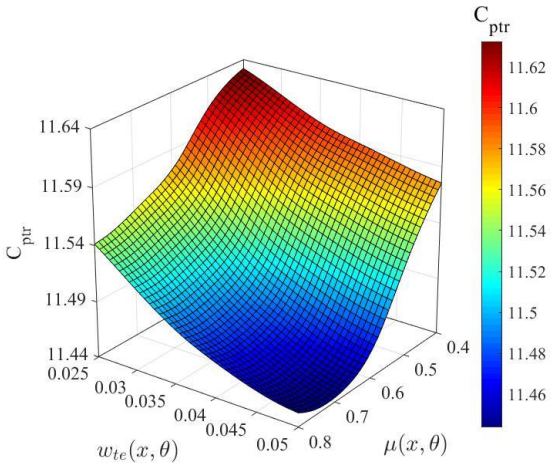

Fig. 2 Optimization of the casing groove using 10 sampling points. in radians.

ADAPTIVE SAMPLING TECHNIQUE

In the case of a black box computer-based optimization, where the system response function is not known, no proactive sampling strategy can be relied upon to optimize the sampling of the design space. Therefore, it is essential to examine the sampling distribution in the design space *a posteriori* and particularly around any predicted system response optimum (in this case, the predicted pressure loss coefficient minimum). This may lead to adding more samples in the neighbourhood of the predicted system response optimum. The distribution of these additional samples in the design space is therefore informed from the results of the previous sample set. This process is commonly known as adaptive sampling.

A sensitivity analysis on the optimized geometry from the previous section is performed by adaptive sampling. In Fig. 3, there are only two initial sampling points (red circles) in the region around the optimal design point ( ), which is identified using green colour. This is not conducive to obtaining accurate predictions from the Kriging model in this region. To examine and enhance the accuracy of the Kriging model, a local adaptive sample of 10 points is added to the initial set of 10 points used in the previous section. The adaptive sample set is also generated using the Optimal Latin Hypercube method and therefore it is not an arbitrary sample.

The extent of the re-sampled region was constrained to the region delimited by ≤ 11.46, which is about 10% of the colour-scale range in Fig. 2 from at . This smaller sample space region includes the optimal design point ( ) from the initial set.

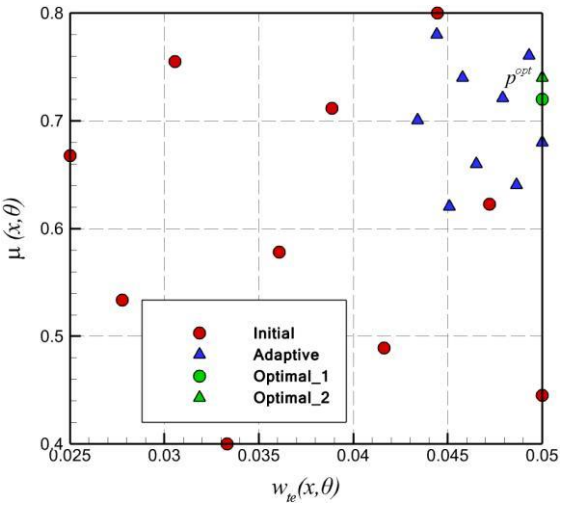

Fig. 3 Initial and adaptive sampling using the OLH.

Figure 3 shows the initial and the adaptively selected samples that are generated using the Optimal Latin Hypercube. The green filled circle represents the geometry parameters for the casing optimized from the set of 10 samples of the initial set. The geometry parameters for the casing optimized by applying adaptive sampling is shown by the green filled triangle.

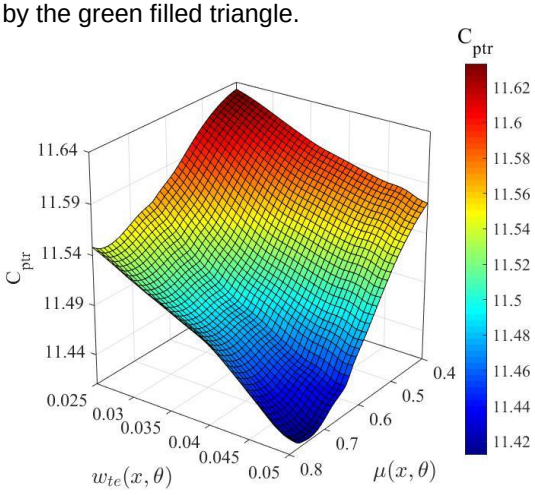

Fig. 4 Kriging model of the total pressure loss coefficient. in radians.

The response function obtained from combining the initial and the adaptively selected samples (20 points) is shown in Fig. 4. By comparing Fig. 2 and Fig. 4, it is possible to appreciate that adding the 10 additional samples shown by the blue filled triangles in Fig. 3 appears to have increased the definition of the shape of the response function in the neighbourhood of the lowest value, denoted by in Fig. 3. There appears to be a steeper valley in Fig. 4 defining this minimum, suggesting a

greater div ( ), which is indicative of a greater localization of the minimum in the (,) space. The (,) location of the optimal value from

Fig. 4 is shown in Fig. 3 to be slightly different than that from Fig. 2.

The minima of predicted from the Kriging models were verified by running CFD simulations at the (,) of . These simulations predicted values very close to the ones from the Kriging models. The difference with the 10-point sample model was 0.2125 %, which is arguably too small to be verified in experiment. With a 20-point adaptive sample, the difference was 0.00276 % and therefore essentially immaterial. The percentage differences between the optimal stage total pressure loss prediction from Kriging and from CFD for both sets confirm a good model data fit. The values of the percentage improvement Δ using the adaptive technique is calculated as

$$\Delta = (- \quad - \quad - \quad) \times 100\% \qquad (2)$$

Table 1 documents the axial turbine performance improvement obtained by using this adaptive technique. The adaptive sampling has shown to be able to improve the selection of over the initial design of 10 points, but the 3.5 % Δ performance gain is rather small. This improvement is arguably worth the additional computational cost of the 20-point sample, which is about double the one from the 10-point sample.

Table 1. Response function percentage improvement

Response function	Baseline	Optimal 1	Optimal 2	%
	11.6205	11.4139	11.4067	3.5

CONCLUSIONS

A newly adaptive sampling technique for optimizing the design of axial turbine endwalls is presented. The technique is used for obtaining more accurate predictions from a Kriging model, based on the design of experiment Optimal Latin Hypercube method.

Whereas in this work the application of adaptive sampling led to modest improvements in performance with respect to judiciously selected initial sampling, the adaptive sampling technique appears to be an interesting approach in its own right. This approach has the potential to identify more optimal configurations in problems where the response function has greater complexity in shape, a complexity that may not be known *a priori* and that the adaptive sampling should be able to uncover.

The results from the optimization and from its *a posteriori* verification gave confidence that a good predictive ability was obtained by the Kriging surrogate model used in the design process. The low cost overhead of the Kriging model and its robustness are attractive for accelerating the design iterations used in industry for turbomachines.

ACKNOWLEDGEMENT

This work has been undertaken under the auspices of the GE Power -University of Leicester framework agreement. The Higher Committee for Education Development in Iraq (HCED) is acknowledged.

NOMENCALTURE

Stage total pressure loss coefficient

Optimized groove parameters point

Groove width at the blade trailing edge, radians

Greek Letters

Maximum groove depth location

REFERENCES

Arabnia, M. (2012). Aerodynamic shape optimization of axial turbines in three dimensional flow. PhD thesis, Concordia University.

Forrester, A. I. & Keane, A. J. (2009). Recent advances in surrogate-based optimization. Progress in Aerospace Sciences, 45(1), pp. 50-79.

Kadhim, H., Rona, A., Gostelow, J. P. & Leschke, K. (2018). Optimization of the non-axisymmetric stator casing of a 1.5 stage axial turbine. International Journal of Mechanical Sciences, 136, pp. 503-514.

Kadhim, H. T. K. (2018). Effect of non-axisymmetric casing on flow and performance of an axial turbine. PhD thesis, Department of Engineering, University of Leicester.

Madavan, N. K., Rai, M. M. & Huber, F. W. (1999). Neural net-based redesign of transonic turbines for improved unsteady aerodynamic performance. AIAA/SAE/ASME/ASEE 35th Joint Propulsion Conference, Los Angeles. Paper No. 99–2522.

Pahl, G. & Beitz, W. (2013). Engineering design: a systematic approach. New York, Springer Science & Business Media.

Panchal, K., Abraham, S., Ekkad, S. V., Ng, W., Brown, B. J. & Malandra, A. (2011). Investigation of effect of endwall contouring methods on a transonic turbine blade passage. ASME 2011 Turbo Expo: Turbine Technical Conference and Exposition, Canada. ASME Paper GT2011-45192.

Poles, S., Fu, Y. & Rigoni, E. (2009). The Effect of Initial Population Sampling on the Convergence of Multi-Objective Genetic Algorithms. Multiobjective Programming and Goal Programming: Theoretical Results and Practical Applications. Berlin: Springer Berlin Heidelberg, pp. 123-133.

Queipo, N. V., Haftka, R. T., Shyy, W., Goel, T., Vaidyanathan, R. & Tucker, P. K. (2005). Surrogate-based analysis and optimization. Progress in aerospace sciences, 41(1), pp. 1-28.

Rai, M. M., Madavan, N. K. & Huber, F. W. (2000). Improving the unsteady aerodynamic performance of transonic turbines using neural networks. Proceedings of the 38th AIAA aerospace sciences meeting and exhibit, USA. NASA/TM-1999-208791.

Shyy, W., Papila, N., Vaidyanathan, R. & Tucker, K. (2001). Global design optimization for aerodynamics and rocket propulsion components. Progress in Aerospace Sciences, 37(1), pp. 59-118.

Søndergaard, J., Madsen, K. & Nielsen, H. B. (2003). Optimization using surrogate models-by the Space Mapping technique. PhD thesis, Technical University of Denmark.

ISSA-2018-010

ROBUST AIRCRAFT PATH PLANNING USING ENSEMBLE WEATHER FORECASTS

Antonio Franco, Damián Rivas, and Alfonso Valenzuela Department of Aerospace Engineering, Universidad de Sevilla School of Engineering, 41092 Sevilla, Spain
antfranco@us.es, drivas@us.es, avalenzuela@us.es

SUMMARY

The optimisation of the aircraft route taking into account wind uncertainty is addressed in this work . The wind uncertainty is obtained from ensemble weather forecasts . A structured airspace is considered, which is defined by a set of waypoints and a set o f allowed connections between each pair of waypoints . The analysis is focused on a cruise flight composed of several segments connecting given waypoints . The optimal route is seen as a path in a graph. A combinatorial optimisation approach is followed, and the stochastic optimal path is obtained by applying a Mixed -Integer Linear Programming algorithm. A trade - off between efficiency (minimum average flight time) and predictability (minimum dispersion of the flight time) is performed. Results are presented for a given trans -oceanic flight, considering a real ensemble weather forecast .

Keywords: Probabilistic trajectory optimisation; wind uncertainty; ensemble weather forecasting

INTRODUCTION

From the operational point of view, trajectory optimisation is a subject of great importance in Air Traffic Management (ATM). It aims at defining optimal flight procedures for a given aircraft mission that lead to cost-efficient flights. Aircraft trajectory optimisation is an important tool to improve the efficiency of operations and, therefore, it contributes to enhance the efficiency of the ATM system.

Furthermore, in order to maintain high safety standards, any new methodology developed to improve the system performance should integrate uncertainty information. Weather is among the uncertainty sources that most importantly affect the ATM system. In particular, weather uncertainty has a major impact on the route planning process.

The main objective of this work is to develop a methodology capable of finding stochastic optimal routes, in the presence of uncertain winds, within a structured airspace, and using a kinematic model for the aircraft motion. The winds are provided by an ensemble weather forecast, which is obtained for an intermediate lead time between departure and arrival, and the analysis is focused on the cruise flight. The main contribution with respect to Gonzalez-Arribas et al. 2018 is the consideration of a structured airspace; this is a more appropriate assumption not only for the traditional air route network, but also for the new free-route airspace concept, because both make use of predefined waypoints.

PROBLEM FORMULATION AND METHODOLOGY

In this Section, the optimisation of the aircraft route taking into account wind uncertainty is formulated, and the resolution methodology is explained. In particular, a stochastic trajectory optimiser has been developed, composed of several blocks depicted in Fig. 1.

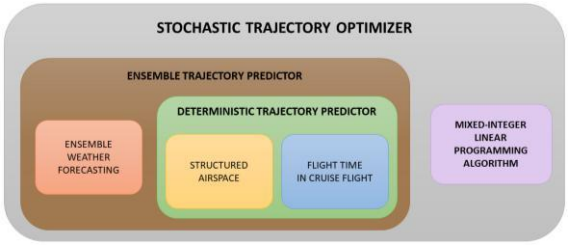

Fig.1. Methodology proposed for optimal path planning.

Ensemble weather forecasting

To model weather for strategic planning horizons an upward trend is to use Ensemble Prediction Systems (EPS), which attempt to characterise and quantify the inherent prediction uncertainty based on ensemble modelling. This technique generates a representative sample of the possible weather realisation (see Steiner et al. 2008); hence, an ensemble forecast (EWF) is a collection of weather forecasts (referred to as members).

Ensemble forecasting has proved to be an effective way to quantify weather prediction uncertainty. The uncertainty information is on the spread of the solutions in the ensemble, and the hope is that this spread bracket the true weather outcome (see Steiner et al. 2008). It is important to notice that, for strategic planning, the analysis of all the individual ensemble members must be included (rather than an ensemble mean).

Airspace Structure

In this work, a structured airspace is considered, which is defined by a set of waypoints and a set of allowed connections between each pair of waypoints, referred to as airways. First, a regular grid of waypoints is defined in the weather forecast retrieval area, with a step in latitude and longitude. Then, as in Dancila and Botez 2016, the geographical search area is restricted to be inside a

spherical ellipse with foci located at arrival and destination airports, and with major axis equal to $(1+)\, r_{gc}$, where r_{gc} is the great circle distance between the departure and destination airports, and $$ is a tuning parameter that controls the extension of the search area.

Furthermore, each waypoint inside the search area is connected to some of its neighbours in a 7x7-waypoint square centred at the waypoint of interest, as depicted in Fig. 2, provided that the neighbours are inside the search area as well.

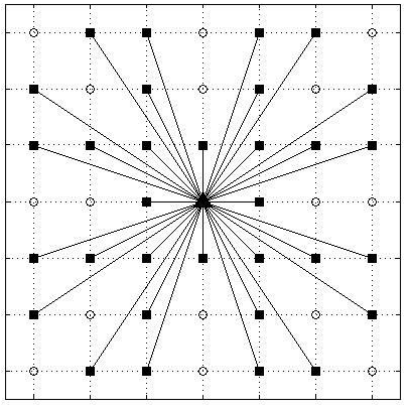

Fig.2. Sketch of connections of a waypoint. Waypoint (black filled triangle); connections (black segments); connected neighbours (black filled squares); not connected neighbours (black circumferences).

Finally, the arrival and destination airports are considered to be connected to those surrounding waypoints closer than 2º in both latitude and longitude, provided that those waypoints are inside the search area.

Flight time in cruise flight

As already indicated, in this paper the flight time in cruise flight is studied. In accordance with the airspace structure defined above, the cruise is considered to be formed by p cruise segments, each one of them defined by a constant course, and flown at constant Mach number and constant pressure-altitude, as required by Air Traffic Control (ATC) practices. The Earth is assumed to be spherical, with mean radius $R_E = 6371\ \text{km}$, and the atmosphere is supposed to be defined by the International Standard Atmosphere (ISA) model plus the winds given by the EPS. The true airspeed is also constant, defined by $V = Ma$, where a is the ISA speed of sound at the given flight pressure altitude. A time-invariant wind field is considered, which comes from an ensemble weather forecast obtained for an intermediate lead time between departure and arrival.

A sketch of a generic cruise segment can be found in Fig. 3. In cruise segment j, the flight is subject to along-track winds, $w_{AT_j}(r)$, and crosswinds, $w_{XT_j}(r)$, which vary along the cruise (note that r represents the distance flown by the aircraft). These wind components are obtained by projecting the wind vector onto the constant course segment connecting the bounding waypoints. Note that the course j and the segment length $(r_f)_j$ can be computed from the navigation equations (see Franco et al. 2017 for more information).

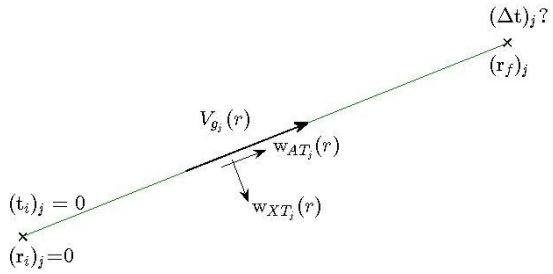

Fig.3. Sketch of a generic cruise segment.

The effects of the crosswinds are analysed by taking them into account in the kinematic equations, ignoring the lateral dynamics, and translating the crosswind into an equivalent headwind. This leads to a reduced ground speed, which for cruise segment j is given by

$$V_{g_j}(r) = \sqrt{V^2 - w_{XT_j}^2(r)} + w_{AT_j}(r) \qquad (1)$$

The kinematic equation of motion for cruise flight, for segment j, can be written as:

$$\frac{dt}{dr} = \frac{1}{V_{g_j}(r)} \qquad (2)$$

The time to fly the cruise segments, namely $(t)_j$, $1 \le j \le p$, are obtained from the numerical integration of Eq. (2), from $r = 0$, to the given length of the segment, $r = (r_f)_j$. Hence, the total flight time t_f is given by

$$t_f = \sum_{j=1}^{p} (t)_j \qquad (3)$$

Ensemble trajectory prediction

Ensemble trajectory prediction is one of the main approaches commonly used for trajectory

prediction subject to uncertainty provided by EWF. Following this approach, for each member k of the ensemble, the procedure previously described for the computation of a deterministic total flight time can be applied, obtaining $t_f^{[k]}$. Therefore, for a given cruise path compatible with the airspace structure, the final result is a set of cruise total flight times ($t_f^{[1]}$, …, $t_f^{[n]}$), where n is the number of weather ensemble members.

Methodology for stochastic optimal path planning

Because the cruise flight is composed of several segments connecting given waypoints (including the origin and the destination), the aircraft route can be seen as a path in a graph. Therefore, the optimisation of the aircraft route with respect to a given objective function becomes a shortest path problem. The graph is defined by a set of m nodes (the waypoints), a set of l links (the constant-course segments) and a set of link costs (the increments of the objective function experienced at the segments).

However, as the problem is affected by uncertainty, it is indeed a stochastic shortest path problem, described with a model based on a discrete set of scenarios (the ensemble members). Therefore, the problem is stated as selecting a unique route to be followed that minimises some function of the possible realisations of an appropriate flight variable (e.g., the flight time).

In this work, this approach can be applied to find the route that minimises some combination of the average value of the total flight time (which is a good measure of the efficiency of the route) and some measurement of the spread of the trajectories, for instance, the difference between the largest flight time and the smallest one (which has an inverse relationship with the predictability); it enables performing a trade-off between efficiency and predictability when addressing aircraft path planning. This objective is stated in the following cost function

$$J = \frac{1}{n}\sum_{k=1}^{n} t_f^{[k]} + dp\left(\max_k(t_f^{[k]}) - \min_k(t_f^{[k]})\right) \quad (4)$$

where dp is the dispersion penalty parameter, which controls the trade-off between efficiency and predictability: the higher it is, the more predictable the trajectory is but the more willing we are to accept a decrease in efficiency.

The problem of finding the path that minimises the objective in Eq. (4) is formulated according to a combinatorial optimisation approach (see Gabrel et al. 2013), leading to a Mixed-Integer Linear Programming (MILP) problem. In this work, the MILP problem is solved by applying MATLAB's *intlinprog* algorithm, which relies on a combination of the branch and bound and the cutting plane methods.

RESULTS AND DISCUSSION

In this section, results are presented for a flight from Philadelphia International Airport (KPHL) to Barcelona–El Prat Airport (LEBL). ECMWF EPS has been chosen. Winds have been retrieved from the TIGGE dataset, available at ECMWF portal. They correspond to 31 August 2016, released at 00:00 with a look-ahead time of 24 hours. Winds are obtained for pressure altitude 200 hPa; this corresponds to an ISA altitude of 11784 m, which is in the stratosphere.

The tuning parameter for the search area is set to $= 0.04$, and the step in latitude and longitude for the regular waypoint grid is $= 1^{\circ}$. In the following, results are presented for a cruise flight performed at Mach number $M = 0.82$, at a pressure altitude 200 hPa, and departing 31 August 2016 at 20:00h.

The optimal routes are presented in Fig. 4, for $dp = 0$, 5 and 10, along with the route of minimum distance as a reference, and a representative wind field (the average along the EPS members). For this weather forecast, one can see that the route is somehow shifted to the South (mainly at the beginning), in order to take advantage of the predominant tailwinds.

The values of the optimal total flight time corresponding to these trajectories are presented in Table 1. The average $E[\cdot]$ is computed along the EPS members, and the spread $[\cdot]$ is defined as the difference between the largest value and the smallest one. Note that $E[t_f] + dp\,[t_f]$ is the minimum value of J.

Results show, as expected, that the higher the value of dp, the lower the dispersion in the total flight time, but the higher the average total flight time. In particular, for $dp = 5$, one can have a decrease of around 2 min in $[t_f]$ (that is, a 37%) at a cost of an increase of 3.7 min in $E[t_f]$ (that is, a 1%).

Table 1. Average value and spread of the total flight time for different values of dp

dp	$E[t_f]$, [min]	$[t_f]$, [min]
0	386.17	5.36
5	389.86	3.40
10	396.98	2.59

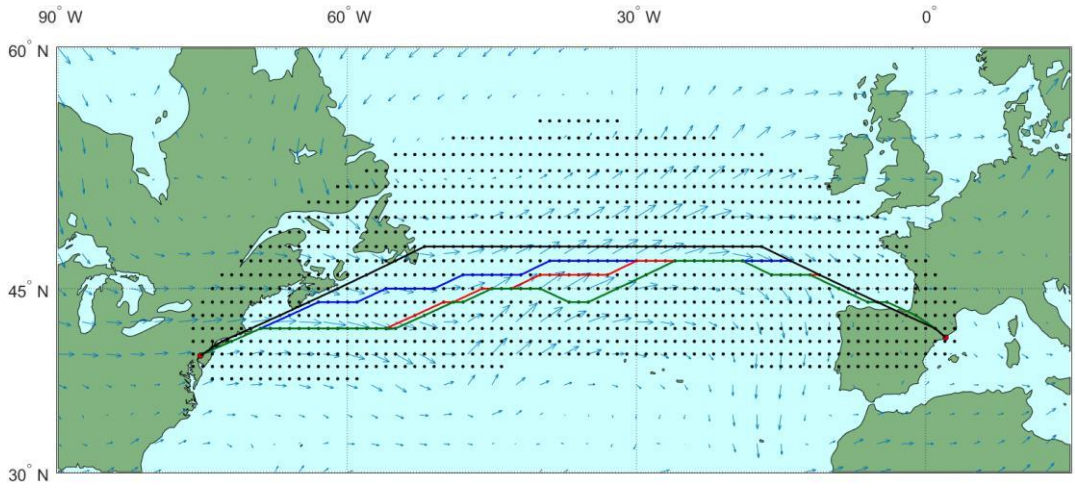

Fig.4. Optimal routes from KPHL to LEBL. $dp = 0$ (blue), $dp = 5$ (red), and $dp = 10$ (green); route of minimum distance (black); average wind field (blue arrows).

From a multi-objective optimisation point of view, any optimal aircraft path that minimises the objective in Eq. (4) is Pareto optimal with respect to the conflicting objectives $E[t_f]$ and $[t_f]$ because no other path can improve neither of the objectives without degrading the other one. In Fig. 5, the Pareto frontier is depicted for *dp* ranging from 0 to 10. This curve is very useful to present the results of the optimisation to the Airspace Users (AUs) in a clear and condensed form, and have the main advantage that the AUs can make a decision without revealing their cost structure.

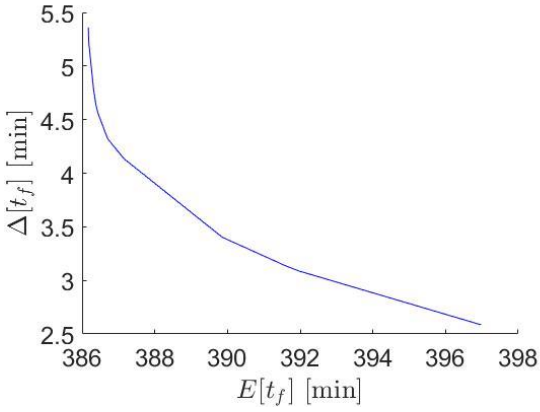

Fig.5. Trade-off analysis between efficiency and predictability: Pareto frontier.

CONCLUSIONS

In this paper, a stochastic methodology has been implemented, which is capable of finding the optimal aircraft path, considering a structured airspace, in the presence of uncertain winds provided by an EPS. Furthermore, the advantages of applying this methodology to obtain efficient and more predictable routes have been quantified.

With only minor changes, this methodology could be extended in the future to include temperature uncertainty, also provided by EPS. Additionally, this methodology can be extended to consider a time-dependent wind field, which is also left for future work. Nevertheless, such an extension would imply a considerable increase in complexity, because the time to fly a path could no longer be expressed as a linear function of the decision variable and the problem would become a Mixed-Integer Nonlinear Programming (MINLP) problem.

ACKNOWLEDGEMENT

The authors gratefully acknowledge the financial support of the Spanish Ministerio de Economía y Competitividad through grant TRA2014-58413-C2-1-R, co-financed with FEDER funds.

REFERENCES

González-Arribas, D., M. Soler, and M. Sanjurjo-Rivo, 2018, Robust Trajectory Planning Under Wind Uncertainty Using Optimal Control. *Journal of Guidance Control and Dynamics*. 41 (3): 673–688.

Steiner, M., C.K. Mueller, G. Davidson, and J.A. Krozel, 2008, Integration of probabilistic weather information with air traffic management decision support tools: a conceptual vision for the future, 13th Conference on Aviation, Range and Aerospace Meteorology, January 20-24, 2008. New Orleans, Louisiana, USA.

Dancila, B. D., and R. M. Botez, 2016. Geographic Area Selection and Construction of a Corresponding Routing Grid Used for in-Flight Management System flight trajectory optimization, *Institution of Mechanical Engineers, Part G: Journal of Aerospace Engineering*, 231 (5): 809–822.

Franco, A., D. Rivas, and A. Valenzuela, 2017, Optimal Aircraft Path Planning Considering Wind Uncertainty, 7th European Conference for Aeronautics and Space Sciences, July 3-6, 2017. Milan, Italy.

Gabrel, V., C. Murat, and L. Wu, 2013. New models for the robust shortest path problem: complexity, resolution and generalization. *Annals of Operations Research*, 207 (1): 97– 120.

EFFECT OF FORWARD VELOCITY ON RECTANGULAR WINGS FLAPPING WITH PIEZOELECTIRIC ACTUATORS

Fadile Yudum Comez
Middle East Technical University
yudum.comez@metu.edu.tr

Assoc. Prof. Dr. Dilek Funda Kurtulus
Middle East Technical University
funda.kurtulus@ae.metu.edu.tr

SUMMARY

In the current study, unsteady aerodynamic forces of two flapping rectangular w ings are investigated using two different materials namely, aluminum and plexigla ss . Two different materials used for the wings are intended to observe the effects of the wing flexibility on instantaneous aerody namic forces . A Lead Zirconate Titanate (PZT) piezoelectric actuator is u sed for flapping the wing models . The wind tunnel tests are performed with velocities ranging from 0m/s to 12 m/s . Output flapping frequencies are measured and compared for the wings investigated.

Keywords: flapping wing, wind tunnel, aerodynamic forces, piezoelectric actuator.

INTRODUCTION

The researches on aerodynamics of flapping wings are mainly based on theoretical, computational, and experimental fluid mechanics methods in recent years. To investigate infinitesimal forces generated by flap motion, some mechanisms might be designed and manufactured and equipped with force/torque sensors. There are lots of experimental studies on this topic. Li et al. (2014) designed a dual-differential four-bar mechanism to control 3 DOF flapping wings. They performed force and moment coefficients measurements in a wind tunnel. Two flapping wings are actuated by six brushless motors. Liu et al. (2012) designed a lightweight flapping-wing micro air vehicle (MAV). To investigate the effects of variations of parameters such as flapping frequencies and flap-pitch amplitudes, they performed also CFD analysis. Finally, the aerodynamic performance tests in a low turbulence and low Reynolds number wind tunnel are performed for verification of the numerical studies of the rigid and flexible flapping wings. Another recent research is focusing on the aerodynamic characteristics of a Bumblebee micro air vehicle (BMAV) developed by Thompson et al. (2015). They have also performed a wind tunnel test to measure aerodynamics coefficients. The angle of attack for the wing was ranged from - 10° to +25° and the wind speed was 12.88 m/s which corresponds to a Re=63000. The mechanism was manufactured using ABS plastic via rapid prototyping 3D printing. Kim et al. (2009) developed a flapping wing by using macro-fiber composite (MFC) actuators. The wing is tested inside the low-speed wind tunnel with the particle image velocimetry (PIV) setup. They particularly investigated the camber effect, the chordwise flexibility effect and the unsteady effects. Comez et al. (2015) investigated unsteady aerodynamic forces for bio-inspired flapping wings actuated with piezoelectric material. In the current study, two rectangular flapping wing models are used to investigate unsteady aerodynamic forces in a low speed wind tunnel. The wings are generated from aluminum and plexiglass materials to observe the effects of the wing flexibility on instantaneous aerodynamic forces. A PZT piezoelectric actuator is used for flapping the wing models to avoid a heavy flapping wing mechanism.

EXPERIMENTAL SETUP

The wind tunnel experiments are performed in the low Reynolds number wind tunnel of Aerodynamic Laboratory in Aerospace Engineering Department of METU. Fig. 1 shows the coordinates of the flapping wings and aerodynamic forces. The wing models are actuated with piezoelectric material are located at the intermediate level of the wind tunnel test section shown in Fig. 1.

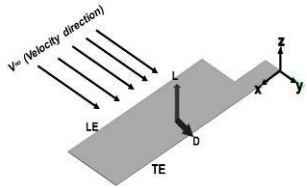

Fig. 1 Rectangle flapping wing and flow CAD model.

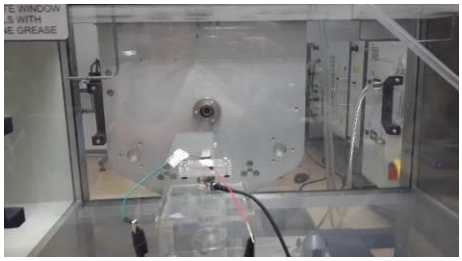
a)

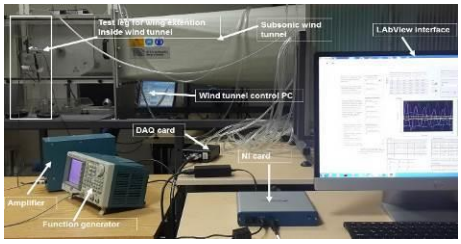

b)

Fig. 2 a) Wing model in the wind tunnel, b) Entire setup.

It is important to note that only the wings are placed into the wind tunnel in order to avoid disturbing the wind tunnel flow with the piezoelectric material cables, test leg body and force/torque sensor body.

In Fig. 2 experimental setup is shown. One of the components of the setup is 6 DOF ATI Nano force/torque sensor. It collects data via NI and DAQ cards. The other components of the system are the actuation suppliers for the piezoelectric material, function generator and amplifier. Function generator and signal amplifier generate a sinusoidal signal which is applied to piezoelectric material to obtain flapping motion of wing models. Final element of the mechanism consists of a control panel of the wind tunnel which includes 32 number of pressure measurement junctions and a software for the wind tunnel data.

RESULTS

Aerodynamics of two different flapping wings at a uniform flow are investigated in the current study. The experiment starts with 0 free stream flow velocity (hover) and increased up to 12 m/s. During the velocity increment, the aeroelastic effects can be observed clearly. To determine the natural frequency of the wing models, FFT analysis is performed and the results are listed in From FFT analysis, it is found that the output frequencies frequently lag behind the input frequencies at some flow velocities.

Table 1 with respect to the maximum amplitude output frequency values and plotted for some velocities in Fig. 3 and Fig. 4.

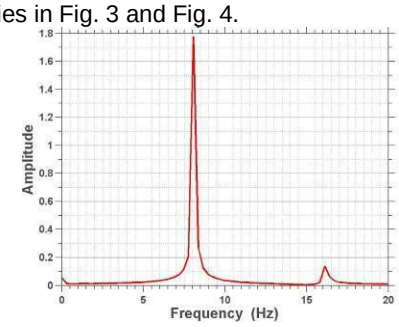

a) V_∞ =0 m/s, f_i=8.1 Hz, f_o= 8.06 Hz.

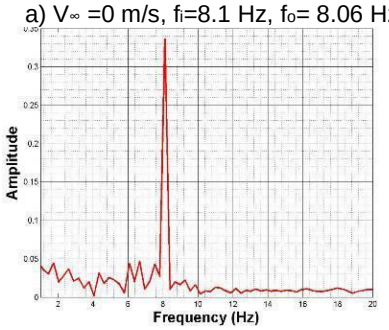

b) V_∞ =6 m/s, f_i=8.1 Hz, f_o = 8.116 Hz.

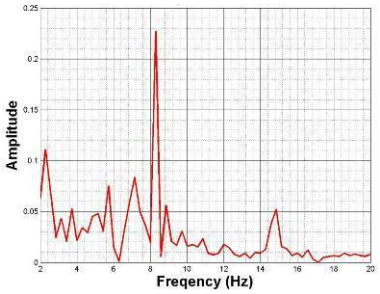

c) V_∞ =10 m/s, f_i=8.3 Hz, f_o = 8.286 Hz.

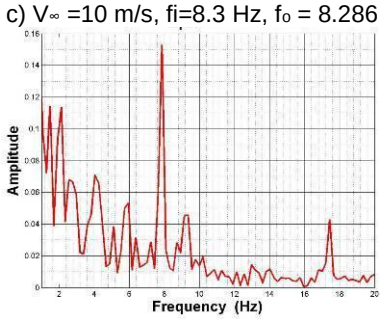

d) V_∞ =12 m/s, f_i=7.9 Hz, f_o = 7.872 Hz.

Fig. 3 Amplitude spectrum of the z- axis direction force of aluminum wing for different velocities.

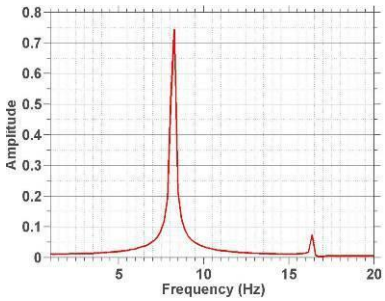

a) V_∞ =0 m/s, f_i=8.2 Hz, f_o = 8.283 Hz.

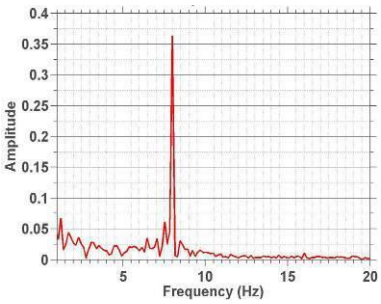

b) V_∞ =6 m/s, f_i=8 Hz, f_o = 8 Hz

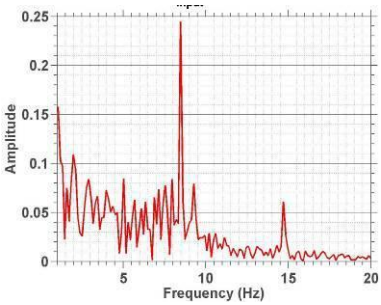

c) V_∞ =10 m/s, f_i=8.5 Hz, f_o = 8.477 Hz

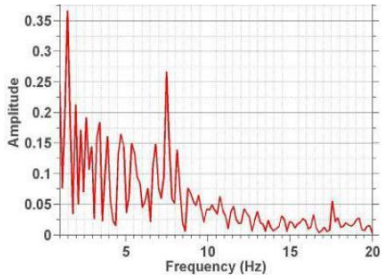

d) V_∞ =12 m/s, f_i=7.5 Hz, f_o = 7.48 Hz

Fig. 4 Amplitude spectrum of the z- axis direction force of plexiglass wing for different velocities.

From FFT analysis, it is found that the output frequencies frequently lag behind the input frequencies at some flow velocities.

Table 1. Aluminum and plexiglass rectangle wing input and output frequencies for different velocities.

V_∞ [m/s]	Input Frequency f_i [Hz]	Output Frequency f_o [Hz]	Difference % $(f_i-f_o)/f_i*100$
Aluminum			
0	8.1	8.06	0.49
2	8.2	8.125	0.91
4	8.1	8.108	-0.098
6	8.1	8.116	-0.197
8	8.2	8.158	0.51
10	8.3	8.286	0.16
12	7.9	7.872	0.35
Plexiglass			
0	8.2	8.283	-1.012
2	8.5	8.466	0.4
4	8.5	8.468	0.37
6	8	8	0
8	8.1	8.088	0.14
10	8.5	8.477	0.27
12	7.5	7.48	0.26

Lift force is generated (along z- axis) by flapping motion at uniform flow condition. To compare the lift forces of the wing models at different velocities, maximum peak frequencies are extracted from From FFT analysis, it is found that the output frequencies frequently lag behind the input frequencies at some flow velocities.

Table 1 and lift forces are investigated at these frequencies. It is imported to state that the flexibility characteristics of the wing materials are highly effective on the lift generation for low velocity values. When the velocity is increased gradually, the lift generation of the plexiglass wing is more contributed than the aluminum one with the increase of air velocity. However, when the velocity is reached to 12 m/s, both wing models show only the vibrating motion at maximum peak frequency values for each wing model.

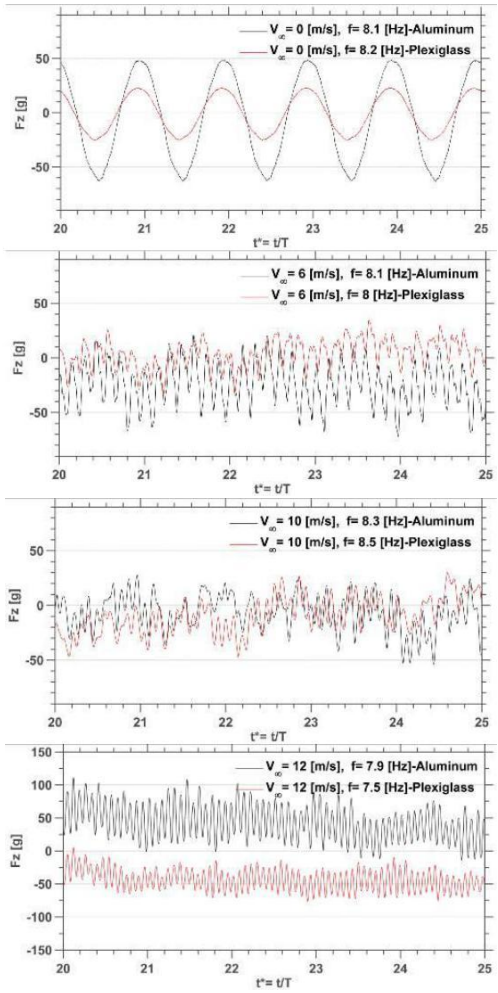

Fig. 5 Lift force at V_∞ =0, 6, 10, 12 m/s for aluminum and plexiglass wings.

In Fig. 6 and Fig. 7 mean C_l values are almost zero at V_∞=0 m/s for both wing models. It is important to note that flat plate rectangular wing models actuated with the piezoelectric material might not generate sufficient lift at hover case. To increase mean C_l values, wing models should have angle of attack or a camber. In addition, the mean lift coefficient fluctuates and increases with the increment of the uniform velocity.

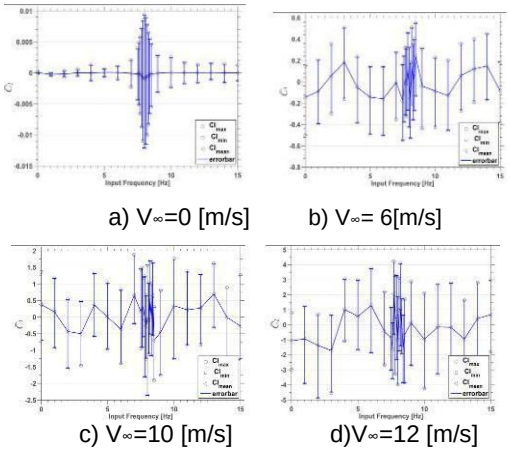

a) V_∞=0 [m/s] b) V_∞= 6[m/s]

c) V_∞=10 [m/s] d)V_∞=12 [m/s]

Fig. 6 Mean lift coefficient and amplitude of oscillations for aluminum wing model.

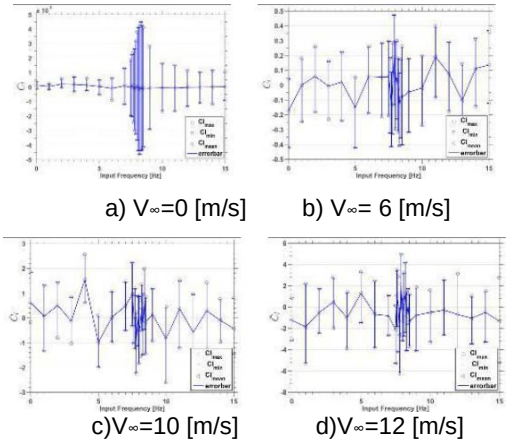

a) V∞=0 [m/s] b) V∞= 6 [m/s]

c)V∞=10 [m/s] d)V∞=12 [m/s]

Fig. 7 Mean lift coefficient and amplitude of oscillations for plexiglass wing model.

In Fig. 8, until 8 m/s freestream velocity, any significant contribution does not occur for the average of C_l value. After 8 m/s velocity, both C_l value almost doubles at 10 m/s for both wings and almost triple at 12 m/s. In Fig. 9, it is seen that the actuation of PZT material has maximum frequency at V∞=10 m/s, for both aluminum and plexiglass wings.

The resulting output frequency magnitude of the plexiglass wing model is larger than the aluminum one; but at 6 m/s and 8 m/s the frequency range of the plexiglass wing model is smaller than aluminum wing model.

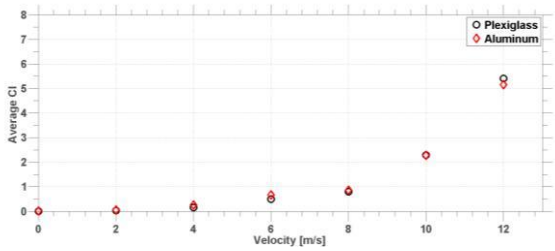

Fig. 8 Mean C_l versus velocity plot for aluminum and plexiglass wing models

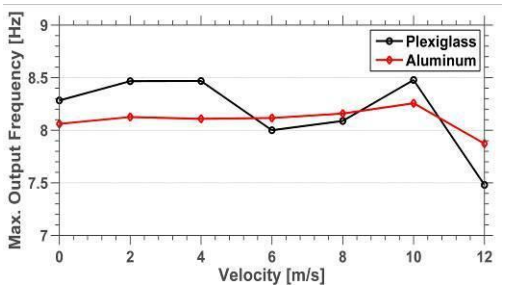

Fig. 9 Velocity versus maximum output response frequencies for both wings.

DISCUSSION

From the results, it can be clearly seen that plexiglass wing generates more lift than aluminum wing. When rigidity of the aluminum wing is considered, the incoming flow is increased, the flapping motion of the wing is mostly affected. It is also found that for both wings actuated PZT material gives a maximum frequency at V∞=10 m/s.

ACKNOWLEDGEMENT

This study was supported by 116M273 TUBITAK project.

REFERENCES

Comez F.Y., Kurtulus D.F., Senol M.G and Arikan K.B, 2015, Unsteady Aerodynamic Analysis of a Flapping Wing Actuated with PZT Material, Workshop on Non-Intrusive Measurements for unsteady flows and aerodynamics, October 27-29, 2015 Poitiers, FRANCE.

Li B., Song B., and Wang L., (2014), A Three-Dimensional Flapping Wing Mechanism for Wind Tunnel Experiments, 29th Congress of International Council of the Aeronautical Science, September 7-12,2014. St. Petersburg, Russia.

Liu, L., Zhang, X. and He, Z. (2012) Aerodynamic Analysis and Wind Tunnel Test for Flapping-Wing MAVs. *Journal of Theoretical and Applied Information Technology* Vol. 45 No.2: 542-550.

Thompson M. J., Burnett J., Ixtab Alan D.M., Tran D., Batra A, Rodriguez A, and Steele B. (2015) Experimental Design of a Flapping Wing Micro Air Vehicle through Biomimicry of Bumblebees, AIAA SciTech Forum, January 5-9, AIAA 2015-1454. Kissimmee, Florida, USA.

Kim D.K., Han J.H., and Kwon K.J., 2009, Wind tunnel tests for a flapping wing model with a changeable camber using macro-fiber composite actuators. *Smart Materials and Structures.* 18 (2009) 024008 (pp.1-8).

International Symposium on Sustainable Aviation 2018
4 – 6 June 2018
Rome, Italy

ISSA-2018-012

THE CONTRIBUTION OF EVTOL TO SUSTAINABLE URBAN AIR TRANSPORTATION

Vieira, Darli R.; Silva, Dreyfus
University of Quebec at Trois-Rivières, C.P. 500
Research Chair in Management of Aeronautical Projects
darli.vieira@uqtr.ca; dreyfus.silva@uqtr.ca

SUMMARY

This article will discus s the contribution of eVTOL (electric Vertical Take -off and Landing) aircraft technology to the sust ainable air transport in the urban environment . The eVTOL is a disruptive technology, which will become reality in the near future, bringing several advantages over conventional helicopters . The discussion will comprise a comparison of the major designs currently under development, their advantages and handi caps, and the challenge of civil certification .

Keywords: aviation, electric propulsion, eVTOL, urban air mobility, sustainable, green operation

1. INTRODUCTION

Shortly after the invention of the first heavier-than-air flying machines in the beginning of the 20th century, aviation pioneers started to pursue developing aircraft capable of vertical take-off and landing (VTOL), avoiding the need for runways. A huge technical evolution was made from the first practical helicopter, the Focke-Wulf Fw 61 (1938) (Watkinson, 2004), up to modern VTOL aircraft, like the Bell Boeing V-22 Osprey or AS350 helicopter, but the main design concepts were kept the same.

Figure 1. From the FW61 to the modern VTOL

Now, in the beginning of the 21st century, a technological revolution promises to insert VTOL aircraft in the life of regular people in the next 5 to 10 years (Uber, 2016). The responsible for this revolution is the eVTOL (electric VTOL) technology.

In October 2016, Uber issued a white paper named *Fast-Forwarding to a Future of On-Demand Urban Air Transportation* (Uber, 2016) which attracted attention from the whole aeronautical industry, describing its vision for the use of eVTOL vehicles for air transportation in the urban environment. Several organizations rushed to develop their eVTOL concepts to cope with Uber´s vision. The proposed designs vary a lot, but all of them are aimed to fulfill the so called UAM (urban air mobility) market, which comprises the transportation of passengers or small cargo, by the air, within the urban environment, or short commuter routes. This role is played nowadays by helicopters. But, despite their flexibility, helicopters have some handicaps that are vastly surpassed by eVTOL vehicles, when considering sustainable operation.

The use of eVTOL will push UAM towards an environmentally friendly operation, while providing higher levels of safety to users. But, the eVTOL technology has still to face huge challenges before coming to the market. It is possible to list a considerably big number of these challenges, but the lack of specific regulations for civil Certification seems to be the toughest to overcome, and was chosen to be addressed in this paper. The discussion will comprise the comparison of the major designs currently under development, their advantages and handicaps, and the challenge of obtaining civil Certification.

As there are no current commercial deployments of this technology, the research was conducted based on literature and public access information of the projects under development.

2. THE EVTOL SOLUTION TO UAM

2.1. The helicopter and UAM

The helicopter (a type of VTOL aircraft) plays an important role in the urban air mobility of some of the world´s largest metropolises (Cwerner, 2006), with unmatched flexibility. Helicopters are used for rescues, police enforcement, air ambulance, among other important services.

As helicopter flights started to popularize and take place within the urban environment, they quickly became a concern for these populations, especially when considering noise and air pollution. So, alternative solutions must be developed to contribute with the overall sustainability of urban air mobility.

2.2. The Convertiplane VTOL

The helicopter, which relies on rotary wings to provide 100% of its lift (and thrust) pays huge penalties during forward flight, when rotors are far less efficient than wings in the generation of lift (Walsh, Bingham, & Riley, 1987). In the late 1940´s, a new design appeared, aiming to mix the helicopter capabilities of vertical flight, with the better cruise efficiency of airplanes. This design was called the Convertiplane, a machine which

takes-off and lands vertically, using the lift generated by rotors, but tilts these rotors to produce forward thrust in cruise flight, relying on wings to generate lift (with much more efficiency).

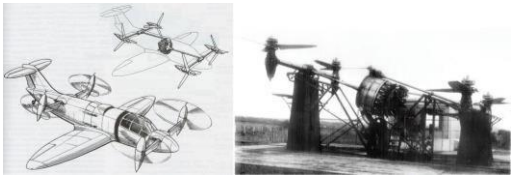

Figure 2. Heliconair HC-1, example of convertiplane

These convertiplane designs were mechanically far more complex than the conventional helicopters. And this is the reason why, despite convertiplane designs have been around for a while (especially for military applications), most of those programs have failed to enter on series production. The complexity of controlling the aircraft in the air, the high number of mechanical rotating parts (including complex transmission system) and the resulting high-weight/low-payload characteristics, are the main reasons why most past convertiplane designs never entered into service. But, at the last decades of the 20th century, new technologies made the Convertiplane VTOL a more practical solution. These technologies were fly-by-wire flight controls and composite materials. Complex mechanical transmission systems were still necessary, until the recent developments made on electric propulsion, giving birth to the concept of the eVTOL.

2.3. The eVTOL

The eVTOL is a category of VTOL aircraft that uses electric motors instead of ICE (Internal Combustion Engine), eliminating the need for complex mechanical transmission systems. There are several advantages when using electric propulsion on the VTOL. Some of the most important advantages are addressed below.

2.3.1. Distributed electric propulsion

Electric motors allow for DEP (Distributed Electric Propulsion) installations. DEP is the use of multiple rotors, each one directly driven by an electric motor, instead of just one main rotor (like in most helicopters) (Borer et al., 2016). DEP installations present graceful degradation, which means that single failures will degrade aircraft thrust and controllability only incrementally.

Figure 3. DEP on NASA GL10 Greased Lightning

DEP is possible due to the fact that electric motors are very efficient in a wide range of sizes, differently of ICE´s (Brown & Harris, 2018). So, it is possible to use multiple small electric motors, instead of a single (or few) ICE that relies on a transmission system to distribute torque to rotors.

The use of electric propulsion also presents the following advantages over ICE (Uber, 2016): higher power-to-weight ratio, possibility to use momentary emergency power in excess of 150% of MCP (maximum continuous power) in case of inoperative motors, lower number of moving parts (within the motor, and no need for transmission), better integration with fly-by-wire, lower noise generation, lower maintenance costs, zero operational emission of gases and a much better overall energy efficiency figure of around 10 times.

2.3.2. Environmental contribution of eVTOL

The operation of helicopters in urban areas brings clear environmental impacts, like noise and air pollution.

2.3.2.1. Noise pollution

Helicopters are perceived by the general population as a very annoying noise source (Amoroso, Castelluccio, & Maritano, 2012). Current helicopter designs present three main sources of noise (ICAO, 2015): the main rotor, the tail rotor (anti-torque) and the engine(s). For each type of helicopter, and each flight phase, one (or more) of these components plays a major role in the overall helicopter noise. For a classic design helicopter, two phenomena are also big contributors to helicopter noise (ICAO, 2015):

- HSI (High Speed Impulsive noise): cruising in high speeds, the helicopter forward speed adds to the advancing blade tip tangential speed, approaching transonic region, and generating shock waves;
- BVI (Blade Vortex Interaction): happens when blade tip vortex recirculates into main rotor and intercepts subsequent blades, creating the characteristic sound of “blade slapping”;

The eVTOL practically eliminates these noise-generating characteristics present in helicopters, due to:

- Use of DEP, with multiple small radius rotors instead of only one (or few) big rotors, practically eliminates HSI and BVI;
- There is no need for anti-torque tail rotors;
- No noisy reciprocating or turbine ICE´s;

2.3.2.2. Air pollution

The air pollution generated by Helicopter engines receives lower importance in the discussions on environmental impact of aviation, when compared to noise. But, these emissions cannot be neglected, due to the proximity to the communities where they happen and the toxicity levels of the emitted substances.

In addition to emitting greenhouse effect gases (like CO_2), helicopter turbines operation also generates a series of contaminating compounds, like: NO/NO_2, CO, unburned hydrocarbons, SOx, non-volatile particulate matter (nvPM), among others (ICAO, 2018). Also, reciprocating engines, like the ones used on the very popular Robinson R-

44 helicopters, use Avgas (100LL) as fuel, which contains TEL (tetraethyl lead) additive, highly poisonous to humans (Storino, 2014).

Due to the use of electric motors, eVTOL aircraft will present zero operational emission of polluting gases.

2.4. Main designs currently under development

2.4.1. Design complexity

The design complexities of the eVTOL aircraft under development can vary significantly depending on the chosen technical solutions. The Figure 7 shows a qualitative comparison of complexity levels of current eVTOL design choices.

Among all the different designs under development, the wingless multicopters present the lowest complexity due to the absence of tilting components (rotors or wings). This characteristic possibly explains the fact that some of the first eVTOL aircraft to perform manned flights were multicopters, like the Ehang 184 (see Figure 4), which is essentially a scaled-up multicopter drone, that has performed several manned flights since 2015 (Vertical Flight Society, 2018), and the Volocopter VC200, which performed its first manned flight in 2016 (Vertical Flight Society, 2018).

Figure 4. Ehang 184 and Volocopter VC200

An intermediary design, in terms of complexity, between the multicopter and the convertiplane is the Hybrid Lift+Cruise. These aircraft present a dedicated set of rotors used during vertical flight, like multicopters, and one (or more) horizontal rotor(s) dedicated to forward flight. No tilting components are used. During the cruise flight, the vertical rotors are stopped and 100% of the lift is obtained from fixed wings. The Kitty-Hawk Cora is an example of this kind of design (see Figure 5).

Figure 5. The Kitty-Hawk Cora Hybrid Lift+Cruise

Design complexity of eVTOL increase when tilting components are added. The *tilt rotors*, *tilt rotors+wing,* and *thrust vector* (examples in Figure 6) are the most complex to develop, due to the need of tilting the lift-generating components while transferring lift from rotors to the wings, during transition phase from hover to forward flight. These designs will possibly have the longest time to develop and fly prototypes.

Figure 6. Tilt rotor, tilt wing+rotor and thrust vector

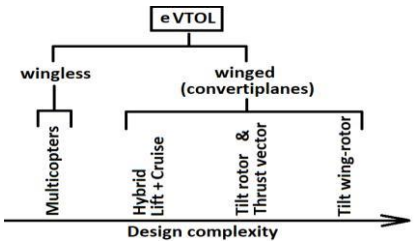

Figure 7. Main types of eVTOL designs under development and a qualitative complexity comparison

2.4.2. Performance and noise

Disc loading (weight of the aircraft divided by the total area of the rotors) is a key design parameter for any VTOL aircraft, as it affects its performance and noise related characteristics. In general, the lower the disc loading, the better the hover performance (less power necessary to maintain hover) (Uber, 2016). Conventional helicopters are examples of very low disc loading VTOL. Also, lower disc loading results in quieter hover characteristics (Brown & Harris, 2018).

Multicopters present some of the lowest disc loading values among eVTOL, resulting in better hover performance and lower hover noise levels. The low disc loading of the multicopters is generally achieved by using a large number of rotors. But, multicopters are not optimized for forward flight, presenting very low L/D (lift-to-drag) ratios, due to the absence of wings. So, multicopters are more suitable for short-range/low-speed applications.

The presence of wings significantly increases cruise performance of convertiplane eVTOL in relation to multicopters. The choice between tilting or non-tilting wings may play an important role in the hover-performance of these vehicles. A non-tilting wing is submitted to downwash from the rotors, reducing hover performance. This is why Tilt wing+rotor design presents better hover performance in relation to both Tilt Rotor and Hybrid Lift+Cruise designs. Lift+Cruise designs also pay a huge penalty in cruise flight, by carrying unused vertical motors and stopped rotors (drag).

Convertiplane designs can be equally employed in within-city-limits air service or inter-urban mid-range routes. But, the benefits that come from the use of wings and possibility to reach higher speeds, may not be perceived on very short trips.

On the other extreme, presenting very high disc loading, mixed with the use of wings, is the thrust vector design. The Lilium Jet (see Figure 6) is an example of this design. The small radius ducted fans used on the Lilium are tiltable between hover (vertical thrust) and cruise (horizontal thrust)

positions. In cruise position, this configuration tends to favor longer distances/higher speed applications. But, the higher disc loading may lead to higher noise levels in hover, which may become a concern for this kind of propulsion.

2.5. Type certification of eVTOL aircraft

No aircraft can operate commercially without a TC (type certificate) from a certification authority. FAA (Federal Aviation Administration) and EASA (European Aviation Safety Agency) are the main authorities under which most of the TC´s of the world are issued. Also, both entities cooperate closely to keep a high-level of harmonization between their regulations. Certification efforts of future eVTOL vehicles, must be made in cooperation with at least one of these two entities.

Differently from military certification (focused on mission requirements), civil certification is focused on demonstrating that the design complies with regulations that aim at guaranteeing the highest level of safety. So, it is expected that a new kind of aircraft, like the eVTOL, will be submitted to a considerable scrutiny before receiving a TC.

The discussions on the certification basis of these aircraft have already started, but due to the multiple types of designs, the definition of a single certification basis is a huge challenge for applicants and authorities. The certification basis for eVTOL aircraft is still not defined, and must be agreed between the manufacturer and the authority, based on the specificities of each design.

To illustrate the difficulties on meeting specific certification requirements, let´s pick the autorotation condition for helicopters, for example. Due to the rotors characteristics of most eVTOL multicopters (small radius, low mass), these vehicles will probably not be capable of autorotation, which is a condition under which helicopters must demonstrate to be controllable (FAA/EASA part 27 or 29, paragraph 27.143(a)(2)(v)).

Most eVTOL designs under development, present maximum take-off weight and passenger number that fit into part 23 (small airplane) or part 27 (normal category rotorcraft) certification. So, it is probable that a mix of part 23 and 27 regulations will be used for the certification of these eVTOL as ***special classes of aircraft***. The certification process of eVTOL may be addressed by *14 CFR part 21.17(b)* (special classes of aircraft), which defines that for those aircraft "*which airworthiness standards have not been issued…*" the applicable requirements will be *"…**portions** of those other airworthiness requirements contained in Parts 23, 25, 27, 29, 33, and 35, found by the FAA to be appropriate for the aircraft and applicable to a specific type design, or such airworthiness criteria as the FAA may find provide an **equivalent level of safety** to those parts*".

The FAA 14 CFR Part 23 regulations passed recently (0August 30, 2017) through a reformulation (amendment 64), which introduced the concept of Consensus Standards for the demonstration of means of compliance. According to AC23.2010-1 (FAA, 2017), Consensus Standards are *"…Industry developed standards the Administrator has accepted for use as a means of compliance to the part 23 regulations…*". This means that recognized non-governmental institutions like ASTM International and RTCA (Radio Technical Commission for Aeronautics), for example, can work together with manufacturers to propose alternative means to demonstrate compliance with part 23 requirements. EASA has harmonized with amendment 64 of part 23 and issued a revision of the CS-23 (amendment 5), effective since 1st April 2017.

3. CONCLUSIONS

In the last decade, the advances in electric propulsion made possible the concept of the eVTOL. These new types of air vehicles will rely on DEP to achieve lighter, less complex, safer and more environmentally friendly VTOL aircraft. eVTOL have many advantages over helicopters, like zero operating emissions of polluting gases and lower noise levels, making them more suitable for the use in the urban environment.

Several companies (and even government agencies) are rushing in this moment to develop eVTOL aircraft. This rush was triggered by UBER´s Elevate initiative (Uber, 2016).

eVTOL vehicles under development in the moment vary a lot in their design choices. These choices may affect significantly their complexity, performance and certification. Multicopters are the simplest kind of design to be constructed and prototyped, have the best hover performance, but pay huge penalties in forward flight. Convertiplanes present more complexity in their design, due to tilting components, but present the best performance in forward flight, due to the use of wings to generate 100% of lift.

The main challenge for the entry-into-service of these aircraft is the certification process. As there are no civil certification requirements for eVTOL aircraft, it is necessary that each manufacturer agrees with certification agencies (like FAA or EASA) the requirements to be fulfilled. A considerable effort is being made in this moment, among industry and authorities, to reach for a common basis to certify these aircraft for civilian use. The *14 CFR part 21.17(b) (Special Class of Aircraft), together with* Amendment 64 of FAR 23 or Amendment 5 of CS23 may be used as the point of start for the certification basis of some of these vehicles. So, it is probable that eVTOL designs that apply for certification with a part 23 approach (for winged designs), requesting classification under special class (21.17(b)), are more likely to reach certification earlier than a part 27 approach (like the case for the multicopters).

4. REFERENCES

Amoroso, S., Castelluccio, F., & Maritano, L. (2012). Helicopter operations: the environmental impact and ground facilities. Procedures and operational standards for the system's acceptance. Paper presented at the 4th International Conference HELI World 2012: Helicopter Technologies and Operations.

Borer, N. K., Patterson, M. D., Viken, J. K., Moore, M. D., Bevirt, J., Stoll, A. M., & Gibson, A. R. (2016). Design and performance of the NASA SCEPTOR distributed electric propulsion flight demonstrator. Paper presented at the 16th AIAA Aviation Technology, Integration, and Operations Conference.

Brown, A., & Harris, W. (2018). A Vehicle Design and Optimization Model for On-Demand Aviation. Paper presented at the 2018 AIAA/ASCE/AHS/ASC Structures, Structural Dynamics, and Materials Conference.

Cwerner, S. B. (2006). Vertical flight and urban mobilities: The promise and reality of helicopter travel. Mobilities, 1(2), 191-215.

ICAO. (2015). Helicopter Noise Reduction Technology, Status Report. Retrieved from

Storino, P. J. (2014). Leads Continued Use In Avgas.

Uber. (2016). Fast-Forwarding to a Future of On-Demand Urban Air Transportation. San Francisco, CA.

Walsh, J. L., Bingham, G. J., & Riley, M. F. (1987). Optimization methods applied to the aerodynamic design of helicopter rotor blades. Journal of the American Helicopter Society, 32(4), 39-44.

Watkinson, J. (2004). Art of the Helicopter. Oxford: Elsevier Butterworth-Heinemann.

AHS (American Helicopter Society), http://evtol.news/, accessed on April 2018

Voom, 2018, https://www.voom.flights/, accessed on April 2018

ICAO, 2018, https://www.icao.int/environmental-protection/Pages/Contaminants.aspx, accessed on February 2018

Fortune, 2018, http://fortune.com/2018/03/13/cora-kitty-hawk-flying-taxi-larry-page/, acessed on April 2018

Vertical Flight Society, 2018, http://evtol.news/aircraft/ehang/ , accessed on April 2018

Vertical Flight Society, 2018, http://evtol.news/aircraft/volocopter/ , accessed on April 2018

INVESTIGATION OF EMISSION EFFECTS OF THE TURBOFAN ENGINE UNDER LAND CLIMATIC CONDITIONS BY EXERGY APPROACH

Kateryna Synylo[2], M.Ziya Söğüt[1], T.Hikmet Karakoç[3]
[2] *Institute of Environmental Safety, National Aviation University, Kiev, Ukranie* [1]
Piri Reis University, Maritime Faculty,Tuzla, Istanbul, Turkey
[3]*Dep.Airframe and Powerplant Maintenance, Anadolu University, Eskisehir-Turkey*
[*]Corresponding author e-mail: mzsogut@gmail.com

SUMMARY

Aircraft engines, which can be defined as fossil fuel consuming mac hines, have significant environmental impacts due to their inefficiency, In this study, a performance study for the turbofan engines, which have become widespread engine for aircraft in recent years, was presented to demonstrate the effect of climate conditions on them. The study examined methodically the losses of the engine with the exergy approach directly related to the climate conditions . In the study, the engine exergy efficiency was calculated as 31. 28% and the effect of humidity condition of the air was found as average 1. 7% in engine performance. At the end of the study, some assessments on climate effects in engine performance were also presented .

Keywords: Aircraft, turbofan engine, thermodynamic analysis, efficiency, emission.

INTRODUCTION

Despite significant economic and social benefits the aviation brings, its activities also contribute to local air quality impact and relevantly affect the health and quality life of people living near the airports. Number of flights has increased by 80% between 1990 and 2014 and is forecast to grow by a further 45% between 2014 and 2035.

In 2012, aviation represented 13% of all EU transport CO_2 emissions, and 3% of the total EU CO_2 emissions. It was also estimated that European aviation represented 22% of global aviation's CO_2 emissions. Similarity, aviation now comprises 14% of all EU transport NOx emissions, and 7% of the total EU emissions. In absolute terms, NOx emissions from aviation have doubled since 1990, and their relative share has quadrupled, as other economic sectors have achieved significant reductions (Parker; 2009).

The aircraft emission inventory is usually calculated on the basis of certificated engine emission indices, which are provided by the engine manufacturers and reported in ICAO engine emission database. Under real circumstances, however, these conditions may vary and deviations from the certificated emission indices may occur due to impact such factors, as: the life expectancy (age) of an aircraft; the type of an engine installed on an aircraft; meteorological conditions.

In aircraft engines that consume fossil fuel, motor performance can be evaluated by thermal analyses in addition to power analyses. Particularly, in emission analyses evaluating the environmental effects, the effects based on the engine irreversibility comprise the directly engine based emissions. Therefore, thermodynamic analyses deal with the fuel based performance with respect to entropy generation and environmental effects in addition to analyses. The analyses based on the second law of thermodynamics, which is also referred as the entropy law, are dealt with multi-dimensionally in sectoral and scientific studies.

Aircraft engines are directly affected by the climate conditions of the environment they are in. Particularly under the atmospheric conditions of the aircraft during the flight processes, the thermo-physical conditions of the moist air have a direct effect on the fuel-air relation in aircrafts running on cycle basis. This effect may be shaped by the effect of excess air in the engine depending on the combustion process. In the combustion process, the air exchange may generate power and performance losses directly based on rich or lean combustion. This affects the directly engine based emission potentials. Scientific studies consider air directly to be theoretical air and it is dealt with independently from the thermo-physical climate conditions. In fact, the effect of the performance analyses to be carried out for the actual atmospheric conditions is important with regards to the evaluation of the actual effects.

This study first examines the performance of the referenced turbofan engine under atmospheric conditions. The main objective of this paper is exergy analysis for turbofan engine CFM 56-5C2/F, by using engine test data for stationary conditions on standing aircraft for different operational modes and meteorological conditions (air temperature, pressure and humidity).

TURBOFAN ENGINE AND INFLUENCE OF MOIST AIR ON THERMAL PERFORMANCE

Turbofan engines have design differences as turbine engines(Figure1). Particularly their first compressor rotor diameters, defined as fans, are bigger than the other engine types. This fan provides a two-way direction of air. The primary air flow is directed to the combustion chamber in inner cycle by compression while the secondary air flow, which is defined to be bypass air flow, is directed to the external surface of the engine from the edges of the fan rotor. The bypass ratio which is defined to be an important parameter, is expressed as the ratio of the bypass air to the internal air flow.

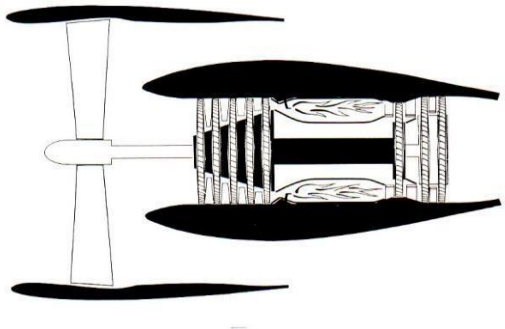

Fig.1 schematic section of fan jet engine(Kimerus,2018).

In turbofans, fans are considered to be low pressured compressor. The fan effect will gradually increase the pressure effect and improve the compressor effect. Another effect of these fans is their direct contribution to thrust generation. Particularly, at low speeds or altitudes, the momentum created by the fan strengthens the thrust generation of the engine. The generated thrust effect of the fan in big turbofan engines used in aircrafts such as B747, B757, B767, A300 and A310 are in the ratio of around 75%(Kimerus,2018).

Like in all engines, the performances of the aircraft engines are directly affected by the atmospheric conditions in flight processes. Almost all analyses are usually based on the standard atmosphere conditions (International standard Atmosphere–ISA) and these values are mainly as follows: the air pressure is 101325 Pa, temperature of an air is equal to 288.15 K, and the air density is 1.225 kg/m^3. These evaluations exclude and ignore the climate conditions or humidity values variations by altitude. However, as shown in Figure 3, only the temperature effect of the climate conditions have different values. This directly affects the aircraft performance.

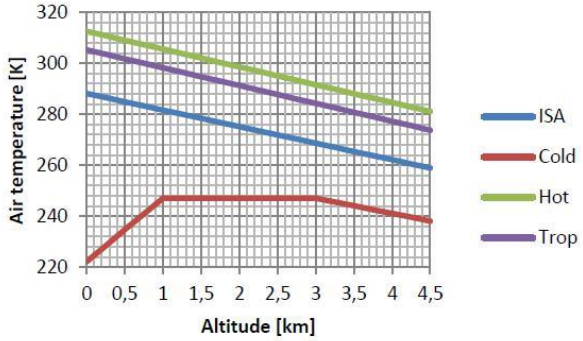

Fig. 3 Change of the air temperature with the altitude (Włodzimierz et al,2014)

In evaluations particularly for turbofan engines, for conditions lower than +35 °C it has a 12% higher effect and for conditions higher than +35 °C it has a 22% lower effect. In case, if that engine will operate from airport situated on altitude close to 4500 m, the thrust will be about 38% less than this can be achieved at the airport, located at sea level. In evaluations particularly for turbofan engines, it is observed that the thrust is directly affected. For conditions lower than +35 °C it has a 12% higher effect and for conditions higher than +35 °C it has a 22% lower effect. (Włodzimierz et al.,2014)

The thrust relation of engine with relative humidity is an important condition. Likewise, the relative humidity and thrust has a reverse change. While relative humidity at +30 °C goes with 100%, a decrease is observed in thrust. As shown in Figure 5, studies revealed this effect to be around 4%.

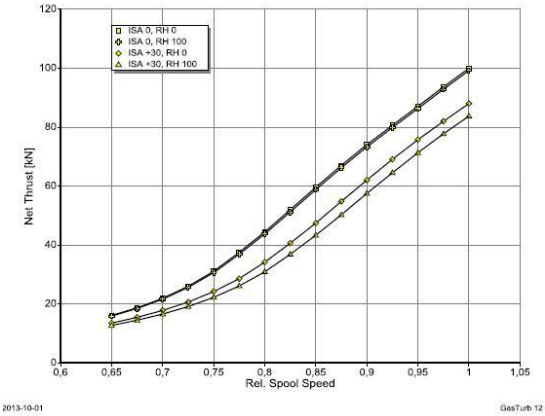

Fig. 5 Changes of the engine thrust with the relative speed N2 for a different relative humidity and OAT (generated by GasTurb 12 program) (Włodzimierz et al., 2014)

Measurement data of aircraft jet engine exhaust was obtained during cooperation between Lufthansa and IMK-IFU and has been used for the exergy analysis of turbofan engine CFM 56-5C2/F, which is usually mounted on aircraft A340-300 (Lufthansa AG, 2007). Engine tests were performed for stationary conditions on standing aircraft for different operational modes at Munich airport.

TURBOFAN ENGINE EMISSION DEPENDENCE ON ENGINE AGE, FUEL FLOW AND AMBIENT TEMPERATURE

Measured emission indices for CO and NOx under real operation conditions of engine tests of A340-300 were proceeded to find their dependence on operational period, engine fuel flow and ambient temperature.

Method of linear regression was used to analyze the measured EINOx, EICO and engine age (t_i). Figure 6, 7 demonstrates correspondingly the linear dependences of EICO at the idle mode (before and after engine test) and EINOx at the cruise mode on the operational hours (engine age), which are fitted in 0.95 prediction interval. Wide range of coefficient correlation is caused by high variation of EICO and EINO depending on operational period (between 166-13000 hours) of tested engines.

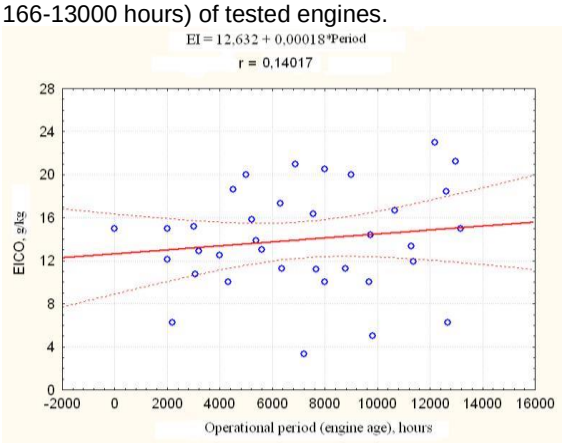

Fig. 6. Dependence of *EI*CO on operation hours of CFM56-5C2/F engine of A340-300 aircraft

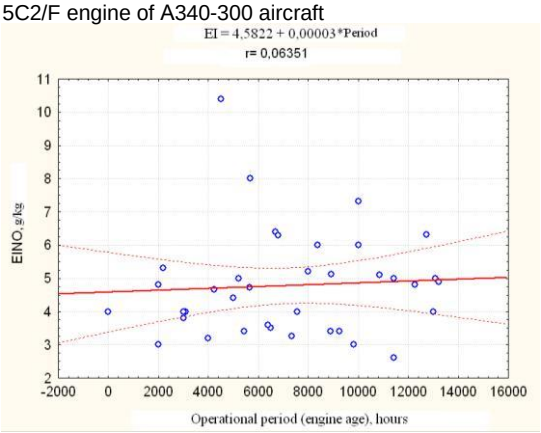

Fig. 7. Dependence of *EI*NO on operation hours of CFM56-5C2/F engine of A340 aircraft

Method of linear regression was also used to analyze the measured EINOx, EICO and ambient temperature (*t*a). On the basis of regression analysis results and evaluated correlation coefficients (*r* below 0.5), it was concluded the weak dependence of EICO and EINOx on ambient temperature. It can be explained by quite small volume of random sample (36 measurements) for considered investigation.

The regression analysis was done for measured *EI*NOx and fuel flow (*FF*) cruise mode. Figure 8 demonstrates correspondingly the linear dependences of *EI*NOx at the cruise mode on the fuel flow, which are fitted in 0.95 prediction interval. The evaluated determination coefficient R^2 obtains 0.112 and correlation coefficient r gets 0.335.

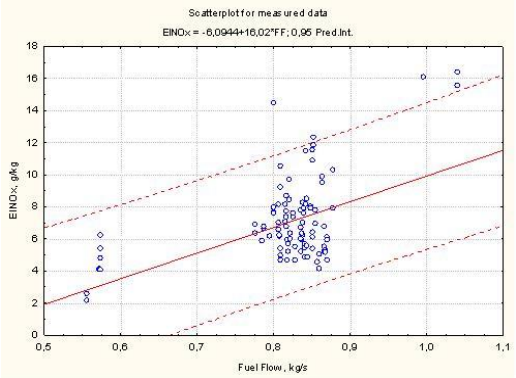

Fig.8. Dependence of *EI*NOx on measured fuel flow for cruise conditions of CFM56-5C2/F engine of A340-300 aircraft

Also it was found, that ffuel consumption index varies in a number of measurements performed in the range of ± 5%, but sometimes there is also an extreme deviation of this indicator, which may be due to sharply increased or decreased parameter of engine shaft rotation (it is used usually for as engine operation control parameter) for the investigated operating mode.

EXERGY APPROACH

Exergy is accepted as useful tool for the thermodynamic evaluation between a system and its surrounding can be considered as measure of the environmental impact related by entropy production. Analysis of some studies concerning assessment of engine performance in aviation sector highlighted, that exergy analysis method can be an effective indicator identify with equations given in Table 1. Besides, this method show that the aircraft engine emission impact on environment can be based on irreversibility (Dincer and Rosen, 2012).

Table 1 Equations of energy and exergy analysis

Name	Equations
Mass balance	$\sum \dot{m}_{in} = \sum \dot{m}_{out}$
Energy balance	$\sum \dot{E}_{in} = \sum \dot{E}_{out}$
	$\dot{Q} - \dot{W} + \sum \dot{E}_{in} - \sum \dot{E}_{out} = 0$
Exergy	$\sum \dot{E}x_i = \dot{E}x_k + \dot{E}x_p + \dot{E}x_{ph} + \dot{E}x_{ch}$
Exergy balance	$\sum \dot{E}x_{in} - \sum \dot{E}x_{out} = \sum \dot{E}x_{dest}$
Exergy work	$\dot{E}x_{work} = \dot{W}$
Exergy flow	$\dot{E}x_{mass} = \sum \dot{m}\psi$
	$\psi = (h - h_0) - T_0(s - s_0)$
Exergy destruction	$\dot{E}x_{dest} = T_0 \dot{S}_{gen}$
Energy efficiency	$\eta_I = \frac{\dot{E}_{out}}{\dot{E}_{in}}$
Exergy efficiency	$\eta_{II} = \frac{\dot{E}x_{out}}{\dot{E}x_{in}} = 1 - \frac{\dot{E}x_{dest}}{\dot{E}x_{in}}$
Improvement potential	$\dot{IP} = (1 - \eta_{Ex})\left(\sum \dot{E}x_{in} - \sum \dot{E}x_{out}\right)$

(Dincer and Rosen, 2012; Cornelissen, R.L. 1997; Moran et al. 2011; Van Gool, 1997).

RESULTS AND DISCUSSION

In this study, first, the energy and exergy analysis have been implemented for turbofan engine CFM 56-5C2/F. In addition, the engine performance under moist climate conditions has also been examined. The study is based on real test results. Reference climate conditions are 1 Atm pressure and ambient temperature. Figure 9 includes the humidity and temperature distributions in the environment.

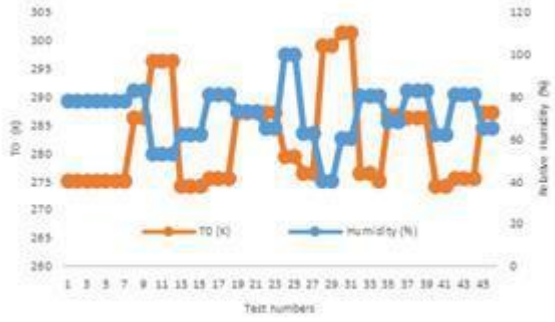

Fig. 9 T_0 and Relative humidity changes

Actual performance relation is directly associated with the intensity of the moist air. This affects the combustion air ratio necessary for the engine. The temperature and mass relation of the moist air has been studied in this aspect. The analyses revealed

that the most important effect was the effect of the moist air directly on the fuel air ratio. Figure 10 includes the relevant distribution of moist and dry air.

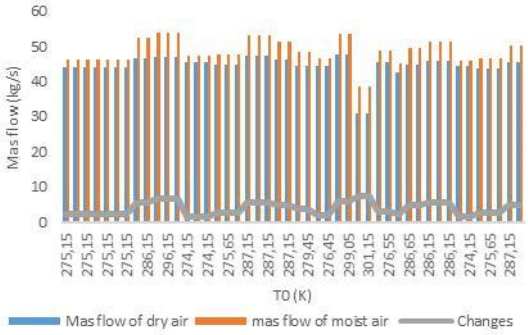

Fig. 10 Mass flow of dry and moist air

In the study, the moist air had a nearly 8.96% effect on the air requirement of the engine depending on the change fuel air ratio. This ratio has a 23.69% change effect with regards to peak values. This condition is important considering the effect of entry of not only the excess air but also the uncontrolled humidity.

Moist air condition has a characteristics that directly affects both energy and exergy efficiencies. The study examines this change primarily from the aspect of thermal efficiency change. Figure 11 includes the relevant performance distribution.

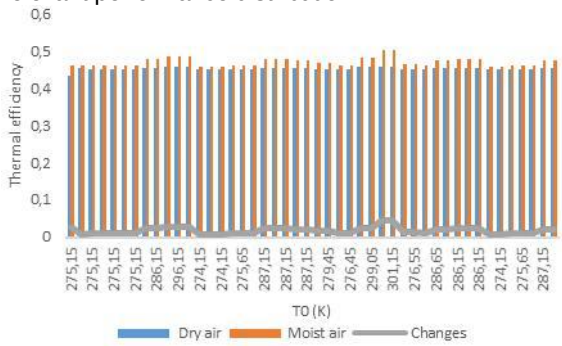

Fig. 11 Thermal efficiency based on dry and moist Air

In engineering analyses, the thermal efficiency analyses are based on the first law of thermodynamics and here air is considered to be the theoretical air. Accordingly, the average thermal efficiency was found to be 45.46%. However, thermal analyses were conducted according to the moist climate condition and the average thermal efficiency of the moist air was found to be 4.30%. This value was found to reach 9.72% under limit conditions. A difference of 4.03% was found between the average effects of the change according to the results of both analyses. In this case, such an error margin appeared in the analyses due to the effect of moist air.

In the definition of irreversibility in energy based analyses, the second law of thermodynamics is used directly which is referred to be the entropy law. In this regard, performance analyses of the engine were done particularly for the actual dead state conditions with results given in Figure 12 and exergy analyses displayed a distribution similar to the change of thermal efficiency.

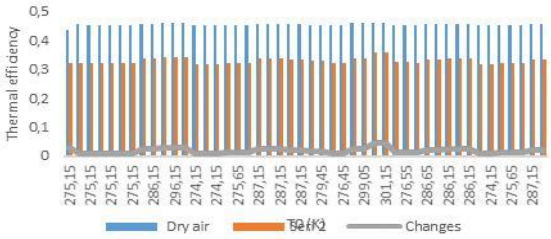

Fig. 12 Exergy efficiency based on dry and moist Air

According to the average values, the average exergy efficiency for dry air was found to be 31.25% and for moist air to be 32.98%. The difference between both average values was found to be 5.53%. This value was found to be 1361% for limit conditions.

CONCLUSIONS

Analysis results of the measured EINOx and EICO under engine (CFM56-5C2/F) testing conditions of A340 have demonstrated dependences of the emission indices on operational period (engine age, hours), fuel flow of the engine and ambient temperature. The results of exergy analysis identify that the exergy efficiency is a quite sensitive to the air humidity. Accordingly, the humid air effect causes an average change of 4.03% in thermal efficiency while this value corresponds to a difference of 5.53% in the exergy efficiency. This study reveals that the dry air analyses in engineering analyses or design processes have an important error margin. Therefore, humid air conditions will be provide a significant contribution.

REFERENCES

Cornelissen, R.L. (1997) Thermodynamics and Sustainable Development: The Use of Exergy Analysis and the Reduction of Irreversibility, PhD Thesis, University of Twente, The Netherlands

Dincer, I. Rosen, M. A. 2012. *Exergy: Energy, Environment and Sustainable Development*, Elsevier

John Golley (1997). *Genesis of the Jet: Frank Whittle and the Invention of the Jet Engine*. Crowood Press. ISBN 1-85310-860-X.

Kimerius, Airplane Turbofan Engine Operation and Malfunctions Basic Familiarization for Flight Crews, Kimerus Aircraft, 2018
http://kimerius.com/app/download/5781574190/Airplane+turbofan+engine+operation+and+malfunctions.+Basic+familiarization+for+flight+crews.pdf

Moran, M.J., Shapiro, H.N., Boettner, D.D. and Bailey, M.B. (2011) Fundamentals of Engineering Thermodynamics, John Wiley & Sons Inc., Hoboken, NJ, USA.

Parker R. From blue skies to green skies: engine technology to reduce the climate-change impacts of aviation. Technology Analysis and Strategic Management 21(1):61-78 · January 2009

Van Gool, W. (1997) 'Energy policy: fairy tales and factualities', Innovation and Technology Strategies and Policies, pp.93–105.

Abschlussbericht zum Kooperationsvertrag zwischen Forschungszentrum Karlsruhe GmbH-IMK-IFU und Deutscher Lufthansa AG–Umweltkonzepte Konzern "Messung von Triebwerksemissionen zur Untersuchung von Alterungsprozessen mit Hilfe optischer Messverfahren", 2007.

STEADY-STATE CFD ANALYSIS OF 3D BIO-INSPIRED FLAPPING WING MODELS

Murvet Bektas
Mechanical Engineering
TOBB University of Economics and Technology, Ankara, Turkey
mbektas@etu.edu.tr

Assoc. Prof. Dr. Dilek Funda Kurtulus
Aerospace Engineering
Middle East Technical University, Ankara, Turkey
funda.kurtulus@ae.metu.edu.tr

Prof. Dr. Mehmet Ali Guler
Mechanical Engineering
TOBB University of Economics and Technology, Ankara, Turkey
mguler@etu.edu.tr

SUMMARY

The aerodynamics of insects flying at low Reynolds numbers is considered for Micro Air Vehicles (MAV) designs . The aim of this study is to analy ze different flapping wing models and to predict generated forces and vortices around the wings . The analyses are significant for understanding properties of flying animals like birds, insects and for improving MAVs more. For three insect species (nam ely, bumblebee, hawkmoth, and hummingbird), three dimensional (3D) wing models are numerically analy zed at different angles of attack with 10° increments from 0° to 50° . The wings have various Reynolds numbers as 1338, 5560, and 10000, respectively depending o n their mean aerodynamic chord . Taking into account the computational results, the efficiencies of insect wings are determined by considering lift -to- drag ratios . The results are also compared with the studies in the literature, and Manduca Sexta wing which is a species of hawkmoth is found to be the most efficient wing model .

Keywords: flapping wing, bumblebee, hawkmoth, hummingbird, CFD analysis, steady-state.

INTRODUCTION

The forces occurred in-flight depend on both the motion of a wing and its 3D shape (Combes et al., 2003). When the wing motion is considered on a preferential basis, MAVs are divided into three parts as fixed, rotary, and flapping wings. In comparison with the others, the flapping wing models have more advantages properties such as being light and small in size, being efficient in low velocities, and working quiet (Kurtulus, 2017).

The sizes of the technological tools become smaller together with the developing technology, and also this leads micro sized unmanned aerial vehicles (UAV). To achieve the targeted micro dimensions, the wing characteristics of flying animal species in the nature are used as reference. When the wing shape is considered at low Reynolds numbers, smaller UAVs have lower Reynolds numbers as defined by Eq. (1)

$$\mathrm{Re} = U\bar{c}/\nu \quad (1)$$

where Reynolds number (Re) is based on the mean aerodynamic chord ($\bar{c}$).

For MAVs, there are different mechanism implementations in the literature (Mueller, 2001). The wing properties of flying animals like bees, moths, or birds are researched to be mimicked for this study.

METHODOLOGY

In the current study, the real wing shapes and flapping properties of flying insects and hummingbirds are investigated. Table 1 shows some of these properties from the literature (Sun and Du, 2003; Altshuler et al., 2004). This table includes the parameters: body mass *m*, wing length *R*, mean aerodynamic chord $\bar{c}$, wing aspect ratio *AR*, Reynolds number *Re* based on the mean aerodynamic chord, and stroke frequency *n.*

Table 1. Wing parameters for various species

Species	*m* [mg]	*R* [mm]	[mm]	*AR*	*Re*	*n* [s^{-1}]
Diptera (Sun and Du, 2003)						
Fruit Fly	0.72	2.02	0.67	6.00	75	254
Cranefly	11.4	12.7	2.38	10.7	251	45.5
Hoverfly	27.3	9.3	2.20	8.45	413	160
Dronefly	68.4	11.4	3.19	7.05	832	157
Coleoptera (Sun and Du, 2003)						
Ladybird	34.4	11.2	3.23	6.95	450	54
Hymenoptera (Sun and Du, 2003)						
Honey bee	102	9.8	3.08	6.37	1067	197
Bumble bee	175	13.2	4.02	6.35	1326	155
Lepidoptera (Sun and Du, 2003)						
Hawkmoth	1648	51.9	18.3	5.68	3852	26.3
Trochilidae (Altshuler et al., 2004)						
Humming-bird	3300	51.6	11.5	8.88	7000	200

Based upon the data in Table 1, information about the wing frequencies and wing sizes are observed. According to their flapping frequencies, Reynolds numbers, and sizes; wings of bumblebee, hawkmoth, and hummingbird are selected to be studied in the current paper. Their wing parameters are obtained in detail in Table 2.

In Table 2, BB01 and BB02 stand for worker bumblebees, and BB03 is for queen bumblebee (Dudley et al., 1990a,b); B27 is also a Bombus Terrestris species (Usherwood et al., 2002b); M1, F1, and F2 represent male and female Manduca Sexta species (Willmott et al., 1997 a,b); AC and SR are abbreviated form of Archilochus Colubris and Selasphorus Rufus (Altshuler et al., 2004). Especially, B27, Derived F1 (Usherwood et al.,

2002a), and about twice scaled SR (Altshuler et al., 2004) are mimicked for modeling Bombus Terrestris (*BT*), Manduca Sexta (*MS*), and twice scaled Selasphorus Rufus (*SR*) in the current study. Area of the wings and mean aerodynamic chord are approximately calculated by using Eqs. (2) and (3)

$$AR = (2R)^2 / (2S) \quad (2)$$

$$S = \int_0^R c\,dr = \bar{c}R \quad (3)$$

where S is the area of a single wing including fore- and hind wings.

Table 2. wing parameters for chosen species

Species	*R* [mm]	[mm]	*AR*	*S* [mm^2]
Bumblebee (Dudley et al., 1990a,b; Usherwood et al., 2002b)				
BB01	13.20	4.0244	6.56	53.122
BB02	13.70	4.0413	6.78	55.366
BB03	15.40	5.3287	5.78	82.062
B27	12.86	4.0696	6.32	52.335
Bombus Terrestris (current study)				
BT	12.86	3.9073	6.58	50.248
Hawkmoth (Willmott et al., 1997 a,b; Usherwood et al., 2002a)				
M1	48.50	18.3712	5.28	891.0038
F1	51.90	18.3717	5.65	953.4903
F2	52.10	18.8768	5.52	983.4819
Derived F1	52.25	18.4629	5.66	964.6864
Manduca Sexta (current study)				
MS	52.25	18.4613	5.66	964.6033
Hummingbird (Altshuler et al., 2004)				
AC	46.5	12.0466	7.72	560.168
SR	51.6	11.5116	8.88	594.000
Scaled SR	100.0	26.1438	7.65	2614.379
Selasphorus Rufus (current study)				
SR	100.0	26.9671	7.42	2696.711

The wing thicknesses are taken as 0.03 ϵ for BT and SR, and as 0.016 ϵ for MS. The left wing couple models used in the current study are shown in Fig. 1.

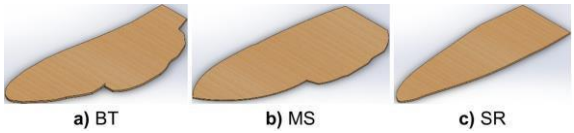

Fig. 1. Isometric views of wing models

Numerical Method

For 3D, steady, incompressible flow, the governing equations are Navier-Stokes equations as given in Eqs. (4)-(7) with eliminated inertial forces.

$$\frac{\partial u}{\partial x} + \frac{\partial v}{\partial y} + \frac{\partial w}{\partial z} = 0 \quad (4)$$

$$u\frac{\partial u}{\partial x} + v\frac{\partial u}{\partial y} + w\frac{\partial u}{\partial z} = -\frac{\partial p}{\partial x} + \mu\left(\frac{\partial^2 u}{\partial x^2} + \frac{\partial^2 u}{\partial y^2} + \frac{\partial^2 u}{\partial z^2}\right) \quad (5)$$

$$u\frac{\partial v}{\partial x} + v\frac{\partial v}{\partial y} + w\frac{\partial v}{\partial z} = -\frac{\partial p}{\partial y} + \mu\left(\frac{\partial^2 v}{\partial x^2} + \frac{\partial^2 v}{\partial y^2} + \frac{\partial^2 v}{\partial z^2}\right) \quad (6)$$

$$u\frac{\partial w}{\partial x} + v\frac{\partial w}{\partial y} + w\frac{\partial w}{\partial z} = -\frac{\partial p}{\partial z} + \mu\left(\frac{\partial^2 w}{\partial x^2} + \frac{\partial^2 w}{\partial y^2} + \frac{\partial^2 w}{\partial z^2}\right) \quad (7)$$

where u, v, w are velocities; x, y, z are directions; is the fluid density; p is the pressure; is the dynamic viscosity.

The lift and drag coefficients are also calculated by using Eqs. (8) and (9) respectively.

$$C_L = \frac{1}{\frac{}{2}} L \, {}^{2}S \quad (8)$$

$$C_D = \frac{1}{\frac{}{2}} D \quad (9)$$

For the computational analysis, a finite volume program (ANSYS/Fluent) is used. Around the wings, O-type unstructured mesh is created. The far field boundary is located at 20 ϵ away from the wing, and also 15 boundary layers are added from the wing surface. The computational domain for MS wing is shown in Fig. 2.

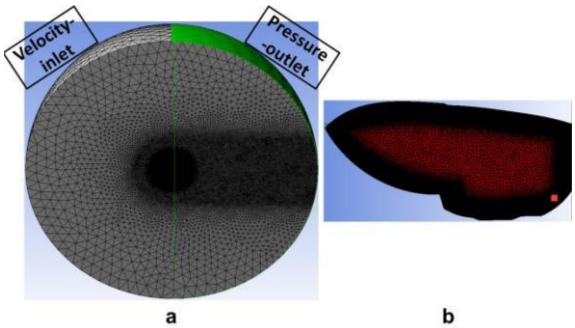

Fig. 2. Computational domain around MS wing

The half of outer domain is chosen as velocity-inlet at the upstream of the wing and as pressure-outlet at the downstream of the wing. The wing is defined as wall, and the face which connected to the wing is defined as symmetry. Boundary conditions for the free-stream velocities are 5 m/s, 4.668 m/s, and 5.414 m/s respectively for BT, MS, and SR wings to obtain Reynolds numbers as 1338, 5560, and 10000. 3D, pressure-based, steady-state, and laminar analyses are performed at different angles of attacks.

RESULTS AND DISCUSSION

The wings are numerically analyzed by applying the flow parameters from the literature (Dudley et al., 1990; Willmott et al., 1997b). To observe the most aerodynamically efficient wing, the maximum lift-to-drag ratios are indicated in Table 3. The numerical results are also compared with the experimental results in the literature.

Table 3. Maximum lift-to-drag ratio

	ρ [kgm^{-3}]	[*kg*/m-s]	*max* C_L/C_D (α=10˚ exp.)	*max* C_L/C_D (α=10˚ num.)
BT	1.23	1.7958* 10^{-5}	2.75 (Dudley et al.,1990b)	2.843 (current study)
MS	1.19	1.8445* 10^{-5}	4.0 (Willmott et al.,1997b)	4.436 (current study)
SR	1.225	1.7894* 10^{-5}	-	4.372 (current study)

Lift-to-drag ratio versus angle of attack curve for these wings investigated is shown in Fig. 3.

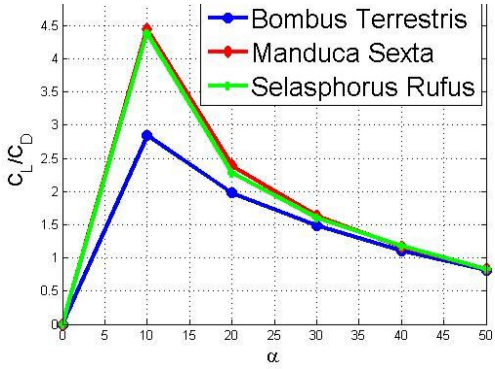

Fig. 3. C_L/C_D vs. α curve

Among the angles of attack analyzed, α=10° is the most efficient angle for all three wings investigated. From Fig. 3, it is also found that MS wing is the most efficient wing, and BT is the least efficient one.

By considering the lift coefficients, the numerical results (solid lines in Fig. 4) and experimental results available in literature (dashed lines in Fig. 4) are also compared in Fig. 4.

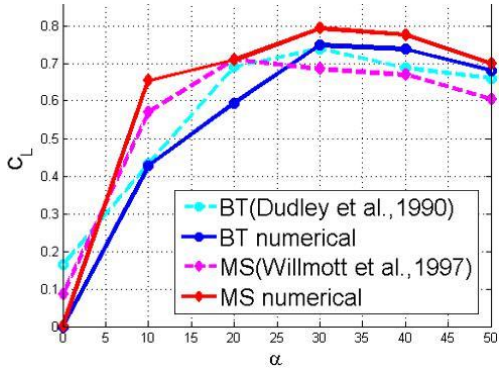

Fig. 4. C_L vs α curve

It should be noted that the wing thicknesses and the camber distribution were unavailable in references investigated. Therefore, the discrepancy between experimental and numerical results could be due to these effects. For both BT and MS wings, the lift coefficients increase from 0° until it reaches a maximum value at 30° angle of attack. After angle of attack 30°, they start to decrease. Considering the experimental and numerical results as shown in Table 3 and Fig. 4 the results give approximately same trends.

The static pressure distributions are also obtained at different angles of attack. For MS wing, the results at α=0˚ and α=10˚ are shown in Fig. 5. It is seen that high pressure is occurred at the lower surface, and it increases while angle of attack increases. In contrast, low pressure is occurred at the upper surface of the wings.

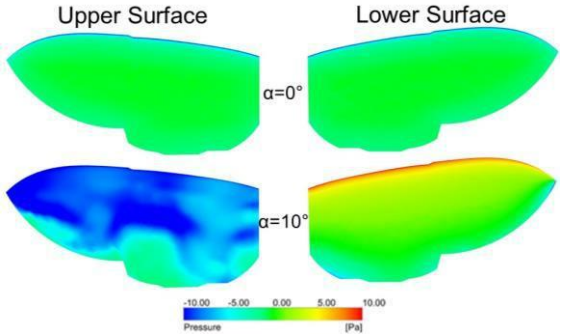

Fig. 5. Pressure distribution on MS wing

The difference between the high and the low pressure generates lift. At α=10°, leading edge vortex (LEV) creates a suction region at the upper surface of the wings. When the results are compared for 3 wings, SR wing has the most pressure change on its surface. LEV is more dominant and strong on the SR wing, so suction pressure is bigger at the upper surface of SR wing compared to other wings investigated in the current study.

To compare the vortex formation for each wing, according to Eq. (10), dimensionless Z-vorticity contours are presented in Fig. 6. The blue parts indicate negative vortices while the red parts indicate positive vortices.

$$ND = z\,c / U \qquad (10)$$

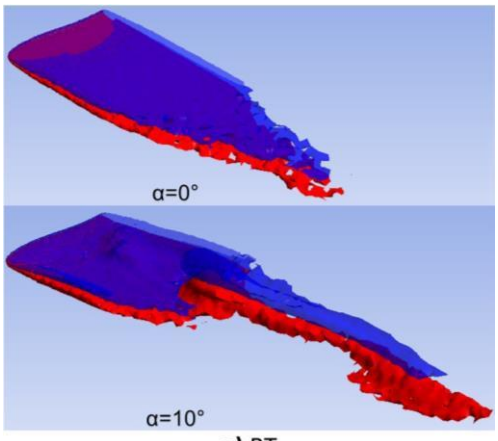

a) BT

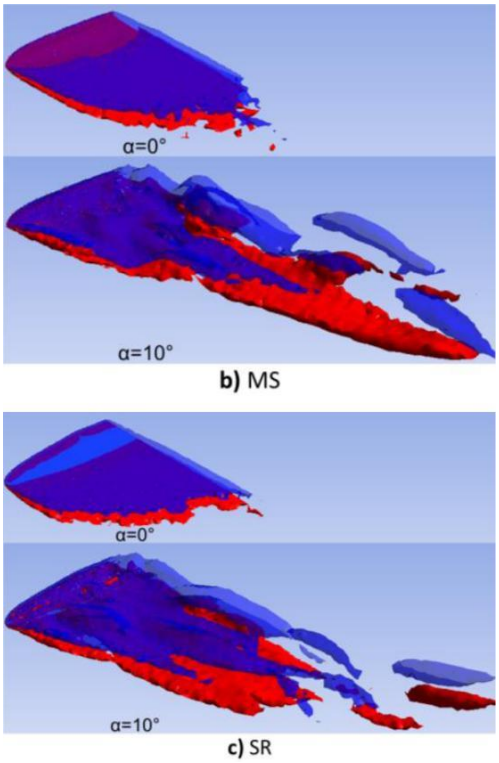

Fig. 6. Non-dimensional iso Z-vorticity contours

For all wings, C_L/C_D is obtained as a maximum value at α=10°. The vorticity contours reveal the wake for motion at the downstream of the wing at α=10° in comparison with α=0° in Fig. 6.

CONCLUSIONS

In this study, we have carried out CFD analysis of 3 different wings as Bombus Terrestris (BT), Manduca Sexta (MS), and scaled Selasphorus Rufus (SR) which are species of Bumblebee, Hawkmoth, and Hummingbird, respectively. These wings have different Reynolds numbers as 1338, 5560, and 10000, respectively depending on their mean aerodynamic chords. The numeric results are compared with the experimental results available in the literature. In addition, considering the lift-to-drag ratio, MS is found to be the most efficient wing type among the wings investigated. The pressure distributions are also obtained, and LEV formation is visualized to form suction region at the upper surface of the wings. Finally, non-dimensional iso Z-vorticity contours are observed for each wing.

ACKNOWLEDGEMENT

This work is supported by TUBITAK Project No: 116M273.

NOMENCLATURE

AR Aspect Ratio
– Mean Aerodynamic Chord, mm
C_D Drag Coefficient
C_L Lift Coefficient
CFD Computational Fluid Dynamics
D Drag, N
L Lift, N
LEV Leading Edge Vortex
m Body Mass, mg
MAV Mikro Air Vehicle
n Stroke Frequency, s^{-1}
p Static Pressure, Pa
RWing Length, mm
Re Reynolds Number
S Wing Area, mm^2
U Free Stream Velocity, m/s
UAV Unmanned Aerial Vehicle
u,v,w Velocity Components, m/s
x,y,z Directions
3DThree-Dimensional

Greek Letters

α angle of attack, degree
μ dynamic viscosity of air, kg/m-s
kinematic viscosity of air, m^2/s
mass density of air, kg/m^3
ω_{ND} Non-Dimensional Vorticity
ω_ZZ-Vorticity, s^{-1}

REFERENCES

Altshuler, D. L., Dudley, R., and Ellington, C. P., 2004, Aerodynamic forces of revolving hummingbird wings and wing models. *Journal of Zoology*, London, 264, 327-332.

Combes, S. A. and Daniel, T. L., 2003, Flexural stiffness in insect wings. I. Scaling and the influence of wing venation. *Journal of Experimental Biology*, 206, 2979-2987.

Dudley, R. and Ellington, C. P., 1990a, Mechanics of forward flight in bumblebees. I. Kinematics and morphology. *Journal of Experimental Biology*, 148, 19-52.

Dudley, R. and Ellington, C. P., 1990b, Mechanics of forward flight in bumblebees. II. Quasi-steady lift and power requirements. *Journal of Experimental Biology*, 148, 53-88.

Kurtuluş, D. F., 2017, MHA tasarımlarına ilham veren kanatlı böceklerin uçuş özellikleri. *Sustainable Aviation Research Society*, 2(2): 66-75.

Mueller, T. J., 2001, Fixed and flapping wing aerodynamics for micro air vehicle applications, Volume 195.

Sun, M. and Du, G., 2003, Lift and power requirements of hovering insect flight. *Acta Mechanica Sinica*, Volume 19 Number 5.

Usherwood, J. R. and Ellington, C. P., 2002a, The aerodynamics of revolving wings. I. Model hawkmoth wings. *Journal of Experimental Biology*, 205, 1547-1564.

Usherwood, J. R. and Ellington, C. P., 2002b, The aerodynamics of revolving wings. II. Propeller force coefficient from mayfly to quail. *Journal of Experimental Biology*, 205, 1565-1576.

Willmott, A. P. and Ellington, C. P., 1997a, The mechanics of flight in the hawkmoth Manduca sexta. I. Kinematics of hovering and forward flight. *Journal of Experimental Biology*, 200, 2705-2722.

Willmott, A. P. and Ellington, C. P., 1997b, The mechanics of flight in the hawkmoth Manduca sexta. II. Aerodynamic consequences of kinematic and morphological variation. *Journal of Experimental Biology*, 200, 2723-2745.

ISSA-2018-015

ELECTRIZATION OF THE RT AVIATION FUEL AS A TECHNIQUE TO GENERATE THE HIGH VOLTAGE ELECTRIC POWER

Ihor. L. Trofimov, Andrian A. Iavniuk,
National Aviation University
Kosmonavta Komarova Ave. 1, Kyiv, Ukraine, UA-03058
troffi@ukr.net, a_yavnyuk@ukr.net

SUMMARY

Generating electric power due to charges differentiation in RT aviation fuel, as well as the application of static electricity charges, to have profitable effect, are discussed in the paper. Development of technological method and installation for generating the electric power due to charges differentiation in dielectric liquids, is described .

Keywords:electrization, electric power generation, static electricity, discharging.

Due to energetic problems escalation, new energy sources and required raw materials search becomes an actual problem. These sources have to satisfy the human heat and electric power demands completely, and they should not contaminate environment, as well as to be easy operating and safe. Researchers of all the countries try to create alternative fuels and to find the alternative energy sources, as opposed to traditional hydrocarbon fuels.

It is known about frequent occurrence of electrostatic charges in different industries [1, 2]: chemical, textile, pulp-and-paper ones, in surgical clinics, coal mines, transportations, etc. According to statistics, damage due to static electricity, for example in the USA industries operating dusts of different substances, achieves 100 $ millions per annum. The most frequently electrization occurs in the industries producing and consuming the huge amounts of volatile flammable liquids. This is the reason why the greatest oil companies, such as “Shell” and “Esso”, were among pioneers of careful investigation of the oil products electrization. These companies are of the first ones who created specific laboratories for investigation of the origins of static electricity appearance and improvement of the electrization reduction techniques.

Hence, significant electric energy source, such as static electricity, should be of high attention. The problems appeared in energy carrier market, obligate not to reduce the static electricity, but to develop the techniques of its profitable application. The use of static electricity occurrence in technological equipment, due to charges distribution when dielectric liquid friction with the equipment surface, is innovative technique and it may have profitable effect, because of insignificant energetic losses and small amounts of required oxidation agents. It is an actual problem nowadays.

Problem formulation. The aim of this work is to investigate the phenomenon of the RT (JET-A analogue) aviation fuel electrization, and to substantiate the possibility of the static electricity application to generate the electric energy due to charges distribution in dielectric liquids.

Carried out research [3] shows that pure liquids of specific volumetric conductivity $\sigma_V = 10^{15}$ Sm m^{-1}, are electrized poorly. With the increase of the liquid conductivity, electrization current increases at constant liquid flow velocity, then it achieves the highest value and reduces up to zero values of $\sigma_V \approx 10^7$ Sm m^{-1}. The increase of elecrization current with the increase of the liquid conductivity may be reasoned by the inner ion concentration growth.

That is why, conductivity growth in certain range may lead to increase of the electrization current. From the other point of view, the conductivity increase leads to the reduction of the double layer thickness, and, as a result, to the reduction of electrization current, which tends to zero at 10^7 Sm m^{-1} conductivity. The electrization current increases also with the growth of the liquid flow speed. Roughness of the pipeline walls enhances the liquid electrization in 1.8-5 times. Extremely higher electrization (in 10-200 times greater than in pipelines) appears in the aviation fuel filters, which have the most rough surface due to specific design. Particularly, high electrization occurs in reusable filters, because of adsorbed fuel addition agents on their parts. It extends the surface, which contacts with the flowing liquid. Due to the same reasons, intensive electrization appears when liquid flows through pumps, losses indicators, measuring hoppers, cocks, gate valves, valves.

Electrization increases in 1.8-4 times when mixing fuel with the nitrogen, and depends on the introduced nitrogen amount. Electrization enhancement occurs in liquids containing fine-dispersed admixtures, dross particles, water, air.

As a result of research, new device for high voltage electric power generation (fig. 1) was designed and tested [4]. It is based on efficient use of the static electricity charges, obtained with the help of INSET when hydrocarbon fuels operation.

Designed installation should solve following tasks: 1. By means of design simplification and making the device economically efficient – to provide the generation of high voltage electric power, to enhance the efficiency of the application of the static electricity reduction devices. 2. Improvement the technique of high voltage electric power generation by means of electrostatic charges trapping from the technological equipment, operation of which is connected with the hydrocarbon fuels; to provide the generation of high voltage electric power without significant energetic losses and oxidation agents application; to solve the problem of static electricity charges completely at the industries operating dielectric liquids in pipelines.

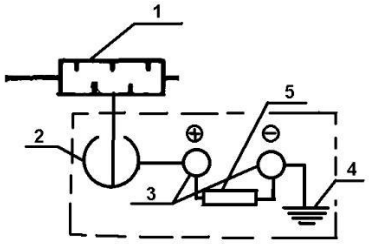

Fig. 1. High voltage electric power generating installation: 1. INSET. 2. Hollow metallic sphere. 3. Discharger. 4. Ground connection. 5. Loading.

The installation operates as follows: static electric charges accumulate in the parts of technological equipment and with the help of INSET 1 they are transmitted into metallic sphere 2, and then – to the discharger 3, one end of which is connected with the sphere 2 and another one – with the earth 4. Loading 5, tension in which leads to electric current appearance, is connected with discharger 3. By changing the amount of clearance of electric discharger, one can determine required potential in the metallic wall 2. If dangerous potential achievement, then air discharging is carried out. To do it, discharger 3 is grounded.

Thus, electrization itself and electrization objects were investigated, opportunity to generate the electric power due to charges distribution in dielectric liquids, application of the static electricity as the electric power source, was grounded. Innovative installation and technique of high voltage electric power generation, due to charges differentiation in aviation

fuels, were designed. Realization of innovations should provide the mankind with chap electric energy. Another advantage is that the use of proposed technology will help to reduce the static electricity in fire-hazardous and dangerously explosive areas efficiently.

REFERENCES

Fasone, V. and Maggiore, P., 2014,Airport development and sustainability: a case of multi-airport system in Italy. *International Journal of Sustainable Aviation*1:13-24. *(for Journal)*

Dahlquist E., E. Thorin, and J. Yan, 2006,Alternative Pathways to a Fossil-Fuel Free Energy System in the Mälardalen Region of Sweden, International Green Energy Conference II, June 25-29, 2006. Oshawa, Ontario, Canada.*(for Conference)*

http://www.proektant.kz/content/52.html

http://www.ngpedia.ru/id611768p1.html

Trofimov I.L. Research electrization of aviation fuels/ I.L. Trofimov / I.L. Trofimov, L.S. Veryagina, L.B. Prymak // THE SEVENTH WORLD CONGRESS “Aviation in the XXI-st centure”, “Safety in Aviation and Space Technologies”, (September 19 – 21, 2016). – Kyiv, Ukraine. – Volume 6, p. 6.21. – 6.31. (*for Conference*)

Pat. 13487U Ukraine. H02N 1/00, H02H 1/06. Installation for high voltage electric power generation / O.M. Zubchenko, I.L. Trofimov, I.A. Kravets. – Valid from 17.04.2006.

International Symposium on Sustainable Aviation 2018
9 – 11 July 2018
Rome, Italy
ISSA-2018-016

COMPUTATIONAL AND EXPERIMENTAL STUDY ON A VARIABLE CAMBER WINGLET

João Paulo Eguea and Fernando Martini Catalano and Alvaro Martins Abdala
University of São Paulo
Av. Trabalhador São Carlense 400, São Carlos, São Paulo, 13566-590, Brasil
Email: joao.eguea@usp.br Email: catalano@sc.usp.br Email: pfalvaro@sc.usp.br

The capability of morphing structures to adapt aerodynamic shape for optimal condition in flight brings potential reducing of aircraft operating fuel consumption. A genetic optimization algorithm is used to optimize the winglet sections camber of midsize business jet aircraft reducing the total drag up to 0.58% when compared to the fixed geometry winglet. Wind tunnel experimental work was carried-out using aerodynamic balance and flow mapping with seven-hole pressure probe to investigate the effects on the aerodynamic forces and tip vortex structure of winglets geometries optimized for climb and cruise conditions. The winglets increase the wing effective aspect ratio by reducing the vortex size and strength resulting on wing total drag reduction on the optimization region. The balance data is fitted to a parabolic drag equation and the induced drag is calculated by the Maskell's equation show similar values, differing in less than 11% from each other.

Keywords: winglet optimization, morphing structures, genetic algorithm.

INTRODUCTION

The International Civil Aviation Organization (ICAO) fuel efficiency improvement goal shows the aviation industry increasing concern on the industry impact on environment. Technologies capable of improving aircraft aerodynamic efficiency are key solutions to reach the yearly 2% fuel efficiency improvement until 2020 proposed by ICAO.

Induced drag can account for about 40% and 80% of total drag in cruise and climb conditions, respectively (Kroo, 2005). Winglets are wing tip devices capable generate additional traction by taking energy from the wing tip vortex flow. Whitcomb (1976) showed that using winglets reduced the induced drag by 20%, increasing the lift to drag ratio (L/D) by 9%. However, the winglets are designed with a fixed geometry optimized for a overall mission performance. This does not mean that the design has optimum performance to every flight phases. Morphing structures that adapt the aircraft geometry to different flight conditions can improve the airplane performance and be used for airplane control (Barbarino et al.,2011).

This combines the concept of morphing structure and winglets, showing a preliminary analysis of a variable camber winglet. The morphed sections are based on the mechanism developed by Martins and Catalano (2003). A genetic optimization algorithm is used to optimize the winglet geometry maximizing the L/D of a midsize business jet for climb and cruise conditions. The results showed an improvement of up to 0.5% on the fixed geometry winglet optimized for the mission overall.

The optimum winglets geometries aerodynamic coefficients and wake velocities are measured on a wind tunnel experiment. The winglet optimized for light cruise condition showed the best performance on the optimization zone, reducing the wing total drag up to 13.3% when compared to a wing with no winglet. The induced drag is calculated using the Maskell's equation and the wake velocities map (Ganzevles et al., 2002). The obtained results are coherent with the induced drag calculated by fitting the balance data to a parabolic drag equation.

METHODOLOGY

The genetic algorithm is a metaheuristic method capable of finding the near optimum solution for complex multidisciplinary optimization problems. The genetic algorithm optimization method is based on the natural selection. An initial random population is generated where the gens on an individual represent different variables. All the individuals are evaluated using the objective function. A percentage of the best individuals of the current population are pre-selected for reproduction (elitism). A roulette wheel selection is performed based on the individual's fitness. The selected individuals are mated and change parts of their genetic code (crossover). Some parts of the new individuals are randomly changed to ensure genetic
variability (mutation), avoiding premature convergence to a local optimum. This process is repeated for the new generation until a convergence criterion is reached. Number of generations and difference between the population's best and worst fit individual are the most common convergence criteria. The method is independent of the objective function shape, being suitable for different nature optimization problems. The method characteristics made it the chosen optimization algorithm for this work.

The genetic algorithm was used to find the winglet geometry with the highest L/D for the flight conditions on Table 1. The angle of the leading and trailing edge of five sections were changed as shown on

The aerodynamic analysis was performed using the full potential model with 3D boundary layer corrections solver implemented on the BLWF software (Johnson et al., 2005). BLWF has a couple mesh generator. The software gives the aerodynamic coefficients and lift distribution over

the wing span. It allows fast aerodynamic simulations for wing-body configurations on transonic flows.

Table 1. Flight conditions used on winglet geometry optimization

Condition	Climb	Heavy cruise	Light cruise	Mid cruise
C_L [-]	0.5150	0.4885	0.4525	0.4165
Re [-] (x10^6)	14.8	9.75	9.75	9.75
Mach [-]	0.6	0.75	0.75	0.75

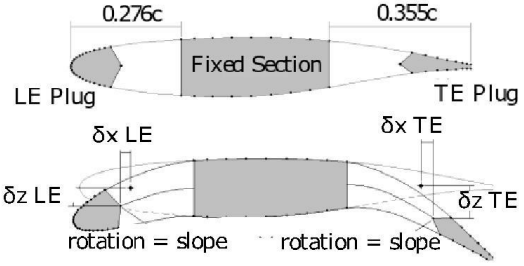

. Every gen defines the angle of the section leading or trailing edge angle.

The aerodynamic analysis was performed using the full potential model with 3D boundary layer corrections solver implemented on the BLWF software (Johnson et al., 2005). BLWF has a couple mesh generator. The software gives the aerodynamic coefficients and lift distribution over the wing span. It allows fast aerodynamic simulations for wing-body configurations on transonic flows.

Table 1. Flight conditions used on winglet geometry optimization

Condition	Climb	Heavy cruise	Light cruise	Mid cruise
C_L [-]	0.5150	0.4885	0.4525	0.4165
Re [-] (x10^6)	14.8	9.75	9.75	9.75
Mach [-]	0.6	0.75	0.75	0.75

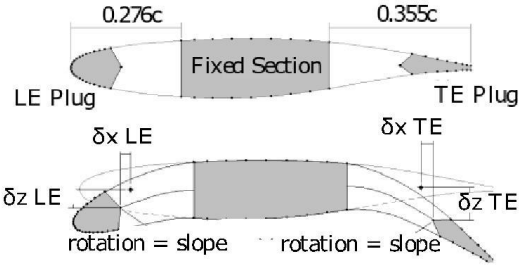

Fig. 1. Camber morphing system representation (Martins and Catalano,2003)

The midsize business jet geometry used on this research is shown on Fig. 2. The dimensions are in millimeters. The main geometry characteristics are listed on Table 2. Only the wing, winglet and body were used on the study.

Table 2. Main aircraft dimensions

Span [m]	19.7
Wing area [m^2]	42.5
Aspect ratio [-]	9
Mean Aerodynamic chord [m]	2.67
Tapper ratio [-]	0.24

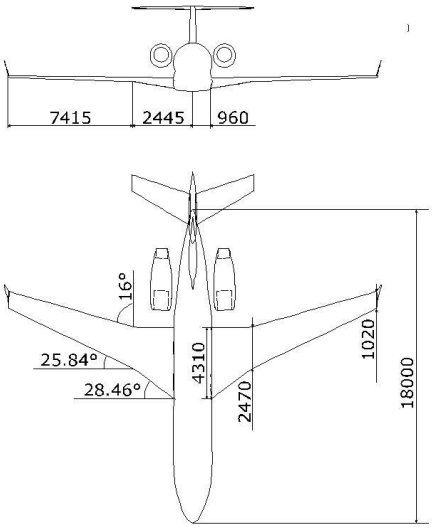

Fig. 2.Analyzed aircraft geometry and dimensions

The genetic algorithm structure scheme and used parameters are shown on Fig. 3 and Table 3. The maximum number of generations was chosen as convergence criteria after a study on the population size and number of generations to reach the optimum solution.

The wind tunnel experiments were carried out at the Experimental Aerodynamic Laboratory (LAE) at School of Engineering of São Carlos (EESC). The tunnel has a closed test section of dimensions 1.7 m x 1.3m on a closed circuit.

Table 3. Genetic algorithm used parameters

Population size	300
Chromosome length	40
Number of variables	10
Gen length	4
Mutation rate [%]	0.25
Elitism [%]	5
Number of generations	30

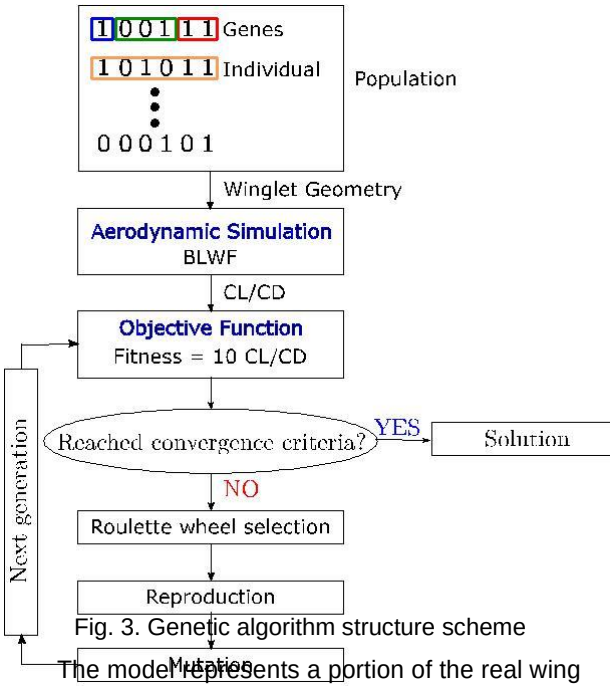

Fig. 3. Genetic algorithm structure scheme

The model represents a portion of the real wing tip on a scale of 1:7.33 with a mean aerodynamic chord (MAC) of 174 mm. The model drawing with the main dimensions are shown on Fig. 4. The wind flow is aligned with the X direction on the drawing coordinate system. The model was produced using a Stratasys Fortus 360MC using ABS M30.

An aerodynamic balance is used to measure the lift and drag coefficients for an incidence angle from -6° to 25° with an angle variation of 1°. The flow conditions are set to at an air speed of 25 m/s. The balance drag coefficient data is fitted to a parabolic function of the lift coefficient (Eq. 1 and 2).

(1)

(2)

The wake flow mapping is performed using a seven-hole probe on the ZY-plane at a distance of one model's mean aerodynamic chord behind the wing tip for a fixed incidence angle of 12°.

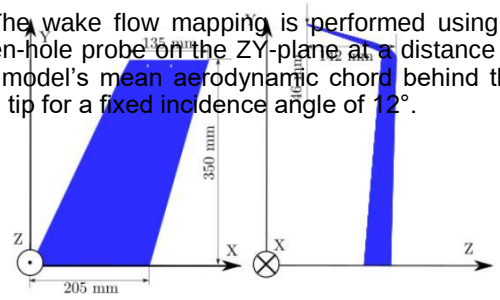

Fig. 4. Model drawing with used coordinate system

Maskell's equation was used for the induced drag calculation from the velocity field (Ganzevles et al. 2002). The induced drag is obtained from the plane vorticity (ω_x) and stream function (Ψ) as shown on Eq. 3 to 5. The velocities and are the velocities components on de z and y directions divided by the free stream velocity (∞) and is the model reference area.

(3)

(4)

(5)

RESULTS AND DISCUSSION

The optimization process described above was used for the wing, winglet and body configurations at the climb, heavy, mid and light cruise conditions. The fitness of the best, mean and worst individual in every generation for the climb condition optimization is shown on Fig. 5. After the 30 generations, the best individual fitness had no significate change and was almost reached by the mean individual. The worst fitness tends towards the best fitness with some oscillations due the mutation factor.

The best individuals after 30 generations total and induced drag coefficients are compared with the fixed geometry winglet (Table 4 and Table **5**). The total drag reduction is greater than the induced drag, showing that the winglet optimizationreducedtheparasitedrag component. The balance measurements results are shown on **Hata! Başvuru kaynağı bulunamadı.** and **Hata! Başvuru kaynağı bulunamadı.**. All the winglets showed an increase on the lift coefficient curve slope ( ) and a drag reduction on the optimization region when compared to the wing with no winglet. The winglet optimized for the light cruise condition show the best performance. The coefficients of the fitted parabolic drag polar are shown on Table 6. All winglet configurations improved the wing effective aspect ratio and increase the zero lift drag (0).

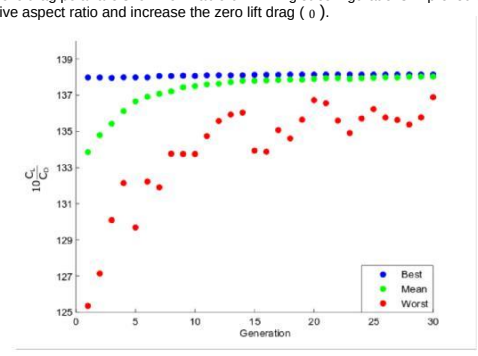

Fig. 5. Individuals fitness at every generation for climb condition

Table 4. Total drag comparison between fixed geometry winglet and optimized geometry

[-]			
Condition	Baseline	Optimum	Δ [%]
Climb	0.03774	0.03752	-0.58
Heavy cruise	0.03626	0.03625	-0.03
Mid cruise	0.03432	0.03427	-0.15
Light Cruise	0.03218	0.03213	-0.16

Table 5. Induced drag comparison between fixed geometry winglet and optimized geometry

[-]			
Condition	Baseline	Optimum	Δ [%]
Climb	0.0075	0.00742	1.06
Heavy cruise	0.00665	0.00661	0.6
Mid cruise	0.00586	0.00582	0.68
Light Cruise	0.00499	0.00496	0.6

Table 6. Parabolic drag polar fit coefficients from wind tunnel data

Winglet configuration	K [-]	[-]
No winglet	0.1090	0.01308
Climb configuration	0.0904	0.02098
Heavy cruise configuration	0.0872	0.02095
Mid cruise configuration	0.0859	0.02114
Light cruise configuration	0.0886	0.01995

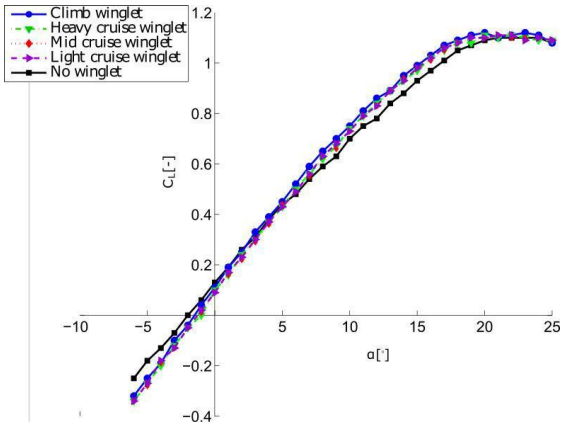

Fig. 6. Lift coefficient results from wind tunnel experiment

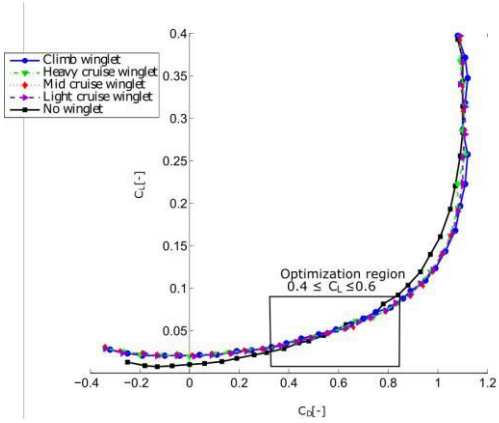

Fig. 7. Drag polar results from wind tunnel experiment

The velocity vector field and vorticity for the wing with no winglet and the light cruise winglet at an incidence angle of 12° (Fig. 8 and Fig. **9**) show that the winglet reduced the vortex size and strength causing the induced drag reduction. The comparison between the induced drag using the parabolic fit for the drag polar and the calculation using Maskell's equation at an incidence angle of 12° is shown on Table 7. The results show that the Maskell's equation and balance measurements are similar with differences of less than 11%.

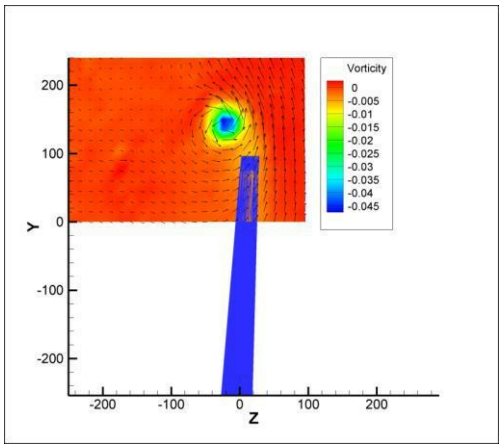

Fig. 8. Mapping of the wing with no winglet

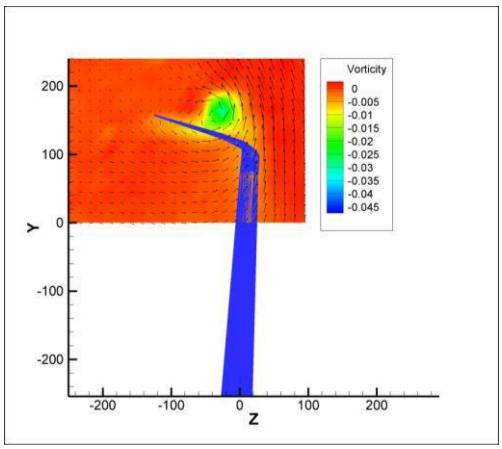

Fig. 9. Mapping of the wing with winglet optimized for light cruise condition

Table 7. Balance and Maskell's equation induced drag comparison

[-]		
Winglet configuration	Balance	Maskell's equation
No winglet	0.0663	0.0679
Climb configuration	0.0669	0.0650
Heavy cruise configuration	0.0615	0.0678
Mid cruise configuration	0.0609	0.0667
Light cruise configuration	0.0610	0.0647

CONCLUSIONS

The optimization process developed in this work shows a method that can be used for a morphing winglet or a brand new winglet project. The morphing winglet improved the optimized fixed geometry winglet performance by reducing the total configuration drag by up to 0.58%.

The experimental results showed that the winglets increased the wing effective aspect ratio, reducing the total drag on the optimization region. Both the balance and Maskell's equation method for induced drag calculation can be used to estimate the induced drag, differing in less than 11% from each other. The flow mapping also gives a good insight of the effectivity of the winglet on reducing the vortex size and strength.

ACKNOWLEDGEMENT

This work has been partially funded by the Department of Aeronautical Engineering of the University of São Paulo and by Coordenação de Aperfeiçoamento de Pessoal de Nível Superior (CAPES).

REFERENCES

Barbarino, S. and Bilgen, O. and Ajaj, R. and Friswell, M.I and Inman, D., "A Review of Morphing Aircraft", Journal of Intelligent Material Systems and Structures, Vol. 22, 2011.

Ganzevles, F.L.A. and de Bruin, Anton and Puffert-Meißner, W, "A quantitative analysis of viscous and lift-induced drag components from detailed wake measurements behind a half model", NLR-TP-2002-320,2002

Johnson, F. T., Tinoco, E. N., and Yu, N. J., "Thirty years of development and application of CFD at Boeing commercial airplanes, Seattle," Computers and Fluids, 2005, p. 1115–1151.

Kroo, I., "Nonplanar wing concepts for increased aircraft efficiency," VKI lecture series on innovative configurations and advanced concepts for future civil aircraft, June 2005.

Martins, A. L., and Catalano, F. M., "Drag optimization for transport aircraft Mission Adaptive Wing," Journal of the Brazilian Society of Mechanical Sciences and Engineering, Vol. 25, No. 1, 2003.

Whitcomb, R. T., "A Design Approach and Selected Wind-Tunnel Results at High Subsonic Speeds for Wing-Tip Mounted Winglets", NASATN D-8260, 1976.

ISSA-2018-017

AN ANALYSIS OF THE RELATIONSHIP BETWEEN TEAMWORK AND JOB SATISFACTION ON AIRLINE CABIN CREW

Dilek CAN
Muğla Sıtkı Koçman Üniversitesi
Dalaman Sivil Havacılık Yüksekokulu
Gazi Bulvarı 291/C 48680 Dalaman Muğla
dilekkozsoy@gmail.com

İlkay Orhan
Anadolu Üniversitesi
Havacılık ve Uzay Bilimleri Fakültesi
İki Eylül Kampüsü 26470 Eskişehir
iorhan@anadolu.edu.tr

SUMMARY

In a highly competitive environment, airline companies can achieve economical sustainability by reducing their costs and ensuring customer satisfaction . Cabin crews are also important customer representatives that provide this sustainability for airline operators . Because of the complex nature of the aviation industry and concurrently operational activities carried out by different employees in limited time, teamwork is essentially important in terms of airlines . Teamwork is also only possible by working with each other in coordination. As a result of working in coordination and establishing positive social relationships, the job satisfaction with employees increases . A high level job satisfaction and teamwork skills provide a competitive advantage for airlines . In this study, the relationship between team work and job satisfaction of 304 employees working as a cabin attendant in an Istanbul - based airline operation was investigated. As a result of this study, it is found out that there is a significant positive relationship between teamwork and job satisfaction.

Keywords: Teamwork, job satisfaction, cabin crew, air transportation.

INTRODUCTION

In recent years, the aviation industry has made rapid progress all over the world with the development of technology. According to the International Civil Aviation Organization data, in 2016, 3.8 billion passengers were carried by air. When it is compared with the year of 2015, there is an increase of 6,8% percent (www.icao.int). According to Boeing data, annual fleet growth is estimated at 3.5% (www.boeing.com). With this growth, there will be an increase in the rate of cabin crew employment in airlines. In airlines, team expenses (salary, premium, etc.) are the second biggest cost after fuel costs (Bazargan, 2012). Increasing the job satisfaction of cabin crews working under stressful factors; such as time management, business family conflict, unlawful passengers, conflict with teammates, other roles the teams take in the plane (police, nurse, firefighter), long working hours, and excessive workload (Karatepe and Vatankhah, 2014; Tungtakanpoung and Wyatt, 2013; Chen and Kao, 2011); will reduce the turnover rate, and this plays a role to eliminate costs such as training and orientation. Additionally, it is obvious that the satisfied employees will be more productive in the workplace, and this will reflect to the passengers positively as well. Therefore, it can be said that job satisfaction will lead to customer satisfaction.

The concurrently operational activities carried by different employees in limited time in the complex aviation industry show that the teamwork in terms of airlines is so important that cannot be denied.

Employing cabin crews which are good-humored, team-oriented, and have high level of communication skills and emotional intelligence will make a difference in order to be preferred airline in a highly competitive environment (Güremen, 2012).

In order to increase competitiveness and to sustain the economic activities, airlines have to have a high quality of service and customer satisfaction (Hussain et al., 2015). According to the studies performed, there is a positive relationship between employee satisfaction and customer satisfaction. Therefore, companies which give a priority to quality of service and customer satisfaction should recognize, support and reward the efforts of their employees (Mendoza and Maldonado, 2014). A cabin attendant with a high job satisfaction can offer a better quality service, and this creates more satisfied customers mass that can affect the profitability of the airline.

In this study, by determining teamwork skills and the level of job satisfactions of cabin crews, the relationship between teamwork and job satisfaction and the differences according to demographic characteristics were determined.

METHODOLOGY

The population of the study is composed of the cabin crew serving in an Istanbul-based airline. According to the information received from the relevant airline, a total of 8,500 cabin crew are working in this airline in 2017. A questionnaire could be applied to 322 cabin crew and 18 of them could not included in the analyzes due to lack of data.

The research results are limited to the cabin crews participating the surveys of teamwork and job satisfaction. It was assumed that participants in the survey gave realistic and genuine responses to all scales and questions.

Minnesota job satisfaction scale was used as data collection tool in the survey. The short form of the Minnesota job satisfaction scale which are scaled with the five point likert scale (1=Not Satisfied; 5=Extremely Satisfied) that widely accepted for measuring of the job satisfaction and demonstrated the reliability and validity with numerous studies is based. In this study, the reliability validity analyzes of the scale were repeated. The overall reliability of the scale was found to be very high at alpha = 0.919.

The scale that is developed by Bateman, Wilson ve Bingham (2002) and that is translated to Turkish by Zehir ve Özşahin (2008), is based in order to determine the teamwork level in the study. The evaluations are realized by giving 5 point to strongly agree, and by giving 1 point to strongly disagree. Reliability validity analysis of the scale were repeated and the overall reliability was found to be very high as alpha = 0.966.

The data obtained from the study were analyzed using the SPSS 22.0 for Windows (Statistical Package for Social Sciences).

T-test was used in order to the comparision of quantitative continuous data between two independent groups, and in addition, One Way ANOVA test was used for the comparision of quantitative continuous data between more than two independent groups. After the Anova test, the Scheffe test was used so as to determine the differences as a complementary post-hoc analysis.

Pearson correlation and regression analysis were applied among the continuous variables of the study. The findings were evaluated at the 95% confidence interval and at the 5% significance level.

RESULTS AND DISCUSSION

For the solution of the research problem, the findings obtained from the analysis of the collected data through the cabin attendant scales participating in the survey are included in this section. Based on the findings obtained from the analysis, the statements and interpretations has been made. The distribution of the descriptive characteristics of the cabin crew is shown in Table 1.The distribution of the cabin crew participating in the study is 53,3% were between 15 to 24, 76,3% were female, 68,8% were single, 61,5% were bachelor's degree, 69,4% were E / Y Class cabin crew. Also, 53.9% have cabin seniority of 2-5 years and 59.2% cabin attendants who have 2-5 years of seniority in the airline where the questionnaires are applied.

Table 1. Distribution of the descriptive characteristics of cabin crew

Tables	Groups	Frequence(n)	%
Age	21-25	53	17,4
	26-30	162	53,3
	31-35	60	19,7
	36 +	29	9,5
Gender	Male	72	23,7
	Female	232	76,3
Marital Status	Married	95	31,2
	Single	209	68,8
Educational Status	High School	19	6,2
	Associate's Degree	48	15,8
	Bachelor's Degree	187	61,5
	Master	50	16,4
Cabin Crew Class	F Class	5	1,6
	Z Class	34	11,2
	E/Y Sınıfı	211	69,4
	Q Class	19	6,2
	Others	35	11,5
Seniority in the Sector	0-1 Year	40	13,2
	2-5 Years	164	53,9
	6-10 Years	66	21,7
	+10 Years	34	11,2
Seniority in the Current Working Business	0-1 Year	49	16,1
	2-5 Years	180	59,2
	6-10 Years	47	15,5
	+10 Years	28	9,2

The diagram of the levels of the cabin crew teamwork and job satisfaction is shown in Fig 1. The level of "Skill and Sourcing" of the cabin crew participating in the survey was high (3,964 ± 0,618); "Coaching and Communication" level was moderate (3,365 ± 0,663); the level of the "Synergy" was high (3,731 ± 0,657); "Leadership" level was moderate (3,281 ± 0,803); "Time Management" level is high (3,709 ± 0,690); "Participation in Decisions" was high (3,568 ±

0,784); and the level of "Teamwork General" was high (3,642 ± 0,568). The level of "Intrinsic Job Satisfaction" of the cabin crew participating in the survey was high (3,768 ± 0,592); "Extrinsic Job Satisfaction" level is high (3,624 ± 0,629); and the level of "Job Satisfaction General" was high (3,710 ± 0,578).

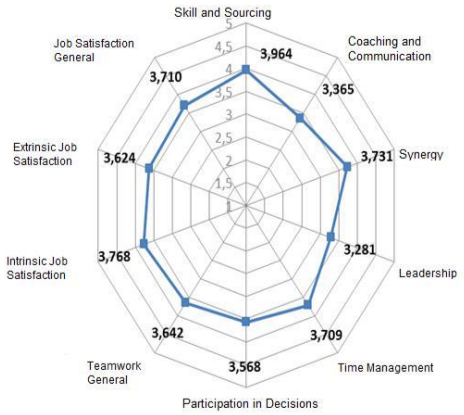

Fig.1. The diagram of the levels of the cabin crew teamwork and job satisfaction

According to the correlation analysis between teamwork and job satisfaction levels of cabin crews, there is a moderate significant positive relationship between intrinsic job satisfaction and teamwork overall (r = 0,516; p = 0,000 <0,05). There is a moderate significant positive correlation between extrinsic job satisfaction and coaching and communication (r = 0,609; p = 0,000 <0,05). There is a moderate significant positive correlation between extrinsic job satisfaction and synergy (r = 0.544, p = 0.000 <0.05). There is a moderate significant positive relationship between extrinsic job satisfaction and leadership (r = 0,522; p = 0,000 <0,05). There is a moderate significant positive relationship between extrinsic job satisfaction and team work overall (r = 0,619; p = 0,000 <0,05). There is a moderate significant positive correlation between job satisfaction overall, coaching and communication (r = 0,545; p = 0,000 <0,05). There is a moderate significant positive correlation between job satisfaction general and synergy (r = 0,521; p = 0,000 <0,05).

The regression analysis performed to determine the cause-and-effect relationship between team work overall and job satisfaction was statistically significant (F = 158,261, p = 0,000 <0,05). As a determinant of job satisfaction overall level, association with team work overall variables (explanatory power) was found to be strong (R2 = 0.342). The overall level of teamwork of cabin crews increases the overall level of job satisfaction (ß = 0.598).

CONCLUSION

With today's developing technology, producing of the large capacity and less fuel-efficient aircrafts, increase the number of airline companies, and preferring the airline which provides faster transportation to the more points lead to an increase in the number of passengers. Providing the satisfaction of this high number of passengers during the flights is only possible by working of the cabin crew in a harmony. In other words, the effective communication of the cabin crew during the flight, synergy, efficient time management, leadership ability, and effective decision making are the key elements for teamwork. However, to be satisfied and get quality service of the passengers is depends on providing cabin crew satisfaction. That is to say when the cabin crews provide both intrinsic and extrinsic satisfaction, this leads to the work performance positively, and therefore the productivity will increase.

In this study, it was tried to measure the effect of team work on job satisfaction. For this purpose, a questionnaire was applied to 304 cabin officers working in an Istanbul-based airline. As a result of the analysis made on the questionnaires, there was a statistically significant positive relationship between teamwork and job satisfaction. With this conclusion, the hypothesis of "There is a significant relationship between teamwork and satisfaction in cabin crews" has been proved. Cabin crews working in a harmony can be more satisfied with the help of teamwork in their works. This is because of the fact that collecting responsibility on a team rather than on a single person will reduce the stress level of workers. In case of a negative situation during the flight, the support of the other team members or the cabin supervisor can provide confidence to their teammates. This can affect job satisfaction positively by ensuring success in jobs that require high performance. The level of skill and sourcing of the cabin crews increases the level of intrinsic satisfaction.

The highest average elements in the teamwork scale can be given as trying to keep the waste of time in minimum level, defining of the objectives of teamwork clearly, and having easy access for team members to required resources for education and development.

The sub-dimensions -such as skill and sourcing, synergy, and time management- of the teamwork scale of the cabin crews participating in the survey were found to be higher. In addition, it's found that the intrinsic level of satisfaction of the cabin crew is higher than the extrinsic level of satisfaction. This may be due to the fact that cabin crews have responsibilities in different roles within their job descriptions, they can benefit others, and they keep busy. In the study; it's seen that the

levels of "Skill and Sourcing", "Synergy", and "leadership" of the cabin crews increase the level of "Intrinsic Job Satisfaction". Additionally, it's seen that the levels of "Coaching and Communication", "Synergy" and "Leadership" of the cabin crews increase the "Extrinsic Job Satisfaction". The reason of this is the fact that in the case of emergencies during the flight, the success with the synergy of the team -even if the limited possibilities- is increases the job satisfaction.

REFERENCES

Bateman, B., Wilson, F.C. and Bingham, D. 2002, Team effectiveness development of an audit questionnaire. *Journal of Management Development* 21 (3): 215-226.

Bazargan, M., (2012). Havayolu operasyonları ve planlaması. (Çev: İ. Orhan). Eskişehir: Anadolu Üniversitesi Yayınları.

Chen, C. and Kao, Y., 2011, The antecedents and consequences of job stress of flight attendants Evidence from Taiwan, Journal *of Air Transport Management* 17: 253-255.

Güremen, F., 2012, The ideal cabin crew? How can we make it happen? Efficient communication and body language trainings for cabin crew. Turkish Aviation Academy 5:30-31.

Hussain, R., Nasser,A. and Hussain, Y. K., 2015, Service quality and customer satisfaction of a UAE-based airline: An empirical investigation. Journal of Air Transport Management 42: 167-175.

Karatepe, O. and Vatankhah, S., 2014, The effects of high-performance work practices and job embeddedness on flight attendants' performance outcomes, *Journal of Air Transport Management* 37: 27-35.

Mendoza M.L. and Maldonado, C.O., 2014, Meta-analytic of the relationship between employee job satisfaction and customer satisfaction, *Suma Neg.* 5 (11): 4-9.

Tungtakanpoung, M. and Wyatt, M., 2013, Spirituality and cultural values in the reported cognitions of female cabin attendants on Thai Airways, *Journal of Air Transport Management* 27: 15-19

Zehir, C. ve Özşahin, M., 2008, Takım yönetimi ve takım etkinliğini belirleyen faktörler: Savunma sanayisinde ar-ge yapan takımlar üzerine bir saha araştırması. *Doğuş Üniversitesi Dergisi* 9 (2): 266-279.

www.boeing.com/resources/boeingdotcom/commercial/market/current-market-outlook-2017/assets/downloads/2017-cmo-compressed_091917.pdf , accessed on October 05, 2017.

https://www.icao.int/sustainability/Documents/AVIATION-BENEFITS-2017-web.pdf ,accessed on October 10, 2017.

INCREASING THE UNMANNED AERIAL VEHICLE LANDING ACCURACY FOR REDUCING ENVIRONMENTAL IMPACT

Nguyen Dinh Dung, Jozsef Rohacs Budapest University of Technology and Economics Department of Aeronautics, Naval Architecture and Railway Vehicles H-1111 Budapest, Műegyetem rkp.3
Authors' e-mails: dungtbhk@gmail.com; jrohacs@vrht.bme.hu

SUMMARY

The automatic landing of an unmanned aerial vehicle (UAV) is a significant challenge for scientists, which requires thorough and thorough research. The environmental factor is an essential role in landing process of UAVs . For take - off or landing, the UAVs need to have a runway and area where does not include obstacles such as tall buildings or ancient trees . The UAV which is researc h object in this paper does not need yard because it is launched from the launcher and recovered with a parachute. This study provides a desired landing orbit which is calculated based on landing areas . These areas are determined by solving aircraft equations of motion and analytical method. The simulation results utilizing MATLAB software show that i) the calculated landing orbit is the shortest, and ii) this orbit is a desired one on which the impact of environmental factors on landing process of UAVs is reduced significantly .

Keywords: orbit, unmanned aerial vehicle, landing, desired landing orbit, environmental impact.

INTRODUCTION

The Unmanned Aerial Vehicles (UAVs) became widely used in civil applications that are in many areas such as agriculture, environmental protection, public safety and traffic flow control. Because increasing their number and their operation rapidly in or close to the urban areas, the reduction of their environmental impacts appears as a new and essential task that required optimization of the operation processes.

In the recent years, most of the research community's attention was centered on a few topics, including self-localization (Weiss et al., 2012), path planning (Achtelik et al., 2011), navigation (Zufferey et al., 2010; Yang et al., 2014) and autonomous take-off and landing (Saripalli et al., 2007; Lee et al., 2012; Lippiello et al., 2016).

In the past years, different research groups around the world have been working on vision-guided autonomous UAV landing (Sharp et al., 2001; Saripalli et al., 2002; Sevcik et al., 2010; Lippiello et al., 2016).

Saripalli et al., (2007) provided the design of a trajectory planning and control algorithm for landing on a moving target based on the variational Hamiltonian and Euler-Lagrange equations. Their research focused on optimal trajectory planning and control for landing a helicopter on a moving target using a cubic spline parameterization of the trajectory. Anitha and Kumar (2012) developed algorithm computes the relative height of the UAV above the runway stripe and the lateral deviation from the runway centerline. Using this method, the UAVs can descend at a constant angle (conventionally 3 degrees below the horizon), align with the runway centerline and the touchdown with the wings level at the beginning of the runway.

Landing approach is one of the critical stages of the entire flight to bring the UAV to land safely at the desired location. Common landing approaches consist of some stages: i) reversing direction of wind direction, ii) lowering altitude, iii) slowing down speed, and implementation at different altitudes. Several factors influence the landing process of the UAV:

- Wind – having a significant and direct effect on the UAV stability and control and - especially in the landing approach - the wind direction and magnitude are the essential parameters determining the trajectory and control parameters;
- Aerodynamic forces – as lift, drag, and side forces determining the landing approach.
- Traction force of an engine – effects of which depend on its integration into the airframe and may create extra moments;
- Propeller reaction moment - affecting the stability of the UAV.

Besides, the takeoff process is influenced by elevation, climatic conditions, and other factors.

In this paper, we present the methodologies using to determine and calculate the landing areas and managing the landing. Based on these areas, the desired landing orbit is estimated, on which the UAV can landing accurately at the desired position without unnecessary environmental impacts causing by non-accurate landing. This research was developed a particular fuzzy control based orbits – straight lines trajectory for increasing the UAV landing accuracy (Dung, Kale and Rohacs, 2018).

METHODOLOGIES

Determining access areas for landing

The UAV landing approach starts by receiving the landing command at current point M (Fig. 1) on landing at predefined point 0. The approach and landing process might be constructed from the

straight lines and orbit curves. The landing orbit may contain two arcs of radius R_{min} (MA and BE) connected by an AB line. From point E, the UAV lowers the altitude (line EF) and reduces the speed (line F0).

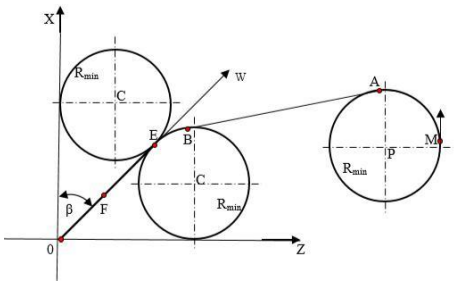

Fig. 1. UAV landing approach process

Based on the method of determining the chosen landing trajectory, we can define the landing areas for UAV landing as follows:

i) Deceleration zone: the smallest circle on the horizontal plane contains the projection of the orbit of the UAV which flies straight with decreasing speed during the landing approach (see Fig. 2).

ii) Lowering altitude zone: this is the smallest circle on the horizontal plane containing the projection of the orbit of the UAV which flies in the process of reducing altitude (see Fig. 2).

iii) Directive zone: the smallest circle in the horizontal plane contains projections of two circles with radius R_{min} which two circles tangent to each other at the opposite of wind direction (see Fig. 2).

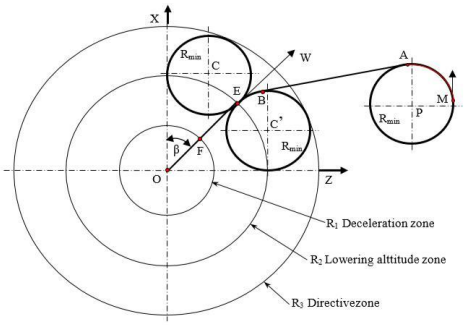

Fig. 2. Landing zones

Calculate the landing areas

To determine the landing areas, the conventional method is to investigate kinetic dynamics of UAV by solving the system of differential motion of UAV.

The forces acting on the UAV are described as in the Fig. 3: The total aerodynamic force ˉ and its components in the coordinate speed Oxcyczc are X, Y, and Z; Gravity ; Traction force of engine ˉ . These forces generate the moments that make the UAV rotate around three coordinate axes.

We only study UAV dynamics to calculate the deceleration zone, then apply the analytical method to determine the remaining landing areas.

Landing areas will be determined by knowing the radius of each region.

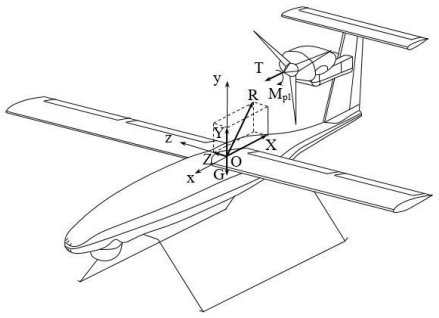

Fig. 3. Flight forces

The calculating the radius of deceleration zone R_1.

The differential equations of motion of the UAV in the deceleration area are described as following:

$$\frac{dV}{dt} = \frac{-X}{m} \quad (1)$$

$$\frac{dx_0}{dt} = V = V - w \quad (2)$$

These equations can be solved by using the fourth level Runge-Kutta and MATLAB software. The calculation results are shown in the Fig.4.

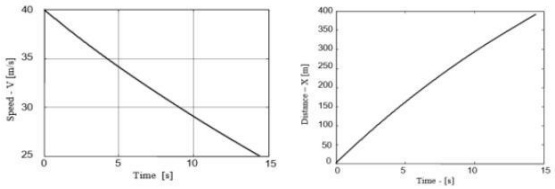

Fig. 4. The speed and distance depend on times

Calculating the radius of lowering altitude area R_2 is described as following steps:

The radius R_2 is determined from the conditions: lowering altitude from H<=500m to H_{min} = 35m and speed $|V_y|$<=5m/s.

The time to decrease altitude from H<=500m to H_{min} = 35m is: $t = \frac{H - H_{\min}}{V_y}$ (3)

The distance of UAV is: $S = t(V-W)$ (4)

The radius of the lowering altitude is:

$$R_2 = R_1 + \sqrt{S^2 - (H - H_{\min})^2} \quad (5)$$

The calculating the radius of directive zone R_3.

$$R_{3\min} = R_{\min} + \sqrt{R_{\min}^2 + R_2^2} \quad (6)$$

Calculating the smallest radius of turning around R_{min}.

R_{min} is the smallest rounding radius of the UAV and determined from the condition of the inclined angle of UAV = $\pm 20^0$.

$$R_{min} = \frac{[V - W\cos(\quad - \quad)]^2}{g.tg} \quad (7)$$

Where, ψ – the direction angle of the UAV compared to the axis Ox; β – the wind direction compared to Ox; γ – the angle of inclination of the UAV.

Calculating the desired landing orbit

Calculating the desired landing orbit on which the landing direction is opposite to the wind direction

As the UAV can turn left or right to connect with the R_{min} circle on the left or the right (following the direction of the wind), thus the UAV from a position with any vector speed can fly to the standard location for landing in four different orbits. After calculating four of these orbits, we compare them to choose the shortest one which is determined by the desired landing orbit.

Case 1: The turning left to reach the left circle (the orbit is MABEO, see Fig. 5)

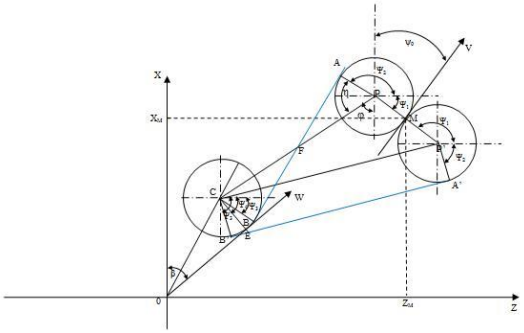

Fig. 5. Landing approach connected to the left circle

$$X_P = X_M + R_{min}.\sin\ _0 \quad (8.1)$$

$$Z_P = Z_M - R_{min}.\cos\ _0 \quad (8.2)$$

$$= arctg\ \frac{Z_P - Z_C}{X_P - X_C}\ ; \quad = arc\cos\ \frac{R_{min}}{FP} \quad (8.3)$$

$$FP = \frac{1}{2}\sqrt{(Z_P - Z_C)^2 + (X_P - X_C)^2} \quad (8.4)$$

$$X_A = X_P + R_{min}.\sin(\ + - \frac{}{2}) \quad (8.5)$$

$$Z_A = Z_P - R_{min}.\cos(\ + - \frac{}{2}) \quad (8.6)$$

$$X_B = X_C - R_{min}.\sin(\ + - \frac{}{2}) \quad (8.7)$$

$$Z_B = Z_C + R_{min}.\cos(\ + - \frac{}{2}) \quad (8.8)$$

$$_1 = arctg\ \frac{X_P - X_M}{Z_M - Z_P}\ ; \quad _2 = arctg\ \frac{X_A - X_P}{Z_A - Z_P} \quad (8.9)$$

$$_3 = arctg\frac{X_C - X_B}{Z_B - Z_C}\ ; \quad _4 = arctg\frac{X_C - X_E}{Z_E - Z_C} \quad (8.10)$$

$$L_1 = R_{min}(\ _1 + \ _2 + \ _4 - \ _3\ ) + \sqrt{(Z_A - Z_B)^2 + (X_A - X_B)^2} \quad (8.11)$$

Case 2: The turning right to reach the left circle (the orbit is MA'B'EO, see Fig. 5)

In this case, the landing distance is:

$$L_2 = R_{min}(\ _1 + \ _2 + \ _3 - \ _4\ ) + \sqrt{(Z_{A'} - Z_{B'})^2 + (X_{A'} - X_{B'})^2} \quad (9)$$

Case 3: The turning left to reach the right circle (the orbit is MABEO, see Fig. 6)

$$L_3 = R_{min}(\ _1 + \ _2 + \ _4 - \ _3\ ) + \sqrt{(Z_A - Z_B)^2 + (X_A - X_B)^2} \quad (10)$$

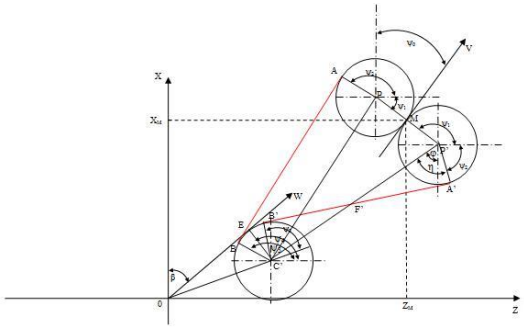

Fig. 6. Landing approach connected to the right circle

Case 4: The turning right to reach the left circle (the orbit is MA'B'EO, see Fig. 6)

$$L_4 = R_{min}(\ _1 + \ _2 + \ _4 - \ _3\ ) + \sqrt{(Z_{A'} - Z_{B'})^2 + (X_{A'} - X_{B'})^2} \quad (11)$$

Choose the situation with the shortest flight distance: $L_{min}=min(L_1, L_2, L_3, L_4)$.

Calculating the desired landing orbit following given direction

Landing in the shortest distance when there is no wind: When the wind speed is less than 1m/s, it can be assumed that there is no wind. In a case where the land area does not have any obstacles, it is allowed to land in any direction, and we should choose the shortest distance. In this case, we just put the wind direction from the position O (the coordinate) to the point M (the current point of UAV) and then usually calculate as when landing in the opposite direction of the wind.

Landing with given direction: In some cases, when the landing ground does not allow to land in any direction, but in a certain one (even when wind speed is less than 1m/s), we can keep the same calculation as in the case when landing in the opposite direction of the wind. In this case, we consider the estimated wind direction is opposite to given landing direction. We should notice that when calculating the radius of the turning arc, it must be the real wind direction.

SIMULATION RESULTS AND DISCUSSION

In the case of the Northern wind and the UAV must land in the opposite of the wind direction, the desired landing orbit is shown in the Fig. 7. At the altitude H =500, the UAV completes two times of turning with the desired angle =20^0, between these two times is a straight flying with speed V=40m/s, to find out the right orbit in opposite direction of the wind, the start step is lowering the altitude, then finally straight flying in decreasing speed. The simulation result given are reasonable and necessary to implement controlling orders. However, when the UAV has to land in the given direction, the landing direction is the given direction

although there was the northern wind.

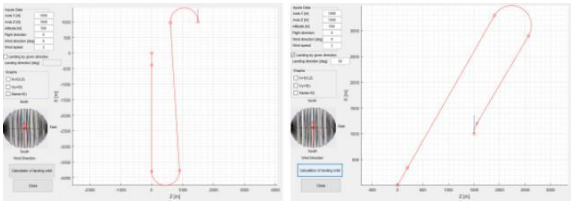

Fig. 7. Landing in the opposite wind direction and given direction with the Northern wind

When there was no wind, and the UAV might land in any direction, the desired landing trajectory is presented in Fig. 8. The result shows that the landing direction is the direction from the current point of the UAV to the desired landing point, and this landing distance is the shortest one. This figure shows the desired landing orbit in the case of landing in the given direction with no wind.

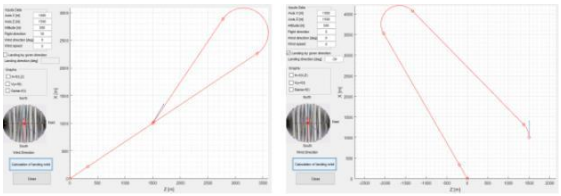

Fig. 8. The desired landing trajectory in any and given directions with no wind

The simulation results are similar when the UAV is landing in the opposite of the wind direction, and provided direction with the easterly wind (see Fig. 9).

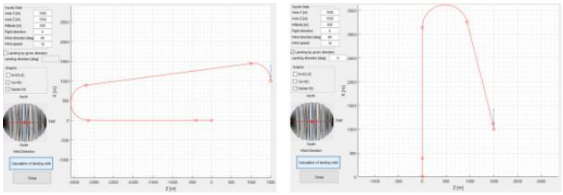

Fig. 9. Landing in the opposite wind direction and given direction with the easterly wind.

CONCLUSION

This paper gave the methodologies for calculating the desired landing orbit of the UAVs. To determine the landing areas, solving the system of differential motion of UAV used as the method in this research. Although the wind is taken into account, the wind impacts in the real-time do not perform in the simulation results.

The developed methodology applied depending on the real situations (wind direction, wind size, humidity, etc.) results in the shortest orbits with considerable reduction of the required landing areas and environmental impact. The improved methods might be applied to more complex task as landing in city areas, or on moving, oscillating platforms (Lippiello, and Ruggieo, 2016), too.

ACKNOWLEDGEMENT

This work was supported by Hungarian national EFOP-3.6.1-16-2016-00014 project titled by "Investigation and development of the disruptive technologies for e-mobility and their integration into the engineering education".

NOMENCALTURE

A, B, C, E, M - all the geometrical data are given *in Fig. 1, 2, 5, and 6.*

H – altitude,

x,y,z – axes of the reference system,

X, Y, Z – aerodynamic forces (Fig. 3.),

T – traction force (Fig.3),

V – velocity of UAV compared to the air,

w – velocity of UAV compared to the ground,

Greek Letters

$\phi, \eta, \varphi, \psi_0, \psi_1, \psi_2, \psi_3, \psi_4$ – angles (Fig. 5, 6)

REFERENCES

Achtelik, M., Achtelik, M., Weiss, S., & Siegwart, R. (2011, May). Onboard IMU and monocular vision based control for MAVs in unknown in-and outdoor environments. In *Robotics and automation (ICRA), 2011 IEEE international conference on* (pp. 3056-3063). IEEE.

Anitha, G., & Kumar, R. G. (2012). Vision based autonomous landing of an unmanned aerial vehicle. *Procedia Engineering*, *38*, 2250-2256.

Dung, N.G., Kale, U., Rohacs, J. Developing the fuzzy control based orbits – straight lines trajectory for increasing the UAV landing accuracy, Repüléstudományi Közlemények (to have appeared), 2018.

Lee, D., Ryan, T., & Kim, H. J. (2012, May). Autonomous landing of a VTOL UAV on a moving platform using image-based visual servoing. In *Robotics and Automation (ICRA), 2012 IEEE International Conference on* (pp. 971-976). IEEE.

Lippiello, V., & Ruggiero, F. (2016, October). Orbital stabilization of a VToL UAV for landing on oscillating platforms. In *Safety, Security, and Rescue Robotics (SSRR), 2016 IEEE International Symposium on* (pp. 131-138). IEEE.

Saripalli, S., Montgomery, J. F., & Sukhatme, G. S. (2002). Vision-based autonomous landing of an unmanned aerial vehicle. In *Robotics and automation, 2002. Proceedings. ICRA'02. IEEE international conference on* (Vol. 3, pp. 2799-2804). IEEE.

Saripalli, S., & Sukhatme, G. S. (2007, April). Landing a helicopter on a moving target. In *Robotics and Automation, 2007 IEEE International Conference on* (pp. 2030-2035). IEEE.

Sevcik, K. W., Kuntz, N., & Oh, P. Y. (2010). Exploring the effect of obscurants on safe landing zone identification. *Journal of Intelligent and Robotic Systems*, *57*(1-4), 281.

Sharp, C. S., Shakernia, O., & Sastry, S. S. (2001). A vision system for landing an unmanned aerial vehicle. In *Robotics and Automation, 2001. Proceedings 2001 ICRA. IEEE International Conference on* (Vol. 2, pp. 1720-1727). IEEE.

Yang, S., Scherer, S. A., Schauwecker, K., & Zell, A. (2014). Autonomous landing of MAVs on an arbitrarily textured landing site using onboard monocular vision. *Journal of Intelligent & Robotic Systems*, *74*(1-2), 27-43.

Weiss, S., Achtelik, M. W., Lynen, S., Chli, M., & Siegwart, R. (2012, May). Real-time onboard visual-inertial state estimation and self-calibration of mavs in unknown environments. In *Robotics and Automation (ICRA), 2012 IEEE International Conference on* (pp. 957-964). IEEE.

Zufferey, J. C., Beyeler, A., & Floreano, D. (2010, May). Autonomous flight at low altitude with vision-based collision avoidance and GPS-based path following. In *Robotics and Automation (ICRA), 2010 IEEE International Conference on* (pp. 3329-3334). IEEE.

International Symposium on Sustainable Aviation 2018
4 – 6 June 2018
Rome, Italy

ISSA-2018-019

TRADEOFFS OF LARGER AIRCRAFT IN AIRPORT OPERATIONS AND INFRASTRUCTURE

Renata Cavion
UFSC - Universidade Federal de Santa Catarina
Departamento de Engenharias da Mobilidade
r.cavion@ufsc.br

SUMMARY

Many airport operations are linked to the physical configuration of the passenger terminal. The increase in size and capacity of aircraft and the provision of flights have resulted in a significant increase in size of airport structures, consequently increasing the distances between operations and impacting on operations delay. In this context, this article analyzes different terminal configurations – linear, satellite and finger- pier - that operates new large aircraft (NLA), identifying some of its challenges and the tradeoffs. To achieve this goal, the passenger terminal layout evolution is analyzed and five of the world's major airports are observed: Hartsfield-Jackson Atlanta International Airport, O'Hare International Airport, London Heathrow Airport, Paris-Charles de Gaulle Airport and Amsterdam Airport Schiphol. This article emphasizes that the efficiency of a terminal will depend not only on the layout concept but also on the operational concept .

Keywords: Airport configuration, walking distance, aircraft movement.

LARGE AIRCRAFT AND AIRPORT TERMINAL CONFIGURATIONS

Over the last few years, airlines and aircraft manufacturers have been discussing the future requirements for new larger aircraft capable of carrying between 500 and 1,000 passengers that, as a result, will weigh in excess of 1 million pounds (FAA, 1998). This new need must cause severe impacts on design, organization and dynamics of airport operations.

The growth of aircraft size and its increasing of capacity added to the offer of new flights have resulted in a significant demand to increase the area of airport structures: passenger terminals, terminal apron, taxiways and runways. With the category of New Large Aircraft (NLA) these measures are even greater and critical, mainly when the characteristics are not compatible with existing airports. The adjustment of airport infrastructure requires also a new planning of operation. In this context, the airport terminal is perhaps the most complex element of the overall airport design that requires modification for new large aircraft operations (FAA, 1998).

FAA (1998) classifies NLA in the largest airplane design group category, Group VI with the following parameters (FAA, 2006): 214 feet (65 m) up to but not including 262 feet (80 m) wingspan. For ICAO (2005), the NLA are the aircrafts of Code F, with wingspan from 213.3' (65m) up to 262.5' (80m).

Today, the aircraft considered NLA are: A380 family, and B747-8 (Fig. 2). The A380 has been in operation since 2007 and it is compatible with over 140 small and large airports for regular service worldwide, and up to 400 airports when adding diversion airports, demonstrating that the A380 was able to be incorporated by the airports' infrastructures (AIRBUS, n.d.). Whereas the first commercial passenger flight of the Boeing 747-8 occurred on 2012, since then the B747-8 family has been approved to serve more than 60 airports around the world, and it is in work on 21 airports (BOEING, 2018).

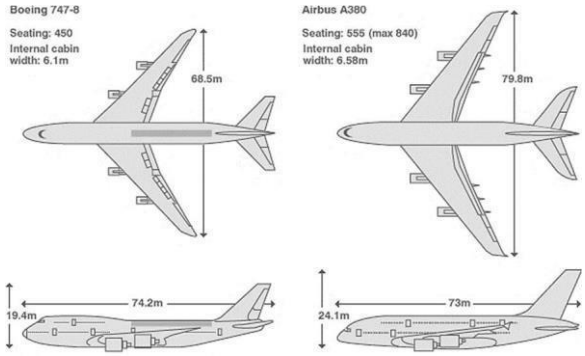

Fig.2. NLA measures: B747-8 and A380-800

. The larger passenger capacity of the NLA can bring some relief to congested airport systems by increasing the number of passengers per aircraft movement. However, several elements must be adjusted to respond properly to expected operational constraints on the airport airside and on the passenger terminal.

On airside, larger aircraft requires gates positions with greater distances between each other, widening the space between gates and between terminals that share the same apron. In order to minimize the space requirement, airport terminals are usually built with gates of different sizes, so that very large aircraft have their operations restricted to a few gates (Barros and Wirasinghe, 1997).

Besides that, the dimensions and routes of taxiway must be increased and adapted to access the gate positions and they must permit the aircraft maneuver with adequate clearance and security.

The passenger terminal requires special attention since the aircraft characteristics have an important role on its planning. Almost all aspects of terminal planning are affected by the size and capacity of the aircraft. Barros and Wirasinghe (1997) identify some of these aspects: number of gates, apron geometry, passenger processing and lounges.

Other aspects can be identified: the greater concentration of passengers in short periods of time (number of passengers per aircraft movement) which requires larger waiting lobbies and boarding rooms, for example. Besides that, the new distance between gates positions generates an increase in distance between boarding areas and requires a longer route to be walked by the passengers. This last aspect is especially relevant for the operation of the airport. Any increase in passenger walking distances results in an increase in arrival time, departure and transfer of passengers, which includes minimum connection time (MCT) and waiting time (Kusumaningtyas, 2007).

NLA requires several components to be simultaneously adjusted. Chicago O'Hare (ORD) has had a runway large enough to handle the A380 since 2013 but lacked a gate suitable for the two-level plane at that time. It was only from 2014 that this Airport started to receive NLA.

All the identified aspects could respond differently according to layout concept and geometry adopted in each passenger terminal. The passenger building may have several configurations, but it does take into account certain concepts that serve to structure it: Linear Terminal, Satellite Terminal and Finger Pier Terminal (Fig.2).

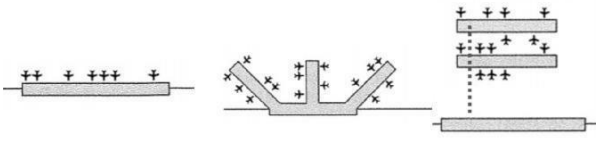

Linear Satellite Finger Pier

Fig.2. Main layout concepts of passenger terminals

FAA (1988) includes as an alternative concept to terminal building the Transporter Concept. In this configuration, the aircraft and aircraft-servicing functions are remotely located from the terminal and the connection to the terminal is provided by vehicular transport. The different concepts of passenger terminal layout result from a historical process of expansion to keep up with the growing public needs, new operational safety conditions and ever larger aircraft wingspan. Each of them has physical characteristics that strongly influence the operations and activities that occur inside and outside the terminal.

The analysis of the physical configuration of terminals that NLA operates shows that there is no single standard. This is due to the fact that until now, the existing terminals have been adjusted to receive these aircraft (Table 1). Recently the O'Hare International Airport announced that the 55-year-old Terminal 2 would be torn down to make way for a new “Global Terminal” with wider concourses and gates to accommodate the larger aircraft that embark on international flights to places like Hong Kong and Dubai (Chicago Tribute, 2018). Another example is the Los Angeles Airport (LAX) with its 2004 Master Plan planned to build a new terminal (Midfield Satellite Concourse) that will serve the NLA up to the beginning of 2020.

Table 1. The different layout of five terminals / concourse that operates NLA

Number of passenger ranking (2017)	Airport	Terminal / Concourse	Layout concept	A380 First Flight	B747-8 First flight
1st	ATL	F International	Pier	2013	Approved
6th	ORD	5 M	Linear / Pier	2016	Approved
7th	LHR	T3	Pier	2008	
		T5	Satellite	2018	
10th	CDG	2F 2E (k) 2G	Pier	2007	.
		2E (l, m)	Satellite		
11th	A MS	G	Pier	2012	Approved

The Hartsfield-Jackson Atlanta International Airport (ATL), O´Hare International Airport (ORD) in Chicago, the London Heathrow Airport (LHR), the Paris-Charles de Gaulle Airport (CDG) and Amsterdam Airport Schiphol (AMS) operate A380 on scheduled flights. However, the newest B747-8 is approved to operate in 3 of them without regular operation though.

Impacts of terminal expansion evolution according to the layout concept

This paper highlights two impacts of terminal expansion associated to the increase of aircraft size and capacity in four different airport generations: the increase in walking distance – that must be covered by the passengers in different landsides operations – , and the increase in airside distance between runway and gates.

The first generation of airport passenger terminal was designed with linear concept throughout the 1930s and 1940s. As examples, Gatwick (London, 1933), Rhein (Frankfut, 1936) and Santos Dumont (Rio de Janeiro, 1937) had a simple structure, with a minimum functional program, few requirements and a flow of boarding and departure in which the passenger used to walk across the apron to the aircraft.

Young and Wells (2014) emphasize that one of the main disadvantages of linear terminals becomes evident as the length of the terminal building begins to grow. Walking distances between facilities, especially between gates at opposite ends,

become excessive for passengers whose itinerary requires aircraft exchanges at the airport, becoming a major problem, especially at airport hub.

Between 1950s and 1970s the finger pier concept emerges as an evolution of linear terminal to respond to the increasing demands for air travel. Several airports design that we see today derive from this period, which configures the second generation. O´Hare Airport (Chicago, 1962) and Schiphol, (Amsterdam, 1967) were designed with pier concept for greater safety and comfort for passengers, allowing a major number of aircraft position along the axis of the pier, preferably in the nose-in position. The expansion of these terminals occurred by increasing the length of the piers axes and the construction of new piers. These changes have caused, in addition to the excessive increase of the distances between the gates and piers, new complexity to passenger routes. At the same time, the expansion reduced aircraft apron movement and maneuverability, inducing the aircraft to spend more time on ground movement until stopping to make arrivals and departures.

These problems tried to be solved by the third generation: the satellite concept (1960s – 1980s). The satellite terminal Concourse C of O´Hare Airport (Chicago, 1987) was constructed in the middle of the airfield as an expansion of Terminal 1, connected to Concourse B by an 850 foot tunnel. The JFK Airport (New York, 1962) is also an example of this layout Concept.

As main disadvantages, a satellite terminal requires high technology for underground transportation system and increases minimum connecting times.

The fourth generation is about hybrid terminal geometries. The hybrid concept is the composition of two or more concepts, considering the advantages and disadvantages of each one according to the operational profile of the airport.

With the volatile changes in the amount and behavior of civil aviation activity in the 1970s, with increasing numbers of large aircraft (with high seating capacities and large wingspans), volumes of passengers, and changes in route structures, airport management had to expand and modify terminal areas to accommodate almost constantly changing environments (Young, Wells, 2014).

Today, the main airports worldwide present a hybrid configuration as the result from each airport historic evolution. It means that there is no single design standard to fit the main airports, and it is also not possible to analyze the terminals as autonomous units, since they depend on the operational concept adopted in the complex airport system.

In a significant number of cases, airports have reached their limit of physical expansion, promoting radical changes in their terminals - such as demolition and reconstruction - to keep pace with rising passenger demand, as well as the rapid technological and capacity development of aircraft in a scenario where major world airports are located in places with saturated airspace.

Most large airfields are completely developed and occupied by runways, taxiways and aprons, leaving no room for relocation without a complete rearrangement of the airfield components – exceptions are airports that were planned for larger aircraft, such as Paris 20 Charles de Gaulle [Chevallier, 1997], Hong Kong Chek Lap Kok and Kuala Lumpur (Barros, 2001).

In an attempt to reconcile these complexities of infrastructure and operation, the airports – international hubs – determine very carefully the number, size, position of gates of NLA, and the specific routes between runway and gates (Fig. 3).

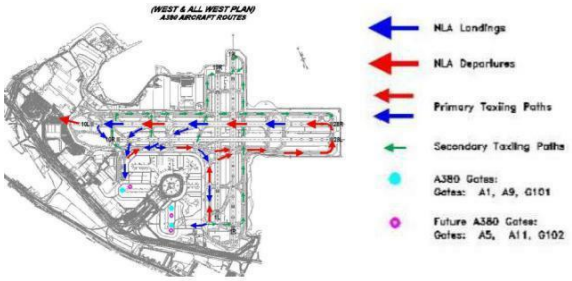

Fig.3. Routes and gates positions planned to receive A380 in San Francisco international Airport (SFO, 2009).

The specific routes and gates used by larger aircraft in hybrid airports have also increased aircraft taxiing distances and time. For flight operations at airports, “bottleneck” areas on the surface where congestion could occur include gates, apron area, taxiways, and runways–with the last two elements often referred to as the airport movement area (Zhang, Wang, 2017).

The longer taxiways are, the more maneuver movements and obstacles the aircraft must face (Fig. 4). As well, longer taxiways impact over surface delay (and consequent excess fuel burn and emissions), widely used to indicate the performance of airport surface movement.

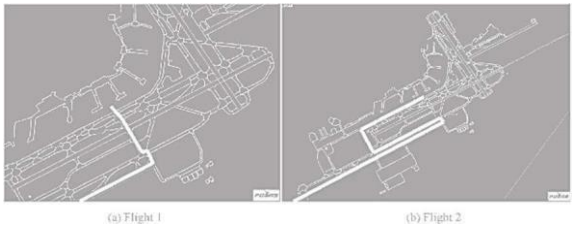

Fig. 4. An example of multiple flight trajectories of two flights with the same gate-runway pair (Zhang, Wang, 2017).

RESULTS: TRADEOFFS OF TERMINAL EXPANSION TO OPERATE NEW LARGE AIRCRAFT

The analysis of passenger terminal evolution contributes to the understanding of the operational and infrastructure complexity reached by airports today. Over the last several years, new commercial transport aircraft has increased in wingspan length, weight, velocity and capacity, impacting on airport infrastructure, planning and operation. With the category of NLA participating in the aircraft mix, the impacts are even greater. The introduction of the NLA, for many airports, will involve significant modifications to accommodate the size and weight of the new aircraft.

Today, the major airports in the world have a hybrid configuration as a result of the historic evolution of each airport. This means that there is no single design standard considered more efficient for new large aircraft, it is necessary to evaluate each airport in its infrastructure and operation as a whole. However, it is possible to see the benefits and losses related to NLAs at airports.

To determine the tradeoffs of terminal expansion to operate new large aircraft (Fig. 5), this paper assume the following scenario: (i) terminals have two types of gates: NLA and conventional jets; (ii) the number of NLA gates and routes from/to runway has been previously determined; and (iii) part of infrastructure is adapted to NLA operation.

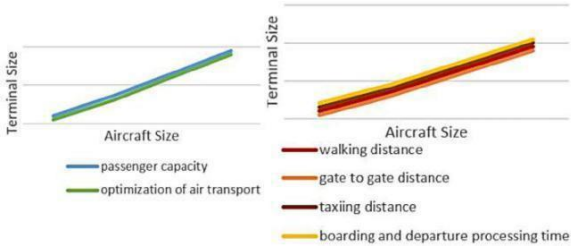

Fig.5. Tradeoffs of terminal expansion and NLA: benefits (left) and losses (right)

The analysis of airport configurations with hybrid terminals that receive the NLA shows that the benefits are related to the air transport operation, whereas the losses are also linked to the infrastructure, in addition to the operation.

Planning for new airports and expansions at existing airports are already taking the proposed new large aircraft into consideration. The new physical and operational characteristics of large aircraft will dictate the design of future airports and their facilities, which, according to the analysis proposed in this paper, deserve special attention.

REFERENCES

BANDARA, S., WIRASINGHE, s. c. (1992). Walking distance minimization for airport terminal configurations. Transpn. Res.-A, Vol. 26A, No. 1, pp. 59-74, 1992. Printed in Great Britain.

Barros, A. G., Wirasinghe, S. C. (1997). New aircraft characteristics related to airport planning. First ATRG Conference Vancouver, Canada June 25-27.

Barros, A. (2001).. Planning of Airports for the New Large Aircraft. Thesis Submitted To The Faculty Of Graduate Studies In Partial Fulfilment Of The Requirements For The Degree Of Doctor Of Philosophy Department Of Civil Engineering Calgary, Alberta

BOEING. (2018) External List of 747-8 Destination Airports with Regulatory Approval Status. Data as of February 23, 2018.

Chicago Tribune (2018).Chicago, airlines nearing $8.5 billion deal to dramatically expand O'Hare. By Bill Ruthhart, published on feb, 26, 2018.

FAA Federal Aviation Administration - U.S Department of Transportation. (1988). Advisory Circular, AC No: 150/5360-13. Subject: planning and design guidelines for airport terminal facilities.

FAA Federal Aviation Administration - U.S Department of Transportation. (1998). Impact of New Large Aircraft on Airport Design Washington D.C.

FAA Federal Aviation Administration - U.S Department of Transportation. (2006). Advisory Circular, AC No: 150/5300-13. Subject: Change 10 to AIRPORT DESIGN.

ICAO International Civil Aviation Organization (2005). Second Meeting Of The New Larger Task Force (NLA/TF/2). Nairobi, 10 May.

Kusumaningtyas, I., Paro, J., Lodewijks, J. (2007). Accelerating Moving Walkways for Quality People Transport in Airports: An Assessment of Their Applicability in Amsterdam Airport Schiphol. AET Papers Repository.

Marinelli, M., Dell'Orco, M., Sassanelli, D. (2015). A metaheuristic approach to solve the flight gate assignment problem. Transportation Research Procedia 5, 211 – 220 2352-1465 Published by Elsevier B.V.

Neufville, R. de, and Odoni, A. (2002) Airport Systems: Planning, Design and Management, McGraw-Hill, New York, NY (in press).

Neufville, R. de (1995) "Designing Airport Passenger Buildings for the 21st. Century," Paper 10284, Transport Journal, Proceedings of the Institution of Civil Engineers (UK), May, pp. 97-104.

R. M. Parsons Co. and Air Transportation Association of America (1973) The Apron-Terminal Complex -- Analysis of Concepts for Evaluation of Terminal Buildings, AD 771, 186/4GI, US National Technical Information Service, Springfield, VA.

SFO – San Francisco International Aiport (2009). A380 AT SFO A380 AT SFO. Presentation available by Airports Council International – ACI.

Wirasinghe, S.C., Bandara, S. and Vandebona, U. (1987) "Airport Terminal Geometries for Minimal Walking Distances," N. Gartner and N. Wilson, eds., Transportation and Traffic Theory, Elsevier, New York, NY, 483-502

Young, S., Wells, A. (2014). Airport Planning & Management. 6th Edition. McGraw-Hill.

Zhang, Y., Wang, Q. (2017). Methods for determining unimpeded aircraft taxiing time and evaluating airport taxiing performance. Chinese Journal of Aeronautics 30, 2, April, 2017.

International Symposium on Sustainable Aviation 2018
9 – 11 July 2018
Rome, Italy

ISSA-2018-020

THERMODYNAMIC ANALYSIS AND ASSESSMENT OF AN INTEGRATED SOLID OXIDE FUEL CELL BASED ENERGY SYSTEM FOR A MID-SIZE AIRCRAFT

Reza Alizade Evren*, Ibrahim Dincer
Faculty of Engineering and Applied Science, University of Ontario Institute of Technology
2000 Simcoe Street North, Oshawa, Ontario L1H 7K4, Canada
Reza.Mohammadalizadeh@uoit.net, Ibrahim.Dincer@uoit.ca

ABSTRACT

Fuel cells are under consideration as a replace ment for traditional technologies , such as jet engines for aircraft applications since they are more efficient at converting chemical energy to electrical energy . A steady progress in developing electric airli ners may win fewer headlines but could generate significant changes over time as well as help save the planet. This paper reports on the results of a study that uses a solid oxide fuel cell (SOFC) system for a mid - si ze airliner, and investigates the thermodynamic limits and conceptual solutions for heating and cooling during various temperatures of the proposed energy system. The results of the thermodynamic energy and exergy analyses , and the performance assessment of the proposed in tegrated system, are presented and discussed. The exergy and energy efficiencies of the major components are calculated and the maximum efficiencies are observed in the SOFC, with energy and exergy efficiencies of 84.54% and 80.31%, respectively. This novel multigeneration al system has overall energy and exergy efficiencies of 57. 53%and 47. 18 %, respectively .

Keywords: Sustainable development, SOFC, Hydrogen, Airplane, Energy and Exergy.

INTRODUCTION

Fuel cell systems are especially beneficial for long range aircraft and can offer solutions for these requirements with the main advantages of higher fuel efficiency, lower to nil emissions, direct current generation, decentralization of power generation and potential water recovery. The integration of solid oxide fuel cells (SOFCs) is acknowledged as one of the clean, energy efficient generating powers for the commercial, domestic, and industrial sectors.

Kadyk et al. (2018) designed and discussed the use of fuel cells as the main energy supply for passenger transportation aircraft. They delivered a physical model of a fuel cell and general design considerations, and discussed different possible design objectives as well as the trade-off between power density and efficiency. Their model uses effective physical parameters, which allows for estimating future development of materials. From the general model-based analysis, it was observed that the optimal size of the fuel cell depends on the interplay of efficiency and power density.

Genç and Sarikoç (2018) presented the performance of a solid-oxide fuel cell/gas turbine hybrid power generation system, with a heat recovery waste unit, based on energy and exergy analyses. The effect of air inlet temperature and air/fuel ratio on exergy destruction and network output was determined.

Waters (2015) investigated the use of gas turbine engine integrated solid oxide fuel cells (SOFCs) to reduce fuel burn in aircraft with large electrical loads, such as sensor-laden unmanned air vehicles.

Fateh (2015) studied the use of bi-directional Solid-Oxide Cells (SOCs) as an auxiliary power unit (APU) on-board commercial aircraft. These bi-directional SOC APU units can be used in an airport energy network to either produce cleaner energy or to produce sustainable fuels, depending on energy demand. This work focusses on the use of these bi-directional SOCs as fuel cells during flight operations and as electrolysers to produce sustainable fuel at an airport when aircrafts are parked. On-board commercial aircraft is explored.

Chinda and Brault (2012) developed two models based on thermodynamic expressions. A comparative study of simulated configurations, based on an energy analysis, is used to perform a parametric study of overall hybrid system efficiency. Some important observations are made by means of a sensitivity study of the complete cycle for the selected configuration.

The objective of the present study is to conduct a comprehensive thermodynamic analysis of a novel multigenerational energy system for an integrated solid oxide fuel cell (SOFC) energy system for a mid-size airliner. The specific objectives are listed as

- To investigate the thermodynamic limits and propose conceptual solutions for heating and cooling during various seasons.
- To design fuel cell needs in the context of a complete energy system.
- To conduct energy and exergy analyses on the proposed system and study energy and exergy efficiencies.

SYSTEM DESCRIPTION

The present system as shown in Fig.1 includes a solid oxide fuel cell (SOFC), a steam bottoming cycle, wing anti- icing and a steam power plant system. During the entire flight of an aircraft, electrical power is presently supplied by generators that are driven by the core of chief propulsion engines.

At point 1 of Fig. 1, the air goes through a preheat exchanger. At stage 2, it goes inside the SOFC and, after reaction, burns in the combustor. At point 9, hot gas goes into the heat exchanger in separator A. At point 8, gas enters the preheater and transfers heat to the system. The gas will mix steam with hydrogen at stage 7 and, at point 6, hydrogen mixes with the steam, passes through the SOFC anode and burns at stage 4. Transfer of heat energy from high

temperature exhaust gas to water and steam takes place by a waste heat recovery boiler in the bottoming cycle. At stage 18, water will condense at point 22, while extra air exits at stage 26. Potable pure water, which is produced during the steam bottoming cycle, is used at stage 24 and changes ti=o steam at stage 12 with exhaust at point 14 with running turbine for producing electricity. Air, which is sucked into the compressor at stage 13 after the compression process in stage 11, enters the heat exchanger and, after increasing the temperature at stage 27, turns the turbine. At stage 14, hot air enters the anti-icing system on the aircraft wings.

Solid oxide fuel cell (SOFC)

A solid oxide fuel cell is an electrochemical contrivance that engenders electrical energy by oxidizing fuel. The system itself consists of a porous anode and cathode that are disunited by an ion conductive solid electrolyte. In this contrivance, the fuel is oxidized at the anode while the reduction of oxygen takes place at the cathode. These reactions are possible if the electrons participating in this process can peregrinate from the anode to the cathode, which is only possible by utilizing an outer circuit. Consequently, this is where electrical energy can be harnessed. SOFC technology has the potential to generate electrical power at a higher efficiency than is achieved by using power from a main engine shaft to run a generator.

Steam bottoming cycle

One of the main issues with power cycles is the ultimate rejection of a significant amount of thermal energy, which exits the system either by heat transfer in a closed cycle or via thermal transport by exhaust gases in an open cycle. During the constant pressure process, the exhaust gases in a gas turbine reject heat. The feed water, as well as the wet and super-heated steam, absorbs some of this heat in the process.

Wing anti-icing system

In flight, ice destroys the smooth flow of air, increasing drag while decreasing the ability of the air foil to create lift. The proposed ice protection system is a fluid-based ice protection system used to help aircraft safely exit in-flight icing conditions. The system uses a fluid to cover the critical surfaces of an aircraft and prevent the risk of any ice forming on the leading edges of the wings.

Steam power plant

In this study, a binary vapour cycle is defined in thermodynamics as a power cycle that is a combination of cycles. In this small power plant, this is the cycle of the steam produced in the heat exchanger, then taken to the steam turbine.

THERMODYNAMIC ANALYSIS

Comprehensive energy and exergy analyses are conducted for the suggested aircraft system. This would provide substantial information about the performance, efficiency and emissions of the cycle. In this section, detailed thermodynamic analyses are conducted to study mass, energy, entropy and exergy balance equations for the system and its components.

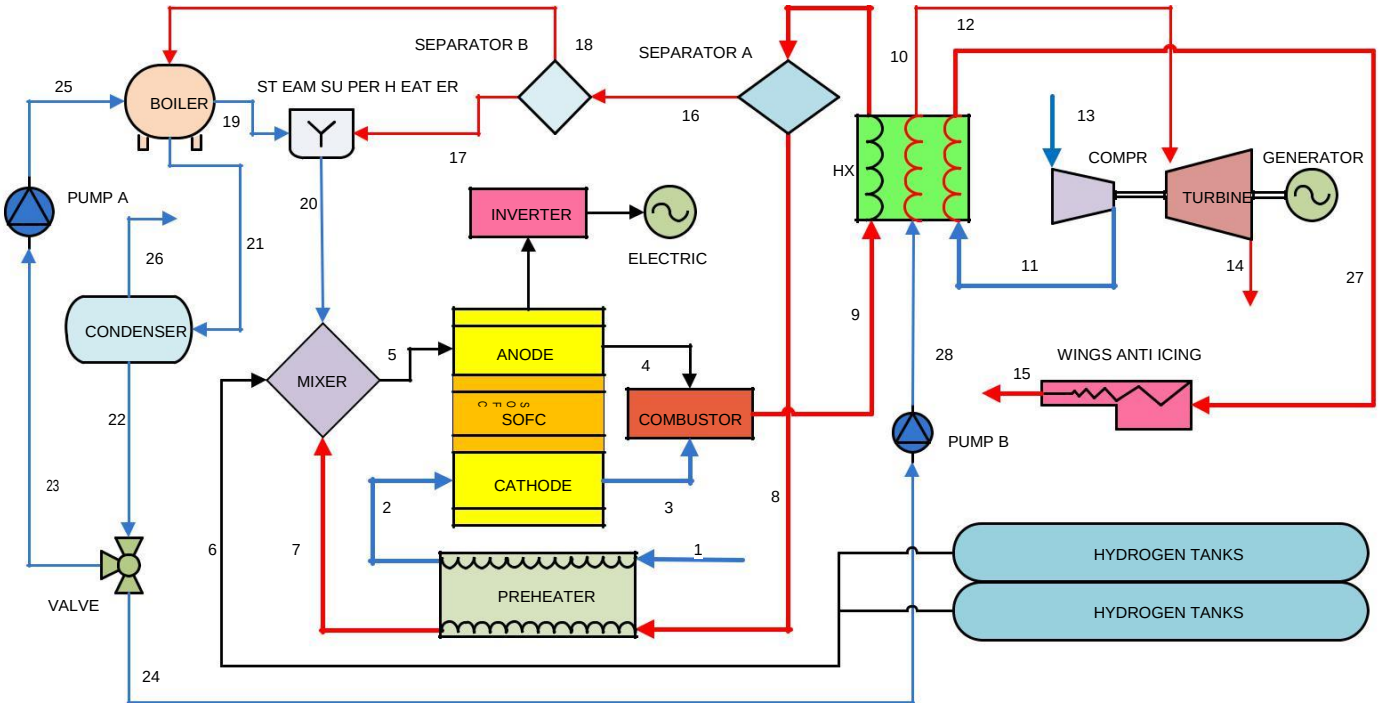

Fig. 1: Proposed system process flow diagram.

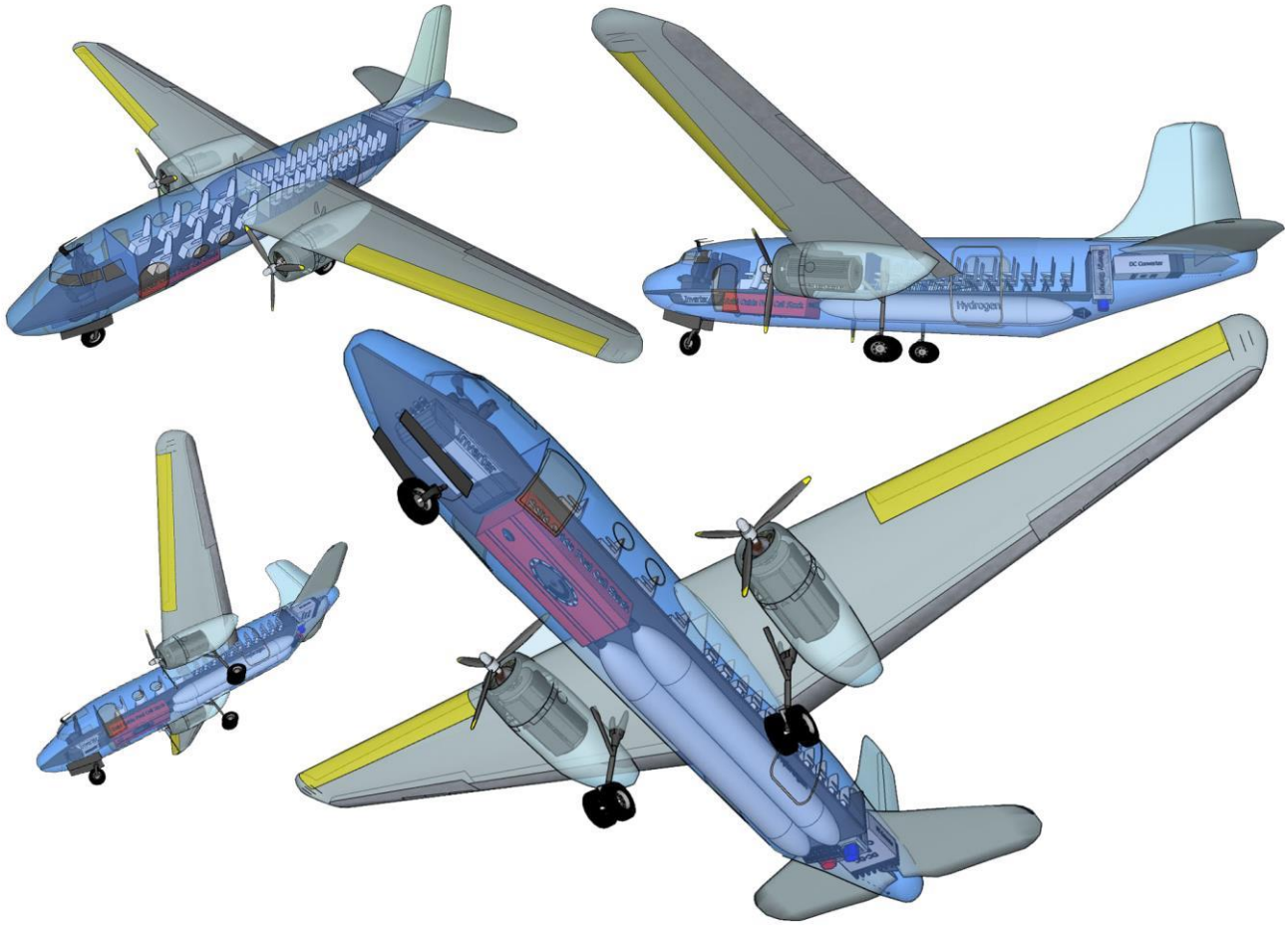

Fig. 2: Mid-size airliner powered by 820 kW solid oxide fuel cell (SOFC).

This section also describes the thermodynamic principles associated with solid oxide fuel cells. Standard reversible voltage is derived from thermodynamic laws followed by definition and calculation of Nernst potential with SOC losses. To model the SOFC, some certain assumptions need to be made as listed below:

- Steady state operation
- Constant utilization factor
- Isobaric electrochemical reaction at SOFC
- Same equivalent area specific resistance assumed for both SOFC models
- Temperature difference of 100K between the inlet and outlet of the SOFC

Table 1: A list of mass, energy, entropy and exergy balance equations.

Components	Mass Balance:	Energy Balance:	Entropy Balance:	Entropy Balance:
preheater				
combustor				

separator				
steam superheater				
boiler				
pump				
condenser				
valve				
mixer				
turbine				
compressor				
heat exchanger				
wing heat exchanger				

SOFC system

The electrochemical oxidation of H_2 takes place at the anode side, according to the equation. This reaction requires oxygen ions, which are released by the reduction reaction of O_2 taking place at the cathode side of the SOFC. Combining the two half reactions, the overall electrochemical reaction can be obtained as:

$H_2+O^{2-} = H_2O$
$\frac{1}{2}O_2+2e^- = O^{2-}$

hydrogen as a fuel, the reactions at the SOFC anode follow the generic mechanism:

$$M + xO^{2-} \rightarrow M[O_x]_M + 2xe^-$$

$$xH_2 + M[O_x]_M \rightarrow M + xH_2O$$

The oxide ions (O^{2-}) are delivered from the cathode via the electrolyte. $[O_x]_M$ is a state of oxygen within the liquid metal anode. The state of oxygen in the metal varies with operating conditions, hence 'x' is used to represent this uncertainty. When using tin, oxygen may form oxide or sub-oxide or remain dissolved in the melt. The state of oxygen may vary, although it has no particular effect on the overall reaction, which is the sum of Reactions:

$$H_2 + O^{2-} \rightarrow H_2O + 2e^-$$

This Reaction is applicable to any liquid metal anode SOFC system, including Sn or Cu.

$H_2+\frac{1}{2}O_2+2e^- = H_2O$

When the product water is considered steam, is known as the lower heating value (LHV). Therefore, to obtain a good comparison with other fuel-using technologies, the efficiency of fuel cells is usually defined as:

SOFC =

max =

The liquid metal anode acts as an intermediary for the oxidation of fuel. Taking a molten metal (M) and

Thermodynamics of SOFC operation

The maximum electrical voltage generated by an electrochemical system can be determined via the standard equilibrium electrode potential (E_{eq}), expressed by the Nernst Equation, as follows:

where a_i and v_i are the activities and stoichiometric factors of the species i (the stoichiometric factors v_i taking positive and negative values for oxidised and reduced species, respectively), R is the molar gas constant, 8.314 J mol-1 K^{-1}, T is the absolute temperature and E^0 is the standard electrode (equilibrium) potential of the reaction that can be defined from the equation:

where $\Delta G^0_{,r}$ is the Gibbs free energy change of electrochemical reaction, *n* is the number of electrons transferred during electrochemical reaction and *F* is Faraday's constant, 96,485 C mol^{-1}.

The mass flow rate of fuel in an aircraft can be related to the rate of change of vehicle mass (assuming fuel burn is the only mechanism for mass change):

=-

where m_f is the fuel mass and m is the aircraft mass. This can be rearranged to form an expression for dt:

Here, endurance, E, can be generally expressed as the integral of time over the duration of the mission, the following general expression can be formed for a fuel burning aircraft:

where and are the initial and final aircraft mass, respectively.

RESULTS AND DISCUSSION

In order to enhance understanding of the system's performance, it is important to use several analyses to identify how this performance varies with design parameters.

In this part, the results of thermodynamic modelling, exergy, and optimization are explained. Exergy analysis can help develop strategies and guidelines for more efficient and effective use of energy and is utilized to study various thermal processes, especially power generation and multigeneration.

The analysis includes a determination of the exergy efficiency of each component in the proposed system and also determines the overall exergy efficiency of the multigenerational system. Exergy analysis also helps to identify and quantify the source of irreversibility that is associated with each component in the proposed systems.

The exergy and energy efficiencies of the major components of the proposed system are calculated and shown in Fig. 3 and Table 2. Maximum efficiencies are observed in the SOFC, followed by the separator, with the third highest efficiency occurring in the pump. To improve the performance of the overall proposed system, efforts need to be made to increase efficiency in the turbine.

The increase in ambient temperature increases the energetic and exergetic output of the system. The proposed system, which offers many advantages, will be successful in comparatively similar systems. Regarding SOFC, one way to scale up a fuel cell based energy generation system is to make a very large "sandwich" of individual fuel cells, referred to as a fuel cell stack.

This novel multigeneration system has overall energy and exergy efficiencies of 57.53% and 47.18%, respectively, as given in Table 3.

The physical reasonableness of the electrochemical model is evaluated by computing fuel cell performance over a range of temperatures and pressures. Fig. 4 shows the operating voltage of the SOFC as functions of current density. They are analogous to button-cell results in that they isolate the electrochemical performance of the designated SOFC without impact from down-the-channel effects of heat loss and reactant depletion.

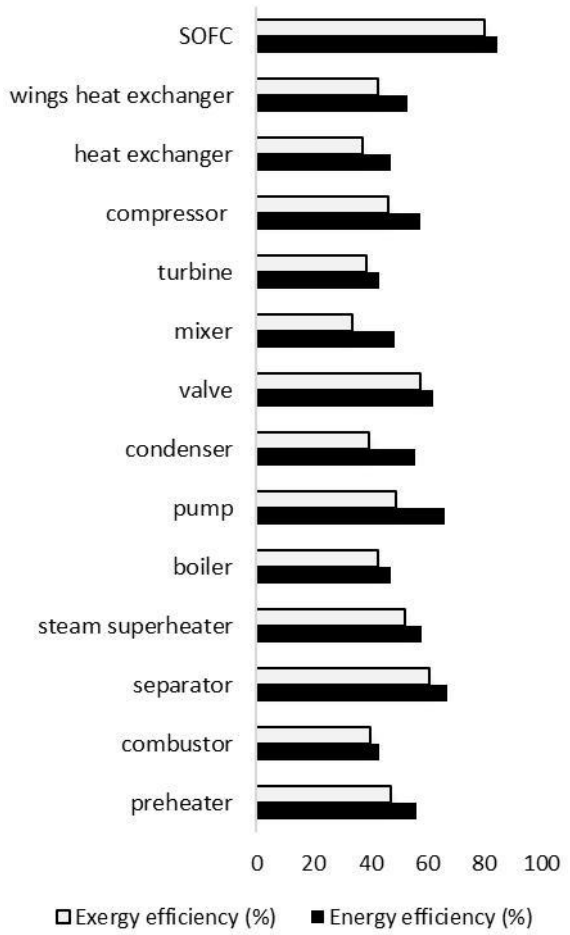

Fig. 3. Energy and exergy efficiencies of the selected units of the proposed system.

Table 2: Energy and exergy efficiencies of the proposed system components.

Components	Energy efficiency (%)	Exergy efficiency (%)
preheater	56.45	47.34
combustor	43.23	39.92
separator	67.14	60.69
steam super heater	58.24	52.34
boiler	47.11	42.92
pump	66.21	49.26
condenser	55.89	39.69
valve	62.11	57.46
mixer	48.78	33.89
turbine	42.94	38.79
compressor	57.48	46.13
heat exchanger	47.19	37.11
wings heat exchanger	53.23	42.89
SOFC	84.54	80.31

Table 3 Overall exergy and energy efficiencies.

Parameter	Value
	57.53%
	47.18 %

Fig. 5 shows the power density of the SOFC as functions of current density. Results are calculated at a constant pressure of 1 atm, in four different temperatures. The solid oxide fuel cell shows best performance at 800oC with maximum power density of 1.2 V. This illustrates the importance of maintaining an appropriate cell temperature as performance drops nonlinearly with decreasing temperature.

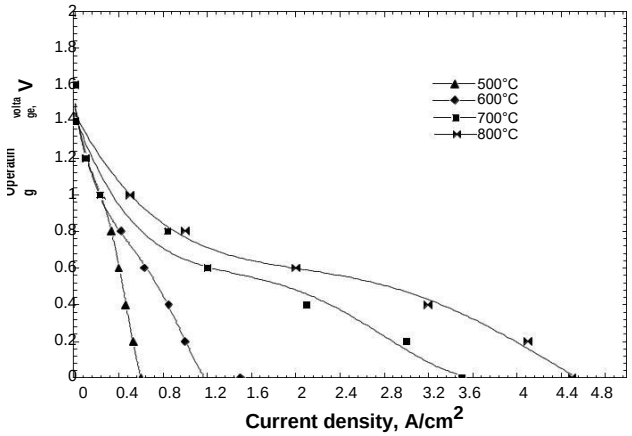

Fig. 4. Operating voltage of SOFC vs current density at 1 atm and various temperatures.

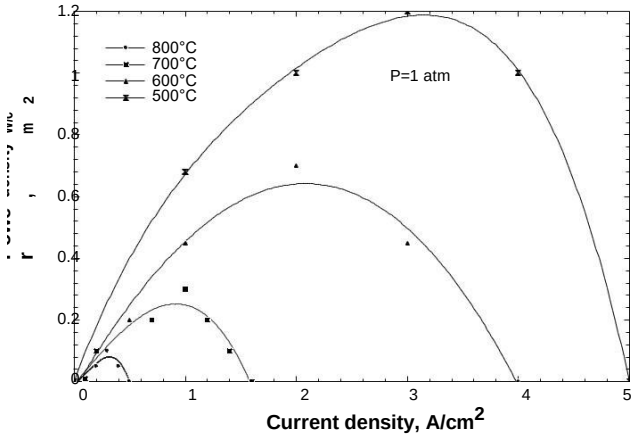

Fig. 5. Power density of SOFC vs current density at 1 atm and various temperatures.

Fig. 6 shows performance at 700℃ and a range of pressures. While raising the pressure from 1 to 10 atm increases power density by ~50%, further increases in pressure yield progressively smaller improvements in power density. Taken together, the characterizations of the fuel cell model suggest that there will be an interesting system-level trade between high-pressure fuel cell performance and low pressure performance.

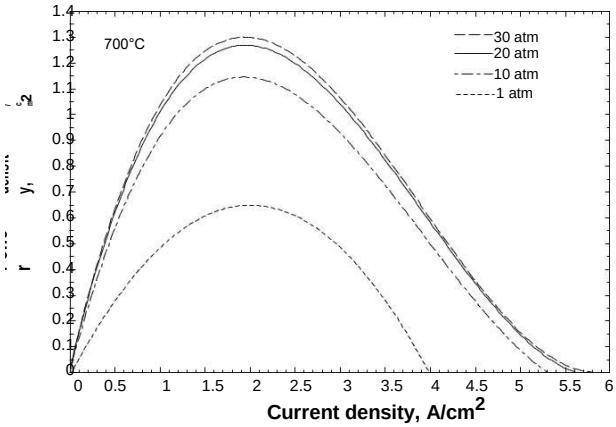

Fig. 6. Operating voltage of SOFC vs current density at 700oC and various pressures.

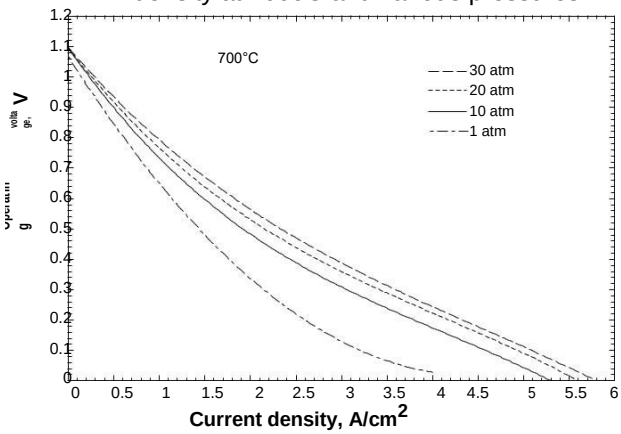

Fig. 7. Power density of SOFC vs current density at 700oC and various pressures.

CONCLUSIONS

The electric flight revolution is now taking place, but it is in the light aircraft and even 'personal air taxi' fields where the first practical uses will occur. Steady efforts may win fewer headlines about developing electric airliners but could generate significant changes over time, as well as help save the planet.

Therefore, to meet growing power demands for futuristic airplanes, the size (output) of these generators needs to increase, as these are currently limited for modern engines by the capability of their core and existing space. Thus, engines need to be redesigned to incorporate the large increase in electrical power that is required for airliners. By replacing heavy generators, an improvement can be achieved with one or more highly efficient, and clean, continuously operating Fuel Cell Power Units. The performance of the proposed system mainly depends upon operating parameters, i.e. turbine inlet temperature and pressure ratio, which were analyzed since they directly affect the proposed system's efficiency and power production. The proposed integrated system showed overall energy and exergy efficiency values of 57.53% and 47.18 %, respectively.

NOMENCLATURE

	exergy rate (kW)
ex	specific exergy (kJ/kg)
	exergy destruction rate (kW)
H	enthalpy (kJ/kg)
	mass flow rate (kg/s)
P	pressure (P)
	heat rate (kW)
s	specific entropy (kJ/kg K)
T	temperature (K)
V	velocity (m/s)
	work rate (kW)

Greek Letters

	energy efficiency
	exergy efficiency
	density (kg/m^3)
	Ohm resistance efficiency

Acronyms

act	actual
G	generator
P	pump
RC	Rankine cycle
LH_2	Liquid Hydrogen
SOFC	Solid oxide fuel cell
GFE	Gibbs free energy
N	Number of cells in series
LHV	Low Heat Value
HHV	High Heat Value

REFERENCES

Chinda, P. and Brault P. (2012) The hybrid solid oxide fuel cell (SOFC) and gas turbine (GT) systems steady state modeling, International Journal of Hydrogen Energy, Volume 37, Issue 11, June 2012, Pages 9237-9248

Genç and Sarikoç (2018) Energy and exergy analysis of a solid-oxide fuel cell power generation system for an aerial vehicle, (ISSA- 2015–139)

Fateh, S., (2015) Bi-directional Solid Oxide Cells used as SOFC for Aircraft APU system and as SOEC to produce fuel at the airport, Faculty of Mechanical, Maritime and Materials Engineering, Delft University of Technology, Master of Science Thesis

Kadyk, T., et al. (2018). Analysis and Design of Fuel Cell Systems for Aviation. Energies 2018, 11, 375; doi:10.3390/en11020375

Klein, S.A. (2017), Engineering Equation Solver (EES). Professional V9.902, Madison, USA. http://www.fchart.com

Waters, D. and Christopher P. Cadou, (2015) Engine-integrated solid oxide fuel cells for efficient electrical power generation on aircraft, Journal of Power Sources 284 (2015) 588e605

International Symposium on Sustainable Aviation 2018
9 – 11 July 2018
Rome, Italy

ISSA-2018-021

EFFECTS OF WEATHER UNCERTAINTY IN SECTOR DEMAND AT TACTICAL LEVEL

Alfonso Valenzuela, Antonio Franco and Damián Rivas
Dept of Aerospace Engineering
Universidad de Sevilla
41092 Sevilla, Spain
{avalenzuela,antfranco,drivas}@us.es

Daniel Sacher
MeteoSolutions GmbH
64283 Darmstadt, Germany
daniel.sacher@meteosolutions.de

Javier García-Heras and Manuel Soler
Dept of Bioengineering and Aerospace Engineering
Universidad Carlos III de Madrid
28911 Leganés, Spain
{javier.garcia-heras, masolera}@ing.uc3m.es

SUMMARY

In this paper, the sector demand at tactical level is analysed with the main objective of quantifying the effects of weather uncertainty due to the presence of thunderstorms . The source of uncertainty is the location of the convective cells, which are to be avoided by the aircraft, resulting in uncertain deviations trajectories and, thus, in an uncertain occupancy count . The analysis is based on the s tatistical characteri zation of this count . Results are presented for a realistic application. Furthermore, it is shown that the dispersion of the occupancy count can be reduced if the convection risk of the individual trajectories is reduced in the mid -term planning phase.

Keywords: sector demand; occupancy count; weather uncertainty; thunderstorms; nowcasts.

INTRODUCTION

In 2005, the European Commission stated the political vision and high level goals for the Single European Sky and its technological pillar SESAR. Accomplishing the goals of increasing capacity and improving safety requires a paradigm shift in operations through innovative technology and research. A promising approach that can improve current prediction and optimization mechanisms towards meeting these goals is to model, analyse, and manage the uncertainty present in Air Traffic Management (ATM). Weather uncertainty is one of the main sources of uncertainty that affect the ATM system (Rivas and Vazquez, 2016).

The objective of the work presented in this paper is twofold. On one hand, to quantify the effects of the stochastic evolution of the thunderstorms on the prediction of the demand of an Air Traffic Control (ATC) sector at tactical level, some minutes before operation. On the other hand, to show that these effects can be reduced when the airspace users plan the route of each individual flight with the objective of reducing the convection risk. Results are presented for a realistic application.

In this work, the location and size of the storm cells is obtained from Nowcasts. They are deterministic short-term forecasts based on the actually observed situation (Kober and Tafferner, 2009). In order to model the weather uncertainty, the location of each convective cell is randomly perturbed within a given margin. This margin models the typical displacement errors of the Nowcasts, which increase as the lead-time increases.

The general framework of this work is the project TBO-Met (https://tbomet-h2020.com). The analysis and reduction of the effects of wind uncertainty on sector demand at pre-tactical level (one day in advance) was already presented in (Valenzuela et al., 2017a).

METHODOLOGY

The general methodology for sector demand analysis is presented in detail in (Valenzuela et al., 2017b); next, it is particularized for the tactical problem.

For each flight the process is as follows. First, a reference trajectory is computed by the airspace user 3 hours in advance of the departure time. This is the trajectory to be filed in the flight plan or the Reference Business Trajectory in the future Trajectory Based Operations (TBO) concept. In this work, this reference trajectory is determined by the trajectory planning algorithm described in (González-Arribas et al., 2017), which is able to reduce the convection risk along the whole trajectory.

It is assumed that the aircraft perfectly executes the reference trajectory until it arrives to the boundary of an extended area that comprises the ATC sector. Thereby, only the uncertainty originated by the thunderstorms inside or close to the sector is considered in this analysis.

Once the aircraft enters the extended area, different possible deviation trajectories are predicted for each flight. These trajectories evade the thunderstorms, taking into account the random location of the storm cells, and reattach to the reference trajectory. They result in different predicted entry and exit times to/from the ATC sector under study. In this work, the DIVMET algorithm (Hauf et al., 2013) generates the deviation trajectories.

The possible deviation trajectories, and thus the predicted times, are updated according to the release of new Nowcasts and the movement of the aircraft. For flights already inside the extended area, the real deviation trajectory followed by the aircraft is considered to be the one obtained using DIVMET along with the latest available deterministic Nowcast.

In this work, the sector demand is described in terms of occupancy count: number of flights inside the sector during a selected time period. The different predicted entry and exit times obtained for each flight lead to different predicted occupancy counts. The analysis is based on the statistical characterization of this count.

Statistical characterization of the occupancy count

It is considered that there exist different flights. For a flight (= 1, …) the DIVMET algorithm performs executions and provides different deviation trajectories considered as equally probable (≤ , corresponding to successful executions, because in some cases there can be spatial distributions of storm cells that DIVMET cannot avoid). The position of flight for the deviation trajectory (= 1, …) at time is named as ( ).

If the trajectory crosses the ATC sector, then

there exist an entry time to the sector , and an exit time from the sector , (≤). If a trajectory crosses the sector multiple times, then the entry and exit times are considered to be the time of the first entry and the time of the last exit, respectively.

An occupancy function is defined for flight , for deviation , and for time period (= 1,2, …), denoted as ( ) . It takes the value 1 when the aircraft is inside the sector during this time period (it enters, exits, or stays in the sector in this period) and the value 0 if the aircraft is outside. If a deviation trajectory does not enter the ATC sector, then , and , are set arbitrarily and it is set to zero.

$$( ) = \begin{cases} 1, & \text{if } (, \in) \text{ or } (, \in) \text{ or} \\ & < (- 1)\delta \text{ and } \geq \delta), \end{cases} \quad (1)$$

, and , respectively) of the occupancy count for time period can be determined from the contributions of all the flights as follows

$$( ) = \sum [\max ( )]$$

$$( ) = \sum [\min ( )]$$

The occupancy-count dispersion at each time period is defined as the difference between the maximum and the minimum values: ( ) =

Reference trajectory

For each flight, the reference trajectory is determined before departure by the trajectory-planning algorithm developed in TBO-Met (González-Arribas et al., 2017). This algorithm is able to reduce the route exposure to convective areas, where individual storms may develop.

The necessary meteorological information is provided by Ensemble Prediction Systems (EPS), a collection of 10 to 50 forecasts, with forecasting horizons of up to 2-5 days (World Meteorological Organization, 2012). A probability of convection, , at each geographical location can be obtained by combining two convection indicators: Total Totals Index and Convective Precipitation. In this work, the wind fields are provided by ECMWF-EPS and the probability of convection is derived from GLAMEPS.

The trajectory-planning algorithm minimises a weighted sum of the average flight time ( ) of the corresponding ensemble members of the EPS and the convection risk, measured as the integral of the probability of convection along the route:

$$\frac{1}{} \quad (3)$$

The relative weight of the convection risk is controlled by the parameter . By changing the value of one can obtain routes that are more efficient on average (they arrive earlier) or routes that are less risky in terms of convection (less probable to run into storms).

Deviation trajectories

DIVMET algorithm (Hauf et al., 2013) obtains an efficient and safe route to the final destination

(2)

according to the fields of existing and forecasted storm cells. It requires an initially planned route (the reference trajectory) and storm data as inputs.

The storm data is provided by the Spanish Agencia Estatal de Meteorología (AEMET). AEMET Nowcasts contain estimates of the location of the centroid of convective cells and a rectangle encompassing the detected convective cells. They are released every 10 minutes, with forecasting horizons every 10 minutes up to 1 hour. Taking this data as input, DIVMET constructs convective cells with elliptical shape, which are further extended by a safety margin.

DIVMET has been adapted to account for weather uncertainty as follows: the location of the centroid of each convective cell is varied randomly within a given range, according to an uncertainty margin. The uncertainty margin models the typical displacement errors of a storm nowcast, which increases as the lead-time increases according to the function ( ) = 0.052 1.56 (maximum is given in minutes).

RESULTS

The demand of the en-route ATC sector LECBLVU is analysed from 6:00 to 13:00 on 19 December 2016; the geographical location of the sector and the extended area are shown in Fig. 1. In this application, 257 flights are considered; the cruise altitude chosen for all flights is 38600 ft. ATC sector and flights data have been obtained from Eurocontrol's NEST and AIRAC cycle 1613.

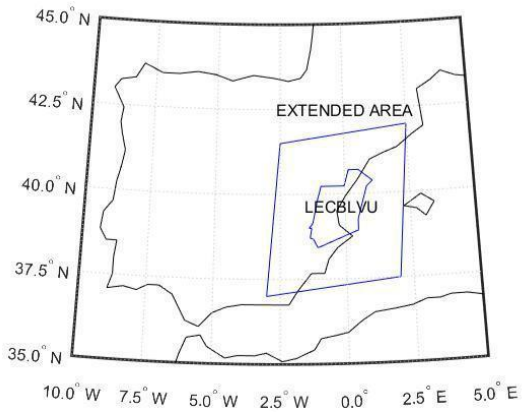

Fig. 1. ATC sector LECBLVU and the extended area

Two different values of the relative weight of the convection risk are considered: = 0 and = 0.005 s/m. Therefore, two different reference trajectories are determined for each flight. Results are shown for both values.

The AEMET Nowcasts released at 08:10, which identifies 55 different storm cells, is depicted in Fig. 2. It can be seen that the sector and the extended area are greatly affected by the storms.

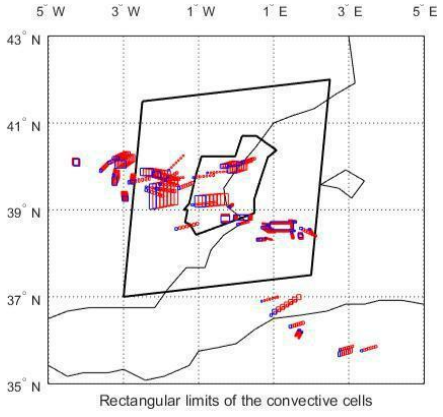

Fig. 2. AEMET Nowcast released at 08:10. Detected storm cells (blue) and estimation for 10,…,60 min (red)

The number of deviation trajectories generated for each flight is = 31. As an example, the deviation trajectories computed at two different time instants for a particular flight and for = 0.005 s/m are shown in Fig. 3. At the first prediction time (09:28), when the aircraft enters the extended area, the deviation trajectories are very disparate among them. The dispersion of the entry time (difference between the maximum and the minimum value) is rather large (294.9 seconds) because the entry point can be located at the Northeast or at the Northwest of the sector. The dispersion of the exit time is even larger (766.3 seconds). As the flight progresses the aircraft comes closer to the storm cells, the dispersion is reduced and the deviation trajectories are more similar to each other. At the second prediction time (09:38), when the aircraft is on the verge of entering the sector, the dispersion of the entry time is nil and the dispersion of the exit time is significantly reduced (386.7 seconds). This behavior can be extended on average to all the flights. In general, the reference trajectories obtained with reduced convection risk, = 0.005 s/m, show a lower dispersion of the entry and the exit times.

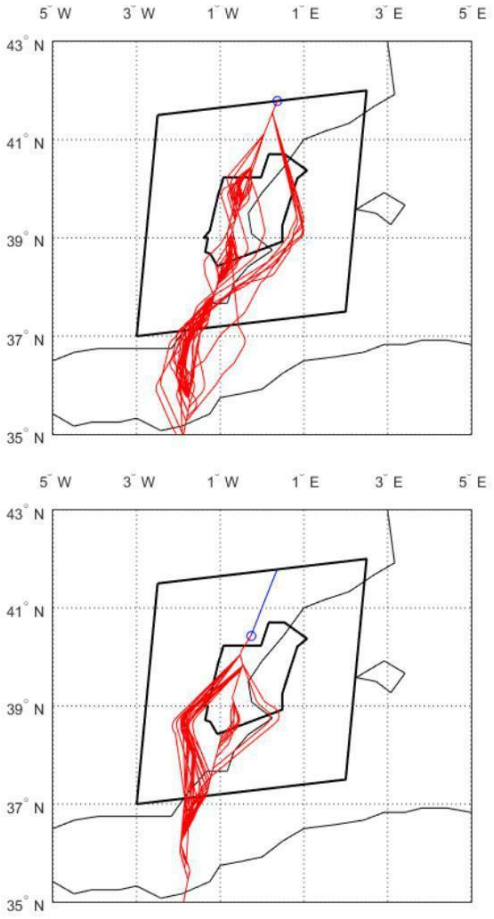

Fig. 3. Flight 203221283 and = 0.005 s/m. Executed trajectory (blue) and deviation trajectories (red). Time instants: 09:28 (top) and 09:38 (bottom)

The occupancy count for = 0 when predicted at two consecutive time instants, 08:30 and 08:40, is depicted in Fig. 4. The average occupancy count is shown as vertical bars, the minimum and maximum counts as whiskers. It is shown for time periods with a duration of 1 minute and a maximum forecasting horizon of 15 minutes. Although the maximum forecasting horizon is short, the dispersion can be rather large, up to 4 flights. One can see how the count dispersion evolves as the predictions are updated. For example, the predicted occupancy count for the period 08:44-08:45 is between 4 and 8 flights when predicted at 08:30, and it is narrowed to be between 5 and 6 flights when predicted at 08:40.

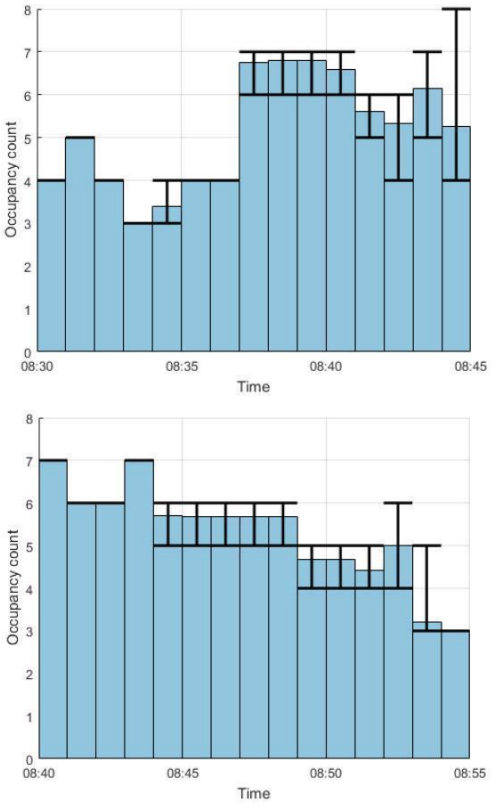

Fig. 4. Occupancy count for = 0 predicted at two time instants: 08:30 (top) and 08:40 (bottom)

The previous example clearly illustrates the reduction of the count dispersion when the predicted time period is closer to the prediction time. The relationship between the dispersion and the forecasting horizon is shown in Fig. 5 for the two values of . In this figure, the average dispersion by forecasting horizon (computed among all the predictions made every 10 minutes between 07:30 and 11:00, when the storm activity is higher) is presented. T_P generically denotes the time instant at which the predictions are made. It can be seen that the average dispersion is almost nil for time periods very close to the prediction time T_P, and that it increases as the forecasting horizon increases. It can also be seen that, as intended, the dispersion decreases as the convection penalty increases, although locally, for some forecasting horizons, it may be larger. The average dispersion among all the forecasting horizons is reduced from 0.52 flights for = 0 to 0.37 flights for = 0.005 s/m.

CONCLUSIONS

In this paper, the effects of the stochastic evolution of thunderstorms on the prediction of the demand of an ATC sector at tactical level have been quantified. Through a particular application, it has been found that the dispersions of the entry and the exit times can be very large, tens of minutes, which lead to large dispersions on the occupancy count. These dispersions increase as the forecasting horizon increases. It has been also found that the dispersions can be reduced if the convection risk is taken into account during the trajectory-planning process before departure.

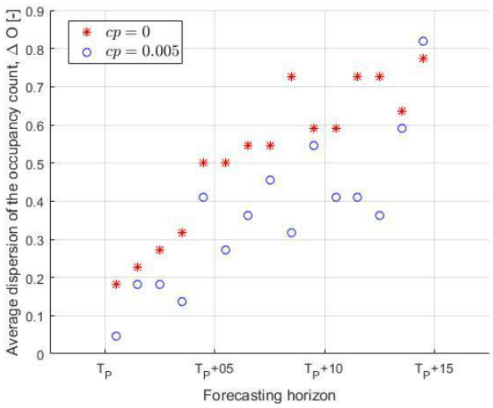

Fig. 5. Average dispersion of the occupancy count

This work is especially relevant for Air Navigation Services Providers: air traffic controllers may know more precisely the future demand of the sectors, being aware of possible workload peaks. Airlines could be also interested in reducing the convection risk to increase not only the predictability of their individual operations but also of the overall air traffic.

ACKNOWLEDGEMENT

This work is part of the project TBO-Met. This project has received funding from the SESAR Joint Undertaking under grant agreement No 699294 under European Union's Horizon 2020 research and innovation programme. The authors thank AEMET for kindly providing the nowcast data employed in this research.

REFERENCES

González-Arribas D., M. Soler, M. Sanjurjo-Rivo, J. García-Heras, D. Sacher, U. Gelhardt, J. Lang, T. Hauf, and J. Simarro, 2017, Robust Optimal Trajectory Planning under Uncertain Winds and Convective Risk, 5th ENRI International Workshop on ATM/CNS, November 14-16, 2017, Tokyo, Japan.

Hauf T., L. Sakiew and M. Sauer, 2013, Adverse weather diversion model DIVMET. *Journal of Aerospace Operations* 2: 115-133.

Kober K. and A. Tafferner, 2009, Tracking and nowcasting of convective cells using remote sensing data from radar and satellite. *Meteorologische Zeitschrift* 1(18): 75-84.

Rivas D. and R. Vazquez, 2016, Uncertainty, In *Complexity Science in Air Traffic Management*, edited by A. Cook and D. Rivas Ed., Ashgate Publishing Limited.

Valenzuela A., A. Franco, D. Rivas, J. García-Heras, and M. Soler, 2017a, Effects of Reducing Wind-Induced Trajectory Uncertainty on Sector Demand, 7th SESAR Innovation Days (SID2017), November 28-30, 2017, Belgrade, Serbia.

Valenzuela A., A. Franco, and D. Rivas, 2017b, Sector Demand Analysis under Meteorological Uncertainty, 7th European Conference for Aeronautics and Space Sciences (EUCASS), July 3-6, 2017, Milan, Italy.

World Meteorological Organization, 2012, Guidelines on Ensemble Prediction Systems and Forecasting, No. 1091.

International Symposium on Sustainable Aviation 2018
9 – 11 July 2018
Rome, Italy

ISSA-2018-022

FURTHER DEVELOPMENT OF A VARIABLE CAMBER MORPHING MECHANISM USING THE DIRECT CONTROL AIRFOIL GEOMETRY CONCEPT

Kai Loudon, Abdessalem Bouferrouk*, Bradley Coleman, Fraser Hughes, Benjamin Lewis, Benjamin Parsons, Alexander Cole, Yufeng Yao

University of the West of England, Bristol, BS16 1QY, UK
*Corresponding author: abdessalem.bouferrouk@uwe.ac.uk

SUMMARY

T hi s paper reports on the design, manufacture and test ing of an improved variable camber morphing wing mechanism following the study by Evans et al . (2016), who employed the so -called Direct Control Airfoil Geometry (DCAG) concept to actuate the trailing edge flap of a NACA 0012 wing . The skin attachment, the skin material and lack of automati on were identified as the major inadequacies withholding proper functionality of the original prototype model . This paper thus discusses how these issues have been addressed and how further advancement was made in demonstrating the feasibility of the DCAG concept on a small -scale wing demonstrator. Specifically, the updated design incorporates a new skin, a flexible corrugated under skin structure, and a controller. It is shown that the new design has an improved aerodynamic efficiency compared with both a single slotted flap, and the original prototype model .

Keywords: DCAG Concept, Variable Camber Morphing, Morphing Skin Material, Corrugation, Controller.

INTRODUCTION

Conventional fixed aircraft wings are constrained by the conflicting requirements of multiple objectives at various flight conditions across a mission cycle (Barbarino et al., 2014). This often results in sub-optimal designs at each condition. A potential solution is the use of morphing High Lift Devices (HLD) and control surfaces to improve the *L/D* performance over a wider flight envelope.

One promising method for realising variable wing camber has been achieved through the use of re-designed Trailing Edge (TE) flaps for which the aerofoil structure is separated and then reattached with a rotary degree of freedom (Monner, 2001). An actuation system is used to generate torque and adjust the relative camber of the flaps. A wing with morphing variable camber TE was shown to optimise the lift-to-drag (*L/D*) ratio between 3 -10 % (Monner, 2001).

Beyond the drag improvements gained aerodynamically, further economic savings may be obtained by reducing the morphing mechanism's weight compared with a conventional TE flap system. This may be achieved via the use of light and smart materials, and by designing innovative variable camber systems which can be used for various roles such as an air brake, aileron, or a lift augmenting flap (Wildschek et al., 2009).

Some progress has been made recently into using morphing technologies to increase the maximum lift coefficient beyond what could be achieved using a conventional TE flap. A key technological challenge in the design of a variable camber morphing wing is that the skin must be able to flex around the altered camber whilst being able to withstand aerodynamic loads and maintain the desired profile, both chordwise and spanwise. Additionally, the actuator mechanism must be able to apply torque evenly over a distributed area.

Much can be learnt from the Fish Bone Active Camber (FishBAC) morphing concept by Woods and Friswell (2012) which employs a skeleton-like structure to impose smooth continuous change in aerofoil camber. For instance, a pre-tensioned elastomer skin was employed to eliminate buckling once deflected. A further design by Takahashi et al. (2016) utilised the highly anisotropic nature of a corrugated structure to give chordwise flexibility and spanwise stiffness. Both designs employed wires to actuate the aerofoil and thus relied on the respective skin attachment structures to provide the main load bearing properties of the device. The Direct Control Aerofoil Geometry (DCAG) mechanism originally conceived by Müller and Müller, (n.d.) and realised by Evans et al., (2016), directly imposes continuous change in both aerofoil camber and surface profile. The device is based on the 'rotational principle' in that by allowing the wing rib to rotate 90°, a profile change is imposed.

The overall aim of this work is to design, manufacture, and test an improved variable camber TE morphing wing mechanism following the study by Evans et al. (2016) to address identified inadequacies withholding proper functionality of the current prototype. The objectives are:

1. Design of an enhanced internal mechanism and skin attachment method.
2. Selection of a suitable skin from tensile testing and fatigue testing.
3. Automation of the manual mechanism.
4. Numerical/experimental testing of design to assess aerodynamic performance.

PRELIMINARY DESIGN

Generally, a TE camber altering morphing wing consists of a load bearing component, a load transferring component, an actuation method, and a flexible skin. Initially, the previous design was evaluated to assess which areas required improvement. Figure.1 depicts the previous model

demonstrating how such design was largely unsuccessful in imposing the aerodynamic profile both chordwise and spanwise through the angles of deflection, especially on the lower surface.

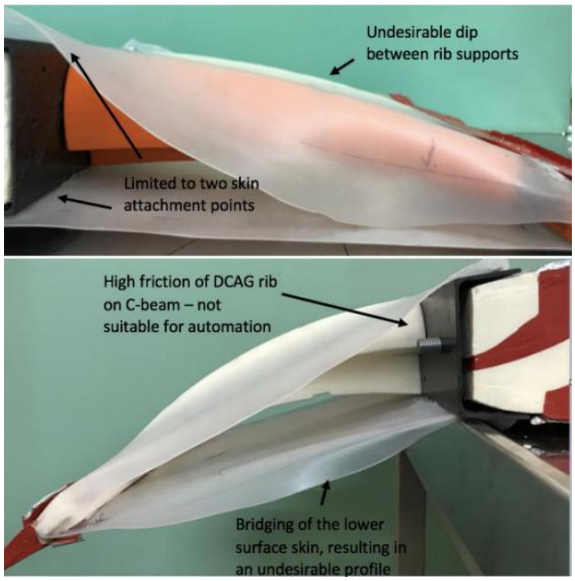

Fig. 1. Demonstration of inadequate skin attachment and internal mechanism from the original manufactured design (Evans et al., 2016) at 0° (upper) and 30° (lower) deflection.

This study has improved the aerodynamic profile of the device by implementing a corrugated structure, taking inspiration from Takahashi et al. (2016). The DCAG ribs were made thinner, to allow them to be encased in the corrugated structure. The anisotropic properties of the corrugated structure gave the device spanwise stiffness, chordwise flexibility and the ability to transfer the aerodynamic loads to the rotating ribs - the main load bearing components of the mechanism. Actuation of the device was applied via the ribs, as in the previous iteration, where the curvature of the rib provides a continuous change in profile geometry.

The four types of shapes for the corrugated structure most commonly employed are sinusoidal, re-entrant, rectangular and trapezoidal. The type of corrugation needs to be carefully selected, as each geometry has different associated structural and flexural properties. Mechanical behaviour analysis by Dayyani et al. (2013) demonstrated how a corrugated structure coated with an elastomer material exhibits changes in its structural properties. Their analysis showed that elastomer coated trapezoidal shapes were superior in terms of bending and tensile stiffness compared with other corrugated shapes. Therefore, for this investigation trapezoidal shaped corrugation was selected as the geometry for the corrugated structure, see Fig. 2 for the CAD model.

To replace a conventional flap, it was known high deflection angles of 25°+ were required. This is larger than TE morphing structures generally seen in literature for an equivalent corrugated structure, e.g. Takahashi et al. (2016) used – 20°, and Thill et al. (2010) used - 12°. To permit the high angle of deflection, a flexible skin such as an elastomer would be required rather than a solid skin such as Carbon Fibre Reinforced Polymer (CFRP) e.g. as used by Takahashi et al. (2016). Fibreglass was chosen as the material for manufacture of the fcorrugated structure due to the low-cost of the material and relative ease of the lay-up into complex geometries compared with alternatives such as CFRP.

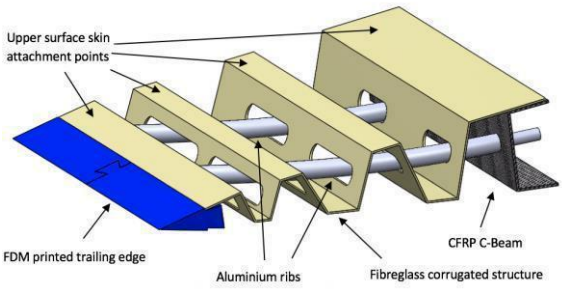

Fig. 2. CAD model of the design of the internal structure at 0° deflection. Note the trapezoidal corrugated shapes for skin attachment, both on the upper and lower surface of the mechanism.

The TE in the design by Evans et al. (2016) was comprised of a Fused Deposition Modeling (FDM) printed piece that the end of the ribs would slot into via a ball bearing. The TE flap mechanism had a chord length of 0.3 m and a span of 0.33 m and once attached to the small scale NACA 0012 demonstrator, resulted in the total aerofoil chord length of 1 m.

SKIN SELECTION

Rigorous skin selection processes were undertaken, via tensile and fatigue tests, to determine a suitable skin to place on top of the internal corrugated structure. Since the morphing flap must undertake deflection angles of 25° +, it was identified that to permit the deflection, an elastomer material would be most suitable. A range of silicone of 0.5 and 1 mm thickness between 30 and 80 Shore were analysed via fatigue and tensile testing.

To allow for automation, the requirement was to minimise the force required to reach full deflection (41.5 mm) with suitable motors. Therefore, it was found that silicone of 40 Shore and 0.5 mm thickness to be most suitable, due to the lowest force of 6.4 N required to reach the required extension. To attach the silicone skin to the corrugated structure, a specialised silicon glue, Elastosil E41, was used. The skin was pre-tensioned using clamps between each skin attachment point. To pre-tension the skin, the wing was set to slightly over maximum deflection and was then attached to the upper and lower surfaces. As a result, undesired skin sagging was largely prevented.

AUTOMATION OF MANUAL MECHANISM

An analogue torque wrench was used to determine the torque required to actuate the mechanism without the skin attached. The torque required was 0.88 Nm and thus allowed a suitable motor to automate the manual mechanism to be chosen. Two 1.9 Nm torque stepper motors were then utilised to actuate the DCAG ribs, controlled via an Arduino Uno microcontroller, see Fig.3 for hardware setup. Subsequently, implementation of the proposed hardware and software proved successful. Automation without skin attachment was achieved up to 23° downwards and upwards deflection. With the skin attached, the controller permitted 15° and 10.27° downwards and upwards deflections, respectively.

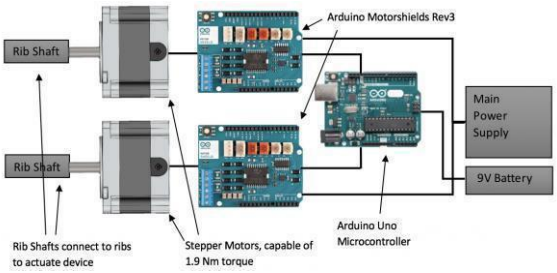

Fig.3. Visualisation of hardware setup for automating the morphing mechanism, showing the Arduino Uno (right) and two Arduino Motorshields Rev3, one for each motor (middle), connected to the wing ribs (left).

A notable improvement the new automation system gave was the ability for 94 points of deflection across the range of morphing motion, permitting an angle setting every 0.31°. By contrast, for the previous prototype only two angles were obtainable: 0° and 30°.

FEA ANALYSIS

Finite Element Analysis (FEA) was utilised to evaluate the design and to better understand the load distribution across the flap. The main use of the FEA was to demonstrate that the location and orientation of the ribs is crucial. Specifically, when the two ribs are placed further apart and rotate in opposite directions it is possible to achieve a more even stress distribution across the load bearing ribs as shown in Fig. 4b. The optimum orientation of the ribs also resulted in 18.7% (von-Mises) stress reduction across the assembly compared with the case when the two ribs were closer to each other and rotate in the same direction (Fig. 4a).

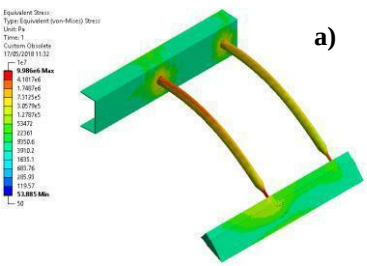

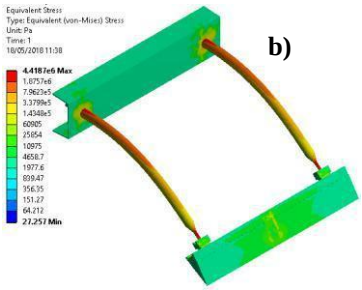

Fig.4. FEA analysis of the (von-Mises) stress on the two different rib orientations.

CFD ANALYSIS AND WIND TUNNEL TESTING

The final improved mechanism (Fig. 5) underwent 2D wind tunnel testing alongside CFD simulations using Ansys Fluent with the RANS k-ε realizable turbulence model. For the wind tunnel tests, a conventional single slotted flap was also tested for comparison purposes. Tests were run at a tunnel velocity of 20 m/s and at 0° angle of attack to match the experimental tests.

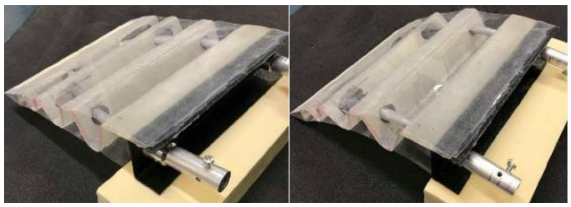

Fig. 5. Final camber morphing flap assembly.

CFD results (not shown) indicates that the lift morphing device gave a 24% improvement in lift-to-drag (L/D) ratio. Wind tunnel testing undertaken in the UWE sub-sonic wind tunnel contradicted this value, demonstrating an increase of *L/D* of only 14.6% compared with the conventional flap. The disparity may be attributed to bridging in the skin, effectively leading to straight sections between the skin attachment points and thus an aerodynamic profile which induced more drag than the geometry simulated in CFD. It is clear from the experimental data in Fig. 6 that the morphing TE flap consistently offers greater *L/D* performance compared with the single slotted flap across the whole range of deflection angles tested.

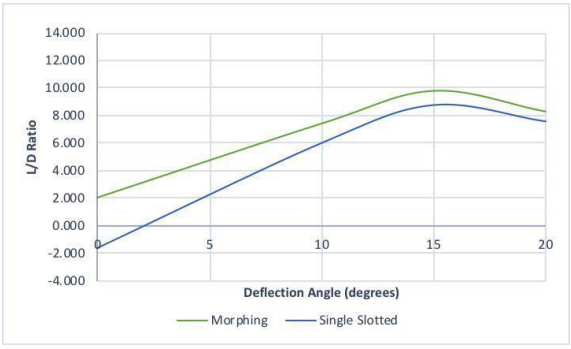

Fig. 6. Wind tunnel results comparing the morphing flap against the single slotted conventional flap at 20 m/s and 0° angle of attack.

Comparing the wind tunnel results (Fig. 6) of the previous iteration against this model, at a deflection angle of 15°, the *L/D* was shown to be 3.8 for the previous design and 9.6 for this design.

FINAL DESIGN

Fig. 5 shows the final improved morphing design with the skin attached. Here, the ribs rotate opposite to one another. As guided by the FEA analysis, this was implemented to spread the aerodynamic loads more evenly across both ribs at full deflection. Additionally, while deflecting the wing, the re-orientation also had the added benefit of stopping the warping out of shape while being deflected, as had previously been the case with the ribs rotating in the same direction. A further addition to the design was a linear guide rail on the FDM printed TE. It had been identified that a lot of friction was being induced by the pin and ball system over the TE. The solution utilised a rail attached to the TE with a carriage of a low coefficient of friction to

one another. The study has advanced the DCAG concept by the implementation of a corrugated structure to offer the required skin support to deliver aerodynamic superiority compared to the previous design as evidenced by wind tunnel testing.

CONCLUSIONS

The present paper describes an approach to achieve chordwise camber variation based on a morphing TE flap. The variable camber morphing wing flap designed in this work has been shown to improve the baseline *L/D* ratio by 14.6% compared to a conventional single slotted flap, aerodynamic profile, structural integrity, and control system of the mechanism compared to the previous iteration. The following are the main achievements:

The DCAG ribs were made thinner to allow for a corrugated structure for the purposes of skin attachment resulting in the aerodynamic profile being more effectively maintained. This was evidenced by an increase in *L/D* from 3.8 to 9.8 for 15° deflection compared to the original model.

The tensile testing of the silicone skins demonstrated the 30 Shore silicone to be most suitable for the improved design as it required the least amount of force (6 N) to reach the 41.5 mm elongation necessary for the full 27° deflection.

CFD analysis compared the performance of the morphing TE flap against a single slotted flap of the same size. On average, a 24.1% improvement in *L/D* was observed over the downwards deflection range at 20 m/s upstream flow velocity, thus justifying the final profile.

Wind tunnel testing demonstrated average *L/D* improvements for the morphing flap compared with the single slotted flap of 14.6%, though testing was limited to 0° angle of attack.

Automation without the skin attached successfully demonstrated both downwards and upwards deflections to 23°. Automation with the skin attached permitted 15.26° downward and 10.27° upward deflections.

ACKNOWLEDGEMENT

The authors would like to thank Zac Kanaa for assistance with the wind tunnel testing.

NOMENCALTURE

x distance along chord length,
m c aerofoil chord length, m

REFERENCES

Müller, J. and Müller, R. (n.d.). How to Simply Change Wing Profile during the Course of a Flight. Available at: http://www.smartairfoil.com/downloads/HowToSimplyChangeWingProfile.pdf.

Evans, C., Harmer, M., Marks, O., Tiley, S., Willis, T., Bouferrouk, A. and Yao, Y. (2016) Development and testing of a variable camber morphing wing mechanism. In: *International Symposium of Sustainable Aviation (ISSA*), Istanbul, Turkey, 29 May - 1 June 2016.

Barbarino, S., Bilgen, O., Ajaj, R.M., Friswell, M.I. and Inman, D.J. (2011) A review of morphing aircraft. *Journal of Intelligent Materials Systems and Structures* Vol. 22. (9)

Monner, H.P. (2001) Realization of an optimized wing camber by using formvariable flap structures. *Institute of Structural Mechanics.,* pp. 445-455.

Wildschek, A., Havar, T. and Plotner, K. (2009) An all-composite, all-electric, morphing trailing edge device for flight control on a blended-wing-body airliner. *Journal of Aerospace Engineering.*

Takahasi, H., Yokozeki, T. and Hirano, Y. (2016) Development of variable camber wing with morphing leading and trailing sections using corrugated strutures*. Journal of Intelligent Material Systems and Structures* pp. 2827-2836.

Thill, C., Ethches, J.A., Bond, I.P., Potter, K.D., Weaver, P.M. and Wisnom, M.R. (2010) Investigation of trapezoidal corrugated aramid/epoxy laminates under large tensile displacements transverse to the corrugation direction. *Journal of Applied Science and Manufacturing* pp. 168-176.

Woods, B.K.S. and Friswell M.I. (2012) Preliminary investigation of a fishbone active camber concept. In: *Proceedings of the ASME 2012 conference on smart materials, adaptive structures and intelligent systems.*

Dayyani I, Friswell MI, Ziaei-Rad S, et al. (2013) Equivalent models of composite corrugated cores with elastomeric coatings for morphing structures. *Composite Structures* pp. 281–292.

ATTITUDE PLANNING FOR THE CONNECTIVITY OF A SWARM OF SPACECRAFT WITH NON-OMNI-DIRECTIONAL COMMUNICATION

Qifeng Chen[1], Song Li[1], Yunhe Meng[2], Yaokun Han[1]
Central South University[1], National University of Defense Technology[2]
1. Changsha, Hunan, 410083, China; 2. Changsha, Hunan, 410073, China
chenqifeng@csu.edu.cn1

SUMMARY

C o n s i d e ri n g a swarm of spacecraft with a directional communication antenna and a payload fixed on each spacecraft, the relative positions and the payload pointing directions of the swarm of spacecraft are given. The problem is to find the attitude s of the spacecraft to meet the connectivity requirement of the interspacecraft communication network . First, possible communication region s of each spacecraft are used to find all allowable communication links, and an allowable communication graph is established . Second, the allowable communication graph is decom posed into a set of 2 -compatible spanning subgraphs in which the neighbors of each spacecraft vertex can be pairwisely covered by their communication cone simultaneously . Third, the spanning trees of 2 -compatible spanning subgraphs are found. For every 2 -compatible spanning tree , a direct search of optimal pointing of the communication antenna is carried out , and the best topology and antenna directions are found . Simulation show s the effectiveness of the proposed method.

Keywords: spacecraft swarm, connectivity, attitude planning.

INTRODUCTION

The concept of a swarm of spacecraft flying closely and working cooperatively is very promising for many space missions, such as distributed sensing, distributed antennas, and replacing an expensive monolithic spacecraft with many low-cost spacecraft [Leonel 2013]. One basic prerequisite for the cooperation of a swarm of spacecraft is the connectivity of the communication network. Each spacecraft in the swarm must be able to communicate with other spacecraft in the swarm, directly or via routing. Thus, connectivity planning and control have become active areas in the field of multi-agent coordinated control [Amir 2010].

Most research in the literature considers the communication omni-directional, where the communication is only restricted by interagent distances. However, in many real cases, the communication antenna is directional, where communication is only possible when the antenna is pointing in the right direction. It may not be economical to have a serving mechanism on the spacecraft for antenna pointing, especially for micro- or nanosatellites. In such cases, the spacecraft attitude must be carefully planned to be appropriate for interspacecraft communication. The spacecraft attitude must also meet the requirement of the mission, such as the pointing direction for the cooperative observation. This paper addresses the attitude planning problem for the connectivity of the communication network for spacecraft with non-omni-directional communication.

PROBLEM STATEMENT

We consider a swarm of n spacecraft. Each spacecraft has a directional communication antenna fixed on its body. The communication region is a cone confined by the maximum communication distance $d_{\max}$. The centerline of the cone is the pointing direction of the antenna, and the half cone angle is . The direct communication between two spacecraft requires that they are both in each other's communication cone.

The mission requires that a main payload fixed on each spacecraft must point along a given direction. Let b_i represent the body frame of the i-th spacecraft, i =1, 2, , n . The unit vector of the payload pointing of the i-th spacecraft is ${}^{b_i}\vec{e}_h^{\,i}$ in its body frame. In a reference frame (such as the inertial reference frame), the unit vector of the payload pointing is represented as $\vec{e}_h^{\,i}$. It is required that $\vec{e}_h^{\,i} \; \vec{e}_p^{\,i}$, where $\vec{e}_p^{\,i}$ represents the required pointing direction of the mission in the reference frame. Let $\vec{e}_c^{\,i}$ represent the unit vector of the pointing of the communication antenna of the i-th spacecraft, and the representation of $\vec{e}_c^{\,i}$ in the body frame of the i-th spacecraft is ${}^{b_i}\vec{e}_c^{\,i}$. The fixed angle between the payload pointing ${}^{b_i}\vec{e}_h^{\,i}$ and the antenna pointing ${}^{b_i}\vec{e}_c^{\,i}$ is .

The positions of the spacecraft in the reference frame are given as $r_i = x_i, y_i, z_i^{\,T}$, i =1, 2, , n , …

where x_i , y_i and z_i are the position coordinate values. The attitude planning problem is to find the proper attitude for each spacecraft in the swarm with the payloads pointing to the required directions, i.e., $\vec{e}_h^{\,i} \; \vec{e}_p^{\,i}$, while the communication network topology composed of the direct communication links between spacecraft is connected. To obtain better communication performance, the communication direction of each direct communication link in the topology should be as near as possible to the centerline of the

communication cone, i.e., the antenna pointing direction.

METHODOLOGY

The attitude solution is closely related to the communication topology and vice versa. The number of topology combination is very large. In this paper, a heuristic mechanism is designed for cutting out nonfeasible topologies to reduce the searching space, and a searching method on this reduced space is provided to find the optimal pointing of the spacecraft antenna.

The Allowable Communication Graph

For the first step, an allowable communication graph composed of all allowable communication links is obtained. Subjected to the payload pointing requirements, each spacecraft can rotate freely about its payload pointing axis, and the communication cone swipes out the allowable communication region. There is an allowable communication link between two spacecraft if they are both in each other's allowable communication region. All allowable communication links constitute an allowable communication graph, in which all possible communication topology are contained.

The condition for deciding whether spacecraft j is inside the allowable communication region of spacecraft i or not depends on the value of the angles and :

$$\begin{cases} \cos(+)\, e_{ij} \quad \vec{} \; e_p^{\vec{}\,i} \cos(-), & \\ \qquad\qquad if and - & \\ \cos(+)\, e_{ij} \quad \vec{} \; e_p^{\vec{}\,i}\, 1, & if- \\ -1 \;\; e_{ij}^{\vec{}} \;\; e_p^{\vec{}\,i} \cos(-), & if\; - \\ -1 \;\; e^{\vec{}} \;\; e^{\vec{}\,l} \;\; 1, & if and\; - \end{cases} \qquad (1)$$

where $e_{ij}^{\vec{}} = \left(\vec{r}_j - \vec{r}_i\right) \Big/ \left|\vec{r}_j - \vec{r}_i\right|$ is the unit vector of the relative position.

The allowable communication graph G is an undirected graph, $G = (V, E)$, where $V = v_1, v_2, \cdots, v_n$ is the vertex set with each vertex corresponding to a spacecraft, and E is the edge set with each edge corresponding to an allowable communication link between its two vertexes. There will be an edge linking the two vertexes in G if and only if the corresponding two spacecraft are in each other's allowable communication region, which can be checked using the condition in Eq. (1). Thus, all the edges in G can be formulated.

The 2-compatible Spanning Subgraphs

For the second step, the allowable communication graph is decomposed into a set of 2-compatible spanning subgraphs. In a 2-compatible spanning subgraph, all the neighbors of each vertex are pairwise compatible, which means that for every pair of neighbors of the vertex, a feasible pointing direction of the antenna for the vertex spacecraft can be found such that its communication cone covers the two neighbors simultaneously. The 2-compatibility is a necessary condition for a graph to be a realizable communication topology for the spacecraft swarm. It is easy to check, thus providing heuristics for reducing the search space. For a communication graph to be realizable, the graph should be fully compatible, i.e., there should exist a feasible antenna pointing direction for each vertex spacecraft such that the communication cone simultaneously covers all the neighbors of the vertex spacecraft.

If v_j and v_k are two neighbors of vertex v_i, the condition for the compatibility of the edges (v_i, v_j) and (v_i, v_k) is that the angle between $\vec{e}_{ij}$ and $\vec{e}_{ik}$ is smaller than 2, i.e.:

$$\cos(2)\, \vec{e}_{ij}\; \vec{e}_{ik} \qquad (2)$$

If the two edges (v_i, v_j) and (v_i, v_k) incident with the vertex v_i are not compatible, they cannot simultaneously exist in one real communication topology. Therefore, they are separated into different 2-compatible spanning subgraphs. Comparing to the allowable communication graph, the set of 2-compatible spanning subgraphs precludes many unfeasible combinations of the edges. Thus, the searching space is reduced.

Fig. 1 shows the algorithm for finding all the 2-compatible spanning subgraphs of the allowable communication graph. A subprocedure named NBR_2CMPT_SETS is called in the algorithm. The subprocedure is illustrated in Fig. 2. It is used for finding all the 2-compatible sub sets of the neighbor set of a given vertex in the graph.

The 2-compatible Spanning Trees

For the third step, all the spanning trees of the 2-compatible spanning subgraphs are found using a standard algorithm such as that in [Harold 1978]. They constitute the set of 2-compatible spanning trees. All connected graphs have at least one spanning tree. Each spanning tree of a connected communication graph for the spacecraft swarm is realizable; thus, they must be 2-compatible. The obtained set of 2-compatible spanning trees covers all the spanning trees of possible connected communication graphs among the spacecraft swarm. Thus, the search can be confined in the set of 2-compatible spanning trees.

The Optimal Antenna Pointing Directions

For the fourth step, optimization of the antenna pointing directions of the swarm spacecraft is carried out on each 2-compatible spanning tree, and the communication performance is compared to find the best solution.

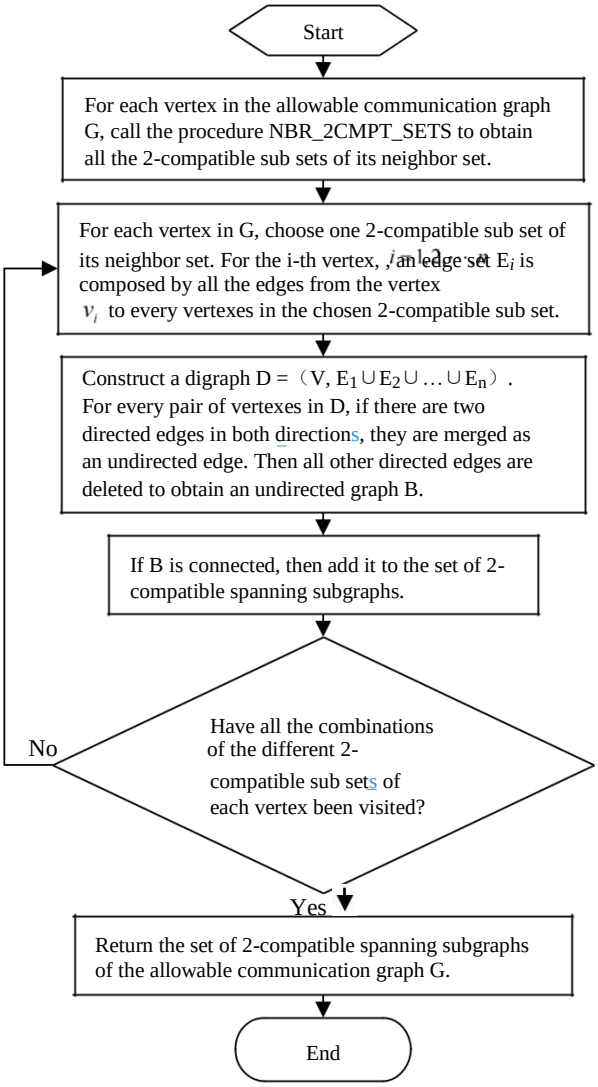

Fig. 1. The procedure of the 2-compatible decomposition.

For a given 2-compatible spanning tree, the search of the antenna pointing direction of each spacecraft is carried out independently. The search is formulated as an optimization problem. Considering the optimization of the antenna pointing of the spacecraft corresponding to the i-th vertex, the antenna pointing direction $\vec{e}_c^{\,i}$ is constrained to rotate around the payload pointing direction $\vec{e}_p^{\,i}$. To quantify the rotation angle, a reference frame pqr_i is defined: the origin is at the barycenter of the spacecraft, and the direction of the 3 axes are $\vec{e}_p^{\,i}$, $\vec{e}_q^{\,i}$, and $\vec{e}_r^{\,i}$, where $\vec{e}_r^{\,i} = \vec{e}_p^{\,i} \times \vec{e}^{\,i}$, $\vec{e}_q^{\,i} = \vec{e}_r^{\,i} \times \vec{e}_p^{\,i}$, and $\vec{e}^{\,i}$ is chosen to be the unit vector of the coordinate direction with the minimal absolute value of the 3 coordinates of $\vec{e}_p^{\,i}$ in the reference frame. The unit vector of the antenna pointing direction is denoted as $e_c^{i,0}$ when it is in the plane spanned by the vectors $\vec{e}_p^{\,i}$ and $\vec{e}_q^{\,i}$, and $e_c^{i,0}$ is used as the starting point of the rotation angle θ_i for quantifying the rotation of $\vec{e}_c^{\,i}$ around $\vec{e}_p^{\,i}$. By the transformation of coordinate systems, $\vec{e}_c^{\,i}$ can be expressed using θ_i as

$$\vec{e}_c^{\,i} = [\vec{e}_p, \vec{e}_q, \vec{e}_{qr}] \begin{bmatrix} 1 & 0 & 0 \\ 0 & \cos\theta_i & -\sin\theta_i \\ 0 & \sin\theta_i & \cos\theta_i \end{bmatrix} \begin{bmatrix} 0 \\ \cos\theta_i \\ \sin\theta_i \end{bmatrix} \quad (3)$$

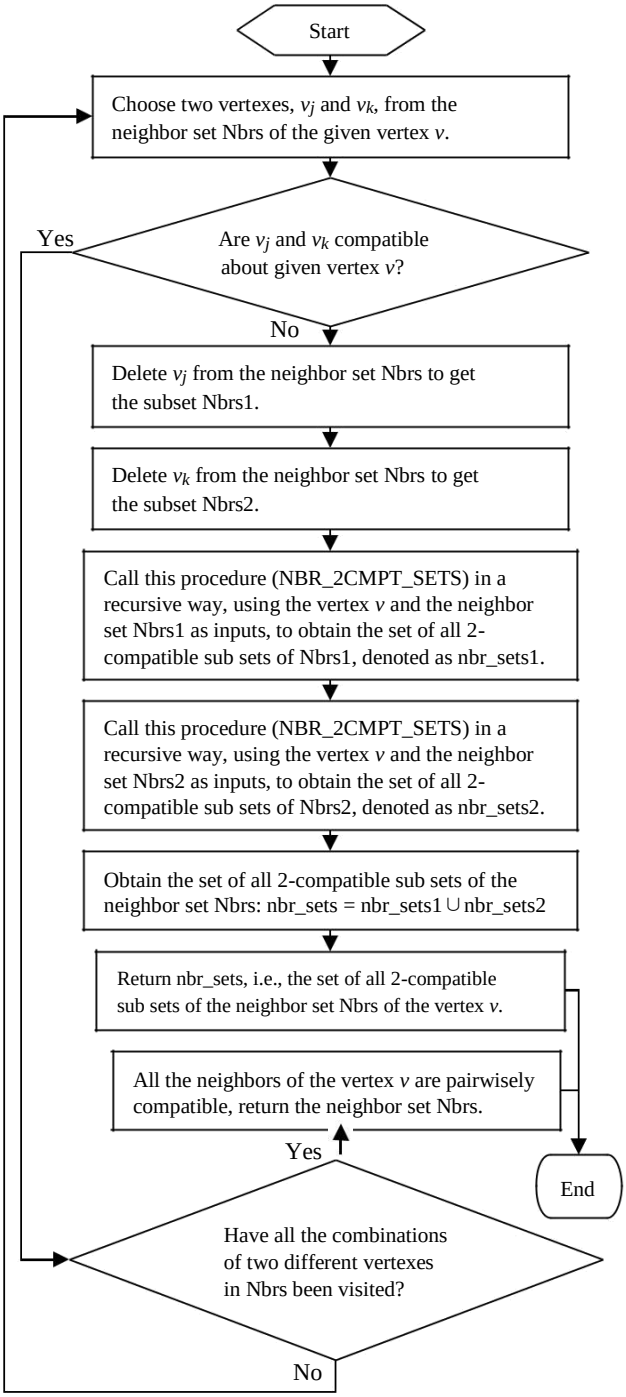

Fig. 2. The algorithm of 2-compatible decomposition of a neighbor set, NBR_2CMPT_SETS.

The optimization of the antenna pointing direction e_c^i is expressed as an optimization of $_i$:

$$\min - \sum_{j \in Nbrs^i} a_{ij}$$

$$s.t.$$

$$-a_{ij} \quad 0, \quad where\ a_{ij} = \vec{e}_c^{\,i}(_i)\vec{r}_{ij} \Big/ \left|\vec{r}_{ij}\right| - \cos \quad (4)$$

$$(\ for\ every\ j \quad Nbrs^i\ )$$

$$0 \quad _i \quad 2$$

where $Nbrs^i$ is the neighbor set of the i-th vertex in the 2-compatible spanning tree. The first constraint requires that every direct communication link of the spacecraft must be within its communication cone, and the objective function requires that the sum of the deviations from the antenna pointing direction of all the direct communication links of the spacecraft is minimum.

For a given 2-compatible spanning tree, the antenna pointing direction of each spacecraft is optimized. If there is no feasible solution, the 2-compatible spanning tree is discarded. Otherwise, it is a completely compatible spanning tree which gives a realizable connected communication graph. The sums of all the objectives of the antenna pointing optimization of every spacecraft show the communication performance of the 2-compatible spanning tree. The one with the best communication performance in those completely compatible spanning trees found is the optimal spanning tree, and the corresponding optimized antenna pointing directions e_c^{i*}(i =1, 2,;;·n) for the tree are the optimal antenna pointing directions.

The Optimal Attitudes of the Spacecraft

The unit vector of the optimal antenna pointing direction can be expressed as $\vec{e}_c^{\,i*}$ in the reference frame, and as $^{b_i}\vec{e}_c^{\,i}$ in the body frame of the i-th spacecraft. Similarly, the unit vector of the payload pointing direction can be expressed as $e_p^{\,i}$ in the reference frame, and as $^{b_i}\vec{e}_h^{\,i}$ in the body frame of the i-th spacecraft. Thus, the cosine matrix to transform from the reference frame to the body frame of the i-th spacecraft can be computed as

$$M_{Rb_i} = {}^{b_i}\left[\vec{e}_c^{\,i}, {}^{b_i}\vec{e}_c^{\,i}, {}^{b_i}\vec{e}_h^{\,i}, \vec{e}_c^{\,i}\left({}^{b_i}\vec{e}_c^{\,i} \quad {}^{b_i}\vec{e}_h^{\,i}\right)\right] \quad (5)$$

$$\vec{e}_c^{\,i*} \quad \vec{e}_c^{\,i*} \quad \vec{e}_c^{\,i} \quad \vec{e}_c^{\,i*} \quad \vec{e}_c^{\,i*} \quad \vec{e}_c^{\,i} \quad -1$$

$$\vec{e}_c \quad , \vec{e}_c \quad \vec{e}_p \quad , \vec{e}_c \left(\vec{e}_c \quad \vec{e}_p\right)$$

which provides the attitude of the i-th spacecraft. **SIMULATION RESULTS**

A swarm of 6 homogeneous spacecraft is considered. The antenna has a half cone angle of $= /4$. The fixed angle between the payload pointing and the antenna pointing is $= 2/5$. All the payload of the swarm spacecraft is in the same pointing direction with $e_p^{\,i} = 0,1,0^{\,T}$, i =1, 2, ,6·: The communication distance of the antenna is 1500 m. The positions of the 6 spacecraft in the reference frame are [853, 648, -486]^T, [276, -156, -770]^T, [-363, 285, 1016]^T, [465, -342, 471]^T, [1001, 532, 714]^T, and [-686, -333, 298]^T.

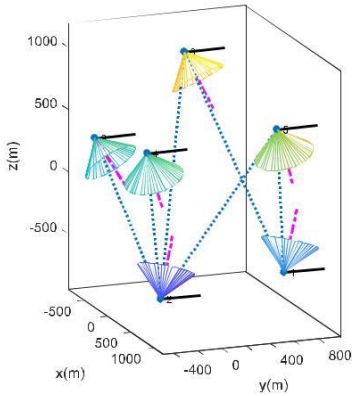

Fig. 3. Pointing directions of the 6 spacecraft.

Fig. 3 shows the attitude planning result for the swarm of spacecraft. The dot point shows the position of the spacecraft. The black lines show the payload pointing, the dashed lines show the antenna pointing, and the dotted lines between dot points show the actual communication links. Parts of the communication cones are also shown.

CONCLUSIONS

This paper investigates the planning of attitudes of a swarm of spacecraft with directional antennae for the communication connectivity. A heuristic mechanism is designed for cutting out nonfeasible topologies to reduce the searching space. The attitude search is carried out on spanning trees to separate the continuous search from the discrete topologies. The simulation of a 6-spacecraft problem shows the effectiveness of the method. The communication connectivity is also affected by the relative positions. The joint planning of spacecraft attitudes and relative positions for swarm connectivity deserves further research.

ACKNOWLEDGMENT

This work was supported by the National Natural Science Foundation of China (61273351).

REFERENCES

Amir Ajorlou, Ahmadreza Momeni, and Amir G. Aghdam, 2010, A Class of Bounded Distributed Control Strategies for Connectivity Preservation in Multi-Agent Systems. *IEEE Transactions on Automatic Control* 55(12): 2828-2833.

Harold N. Gabow and Eugene W. Myers, 1978, Finding All Spanning Trees of Directed and Undirected Graphs. *SIAM Journal on Computing* 7(3): 280-287.

Leonel Mazal and Pini Gurfil, 2013, Cluster Flight Algorithms for Disaggregated Satellites. *Journal of Guidance, Control, and Dynamics* 36(1): 124-135.

ISSA-2018-024

RELIABILITY AND SAFETY ASSESSMENT OF UNMANNED AERIAL VEHICLE SYSTEMS

P. Gonçalves [a,*], J. Sobral [b], L.A. Ferreira [c]
[a] Portuguese Air Force Research Centre (CIAFA)
[b] Mechanical Engineering Department, ISEL – Instituto Superior de Engenharia de Lisboa [b] Centre for Marine Technology and Engineering (CENTEC), Instituto Superior Técnico
[c] Faculty of Engineering of University of Porto (FEUP), Universidade do Porto
[a] Academia da Força Aérea, Av. Leite de Vasconcelos, N.º 4 2614-506 Amadora, Portugal [b] Rua Conselheiro Emídio Navarro, 1, 1959-007 Lisboa, Portugal
[c] Rua Dr. Roberto Frias, s/n 4200-465 Porto, Portugal
Authors' e-mails: pagoncalves@academiafa.edu.pt ; jsobral@dem.isel.ipl.pt ; lferreir@fe.up.pt

SUMMARY

In this work, it was addressed the problem of developing the Initial Maintenance Plan for Remotely Piloted Aerial Systems (RPAS), previously designated by Unmanned Aerial Systems (UAS), for which there is often a lack of reliable data. The approach is two -fold. It was proposed a model for the creation of the Initial Maintenance Plan for use in the UAS certification based on the reliability princ iples and on morphological analysis and also a Petri nets modeling of the UAS Safety Assessment process . The proposed models are applic able to UAS whose operation depends on obtaining an Airworthiness Authori zation / Certification. The objectives were structured according to three aspec ts: the reliability of assets (through a methodology for obtaining reliability data), the initial maintenance plan of the UAS and their respective airworthiness certification.

Keywords: MSG-3, Initial Maintenance Plan, Reliability; Safety Assessment, Unmanned Aerial Vehicle, Unmanned Aerial System, Petri Nets.

INTRODUCTION

The increasing interest in Unmanned Aerial systems (UAS) is well known all over the world, and several efforts are being made to integrate safe operations into civil air space. The development of an initial maintenance plan for newer systems sets up a huge challenge, that can be overcome by scientific methods and supporting tools.

In the aviation sector the risk is widely analyzed and evaluated in order to have an acceptable risk level, or if needed to decrease or mitigate its consequences. Hence, risk and safety are considered in the design phase of new aeronautical products. When dealing with UAS it requires a demonstration of an equivalent level of safety to that of manned aircraft (Clothier & Rodney, 2012).

In order to obtain the aircraft's airworthiness certificate for the UAS an analysis must be conducted in terms of safety assessment and quantifying and classifying the risk associated with the UAS functions (AAN, 2013). The safety assessment process is used in order to demonstrate compliance with the airworthiness requirements and the established manufacturing requirements.

So, in Portugal under the Research and Technology on Unmanned Aerial Vehicles Project (PITVANT) from Portuguese Air Force Academy (AFA), three different models of platforms from two classes of UAS were developed: micro-UAV, ANTEX-X02 (UAV from 15 to 25 kg and with three meters of wingspan) and ANTEX-X03 (UAV of 110 kg and with six meters of wingspan) (AFA and FEUP, 2011).

First, in order to the developed UAS obtain the airworthiness certificate, was developed methodology based on reliability principles and the Morphological Analysis to create the initial maintenance plan. Then, a Safety Assessment Modeling was developed representing the real dynamics of the UAS on the presence of the failure condition that lead to Most Feared Events (MFE). Petri Nets (PN) tool was used to model it, considering isolated or combined failures. The tool was used to determine the average events (Minor, Major, Hazardous and Catastrophic) that will occur in during the expected service period.

UAS SAFETY ASSESSMENT

The aircraft safety assessment process is used in order to demonstrate compliance with the airworthiness requirements (e.g. CS VLA, CS 23 and 25) as well as the established manufacturing requirements (SAE, 2010).

The evaluation process of the basic safety is detailed in ARP 4761 encompasses a set of analysis (SAE, 1996): Functional Hazard Assessment (FHA); Preliminary Aircraft Safety Assessment or Preliminary System Safety Assessment (PASA/PSSA), and Aircraft Safety Assessment or System Safety Assessment (ASA/SSA).

The Functional Hazard Assessment is an analysis of aircraft functions, performed to identify and classify the failure conditions of these functions according to their severity (SAE, 1996). The Preliminary Aircraft Safety Assessment or Preliminary System Safety Assessment is a systematic evaluation of the systems architecture and its implementation is based on the results obtained in the FHA, and the classification of the identified failure conditions allows to establish the

objectives to be achieved for all items (SAE, 1996).The Aircraft Safety Assessment or System Safety Assessment is a systematic evaluation of all systems that make up the UAS, performed to demonstrate that the defined requirements are met (SAE, 1996).

At the military level, the airworthiness requirements for unmanned fixed wing aircraft are defined in several military airworthiness publications such as STANAG 4671, STANAG 4702 and STANAG 4703.

The driving Safety Assessment process recommended in ARP 4761 can be, in essence, applied directly to UAS (NASA, 2007).

It began with the decomposition of UAS functions. The functional decomposition is a structured way to identify all the functions of a system. The functional decomposition is conducted different subsystems.

According to NASA (2007) the main functions of UAS are: aviate, navigate, communicate and mitigate. Following the methodology it is necessary to make a complete decomposition of the four main functions of the UAS.

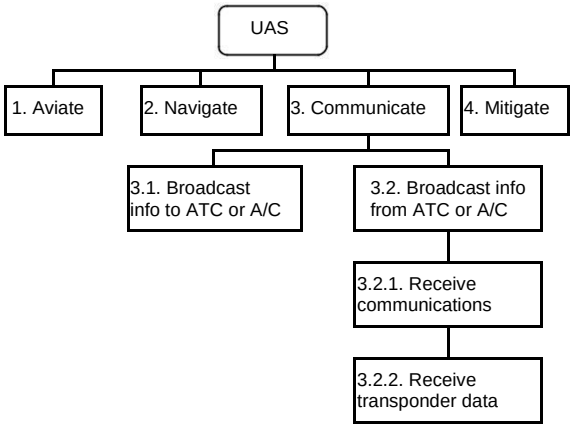

Fig 1- Top-level of the Functional Decomposition (Adapted from NASA, 2007).

Therefore, for each of these functions, all low-level functions, their failure conditions and the operational effects were identified, and evaluated their severity.

Based on the results obtained in the FHA it was: developed a complete list of aircraft and system level safety requirements; determined whether the architecture will met the safety requirements and objectives and, derived the safety requirements for the design, aircraft installation, and operations which are the basis of operation and maintenance plan.

INITIAL MAINTENANCE PLAN METODOLOGY

Due to the lack of reliability information available on UAS systems, and the need to obtain the airworthiness certificate, it was developed a method to create the initial maintenance plan.

The methodology for developing the initial maintenance plan was based on the application of the Morphological Analysis in determination of initial failure rate of the UAS systems, similar to the method presented by Moss and Andrews (1996).

According to Ritchey (2009), Morphological Analysis is the method for investigating and identifying the set of configurations and interfaces associated with a given complex problem. This method is valid whenever there are similar products and services, and is very useful when there is a lack of data available (Vanston, 1998).

The proposed methodology comprises several stages, starting with data collection related to reference failure rates and finishing with the development of the initial maintenance plan of the systems installed on the UAS, is shown in Fig. 2.

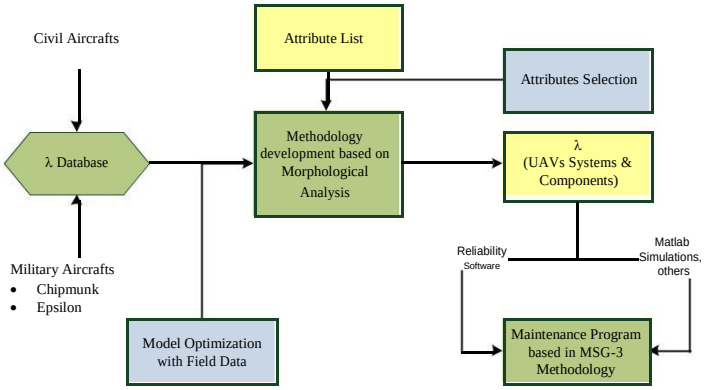

Fig 2 - Method based on the Morphological Analysis.

The process starts with the identification of all systems that comprising the UAS architecture.

The systems that equip the UAS are similar to those of other manned aircraft operated by the Portuguese Air Force, therefore the systems of the manned aircraft, CHIPMUNK MK 20, were used as reference.

The CHIPMUNK MK 20 data collection and analysis allowed the identification of the most significant failure modes. The results permitted to foresee which UAV systems will be considered as critical, as well as to know the potential failure modes that could be present on the UAS.

The UAS Systems failure estimation was based on the identification of similar systems (reference) with known failure rates and subsequent comparison and assignment of the design (D), operation (O) and environment (E) weights. Each one of these categories is evaluated taking into account some attributes.

The estimated failure rates for all systems of the UAS were used to establish and set the time intervals for preventive maintenance activities, for this purpose it was used the Maintenance Steering Group (MSG-3) methodology. This method ensures uniformity and compliance to develop minimum

requirements for scheduled maintenance in accordance with instructions for continuing airworthiness enacted by most regulatory authorities. The logic of MSG-3 consists on a task-oriented approach derived maintenance requirements identified by the manufacturer throughout the Safety Analysis.

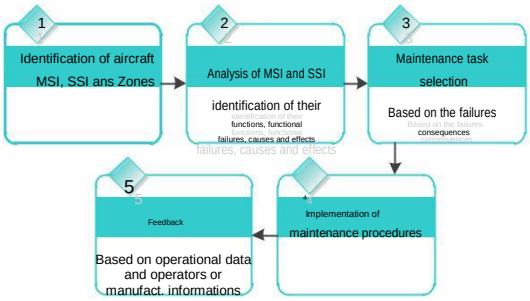

Fig 3 - Development process of Maintenance Plan through MSG-3 logic.

Since MSG-3 was created for manned aircraft, it was necessary to adjust the analysis criteria for the UAS, that is, the risk matrix was adjusted according to the parameters recommended in STANAG 4671 regarding risk acceptance. Subsequently, adopting the procedure recommended in the publication S1000D of AECMA (AECMA, 1999), the Maintenance Plan for the UAS was developed.

The development of initial maintenance plan embodies and materializes the safety requirements and airworthiness derived from the Safety Assessment process. Due, the demonstration phase of compliance with the requirements is crucial to the success of the certification process, it is presented in the following section the model developed for conducting the Safety Assessment of UAS.

UAS SAFETY ASSESSMENT MODELING

The developed model intends to contribute to the increase of confidence in relation to the UAS by the regulators, through the simulation of its behavior in the presence of failure conditions. For this model the Petri Nets (PN) were used, that lead to Most Feared Events with the integration of real UAS dynamics.

Petri Nets are a graphical and mathematical modeling tool applicable to several systems. It is a promising tool for describing and studying information processing systems that are characterized as being concurrent, asynchronous, distributed, parallel, nondeterministic and/or stochastic (Murata, 1989).

The STANAG 4671 defines: failure condition; the risk reference system, which is a combination of severity and probability; as well as a classification of failure conditions and the relationship between the severity of the failure conditions and the effects on the UAS (NATO, 2009). So, failure condition *is a condition having an effect on either the airplane or its occupants, or both, either direct or consequential, which is caused or contributed by one or more failures or errors considering flight phase and relevant operational or environmental conditions or external events* (NATO, 2009).

For the evaluation of failure conditions several analytical tools can be used as the Failure Mode and Effects Analysis (FMEA), Failure Modes and/or Effects Summary (FMES), Fault Tree Analysis (FTA) or Reliability Block Diagrams (RBD). The result of the failure conditions evaluation should be the identification of the Most Feared Events.

Table 1 - Definition of the Most Feared Events (Adapted from (SAE, 2010)).

Feared event	Effects
Uncontrolled flight and/or uncontrolled crash.	Can potentially result in fatalities. Result in loss of UAV control and / or maneuverability.
Controlled-trajectory termination or forced landing	Potentially leading to the loss of the air vehicle, but which can reasonably be expected to avoid fatalities. Prevents the UAV from landing on its planned main landing site although UAV control and / or maneuverability is maintained.
Forced landing	Landing of the UAV on a predefined site where it can be reasonably expected that fatality will not occur.; Prevents the UAV from landing on its planned main landing site although the UAV is controllable and maneuverable and can also able perform a forced landing on a predefined area that as far as is reasonably practicable has been cleared of people.

Given a particular type of UAS (waypoint navigation, path defined by a set of points in the map), the aim is to identify the failure conditions that may lead to the feared events as they are defined in STANAG 4671, during normal operation, using PN. The problem statement is defined on the following questions about UAS:

1- Will it ever get in a certain particular state, (e.g one of the most feared events)?
2- Will it have the ability to react to inputs?
3- Will it be able to achieve a desired state?

Therefore, the proposed Safety Assessment model will only consider isolated or combined failures from propulsion system, communications and flight controls as stated in NASA (2007). Some assumptions have been considered on the implementation:

1- If the failures are evident to the crew, it is considered that transitions are observable and detectable by the system and shown to the UAS crew;
2- The failures considered in the model are those that lead to the Most Feared Events,

in particular those which are classified as catastrophic, hazardous and major;

3- Simultaneous failures will lead to an unique Most Feared Event;

4- The UAS mission is interrupted whenever there is one or more failures that lead to Most Feared Events;

5- G= (P, T, I, O) be the Petri Net that represent the event model of the UAS to safety assess, where P corresponds to a finite set of places ({p_1, p_2, ..., p_n}), T to a finite set of transitions ({t_1, t_2, ..., t_s}), I is an input function ((T x P) --> {0, 1}) and O an output function ((T x P) --> {0, 1}).

The proposed model comprises the following modulations:

A - Modeling of UAV Reconnaissance and Surveillance mission flight phases;
B - Modeling the failure occurrence and Safety Assessment of Most Feared Events;
C - Modeling a UAV Flight Phases with failure occurrence.

It was used the module PN from GRIF 2015 software to perform the analysis to determine the average events (Minor, Major, Hazardous and Catastrophic) that will occur in 36500 hours of operation, corresponding to the average number of tokens in each place. Likewise, it was determined the number of missions that have been accomplished in the assumed period of time, as well as the mission reliability (shown in Table 2). This last parameter lists all the UAV missions that were accomplished by removing those that suffered a failure but after performing mitigation actions preceded.

Table 2 - Average number of tokens achieved in each Place.

Number	Name	Number of Tokens
17	Mission Accomplished	4696
103	Uncontrolled Crash	3
104	Controlled Crash	3252
105	Mission Unaccomplished	5697
110	Mission Proceeded	4040
111	Forced Landing	2442

From Table 2, it can be concluded that during the period defined as UAS service time it will occur all three Most Feared Events. It is expected to occur 3 Uncontrolled Crashes, 3252 Controlled Crashes and 2442 Forced Landings in that period of time. Note that despite the failure occurred in one of the critical systems of the UAS (Propulsion System, Flight Controls and Communications) after performing mitigation actions, the UAV continued its mission about 4040 times, from which it can be inferred that mitigation actions are suitable and effective for a huge number of cases.

CONCLUSIONS

One result of this research is the development of a reliability database to be applied to UAS based on Morphological Analysis. Another result is the development of a systematic process for creating an Initial Maintenance Plan for UAS using the MSG-3 methodology. The third result is a modeling of the Safety Assessment process of the UAS through PN representing the real dynamics of the UAS. Through the proposed model it was possible to identify the critical points of the UAS that need to be improved in order to obtain the authorization for flight or airworthiness certification, and it also allowed to enhance demonstration of evidence that an acceptable level was achieved (or not) related to safety and reliability of UAS operations. It was also possible to demonstrate that despite a failure be classified major, hazardous or catastrophic may not lead to MFE, because it also depends on the flight phase where it occurs.

These results are related to specific UAS and are expected to increase the capacity of making effective and efficient decisions during the development and certification of unmanned aerial systems.

REFERENCES

AAN, 2013, Emissão de Licenças Especiais de Aeronavegabilidade para Sistemas de Aeronaves Não Tripuladas. Alfragide: EMFA.

AECMA, 1999, SPEC 1000D-Iternational Specification for Techinacal Publications utilising acommon source data base. Bruxelas: AECMA.

AFA and FEUP, 2011, Projecto de Investigação e Tecnologia em Veículos Aéreos Não-Tripulados. Sintra: FAP.

Clothier, R. and Rodney, W., 2012, Determination and Evaluation of UAV Safety Objectives, Australian Research Centre for Aerospace Automation, 25th Bristol International UAV Systems Conference, Bristol, UK.

Murata, T., 1989, Petri Nets: Properties, Analysis and Applications. Proc. IEEE, Volume 77, nº4, pp. 541-580.

NASA, 2007, Preliminary Considerations for Classifying Hazards of Unmanned Aircraft Systems. Washington: NASA/TM-2007-214539.

NATO, 2009, STANAG 4671 - Unmanned Aerial Vehicle Systems Airworthiness Requirements (USAR), Brussels, Belgium: NSA.

Ritchey, T., 2009, Futures Studies using Morphological Analysis_Adapted from an Article for the Millennium Project: Futures Research Methodology Series, Version 3.0, and Sweden: Swedish Morphological Society.

SAE, 1996, ARP 4761_Guidelines and Methods for Conducting the Safety Assessment Process on Civil Airborne Systems and Equipment. Washington DC: SAE.

SAE, 2010, Guidelines for development of civil aircraft and systems. Washington DC: SAE.

Vanston, J., 1998, Technology Forecasting: Na Aid to Effective Technology Management. Austin: Technology Futures Inc.

ISSA-2018-025

EFFECT OF DIFFERENT WEIGHTAGE OF ENOVA® IC3100 SILICA AEROGEL ON ALUMINIUM ALLOY COMPOSITES IN ISO2685 AVIATION STANDARD FIRE-TEST

A.R Abu Talib[1,2*], I. Mohammed[1,3], W. Rujhan[1] and N. Bheekhun[4]
[1]Aerodynamic, Heat Transfer & Propulsion (AHTP) Group, Department of Aerospace Engineering, Faculty of Engineering, Universiti Putra Malaysia, 43400 Serdang, Selangor, Malaysia
[2]Aerospace Malaysia Research Centre, Faculty of Engineering, Universiti Putra Malaysia, 43400 Serdang, Selangor, Malaysia
[3]Department of Mechanical Engineering, College of Engineering, Hassan Usman Katsina Polytechnic, Katsina, 2052 Nigeria.
[4]Aerospace and Communication Technology Research Group, Faculty of Information Sciences and Engineering, Management & Science University, 40100 Shah Alam, Selangor Malaysia

*Corresponding author: abdrahim@upm.edu.my

SUMMARY

The main objective of the study is to determine the perc entage amount of Enova ® IC3100 and epoxy resin/hardener on the hybrid composite. The composites were fabricated using different percentage of aerogel in an epoxy (0. 8 to 1. 3); the percentage of aerogel in an epoxy was very small in order to reduce the brittleness nature of the a erogel, whereby mechanical stirrer and ultrasonic machine were used in mixing and dissolving the aerogel in an epoxy . The composites undergo a fire test using a standard ISO2685 propane -air burner. The results obtained clearly indicate that a less layered aluminium alloy coated with greener and lighter substance mix with epoxy resin/hardener can be used in a high - temperature application of an aircraft with higher thermal conductivity resistance. The hybrid composite with flax fibre presents 5 -10% greater th an the other composite in terms of fire resistance.

Keywords: Aluminium alloy; composite; Enova® IC3100; Flax fibre; ISO2685 standard.

INTRODUCTION

To delay the flame fire penetration into aircraft fuselage and cabin, there is need to develop a composite that will act as a firewall in the aircraft components, especially around the high-temperature location of the aircraft. One of the test to be carried out on such composite is fire certifications test, which is required to validate the fire resistance of the component. There are the different standards used in conducting the fire test, but the most two being used are the ISO2685 (1990) and AC20-135 (1998). Different types of materials and composites were used as fire blanket in such areas, but still, there is a need for improvement in the location using greener materials. Also, many different type of instruments were used to measure the temperature and heat flux in the fire test (Mohammed *et al*., 2016). Various types of composite materials were used in the fabrication of new aircraft generation components which include carbon fibre reinforced plastic and fibre metal laminates composites, but its main problems are weight and delamination by using so many layers (Sikoutris, 2012, Tranchard *et al*., 2015, Mohammed *et al*., 2017). To avoid delamination due to thermal shock and a reduced weight, a greener material is required for a component of such locations (Bheekhun *et al*.,, 2016).

Enova® IC3100 is among the type of silica aerogels made synthetically, it has properties that form an open nanostructure by interconnected particles of size 2-4 nm, thermal conductivity of 0.012 W/mK, density of 124 kg/m^3 and a specific surface area of 901 m^2/g (Gorle *et al*., 2008, Lou *et al*., 1995). The Enova® IC3100 is hydrophobic in nature with low gas convection and solid conduction. The different polymer was used with aerogel to produce a different type of mixed polymer-aerogel composite such as those produced by Kim *et al*., (2008). Silica aerogel was used in different applications in an aircraft due to its thermal insulation such as in deforesting of the window and in acoustic barrier (Fricke and Emmerling, 1992, Gibiat *et al*., 1995). The aerogel can be used to coat materials to form a composite of aerogel by using many different approaches. Among the approach was thermal spray coating, which is used to coat the metal, ceramic, and superalloy components; the coat components surface will be protected against corrosion, high temperature, wear and chemical attack (Longo, 1992).

The most metal/metal alloy used in aircraft is an aluminium alloy. In the past decades, aluminium alloys attracted so many interests in the aerospace and automotive industries due to its properties such as resistant to corrosion, lightweight, weldability, among others Prillhofer *et al*., (2014). The most common material in aircraft component is aluminium alloy. Aluminium alloys are used extensively in aircraft due to their high strength-to-weight ratio (Sanders 2001). The following are the most common types of aluminium alloy used in aerospace as stated by Shevell and Shevell (1989); 7068 aluminium, 7075 aluminium, 6061 aluminium, 6063 aluminium, 2024 aluminium, 5052 aluminium, but 2024 aluminium and 7075 aluminium are the most common alloys used in aerospace industries (Sriramkumar 2014, Voevodin *et al*., 2001). Aluminium alloy 2024-T3 has high strength, excellent fatigue resistance, and excellent

machinability. Typical uses of 2024-T3 Alclad aluminium sheet are in aircraft skins, cowls, aircraft structures, and also for repair and restoration because of its shiny finish (2024-T3 Alclad). Its ultimate strength is 427.48 MPa with a shearing strength of 275.80 MPa (Shenglong, 2005).

Reinforcing polymer-aerogel composite with fibre was one of the method used in increasing both the thermal and mechanical properties as in fibre-metal laminate (Mohammed *et al*., 2018), the reinforced fibre polymer-aerogel composites produce a composite with better thermal insulation and mechanical properties. Reinforced fibres such as mullite, ceramic and glass were among the fibre used in the polymer-aerogel composite that improved its thermal and mechanical properties (Karout *et al*., 2005, Yang *et al*., 2011). The composite of the reinforced fibre with polymer-aerogel was affected by the reinforced fibre alignment, which reduces the mechanical properties of the composite (Lioa *et al*., 2012). Carbon reinforced fibre polymer-aerogel composite was developed whereby the reinforced fibre used handled the backing of the composite for the desired properties as reported by Karout *et al*., 2005.

The main goal of the work is to develop and assess the physical fire behaviour of composites of aluminium alloy with Enova® IC3100/epoxy and a hybrid composite of aluminium alloy, reinforced flax fibre with Enova® IC3100/epoxy using a different percentage of Enova® IC3100/epoxy according to ISO2685 standard. The fabricated composites undergo a fire test three-inches from the burner face to the front face of the flat plate after burner calibration, the rear face temperature was measured by thermocouples and recorded by the data logger. The preparation aerogel-polymer with reinforced fibre and aluminium composites were studied and the effects of the percentage of Enova® IC3100/epoxy investigated, analysed and discussed.

MATERIALS AND METHODS

In this section, the materials and the methods used in fabricating and test carried out in the experiment were considered.

The materials used were 300 mm x 300mm x 0.4 mm aluminium alloy 2024-T3, 300 mm x 300 x 0.6 mm flax, Enova® IC3100 powder, and HL002-TA/B epoxy resin/hardener. Specific equipment used includes mechanical stirrer, ultrasonic machine, release wax, mould, propane gas, air gas (primary), compressed air (secondary), manometers, data logger, thermocouples, heat flux meter (SBG01), and gas burner.

Enova ® IC3100 was mixed with epoxy resin at different percentages from 0.8 to 1.3% for different composite. The mixture of Enova ® IC3100 and epoxy resin was conducted using mechanical stirrer at a lower speed for about seven minutes; the mixture was then put in ultrasonic machine for homogenisation of the Enova ® IC3100 pore as reported in Cho (2013) for about 30 minutes at a temperature greater than the boiling point of epoxy resin. The mixture was allowed to cool to room temperature and then mixed with epoxy hardener at high speed for about three to four minutes.

The composites were fabricated by hand lay-up methods by laying one sheet of aluminium alloy and applying the mixture of Enova ® IC3100 with epoxy resin/hardener on it and covering the mixture with another sheet of aluminium alloy (two sheets of aluminium alloy were used in each composite). For the other composite, a layer of flax fibre was placed in between the two sheets of aluminium alloy and bonded together by a mixture of Enova ® IC3100 and epoxy resin/hardener. The composites were allowed to cure for at least 48 hours. A composite of about 1.5 ± 0.2 mm was fabricated for the Enova ® IC3100 and aluminium alloy composite and 2.0 ± 0.2 mm for the hybrid composite.

Fire test rig was set-up according to ISO2685 standard and the fabricated plate was placed in its housing for fire test after calibrating the burner using seven R-type thermocouples and a heat flux meter (SBG01) for about five minutes. The fire test was conducted by placing two thermocouples at the rear face of each composite at the centre and 25.4 mm distance right away from the centre. The average reading of each composite was recorded using data logger. While the pressure of propane gas, primary air and secondary air where set-up and controlled by manometers. Figure 1 shows the configuration of the fire test experimental set-up.

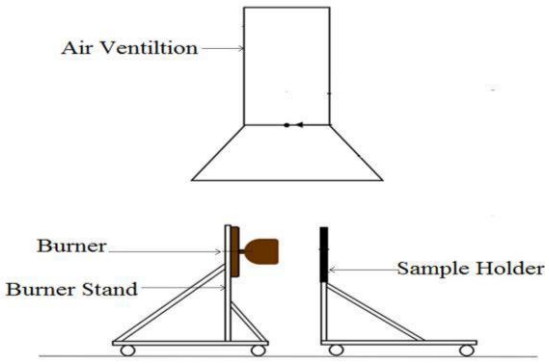

Fig. 1. Fire Test Experimental Set-up

RESULTS AND DISCUSSION

The result of different percentage weight of aerogel to the polymer on 0.4 mm aluminium alloy 2024-T3 was presented in this section. The average of flame fire burn-through time using ISO2685 standard was recorded accordingly as for aluminium alloy coated with aerogel/epoxy and the hybrid composite of aluminium alloy with flax fibre and aerogel/epoxy.

The first set of tests was conducted on three samples of 1.0, 1.1, 1.2 and 1.3% of Enova®

IC3100 silica aerogel to the epoxy polymer. Table 1 shows the result obtained.

Table 1. Result of Percentage of Enova® IC3100 to Epoxy Polymer in Aluminium Alloy 2024-T3

Percentage Enova® IC3100 l (%)	Percentage Epoxy Polymer (%)	Penetration Time (s)	Remarks
1.0	99.0	760	Fire Resistant
1.1	89.9	830	Fire Resistant
1.2	89.8	>900	Fire Proof
1.3	89.7	>900	Fire Proof

The result shows that increase in Enova ® IC3100 in the composite produces a fireproof composite according to ISO2685 standard, with 1.2 and 1.3% produces the best result for the composite.

The temperature result obtained for the two thermocouples at the rear face of the composite show that the centre of the composite received more flame than the other side of the composite as recorded by data logger, indicated in Figure 2.

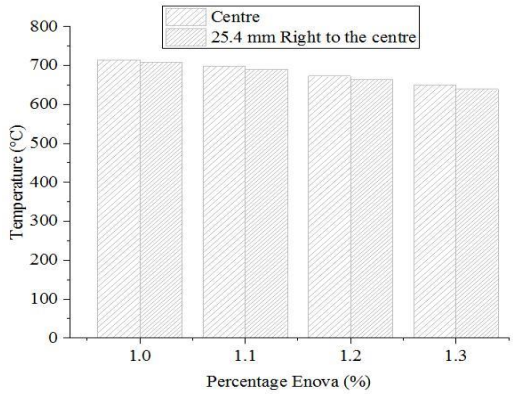

Fig. 2. Rear Face Temperature of Percentage Enova® IC3100 with Aluminium alloy

The rear face temperature of the two thermocouples indicates that more Enova ® IC3100 powder to the mixture produces more fire retardant composite, due to the decrease of thermal conductivity in the mixture as reported in Abu Talib *et al*., (2018).

The second test result was percentage Enova® IC3100 coating aluminium alloy 2024-T3 and flax fibre. Table 2 shows the result obtained.

The result shows that addition of a natural fibre (flax) increase the thermal stability and fire resistant of the composite when compared with the result of only Enova ® IC3100 and aluminium alloy.

Table 2. Result of Percentage of Enova® IC3100 to Epoxy Polymer in Aluminium Alloy 2024-T3 and Flax Fibre

Percentage Enova® IC3100 l (%)	Percentage Epoxy Polymer (%)	Penetration Time (s)	Remarks
0.8	99.2	790	Fire Resistant
0.9	99.1	797	Fire Resistant
1.0	99.0	>900	Fireproof
1.1	89.9	>900	Fireproof

The rear face result obtained for the two thermocouples at centre and 25.4 mm distance from the centre shows that the centre of the composite received more flame than the other side of the composite as presented in Figure 3.

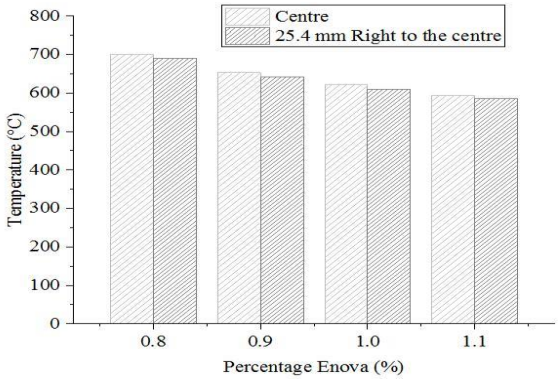

Fig. 3. Rear Face Temperature of Percentage Enova® IC3100 with Aluminium Alloy and Flax Fibre

The rear face temperature shows that flax fibre also decreases the thermal conductivity of the composite, likewise, the increase of Enova® IC3100.

CONCLUSIONS

The results obtained from the study indicated that more percentage of Enova® IC3100 produces more fire resistance composite and also, hybrid composite using flax fibre yield more fire resistance composite with almost 5-10% increase in thermal stability. Therefore, from the result, it is clearly showing that a composite of aluminium alloy 2024-T3 coated with Enova® IC3100 silica aerogel can be used in the high-temperature application of an aircraft components.

ACKNOWLEDGEMENT

The authors would like to thank the Universiti Putra Malaysia for providing the financial support through the IPS Grant scheme no. 9538500 and to the Ministry of Higher Education Malaysia for the support given through the Fundamental Research Grant Scheme FRGS/TK05/UPM/02/7 No. 5524896.

REFERENCES

Abu Talib, A.R., I. Mohammed , K.A. Mohammed , and N. Bheekhun, *Aerogel Application on Fire Certification Techniques and Heat Transfer.* International Journal of Pure and Applied Mathematics, 2018, 119(16): 1783-1790.

AC20-135, *Draft Advisory Circular, Power Plant Installation and Propulsion System component Fire Protection Test Methods, Standards and Criteria, Advisory Circular No: 20-135.* 1990.

Bheekhun, N., A.R Abu Talib, S. Mustapha, R. Ibrahim, and M. Hassan. *Towards an aerogel-based coating for aerospace applications: reconstituting aerogel particles via spray drying*. in *IOP Conference Series: Materials Science and Engineering*. 2016. IOP Publishing.

Cho, M.D., *Fused aerogel-polymer composite, methods of manufacture thereof and articles comprising the same*. 2013, US Patent US8552076B2.

Fricke, J. and A. Emmerling, *Aerogels—Preparation, properties, applications*, in *Chemistry, Spectroscopy and Applications of Sol-Gel Glasses*. 1992, Springer. p. 37-87.

Gibiat, V., O. Lefeuvre, T. Woignier, J. Pelous, and J. Phalippou, *Acoustic properties and potential applications of silica aerogels.* Journal of Non-Crystalline Solids, 1995. 186: p. 244-255.

Gorle, B., I. Smirnova, M. Dragan, S. Dragan, and W. Arlt, *Crystallization under supercritical conditions in aerogels.* The journal of supercritical Fluids, 2008. 44(1): p. 78-84.

ISO2685, *Aircraft Environmental test procedures for airborne equipment – Resistance to fire in designated fire zones (pp. 29).* 1998: p. 29.

Karout, A., P. Buisson, A. Perrard, and A. Pierre, *Shaping and mechanical reinforcement of silica aerogel biocatalysts with ceramic fiber felts.* Journal of sol-gel science and technology, 2005. 36(2): p. 163-171.

Kim, C.-Y., J.-K. Lee, and B.-I. Kim, *Synthesis and pore analysis of aerogel–glass fiber composites by ambient drying method.* Colloids and Surfaces A: Physicochemical and Engineering Aspects, 2008. 313: p. 179-182.

Liao, Y., H. Wu, Y. Ding, S. Yin, M. Wang, and A. Cao, *Engineering thermal and mechanical properties of flexible fiber-reinforced aerogel composites.* Journal of sol-gel science and technology, 2012. 63(3): p. 445-456.

Longo, F., *Industrial guide—markets, materials, and applications for thermal-sprayed coatings.* Journal of Thermal Spray Technology, 1992. 1(2): p. 143-145.

Lu, X., R. Caps, J. Fricke, C. Alviso, and R. Pekala, *Correlation between structure and thermal conductivity of organic aerogels.* Journal of Non-Crystalline Solids, 1995. 188(3): p. 226-234.

Mohammed, I., A.R. Abu Talib, M.T Hameed Sultan, and S. Saadon. *Ballistic impact velocity response of carbon fibre reinforced aluminium alloy laminates for aero-engine*. in *IOP Conference Series: Materials Science and Engineering*. 2017. IOP Publishing.

Mohammed, I., A.R. Abu Talib, M.T Hameed Sultan, and S. Saadon. *Temperature and heat flux measurement techniques for aeroengine fire test: a review*. in *IOP Conference Series: Materials Science and Engineering*. 2016. IOP Publishing.

Mohammed, I., A.R. Abu Talib, M.T.H. Sultan, M. Jawaid, A.H. Ariffin, and S. Saadon, *Mechanical Properties of Fibre-Metal Laminates Made of Natural/Synthetic Fibre Composites.* BioResources, 2018. 13(1): p. 2022-2034.

Prillhofer, R., G. Rank, J. Berneder, H. Antrekowitsch, P.J. Uggowitzer, and S. Pogatscher, *Property criteria for automotive Al-Mg-Si sheet alloys.* Materials, 2014. 7(7): p. 5047-5068.

Sanders Jr, R.E., *Technology innovation in aluminum products.* JOM, 2001. 53(2): p. 21-25.

Shenglong, Y.S.D., *A Glimpse at the Development and Application of Aluminum Alloys in Aviation Industry [J].* Materials Review, 2005. 2: p. 22.

Shevell, R.S. and R.S. Shevell, *Fundamentals of flight*. Vol. 2. 1989: Prentice Hall Englewood Cliffs, New Jersey.

Sikoutris, D.E., *Fire Response of Composite Aerostructures.* PhD Thesis, University of Patras Greece, 2012.

Sriramkumar, J., *Mixture of Alloys Used for Building a Regenerator to Bring Down the Temperature of Liquid Hydrogen (Lh_2) Below 20k,* International Review of Applied Engineering Research. ISSN 2248-9967 Volume 4, Number 1 (2014), pp. 47-56.

Tranchard, P., F. Samyn, S. Duquesne, M. Thomas, B. Estèbe, J.-L. Montès, and S. Bourbigot, *Fire behaviour of carbon fibre epoxy composite for aircraft: Novel test bench and experimental study.* Journal of Fire Sciences, 2015. 33(3): p. 247-266.

Voevodin, N., N. Grebasch, W. Soto, L. Kasten, J. Grant, F. Arnold, and M. Donley, *An organically modified zirconate film as a corrosion-resistant treatment for aluminum 2024-T3.* Progress in Organic Coatings, 2001. 41(4): p. 287-293.

Yang, X., Y. Sun, D. Shi, and J. Liu, *Experimental investigation on mechanical properties of a fiber-reinforced silica aerogel composite.* Materials Science and Engineering: A, 2011. 528(13-14): p. 4830-4836.

International Symposium on Sustainable Aviation 2018
9 – 11 July 2018
Rome, Italy

ISSA-2018-026

EXPERIMENTAL AND THEORETICAL STUDY ON THE FATIGUE LIFE OF BONDED JOINTS USING HOT-CURING EPOXY FILM ADHESIVE

Christof Nagel, Oliver Klapp
Fraunhofer Institute for Manufacturing Technology and Advanced Materials - IFAM
Wiener Straße 12, 28359 Bremen, GERMANY
christof.nagel@ifam.fraunhofer.de

SUMMARY

The fatigue life of commercial epoxy film adhesive used in initial design and bonded repair of civil aircraft was investigated. Fatigue tests were performed in order to explore the influence of the multiaxial stress state in the bond line on the fatigue life of bonded joints . The capability of different approaches to predict the measured fatigue life based on the stress state in the bond line was investigated . I t was found that models dominated by normal stresses worked well while models with dominating shear stresses failed to describe the measured data. The consequences of applying specific approaches to predict bond line failure due to fatigue in structural analysis and design of civil aircraft are discussed.

Keywords: adhesive joint, fatigue, film adhesive

INTRODUCTION

Hot-curing epoxy film adhesives are used for structural bonding in initial design and bonded repair of composite aircraft (CMH-17-3G, 2012). Related standards require that damage growth must be limited in order to ensure safe operation. This may be approved by testing or structural analysis (AMC 20-29, 2010, and CS-23, 2012).

Within structural analysis, the stress-life approach is frequently used in order to confirm that damage growth is limited. Within this approach, the number of cycles to failure is estimated from the initial stress state under cyclic load based on a stress-life, or S-N, curve. A failure condition is used to describe the influence of stress multiaxiality on fatigue. In steel construction, maximum principal stress, Tresca, von Mises, or critical plane approaches are used (Socie and Marquis, 2000, Radaj et al., 2006).

Polymers are known to exhibit pressure-dependent yield under static load, see e.g. and Ward and Sweeney, 2013. This was also confirmed for the current EA9695 film adhesive (Nagel and Klapp, 2018). Known damage mechanisms in polymers include the formation of shear bands, crazes, and voids (Riew and Kinloch, 1993, and 1996) which may explain why yield does not only depend on the deviatoric part but also on the hydrostatic part of the stress tensor. If similar mechanisms are assumed to be active also in fatigue, it may be expected that a valid fatigue failure condition would be dominated by normal or hydrostatic stress rather than shear or deviatoric stress.

The aim of this study is to present experimental data and material theory on the fatigue of bonded joints with EA9695 050 NW film adhesive. The ratio of normal and shear stresses has been varied in order to explore its effect on the measured fatigue life. Experimental data were used to identify potential fatigue failure conditions for structural analysis and design.

METHODOLOGY

Experiments

Thick adherend shear joints (TASJ), butt joints (BJ), and scarf joints (SJ) were used in order to produce a homogeneous stress state within the adhesive layer. The adherends were made of mild steel. The TASJ geometry is given in ISO 11003-2. The SJ geometry is shown in Fig. 1. BJ were similar to Fig. 1 but with an angle of 0°. Surfaces were cleaned by immersion in methyl ethyl ketone in an ultrasonic bath followed by sand blasting using F100 corundum. Thereafter, surfaces were rinsed in methyl ethyl ketone.

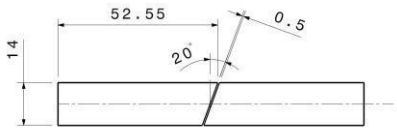

Fig.1. Dimensions of scarf joints.

A joining device was used which allowed for ex-act alignment and avoidance of residual stresses due to temperature. Before bonding, the adhesive was allowed to warm up after cool storage in order to avoid condensed moisture. One layer of adhe-sive film (approx. 0.2 mm thickness) was used. After bonding, pressure was applied in order to achieve sufficient consolidation. Springs were used for BJ and SJ such that a pressure corresponding to the recommended autoclave pressure of 3 bar was achieved. Joining devices containing spring-loaded BJ and SJ were held for 2 hours at 130°C in a convection oven. The temperature ramps were approx. 1K/min. Fully bonded steel plates were used for the production of TASJ. Bonded plates were autoclave-cured for 2 hours at 130°C with a ramp of approx. 1K/min and a pressure of 3-4 bars in a vacuum bag evacuated to 0.1 bar. Samples were machined after curing. The bond line thickness was ≈ 0.1 as obtained by microscopy.

Constant amplitude mechanical fatigue tests were performed at room temperature in an air-conditioned test laboratory in an MTS servohydraulic material testing system. Cardan joints were used to enable free rotating sample ends in order to avoid loads perpendicular to the loading direction. Tests were performed under load control using a sinusoidal load-time history with constant load amplitudeand constant load ratio= / . The test frequency was 7.5 Hertz. Tests were stopped at final fracture of the samples. The temperature of the samples was eventually checked in order to avoid excessive heating.

Evaluation

Stress components were obtained from the nominal stresses, i.e. applied load and the bond area. In TASJ test, the shear stress is given by = / and all normal stresses are zero. Shear stress indices are neglected since all other shear components are zero. In BJ test, 11 = / and 22,33 = 11/(1−) due to transverse strain confinement. In the SJ test, 11 = / , = 0/ , and 22,33 = 11/(1−). Indirect shear stresses are zero due to transverse strain confinement. A value of = 0.465 was used which was measured for the same adhesive system with the same type of samples (Nagel and Klapp, 2018). It considers that transverse strain is zero only in the center of the adhesive layer of the BJ, using an approach proposed by Tsai, 2005.

Principal stresses were needed in order to calculate some of the failure conditions. In the current case they are given by:

$$_{1,2} = \frac{1}{2}\left[_{11} + _{22} \pm \sqrt{(_{11} - _{22})^2 + 4 _{}^2} \right] \quad (1)$$

$$_3 = _{33} \quad (2)$$

For a failure condition based on stress invariants, deviatoric equivalent stress and hydrostatic pressure were calculated as:

$$= \sqrt{\frac{1}{2}\left[(_1 - _2)^2 + (_2 - _3)^2 + (_3 - _1)^2\right]} \quad (3)$$

$$= - \frac{_1 + _2 + _3}{3} \quad (4)$$

where = √3 2 , = − 1/3, 2 is the second stress deviator invariant and 1 is the first stress tensor invariant. For the definition of principal stresses and invariants, see, e.g. Rösler et al., 2007.

A fatigue failure condition was formulated in the sense that equivalent states of stress lead to the same fatigue life:

$$= - ^{-1/} = 0 \quad (5)$$

Eq. (5) has the common form of an S-N curve, where denotes a damage measure, describing equivalent states of stress, denotes the number of cycles to failure, and 0 andare material dependent parameters, i.e. the fatigue coefficient and the slope parameter of the S-N curve.

Five hypotheses aboutwere tested against experimental data:

H1. is equal to the maximum principal stress
H2.is equal to the linear Drucker-Prager equivalent stress
H3. is equal to the Findley-Parameter
H4. is equal to the maximum shear stress
H5. is equal to the von Mises equivalent stress

In H1, is defined as the largest of the principal stresses:

$$= \max\{ _1, _2, _3\} \quad (6)$$

In the current geometry and loading situation this is 1 as given by Eq. (1).

H2 represents a pressure-dependent failure condition, which is used in static loading situations in order to calculate the onset of yield or fracture. It can be formulated as (Rösler et al., 2007, Ward and Sweeney, 2013):

$$= - \quad (7)$$

where denotes a material-dependent parameter which describes the sensitivity to and is given by Eq. (3).

Following H3, the shear stress amplitude and the upper value of the normal stress in the cycle are combined (see e.g. Socie and Marquis, 2000):

$$= (+) \quad (8)$$

Herein,denotes a material dependent parameter and the braces indicate that a sectional plane, where (8) reaches a maximum, has to be identified by rotating the coordinate frame. The procedure is described in Socie and Marquis, 2000.

In H4, the largest of the principal stress differences is used (Rösler et al., 2007):

$$= (_1 - _2)/2 \quad (9)$$

In the current situation, 1 and 2 are given by Eq. (1).

H5 uses the von Mises equivalent stress, as defined in Eq. (3) (Rösler et al., 2007).

The values of were calculated from the amplitudes of the experimental stress components using Eqs. (3) and (6)-(9), and were subsequently plotted against the measured number of cycles to failure. The squared correlation coefficient 2 between log and log was calculated. A power law:

$$= ^{-1/} \quad (10)$$

was least-squares fitted to the data in order to find fatigue coefficient 0 and fatigue slope parameter of the corresponding S-N curve. The

value of in Eqs. (7) and (8) was identified by repeating this procedure, thereby iteratively changing until the root of the mean squared error ( ) between measured and predicted fatigue life according to Eq. (10) reached its minimum.

In all cases except H3, stresses were treated as amplitudes, i.e. half of the difference between stress at maximum stress at minimum load. Within Eq. (8) of H3, shear stress amplitude and upper normal stress are used, which is denoted by subscripts.

RESULTS AND DISCUSSION

Fracture patterns indicated predominantly cohesive failure within the adhesive layer. Therefore, the following discussion is related to the mechanical behavior of the cured adhesive material within the bond line, not to adhesion of the bond line on the surface.

A graphical representation of the test data based on the amplitude of the von Mises stress, Eq. (3), is shown in Fig. 2. It can be seen that the test data appear on different S-N curves since the deviatoric fraction of stress is high in the TASJ while it is low in the BJ. The SJ data lie in between those of TASJ and BJ due to intermediate deviatoric stress.

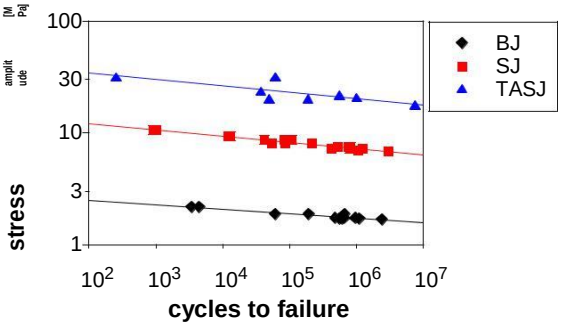

Fig. 2. Representation of fatigue test results in terms of the von Mises stress amplitude – butt joints (BJ), scarf joints (SJ), thick adherend shear joints (TASJ)

It is clear from Fig. 2 that the von Mises stress is not useful in fatigue failure prediction of the current adhesive since a valid fatigue failure condition should unify all test data on a common S-N curve. The same conclusion was drawn for the maximum shear stress, Eq. (9), since it was found that the representation of the test data appeared to be similar to Fig. 2 (not shown).

A representation of the test data in terms of the maximum principal stress (H1), the Drucker Prager equivalent stress (H2), and Findley's parameter (H3), which can be distinguished by color, is shown in Fig. 3. BJ, SJ, and TASJ data are presented using individual symbols for easier assignment. As compared to Fig. 2, it can be seen that BJ, SJ, and TASJ data no longer appear on different levels but fall on a common S-N curve in the case of H1, H2, and H3. It can hence be deduced from the comparison of Fig. 3 and Figs. 2 that H1-H3 represent potential fatigue failure conditions while H4 and H5 are not valid.

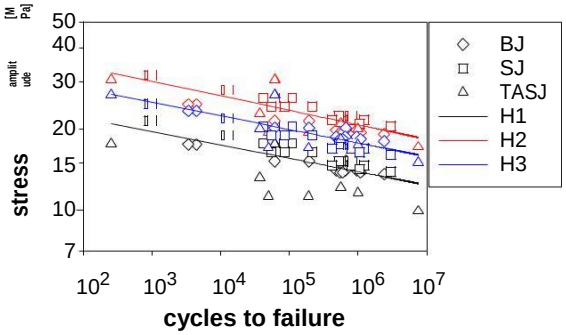

Fig. 3. Representation of fatigue test results in terms of indicated fatigue failure conditions

The major difference is that H1-H3 contain normal stresses while H4, H5 can be interpreted as shear stresses: H1 represents the maximum of the normal stresses that remain after rotating the coordinate frame such that the shear components vanish. H2 includes which can be interpreted as the average normal stress; H3 also includes a normal stress. H4 represents a shear stress (Rösler et al., 2007) and H5 can be interpreted as octahedral shear stress (Socie and Marquis, 2000). From this consideration, it can be concluded that the mechanical fatigue of the current film adhesive is governed by normal stresses.

The results of the correlation and regression analyses are given in Table 3. Considering the value of ^{2}, it can be seen that H1-H3 result in a better reproduction of experimental data than H4, H5, which is in agreement with the conclusion.

Table 3. Fatigue life prediction based on different approaches: H1 – maximum principal stress, H2 – Drucker-Prager equivalent stress, H3 – critical plane model (Findley), H4 – von Mises equivalent stress, H5 – maximum shear stress

H1	0.51	--	9.81	50.84	0.73
H2	0.65	1.40	11.81	62.56	0.62
H3	0.68	0.51	13.29	47.59	0.59
H4	0.07	--	0.60	--	1.01
H5	0.07	--	0.65	--	1.01

Considering the value of in H2 it can be seen that and hence normal stresses have a large influence on fatigue life. In H3 the value of is smaller as compared to H2 but the normal stress effect is large because the normal stress in Eq. (8) is the upper value in the cycle while the shear stress represents the amplitude.

Regression analysis of the data in Fig. 3 indicated that the slope parameter of the respective S-N curve was close to a value of = 10 and the fatigue coefficients ranged between 50 and 60 Megapascals, Table 3. The accuracy of a fatigue life prediction which could be achieved based on

the scatter of the measured data can be estimated by raising the RMS error in Table 3 to the power of ten. It can then be seen that the fatigue life may be determined up to a factor of 4 or 5, depending on the failure condition used. As compared to H2 or H3, H1 is only slightly less accurate but it works without a free parameter.

The maximum principal stress condition (H1) is easy to be used within commercial FE packages since $_1$ (Eq. (6)) is directly available as a standard output variable. The Drucker-Prager stress (H2, Eq. 7) can be obtained from invariants in post-processing using from Table 3. Determination of the Findley parameter (H3) is possible in post-processing by iteratively rotating the coordinate frame and calculating Eq. (8), using from Table 3. This is more complex than using H1 or H2, but H3 can also be useful in cases of non-proportional loading (Socie and Marquis, 2000). After has been calculated following H1, H2, or H3, the number of cycles to failure as well as its lower and upper limits can be calculated from $_1$ using $_0$, , and from Table 3. Alternatively, some allowable value of could be calculated based on a fixed number of and parameters in Table 3, and subsequently be compared to the value of obtained from FEM.

SUMMARY AND CONCLUSIONS

For adhesive joints containing thin layers of EA9695 film adhesive, constant amplitude fatigue tests were performed at room temperature under conditions including different fractions of normal stress. It was found that failure conditions involving normal stresses led to a better reproduction of the measured data then failure conditions involving just shear stresses. From this finding it was concluded that fatigue of the current film adhesive is domi-nated by normal stresses while shear stresses are of minor importance. Consequently, failure condi-tions including normal stresses were found to give useful predictions in the present case.

If fatigue of EA9695 film adhesive has to be considered in structural analysis and design, it is suggested to use maximum principal stress, linear Drucker-Prager stress, or Findley's parameter as a failure condition. Maximum shear or von Mises stress lead to unreliable results if applied to stress states other than shear.

From a comparison of the applied hypotheses, it was found that the maximum principal stress condition was quite accurate despite its simplicity. The Drucker-Prager or Findley conditions were more accurate but they are also more complex and involve additional parameters.

ACKNOWLEDGEMENT

Funding by the Federal Ministry for Economic Affairs and Energy on the basis of a resolution of the German Bundestag is gratefully acknowledged.

NOMENCLATURE

A adhesive bond area, mm^2
b normal stress sensitivity parameter
d adhesive layer thickness, mm
f failure or damage measure, MPa
f_0 S-N coefficient, MPa
F applied load, N
I_1 1^{st} invariant of hydrostatic stress tensor, MPa
J_2 2^{nd} invariant of stress deviator, MPa^2
k S-N slope parameter
N fatigue life (i.e. number of cycles to failure)
p hydrostatic pressure, MPa
q von Mises equivalent stress, MPa
R load or stress ratio

Poisson's ratio
correlation coefficient
normal stress, MPa
shear stress, MPa

Subscripts

a stress or load amplitude
u upper value of stress or load l lower value of stress or load ⊥ component acting normal to A
∥ component acting parallel to A
ii stress component numbering i = 1, 2, 3 i principal stress numbering i = 1, 2, 3

REFERENCES

AMC 20-29, 2010, *EASA AMC 20-29 Composite Aircraft Structure,* https://www.easa.europa.eu, accessed on May 31, 2018.

CMH-17-3G, 2012, Design and analysis of bonded joints, In *Composite Materials Handbook*, Vol. 3, Wichita, Kansas: SAE International, 10-1–10-54.

CS-23, 2012, *EASA Certification Specifications for Normal, Utility, Aerobatic, and Commuter Category Aeroplanes,* https://www.easa.europa.eu, accessed on May 31, 2018.

Nagel, C. and Klapp, O., 2018, *Yield and Fracture of Bonded Joints Using Hot-curing Epoxy Film Adhesive*. Presented at this conference.

Radaj, D., Sonsino, C.M., Fricke, W., 2006, *Fatigue assessment of welded joints by local approaches.* Cambridge: Woodhead.

Riew, C.K. and Kinloch, A.J., 1993, *Toughened plastics I*. Washington: American Chemical Society

Riew, C.K. and Kinloch, A.J., 1996, *Toughened plastics II*. Washington: American Chemical Society

Rösler, J., Harders, H., Bäker, M., 2007, Mechanical Behaviour of Engineering Materials, Berlin: Springer

Socie, D.F. and Marquis, G.B., 2000, *Multiaxial Fatigue.* Warrendale: Society of Automotive Engineers.

Tsai, H., 2005, Compression analysis of rectangular elastic layers bonded between rigid plates. *International Journal of Solids and Structures* 42: 3395-3410.

Ward, I. M., and Sweeney, J., 2013, *Mechanical Properties of Solid Polymers*, 3 ed., Sussex: Wiley

International Symposium on Sustainable Aviation 2018
9 – 11 July 2018
Rome, Italy

ISSA-2018-027

YIELD AND FRACTURE OF BONDED JOINTS USING HOT-CURING EPOXY FILM ADHESIVE - MULTIAXIAL TESTS AND THEORETICAL ANALYSIS

Christof Nagel, Oliver Klapp
Fraunhofer Institute for Manufacturing Technology and Advanced Materials - IFAM
Wiener Straße 12, 28359 Bremen, GERMANY
christof.nagel@ifam.fraunhofer.de

SUMMARY

The static strength of commercial epoxy film adhesive used in initial design and bonded repair of civil air - craft was investigated. Bonded joints which combine normal and shear stresses in different fractions were tested in order to determine the influence of multiaxial stresses in the bond line on the limits of yield and fracture. The low value of Poisson's ratio, which was derived from the same set of tests, led to a critical review of the assumptions used in the evaluation of the butt joint tests . A modified data evaluation ap - proach led to a more realistic value. The capability of different approaches to describe the experimental failure limits based on the state of stress in the bond line was investigated. It wa s found that models combining the second invariant of the deviator and the first invariant of the stress tensor worked well for general states of stress while the von Mises model performed well only in shear.

Keywords: adhesive joint, yield, fracture, film adhesive

INTRODUCTION

Structural adhesive joints are used in initial design and bonded aircraft repair. Safety rules require limited damage growth in order to preserve defined load bearing capacity of the bonded structure in operation. This may be approved by structural analysis or testing, see CMH-17-3G, 2012, AMC 20-29, 2010, and CS-23, 2012.

Linearity is usually assumed in applied static analysis if the loads are low. Elastic constants are needed in order to calculate stress and strain components in the bond line, from which a scalar equivalent is obtained which in turn is compared to a failure condition that contains material-dependent yield or strength parameters. In contrast to ductile metals, yield and fracture of polymers are influ-enced by hydrostatic stresses, see e.g. Ward and Sweeney 2013. A valid failure condition must there-fore consider the hydrostatic part of the stress tensor, Rösler et al., 2007. The deviatoric part, measured by the von Mises equivalent stress, is not adequate for adhesives unless they are loaded in pure shear, see Ban et al., 2008 and Kumar et al., 2006. If ultimate strength or yield limits have been measured for specific multiaxial stress states,
a pressure-dependent failure condition can be derived which may be used to predict failure for general states of stress within structural analysis.

It may be necessary in the case of structural adhesive joints to perform local plastic analyses in the design phase in order to verify global linearity assumptions. Plasticity considerations require a plastic potential and a strain hardening curve, which are also influenced by hydrostatic stresses. Since the determination of material parameters is always a matter of cost, it may be useful to obtain the required parameters from a common set of tests.

The aim of this study is to present elastic constants, static failure conditions, and base data for plasticity of EA9695 050 NW film adhesive based on a limited number of tests.

METHODOLOGY

Experiments

Thick adherend shear joints (TASJ), butt joints (BJ), and scarf joints (SJ) were used in order to produce a homogeneous stress state within the adhesive layer. The adherends were made of mild steel. The TASJ geometry is given in ISO 11003-2. The SJ geometry is shown in Fig. 1. BJ were similar to Fig. 1 but with an angle of 0°. Surfaces were cleaned by immersion in methyl ethyl ketone in an ultrasonic bath followed by sand blasting using F100 corundum. Thereafter, surfaces were rinsed in methyl ethyl ketone.

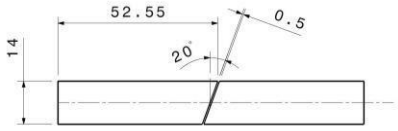

Fig.1. Dimensions of scarf joints.

A joining device was used which allowed for exact alignment and avoidance of residual stresses due to temperature. Before bonding, the adhesive was allowed to warm up after cool storage in order to avoid condensed moisture. One layer of adhe-sive film (approx.. 0.2mm thickness) was used. After bonding, pressure was applied in order to achieve sufficient consolidation. Springs were used for BJ and SJ such that a pressure corresponding to the recommended autoclave pressure of 3bar was achieved. The joining device containing spring-loaded BJ and SJ was heated to 130°C in a convection oven, held for 2 hours and then cooled down using temperature ramps of approx. 1K/min. Fully bonded steel plates were used for the production of TASJ. Bonded plates were autoclave-cured for 2 hours at 130°C with a ramp of approx. 1K/min and a pressure of 3-4 bars in a vacuum bag evacu-

ated to 0.1 bar. Samples were machined after curing. The bond line thickness was measured prior to tests. An average value of = 0.135 was obtained by microscopy.

Mechanical tests were performed at room temperature in an air-conditioned test laboratory with a constant displacement rate in a Zwick Z050 material testing system. Test speed was chosen such that nominal strain rates were in the order of 0.001 per second. Local strain measurements were performed using extensometers or COD clips in order to evaluate adhesive strains. TASJ were equipped with inductive ALTHOF extensometers set symmetrically about the adhesive layer on either side of the joint with an initial distance between the contact points of $_0 = 3.0$. BJ were equipped with a total of four COD clips set symmetrically about the adhesive layer using $_0 = 5.0$.

Evaluation

Load vs. local displacement curves obtained in each test were carefully considered with respect to their equality in order to avoid erroneous results due to sample rotation. Tests showing major differences between the two local measurements were not used. Valid load vs. local displacement curves were evaluated until the maximum load.

Adherend deformation between sensor tips and bond line was corrected for by assuming proportional response to the applied load. A procedure described in ISO 11003-2 was used for TASJ tests. After a straightforward modification for uniaxial tension, the same procedure was used for BJ tests. For SJ tests, an equivalent procedure containing normal and shear deformation was used.

The shear modulus was obtained from TASJ data as described in ISO 11003-2. The apparent elastic modulus * was obtained from BJ data as the slope of the nominal stress = / vs. nominal strain = / curve in the linear range. Nominal values in TASJ are = / and = / . In case of SJ, = ⊥/ , = ∥/ .

Yield limits were defined as 0.2% offset values of the nominal stresses. Fracture limits were defined as maximum measured nominal stresses.

A pressure-dependent failure condition was formulated using invariants $_1$ and $_2$, which are related to hydrostatic pressure and von Mises equivalent stress as

$$= \sqrt{\frac{1}{2}[(-)^2 + (-)^2 + (-)^2]} \quad (1)$$

$$= - \frac{_1 + _2 + _3}{3} \quad (2)$$

where refer to the principal stresses. In the TASJ test, $_{1,2} = \pm$. In the BJ test, $_1 =$ and $_{2,3} = _1/(1 -)$. In the SJ test,

$$\frac{1}{} \quad (3)$$

$$_3 = _{33} \quad (4)$$

where $_{11} = _⊥/ . = _∥/ .$ and $_{11}/(1 -)$.

Hydrostatic pressure and deviatoric equivalent stress are related to the invariants as $= - _1/3$ and $= \sqrt{3}\ _2$, where $_1$ is first stress tensor invari-ant and $_2$ is second stress deviator invariant.

RESULTS AND DISCUSSION

The elastic constants derived from TASJ and BJ tests are listed in Table 1. The average shear modulus is in good agreement with a tubular butt joint torsional (TBJ) test on the same adhesive system, = 670 , Kosmann et al, 2018.

Table 1. Test results, elasticity data in MPa. Mean (*m*), standard deviation (*s*), number of tests (*n*)

	m	*s*	*n*
	774.24	153.22	6
*	2422.80	247.24	9

Using linear elasticity theory and zero trans-verse strain of the adhesive layer in BJ test, = 0.265 and = 1959 were obtained from the numbers in Table 1 (see, e.g. Irgens, 2008). The value of seems to be low as compared to plastics or even steel. In fact, transverse strain is approximately zero only in the center of the adhe-sive layer but increases towards the free edges. An analytic solution to the stress state in a com-pressed, rectangular elastic layer between rigid plates has been proposed by Tsai, 2005. This solution was applied to BJ tension data. As a re-sult of this evaluation, = 0.467 and = 2272 were obtained. This solution seems to be more plausible since is within the meaningful range, see, e.g., Lee et al., 1986, and Adams et al., 1997.

Yield and fracture limits are given in Table 2. In case of TASJ, the values are close to the aforemen-tioned TBJ test, which were = 30 and = 55 . In SJ, yield or fracture limits are lower than in pure tension or pure shear due to the superposition of tensile and shear loads. A yield point was not clearly visible in the SJ shear stress, probably due to the complex strain measurement. Considering the strains, it can be seen that, as compared to pure shear, plasticity is absent in the presence of tension with constricted transverse strain.

Fracture patterns indicated predominantly cohesive failure within the adhesive layer. It should be noted that the bond lines in TASJ contained imperfections from manufacturing, which was later opti-

mized. There was, however, no large influence on the test results.

Table 2. Test results, strength values. Mean (*m*), standard deviation (*s*), and number of tests (*n*)

		[MPa]	[MPa]		[MPa]	[%]	[%]
TASJ	*m*			32.78	51.28		18.30
	s	--	--	2.73	7.22	--	4.58
	n			6	9		10
BJ	*m*	46.78	51.94			3.08	
	s	1.62	2.41	--	--	0.49	--
	n	9	10			9	
SJ	*m*	38.67	43.69		15.90	3.30	1.45
	s	3.91	4.41	--	1.61	0.62	0.94
	n	9	9		9	9	6

Values of and were calculated from Table 2, using Eqs. (1), (2), and = 0.467. The result is depticted in Figure 2. It can be seen that, at a given stress state, fracture or yielding of the adhe-sive are dependent on the magnitude of . Under pure shear (TASJ), = 0 and is highest. In ten-sion (BJ), ≫ 0 and → 0. The SJ tests take an intermediate position since the value of is be-tween BJ and TASJ values. Negative values of imply triaxial tension, which is known to be detri-mental to the strength of adhesive joints, see e.g. Adams 1997.

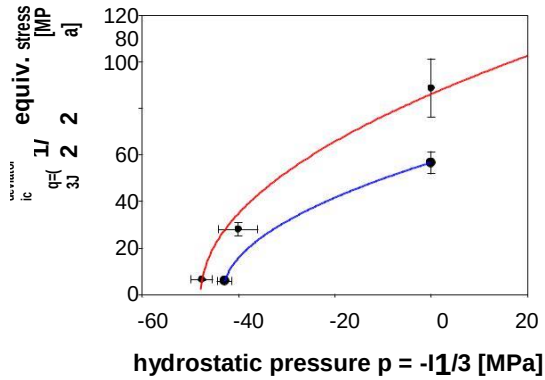

Fig.2. Representation of static test data in the meridian plane. Drucker-Prager model for yield (blue) and frac-ture (red)

The von Mises equivalent stress does not de-scribe such behavior. Related to the adhesive shear strength, the von Mises model would be represented by a horizontal line through the data points at = 0. This motivates the introduction of a Drucker-Prager type material model

$$^2 = + ^2 \qquad (5)$$

which describes the influence of hydrostatic stresses on strength, see Drucker, 1953, and Drucker and Prager, 1952. Herein, denotes a material-dependent parameter which describes the sensitivity to , and is the strength parameter of the adhesive material. This model represents a specific case of the exponential model which is available in commercial finite element codes such as ABAQUS or ANSYS. The linear form of (5), which can be found in Ward and Sweeney, 2013, was also used. It is however not suited as plastic potential due to lacking convexity. Due to lacking SJ data, Eq. (5) was solved analytically in order to identify the material parameters at the yield limit. At the fracture limit, Eq. (5) was fitted to available data. The results are given in Table 3 and the corresponding graphs are depicted in Fig. 2.

Table 3. Parameters of Drucker-Prager type material models for yield and fracture 1 – linear 2 – parabolic

		b	*c*	
yield	1	1.19	56.77	(1)
	2	74.32	56.77	(1)
fracture	1	1.66±0.18	89.60±6.46	0.988
	2	155.27±24.40	86.19±34.00	0.986

It can be shown that is related to measured shear or yield limits in Table 2 by

$$= \sqrt{3}\,(= .) \qquad (6)$$

A failure condition or plastic potential can now be formulated which allows any stress state in the bond line to be evaluated with respect to static failure based on the shear or yield limits.

A strain hardening curve is needed in order to simulate plastic Drucker-Prager type material behavior. Since substantial plasticity was only present in shear, a strain hardening curve was derived from TASJ tests.

Elastic shear strain = / was subtracted from the measured total shear strain in order to obtain plastic shear strain . Then, a power law of the form

$$= + \qquad (5)$$

where and are material-dependent parameters, was chosen in order to empirically describe the observed hardening curve. The shear yield stress was set to = 32.78MPa, as identi-fied in TASJ tests. Different values were chosen for since no stable fit was obtained. Values of were then identified by a weighted non-linear least squares fitting procedure to measured values of

and using 1/ ^{2} as weight. The results are given in Table 4. Although ^{2} indicates a better fit at high values of , it was decided that a value of = 0.3 is realistic since it did not over-predict stress at high values of .

Table 4. Strain hardening parameters. Shear yield stress set to 32.78 MPa

exponent	0.2	0.3	0.4	0.5	0.6
coefficient	17.48	25.19	35.42	48.65	65.38
	0.456	0.633	0.763	0.839	0.861

SUMMARY AND CONCLUSIONS

For a thin layer of EA9695 film adhesive, a consistent and sound set of elastic constants, a pressure-dependent failure condition, and a strain

hardening curve were obtained from a combination of TASJ, BJ, and SJ tests. Low values of Poisson's number were addressed to the assumption of zero transverse strain in BJ tests. This was overcome by using Tsai's approach.

Hydrostatic stresses were observed to have a large influence on the yield and fracture limits. Accordingly, failure conditions were formulated based on forms of the Drucker-Prager model, using a pressure coefficient and the shear strength as material parameters. For the current adhesive, a von Mises model could only be used in shear loading, which is a serious limit for the common case of multiaxial loading.

Significant plastic strain was observed in shear while it appeared to be absent in states containing hydrostatic tension. This suggests Drucker-Prager type behavior also for strain hardening. A strain hardening curve was extracted from shear tests and a power law was used to model strain hard-ening.

It can be concluded that, for similar structural adhesive films, a combination of TASJ, BJ, and SJ tests could be used in order to obtain elastic con-stants, pressure-dependent yield or fracture limits, and plasticity at once. It is important to use carefully manufactured samples with highly accurate align-ment, adequate test equipment, and well devel-oped data evaluation methods. Low values of Pois-son's number may be avoided by using realistic assumptions on transverse strain in BJ tests.

ACKNOWLEDGEMENT

Funding by the Federal Ministry for Economic Affairs and Energy on the basis of a resolution of the German Bundestag is gratefully acknowledged.

NOMENCLATURE

A adhesive bond area, mm^2
b pressure sensitivity parameter in DP model
c strength parameter in DP model, MPa
C strain hardening coefficient
d adhesive layer thickness, mm
D strain hardening exponent
E adhesive elastic modulus, MPa
E* apparent adhesive modulus in BJ test, MPa
F applied load, N
G adhesive shear modulus, MPa
I_1 first invariant of hydrostatic stress tensor , MPa
J_2 second invariant of stress deviator, MPa^2
L_0 distance between sensor tips, mm
p hydrostatic pressure, MPa
q von Mises equivalent stress, MPa
u corrected displacement, mm

Greek letters

shear strain, % or mm/mm
normal strain, % or mm/mm
Poisson's ratio
correlation coefficient
normal stress, MPa
shear stress, MPa

Subscripts

el elastic
f fracture
n nominal quantity
y yield
. (i) component acting normal (parallel) to A
iistress component numbering i = 1, 2, 3
iprincipal stress numbering i = 1, 2, 3
plplastic

REFERENCES

Adams, R., Comyn, J., and Wake, W., 1997, *Structural adhesive joints in engineering.* London: Chapman & Hall, 167-220.

AMC 20-29, 2010, *EASA AMC 20-29 Composite Aircraft Structure,* https://www.easa.europa.eu, accessed on May 31, 2018.

Ban, C. S., Lee, Y. H., Choi, J. H., and Kweon, J. H., 2008, Strength Prediction of Adhesive Joints Using the Modified Damage Zone Theory. *Composite structures* 86(1): 96–100.

CMH-17-3G, 2012*,* Design and analysis of bonded joints, In *Composite Materials Handbook*, Vol. 3, Wichita, Kansas: SAE International, 10-1–10-54.

CS-23, 2012, *EASA Certification Specifications for Normal, Utility, Aerobatic, and Commuter Category Aeroplanes,* https://www.easa.europa.eu, accessed on May 31, 2018.

Drucker, D. C., 1953, Limit Analysis of Two and Three Dimensional Soil Mechanics Problems. *Journal of the Mechanics and Physics of Solids* 1: 217–226.

Drucker, D. C., and Prager, W., 1952, Soil Mechanics and Plastic Analysis or Limit Design. *Quarterly of Applied Mathematics* 10: 157–165.

Irgens, F., 2008, *Continuum mechanics*. New York: Springer Science & Business Media.

Kosmann, J., Klapp, O., Holzhüter, D., Schollerer, M., Fiedler, A., Nagel, C., and Hühne, C., 2017, Measurement of Epoxy Film Adhesive Properties in Torsion and Tension Using Tubular Butt Joints, 4th International Conference on Structural Adhesive Bonding, Porto.

Kumar, S. B., Sridhar, I., Sivashanker, S., and Osiye, S. O., 2006, Tensile failure of adhesively bonded CFRP composite scarf joints. *Materials Science and Engineering B* 132: 113–120.

Lee, C. S., Jones, E., and Kingsland, R., 1986, Poisson's Ratio of Engineering Plastics. *Advances in Polymer Technology* 6(1): 85-90.

Rösler, J., Harders, H., Bäker, M., 2007, Mechanical Be-haviour of Engineering Materials, Berlin: Springer

Tsai, H., 2005, Compression analysis of rectangular elastic layers bonded between rigid plates. *International Journal of Solids and Structures* 42: 3395-3410.

Ward, I. M., and Sweeney, J., 2013, *Mechanical Properties of Solid Polymers*, 3 ed., Sussex: Wiley

International Symposium on Sustainable Aviation 2018
9 – 11 July 2018
Rome, Italy

ISSA-2018-028

AN APPLICATION OF TECHNIQUES FOR PAV OPERATION AND RESEARCH TREND IN REP. OF KOREA

ARim Ko[1], DaUn Kim[1], SungKwan Ku[2*]
[1]Dept. of Aeronautical System Engineering, Hanseo University Graduate School
[2]Dept. of Aviation industrial and system engineering, Hanseo University
Nam-myeon, Taean-gun, Chungcheongnam-do, Republic of Korea
Authors' e-mails: skku@hanseo.ac.kr

SUMMARY

In this paper, we conducted a research on technologies and operation related to PAV in Korea and overseas and described on the need for technologies .

Keywords: PAV, Operation, Trend of Technology.

INTRODUCTION

A personal air vehicle (PAV) refers to a small air vehicle for 1-4 persons that can be used as a personal transportation. It means an air vehicle directly controlled by the owner or navigated automatically from a point of departure to a destination. The ground transportations that have been gradually saturated recently demanded the appearance of a new transportation as an alternative. PAV, which can utilize all the transportation networks in the air and on the ground, is under research as the next-generation transportation.

The industry associated with PAV is a multi-area convergence industry that includes technical scopes, such as aeronautical engineering, electronics, communication, software, control, and automobiles, as well as airplane flight control and flight support. Therefore, PAV is a high-value-added industry with technical ripple effects on the growth of related industries. In addition, unlike the existing aviation industry with high entry barriers, the competition for PAV has not started yet. Therefore, it is necessary to develop the PAV industry as a growth engine for new future industries that can be preempted.

The generally suggested PAV reaches a destination through both ground movement and flight. The operation of PAV requires a three-dimensional (3D) transportation system. Since current aviation traffic systems are not capable of handling different transportations, system modification is necessary. Overseas, projects related to the PAV operation and air vehicle development have been performed since the end of the 1990s. For the PAV industry development in Rep. of Korea, it is necessary to review the previous studies and prepare plans to operate and develop PAV according to the Korean situation.

In this study, domestic and overseas PAV research trends were investigated for the PAV operation. Based on the results, methods to apply PAV to Rep. of Korea were researched.

REVIEW OF THE OVERSEAS PREVIOUS STUDIES ON PAV

For the PAV operation, support-related systems, and air vehicle design area, the overseas research trends related to PAV were investigated.

Operation and System

Overseas, projects, such as Advanced General Aviation Transport Experiments(AGATE), Personal Air Vehicle Exploration(PAVE), Small Aircraft Transportation System(SATS), Next Generation Air Transportation System(NextGen), Personal Plane(PPlane), and METROPOLIS, have been performed in relation to the PAV operation and system. Fig. 1 shows such projects in chronological order.

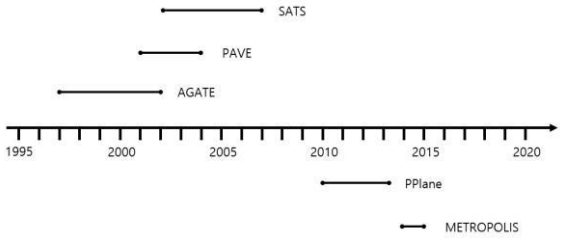

Fig. 1. Projects related to the PAV operation and system

AGATE is a project targeting at the activation of the personal small aircraft market. It is focused on developing key technologies required to develop small aircraft that is safe, easy to control, comfortable, and inexpensive.

PAVE is a project led by the NASA Langley Research Center. It established the concept of PAV and conducted research on the concept of a future air vehicle. It classified the required conditions, shape concept, and required technologies, and proposed the platforms of various PAV shapes.

SATS is a project for creating a new small aircraft transport system after AGATE. Its target is to develop national airspace, in which free flight is possible, using more than 5,000 small airplanes. The

optimal target of SATS is to construct a highway in the sky as shown in Fig. 2.

Fig. 2. Sky highway image system

NextGen is a program conducted in the United States. Its target is to effectively control air traffic by connecting all airplanes in the US airspace to a network in real time by 2025 and sharing the information. The current air traffic system is focused on ground control and human-oriented. The concept of the future air traffic system utilizes a communication group (including unmanned aerial vehicles (UAVs), communication satellites, and high-altitude airships).

PPlane is a project to find an optimized PAV operation system by 2030. In this project, the ground travel function is excluded from the PAV concept. The purpose of this project is to develop a system operated through automatic flight without a need for a pilot.

METROPOLIS investigates the alternatives to city airspace design for the operation of a number of personal airplanes and UAVs. The METROPOLIS airspace design is divided into four concepts (Full Mix, Zones, Layers, and Tubes). These four concepts are used to separate and construct the traffic system. Fig. 3 shows the conceptual diagrams of the METROPOLIS airspace.

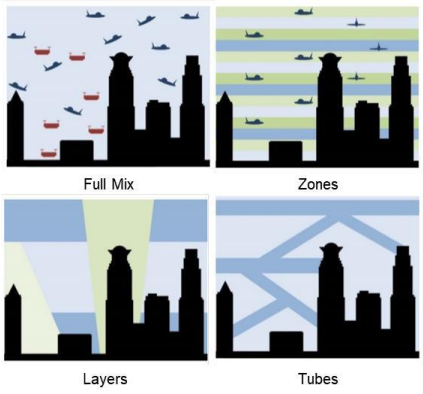

Figure 3. Conceptual diagrams of METROPOLIS

Air Vehicle Design

Air vehicle design has been conducted in various countries. Fig. 4 shows the PAV-type air vehicles already developed or under development.

Fig. 4. Historical development of PAV models

In this study, the overseas PAV development status was surveyed for the PAV operation. Table 1 summarizes the surveyed PAV air vehicle status of each country.

Table 1. PAV development status by country

Country	PAV name
The US	Transition
	TF-X
	Joby S2
The UK	Skycar
Israel	X-Hawk
Slovakia	Aeromobil 3.0
Europe	myCopter

Terrafugia from the US developed Transition, TF-X in which the wings can be folded. It is a dual-mode PAV capable of both road travel and flight. Joby S2 developed in the US is a two-seater PAV that uses an electric propulsion system. Joby S2 is a single-mode PAV capable of flying only.

In the UK, Skycar, a four-seater PAV, was developed. Skycar is a VTOL type capable of taking off and landing without runway. The duct fan of Skycar uses a tilting method. Skycar is equipped with devices controlled by the computer and the pilot can input the desired flight control.

In Israel, X-Hawk was developed, which can be used by civilians and armed forces. X-Hawk can be used for public purposes, such as the transport of emergency patients. It is known that X-Hawk finished the test flight in 2009.

In Slovakia, a dual-mode PAV AeroMobil was developed. AeroMobil is a new transportation capable of taking off and landing on the water. It has wings that can be folded backwards.

Europe has twice the population density of the US. As a measure to solve extreme traffic congestion, the myCopter project was conducted. The developed type was the VTOL type capable of taking off and landing without runway.

PAV RESEARCH TREND IN REP. OF KOREA

The Korea Aerospace Research Institute in Rep. of Korea conducted research on the PAV concept in 2010 after a need for the development of PAV key technologies was recognized on a national level. A technology development promotion strategy was established to intensively develop PAV-related competitive technologies. The researched PAV technology road map suggested technology development strategies in four steps. Table 2 shows the phased technology development strategies in the PAV technology road map.

Table 2. Technology development strategies by step in the PAV technology road map

1st step (2011-2015)	2nd step (2016-2020)	3rd/4th steps (2021-2030)
Key technology construction	Key technology verification	Key technology commercialization
Technology unit test-bed	Certification test development	Flight prototype development/commercialization prototype development

In Rep. of Korea, the concept design and demonstration flight of PAV-type air vehicles with various shapes were conducted.

The Pusan National University developed a reduction model of the quad-tilt-prop-type dual-mode PAV. A prototype for the flight test assessment in the VTOL mode was fabricated as shown in Fig. 5. The automatic travel and flight experiment was performed, confirming the stable driving performance and maneuverability. The efficiency of the reduction model will be improved through further research.

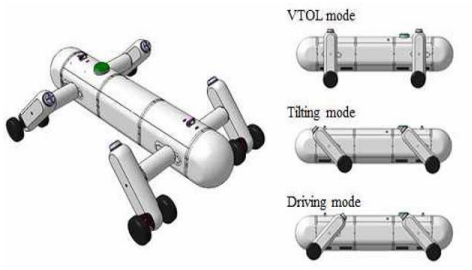

Fig. 5. Quad-tilt-prop-type PAV

The Chungnam National University developed a tilt-prop-type dual-mode Flying Car as a Korean PAV as well as a CNUPAV-01 reduction model. Fig. 6 shows the tilting-type Flying Car. The entire vehicle adopted an airfoil shape to reduce complicated mechanisms, such as folding-type wings. A folding mechanism, in which the main propeller can be folded into the fuselage, was reflected to meet road width restrictions.

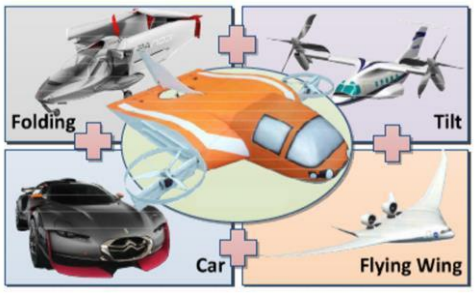

Fig. 6. Tilting-type Flying Car

Fig. 7 shows the CTOL-type CNUPAV-01. CNUPAV-01 is equipped with two-stage folding wings like the commercialized fuselage transition. The flight stability and maneuverability of the CNUPAV-01 model were confirmed by flight testing.

Fig. 7. Configuration of the CNUPAV-01

In addition, government-funded research on the intelligent precision navigation for PAV and manned/unmanned aerial vehicle composite operation technology has been conducted based on the aviation electronics and communication technologies of Rep. of Korea. This suggested that effective outputs can be expected if the intelligent traffic system (ITS), which uses domestic transportation and IT technologies, is utilized.

Recently, base technology to support the safe navigation of PAV has been developed. PAV is operated at a very low altitude compared to the airspace and airway in which aircraft operates. Its operators are expected to be those who have not received professional aviation education. The weather information provision method for PAV operators is being researched so that safe flight can be possible under these flight conditions. Base technology for non-experts to easily access the navigation weather (aviation weather) information is under research using the existing aviation weather information and other various information sources.

PAV OPERATION TECHNOLOGY APPLICATION METHOD OF REP. OF KOREA

Overseas countries proposed the PAV operation method in a way that information sharing through real-time networks and traffic systems are separated. Rep. of Korea needs to follow the same way. For the PAV operation in Rep. of Korea, a basis must be prepared first to provide the stability and maneuverability for the aircraft flying in 3D space on the automotive level. Technologies for the stability and maneuverability of PAV are required. Technologies to secure the stability of PAV are being developed in the areas of the PAV certification system, navigation system, and aviation communication system.

The control system of PAV will be developed based on the satellite navigation system, which is currently being standardized worldwide. However, technologies related to air vehicles and engines must be further established to meet the operating environment pursued by PAV. Rep. of Korea has technologies accumulated through the small plane development experience. In addition, it acquired new-concept air vehicle technology through the development of smart UAVs. In Rep. of Korea, it is possible to apply IT technology to flight control devices for automatic taking off and landing as well as safe navigation based on the semiconductor IT area, which is the world leader. The Korea government is growing the related industries by investing in the ITS. Automotive technologies and intelligent vehicle technologies can be a strength in developing PAV and preempting the market. Rep. of Korea's utilization of the accumulated technologies will advance the development of the PAV industry.

Unlike commercial aircraft, PAV will be operated at low altitudes. The airspace and airway for PAV must be secured. The weather in the airspace and airway, in which aircraft operates, affects the stability and maneuverability of PAV. For this reason, a weather-related observation system is required. The weather radar of Rep. of Korea has a sufficient probing area to cover the entire land and waters. However, it is necessary to develop high-level contents to indicate the presence of turbulence and heavy rain accompanied by cumulonimbus that inhibit safe flight.

CONCLUSIONS

Domestic and overseas studies were examined for the application of the PAV technology and operation method to Rep. of Korea. The overseas PAV-related technology development has been performed since the end of the 1990s. Rep. of Korea conducted preliminary PAV development research in the early 2000s after recognizing a need for PAV technology development.

Rep. of Korea needs to adopt the same PAV operation method as proposed by overseas countries in which network communication was separated from the traffic system. Technologies for the stability and maneuverability of PAV, which flies in 3D space, are being developed in various areas. It is necessary to establish technologies related to air vehicles and engines that meet the operating environment.

ACKNOWLEDGEMENT

This research was supported by a grant (18CTAP-C129733-02) from technology advanceme -nt research program funded by Ministry of Land, Infrastructure and Transport of Korean government.

REFERENCES

B.J. Holmes, M.H. Durham, S.E. Tarry, Small aircraft transportation system concept and technologies, 2004, Journal of Aircraft, 41: 26–35.

Dae-Seong Lee, 2010, Personal Air Vehicle Development precedent research, Korea Aerospace Research Institute.

H. Blülthoff, myCopter personal aerial vehicles: the next big game-changer? 2016, EASA-OPTICS Safety Conference, 2016.

Jin-Deog Chung, 2014, Current Development status of Personal Air Vehicles(PAVs), The Korean Society of Mechanical Engineers Conference, November 11-14, 2014. Seo-gu, Gwangju, Republic of Korea.

Jin-Suk Jeong, Young-Seop Byun, Jun-Beom Song, Jae-Nam Kim, Hyeong-Ho Kim, Woo-Jin Song, Beom-Soo Kang, 2013, Design and Fabrication of Scaled-down Quad Tilt Prop PAV, The Korean Society for Aeronautical and Space Sciences Conference, April, 2013, Republic of Korea.

Ki-Sang Lee, 2008, Development Prospects and Opportunities for future Personal Air Vehicles(PAV), The Journal of Aerospace Industry, 70: 70-93.

METROPOLIS – Urban Airspace Design: Concept Design (D2.2), 2014.

Seong-Hun Yoon, Dong-Hun Chang, Il-Won Seo, Chung-Gil Ra, Jin-Yeoung Seok, Seong-Jun Yoon, Seong-Nam Kim, 2013, Development and Test of Tilting-Type Scaled Flying Car, The Korean Society for Aeronautical and Space Sciences Conference, Aprile, 2013, Republic of Korea.

Tae-Hyeong Yi, Keun-Taek Kim, Seokmin Ahn, Dae Sung Lee, 2011, Technical Development Trend and Analysis of Futuristic Personal Air Vehicle, Current Industrial and Technological Trends in Aerospace, 9.1: 64-76.

Yaolong Liu, Michael Kreimeier, Eike Stumpf, Yaoming Zhou, Hu Liu, 2017, Overview of recent endeavors on personal aerial vehicles_A focus on the US and Europe led research activities, Progress in Aerospace Sciences.

https://www.terrafugia.com/, accessed on April 19, 2018.
https://www.moller.com/, accessed on April 19, 2018.

RESEARCH OF WAYS TO IMPROVE ENVIRONMENTAL CHARACTERISTICS OF A HEAVY LONG-HAUL AIRCRAFT

V. LOGINOV; S. DMYTRIYEV; V. SHLAPATSKYI

Private Joint Stock Company "FED"; State Enterprise "Ivchenko-Progress";
State research test centre of Armed Forces of Ukraine Chernigiv;

132, Sumskaya Street, Kharkov, 61023, Ukraine;
2, Ivanova Street, Zaporozhye, 69068, Ukraine;
1, Striletska Street, Chernigiv, 14013, Ukraine;

login_w@ukr.net;
s.dmytriyev@ivchenko-progress.com
bezpilota@ukr.net

Europe is moving to a new level of development in the context of global globalization, financial reforms, climate change and the growing scarcity of resources. The main purpose of ACARE is to initiate cooperation among stakeholders, aimed at achieving the goals Flightpath 2050. For achieving ACARE goals, one of the purposes of PARE project research is to evaluate methods for reducing the drag of a heavy long-haul airplane of the A340-600 type based on the implementation of the adaptive wing concept, as well as the influence of the electric landing gear on the fuel efficiency of the airplane. Analysis of the results of the research showed that the laminarization of the surface of the airframe without taking into account the energy costs of extracting the boundary layer reduces fuel consumption by approximately 20 %. Taking into account the energy costs of laminarization, this gain may reach 13...15 %. Reducing the time of using the airplane's march engines during taxiing is an action that is comparable in its effectiveness with the reduction in the size of the slits and ledges in the controls and mechanization of the wing of the airplane. Thus, even without considering the development of the resource of marching engines, an airplane equipped with a device of the WheelTug type has an advantage over the original airplane only when taxiing for more than 30 minutes.

Keywords: aircraft, drag, laminarization, jet engine, electric drive, fuel efficiency.

INTRODUCTION

Aviation contributes significantly to anthropogenic pollution of the environment. This problem is especially important for large airports with intensive air traffic [1, 2]. Pollution of the upper troposphere and stratosphere has global climatic and environmental impacts on humans and the biosphere [3]. Therefore, the leading countries of the world aircraft industry set long-term goals for the development of aviation based on environmental efficiency [4, 5], the development of new technologies and the search for new technical solutions in aviation at the level of revolutionary approaches [6-9].

In the European Union, the Advisory Council for Aeronautics Research in Europe (ACARE) plays a key role in -termhe longstrategy for research aimed at reducing the impact of aviation on the environment and increasing the competitiveness, sustainability of the European aviation industry.

The main task of ACARE is to initiate cooperation between stakeholders, aimed at achieving the goals of Flightpath 2050 [2]. To analyze the fulfillment of all the goals, outlined in the Flightpath 2050, at the present time, on the initiative of the partners of the project PARE-Perspectives for Aeronautical Research in Europe (www.pareproject.eu),research is being conducted to determine the level of progress, gaps and barriers for each of these objectives and to develop recommendations for their elimination. One of the research tasks in the PARE project is the assessment of methods for improving the fuel efficiency of an aircraft based on the implementation of the concept adaptive wing to reduce the drag of the aircraft [10] and the electric drive of the chassis wheels.

To ensure the competitiveness of aircraft, an urgent task for modern and future aircraft is to study environmental characteristics and fuel efficiency.

The aim of the presented investigations is to evaluate the influence of perspective methods of reducing fuel consumption of a heavy long-range aircraft based on improving aerodynamic characteristics.

METHOD OF RESEARCH

The research of the aircraft environmental characteristics is based on the knowledge of the parameters of the working process of the propulsion engine and the aerodynamic characteristics of the airframe. Advanced methods to increase the aerodynamic quality of the aircraft are the abandonment of mechanization of the leading and trailing edges of the wing, deflected controls of the aircraft, artificial laminarization of the airframe elements [6, 10]. As a result, the effect of increasing the aerodynamic quality of the aircraft is the increasing of some extent its fuel efficiency. Another example of improving the fuel efficiency of the aircraft is the use of an electric drive of WheelTug chassis racks for taxiing the aircraft with the engines switched off [11]. However, such solutions require careful research.

For carrying out the research, a heavy long-haul aircraft of the A340-600 type was chosen.

The researches were carried out for two directions: parametric researches of the aircraft performance characteristics (APC) and the assessment of the application of the chassis landing gear during the taxiing of the aircraft with the engines shut off to the runway.

Parametric researches of the APC of a heavy long-range aircraft were carried out with the help of a developed modular software package based on the methodology described in [12, 13]. The modular software package allows to carry out research with both subsonic and supersonic flight speeds.

The basis of reduction the aerodynamic drag of the aircraft is to improve the quality of the streamlined surface, reduce the number of external superstructures and structural elements, and conduct other design and technological actions. To eliminate errors associated with the definition of areas of small elements, data on their drag are represented as the product $\Delta(C_D \cdot A)$ [14]. The necessary values of the coefficients of drag are obtained by dividing $\Delta(C_D \cdot A)$ by the characteristic area: $C_D = \Delta(C_D \cdot A)/A$. If necessary, additional drag can be taken into account for the engine nozzle with a noise attenuation system

$C_D=0{,}025\ n\ (A_{noz} / A)$.

RESULTS AND DISCUSSION

The advanced means of reducing drag of subsonic aircraft are artificial and natural laminarization of flow. Using profiles of special shapes with favorable pressure gradients in the front part of the wing, natural laminarization can be carried out on the wing of the aircraft and, as a result, reduce the drag [15].

The aerodynamic characteristics of the initial and modernized version of the aircraft are presented in the form of polar (Fig. 1) and aerodynamic quality dependencies on the lift coefficient of the aircraft (Fig. 2) for the cruising flight regime.

The results of the calculation of the polarity and the dependence of the aerodynamic quality on the lift coefficient of the modernized aircraft are shown in the absence of mechanization of the leading and trailing edges of the wing, the deflected controls of the aircraft, laminarization of the fuselage, wing, tail, and nacelles. The data correspond to the cruise mode of the aircraft flight.

Table 1 shows the results of calculating the consumption characteristics of an aircraft with influence (turbulizes the boundary layer) and without effect of the slat on the structure of the boundary layer on the main profile. Also, the results of calculating the value of the additional fuel consumption ΔG_{fuel} under the influence of the slat in the absence of mechanization of the wing, ailerons and rudders are given.

To improve the environmental characteristics of the aircraft, it is necessary to use the electric drive of the chassis wheels [11]. The use of this device reduces the number of harmful emissions and noise levels, and also allows the aircraft to move in reverse without using ground equipment. Due to the increased mobility of the aircraft, the traffic intensity increases, which leads to a shortening of its time on the ground and increases the profitability of air transportation.

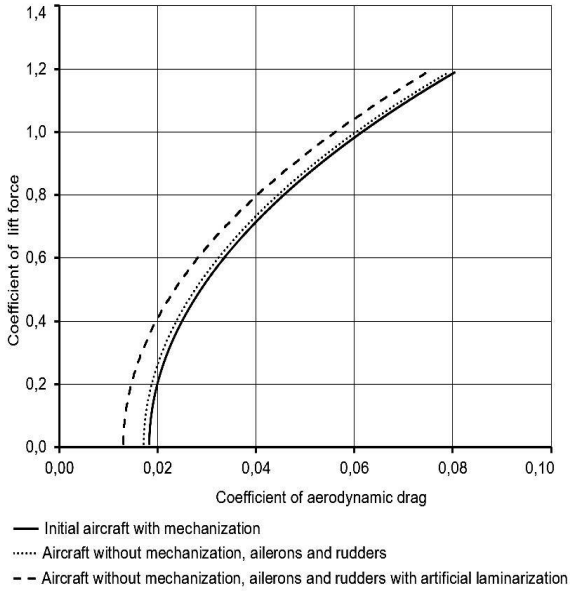

Fig. 1. Polaris of the initial and modernized aircraft

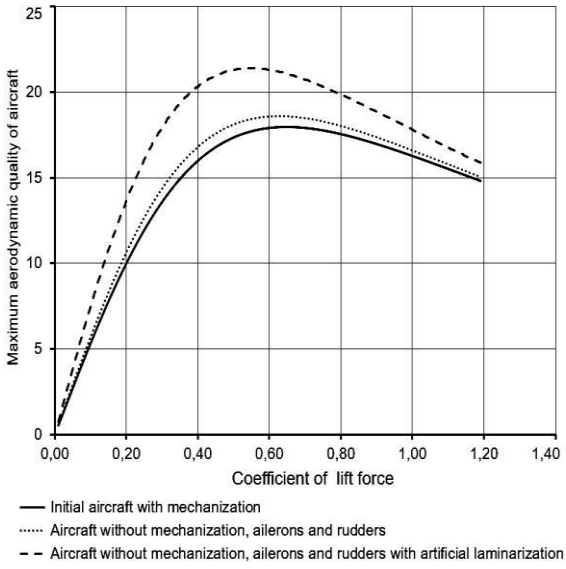

Fig. 2. Dependence of aerodynamic quality on the lift coefficient of the aircraft.

An increase in fuel consumption with an increase in the taxiing time of the aircraft (the operating mode of the "idle" engine) is shown in Fig. 3.

Table 1. Results of calculating the consumption characteristics of A340-600 aircraft with the influence of the slat on the boundary layer structure on the main profile

Parameter name	Initial aircraft (influences/ does not influence)	Without slats (influences/ does not influence)	Without flaps (influences/ does not influence)	Without ailerons (influences/ does not influence)	Without mechanization and ailerons (influences/ does not influence)	Without mechanization, ailerons and rudders (influences/ does not influence)	Artificial laminarization (influences/ does not influence)
Fuel consumption per flight, kg	139195,8	133513,4	137213,3	138657,3	131004,4	128855,3	111140,6
	134080,5	133513,4	132105,9	133544,3	131004,4	128855,3	111140,6
Fuel consumption in the horizontal part of the flight, kg	125505,3	120152,3	123640,3	124999,1	117782,1	115748,9	98906,3
	120687,4	120152,3	118823,1	120181,4	117782,1	115748,9	98906,3
Remaining fuel, kg	16404,2	22086,6	18386,7	16942,7	24595,6	26744,7	44459,4
	21519,5	22086,6	23494,1	22055,7	24595,6	26744,7	44459,4
Hourly fuel consumption of aircraft propulsion, kg/h	11242	10798	11087	11200	10601	10432	9030
	10842	10798	10687	10800	10601	10432	9030
Hourly fuel consumption of aircraft propulsion at cruising speed, kg/h	10914	10448	10751	10869	10242	10065	8601
	10495	10448	10332	10451	10242	10065	8601
Kilometer fuel consumption of aircraft propulsion on cruise control, kg/km	14,42	13,81	14,21	14,37	13,54	13,30	11,37
	13,87	13,81	13,66	13,81	13,54	13,30	11,37
Gain on fuel ΔG_{fuel} in comparison with initial one, kg	-	5682	1982	538	8191	10341	28055
	-	567	1975	536	3076	5225	22940
Gain on fuel ΔG_{fuel} in comparison with initial one, %	-	4,1	1,4	0,4	5,9	7,4	20,2
	-	0,4	1,5	0,4	2,3	3,9	17,1

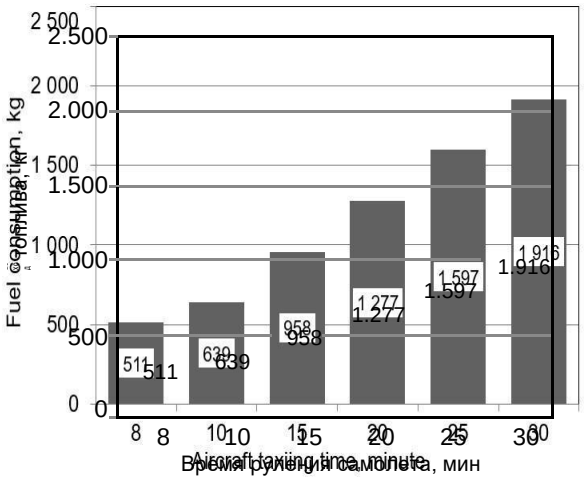

Fig. 3. Fuel consumption with increasing taxiing time of the aircraft (engine mode "idle")

The results of a study of the fuel efficiency of the initial aircraft for a typical flight cycle with a device of the WheelTug type are obtained for different aircraft taxiing times on the ground. The device weighs 1 000 kilograms, including the cab interface and controllers and consists of electric motors installed in the wheels of the bow rack. It should be noted that the installation of such systems reduces the weight perfection of the aircraft [10].

Researches have shown that for this aircraft the use of an electric drive of such weight is effective in case of taxiing for more than 30 minutes. With less taxiing time with the device type WheelTug, the weight of the saved fuel during taxiing becomes much less than the weight of fuel that is expended for the air transportation of the additional weight of the electric drive in the aircraft. Therefore, in future researches, it is expediently to take this feature into account when calculating the characteristics of the aircraft, and the weight of the electric drive must be reduced.

CONCLUSIONS

Based on the obtained results it is possible to draw the following conclusions:

1. The most effective method of increasing the aerodynamic quality of the aircraft is the laminarization of the airframe surface. Laminarization of the surface without taking into account the energy losses of extracting the boundary layer allows reducing fuel costs by approximately 20%. Estimated, taking into account the energy losses for laminarization, it may be 13…15 %.

2. Reducing the time of using the aircraft's cruising engines during taxiing is an activity that is comparable in its efficiency with the reduction in the size of the slits and ledges in the controls and mechanization of the wing of the aircraft. It is established that even without taking into account the reaching the end of cruising engines service life, a heavy long-distance aircraft equipped with a device of the WheelTug type has an advantage over the initial airplane when taxiing for more than 30 minutes.

3. The results are preliminary and allow one to evaluate the limiting possibilities for improving the fuel efficiency of a heavy long-range aircraft of the chosen type.

NOMENCALTURE

n – number of engines,
A – reference area, m^2,
A_{noz} – nozzle exit area, m^2,
G_{fuel} – fuel consumption, kg,
C_D – aerodynamic drag coefficient.

SUBSCRIPTS

noz – nozzle,
D – drag,
fuel – fuel.

REFERENCES

1. https://ec.europa.eu/commission/future-europe_en, accessed 26 May 2018.
2. http://www.acare4europe.org/sria/flightpath-2050-goals, accessed 25 May 2018.
3. environmental-report-2016-72dpi.pdf: 84.
4. http://www.airbus.com/newsroom/press-releases/en/2017/09/airbus_-_blade_-laminar-flow-wing-demonstrator-makes-first-fligh.html, accessed 10 September 2017.
5. Nickol, C., Haller, W., 2016, Assessment of the Performance potential of Advanced Subsonic Transport Concepts for NASA's Environmentally Responsible Aviation Project.
6. A. Concilio, I. Dimino, L. Lecce, R. Pecora, 2017, Morphing Wing Technologies. Large Commercial Aircraft and Civil Helicopters, 1st Edition, Butterworth-Heinemann: 978.
7. Grahamn, W.R., Hall, C.A., Morales, V., 2014 The potential of future aircraft technology for noise and pollutant emissions reduction. *Transport Policy*, Volume 34: 36–51.
8. L. Leylekian, M. Lebrun, P. Lempereur, 2014, An Overview of Aircraft Noise Reduction Technologies. *Aerospace Lab Journal*, Issue 7: AL07-01.
9. Nae, C., 2014, Advanced Aerodynamic Technologies for Future Green Regional Aircraft. *INCAS BULLETIN*, Volume 6, Special Issue 1: 99 – 110.
10. В.А. Белкин, 2015, К проблеме повышения топливной эффективности гражданских самолетов. *Научный вестник МГТУ ГА.* № 219: 121-126.
11. https://www.safran.ru/file/download/safranmag11_rus.pdf: 21.
12. В.В. Логинов, 2015, Программный комплекс по формированию эксплуатационных характеристик двигателя силовой установки самолета. *Авиационно-космическая техника и технология*. № 9: 149–152.
13. V. Loginov, Y. Ukrainets, 2016, Analysis of operational characteristics of aviation diesel and gas turbine engines for light passenger aircraft, *Transactions of the institute of aviation*. Warsaw, №4(245): 103-115.
14. Н.Ф. Краснов, 1981, Основы аэродинамического расчёта. М.: Высшая школа.
15. C.L. Burley, E.D. Olson, R.H Thomas, 2017, Hybrid wing body aircraft system noise assessment with propulsion airframe aeroacoustic experiments. *International Journal of Aeroacoustics.* Vol. 11, No. 3&4.

ISSA-2018-030

FOR A MORE SUSTAINABLE AND SAFE AVIATION

Jean-Michel Most[1] and Michel Champion Institut Pprime UPR 3346 au CNRS, ISAE-ENSMA,Université de Poitiers, France 1 avenue Clément Ader, BP 40109, 86961 FUTUROSCPE Cedex jean-michel.most@ensma.fr, michel.champion@ensma.fr

SUMMARY

The reduction of aircraft weight is the major key to save energy and decrease the emission of greenhouse gases . In new generation of aircraft, composite materials are massively introduced for structure, fuselage, wings, fuel tanks, cowling and fire walls. Indeed the flammability of these materials must not increase the fire hazard whose probability must remain at least lower than those of aluminum planes in term of safety for passengers and crew.

This work is focused on the experimental characterization of resistance to fire of aeronautical thermoset and thermoplast composite materials used in the new generation of aircraft.

*An original experimental setup is described to characterize the materials in standard conditions of fire scenario (postcrash, engines or flight fires). Main flammability and burning properties of these composites are determined and a material ranking is proposed. Conclusions of the analysis involve a cl*ear description of the potential toxicity of the degradation products and their sustainability factors.

Keywords: Resistance to fire of materials, thermosets, thermoplasts, composite ranking

INTRODUCTION AND OBJECTIVES

Current challenges for a sustainable aviation involve key-points related to the energetic transition whose goal is to make a green planet great again. To do so the aviation sector must clearly play a significant part. The reduction of the aircraft weight is considered as a major issue to decrease the exhaust of greenhouse gases (soot particles, Nox and CO_2). This involves developing new materials, using green energy, increasing the role of electricity, and recycling the aircraft materials at the end of their life.

One of the main objectives is the development of lighter aircraft where composite materials are widely substituted by aluminium elements which are the best alternative in term of density and mechanical resistance (composites compose around 53% of the primary structure of 350 XWB). In this new generation of aircraft, the polymer are not used only for indoor decorative panels for passenger convenience or avionics devices, but, they are more and more introduced in the aircraft structure itself, fuselage, empennage, wing, cowling, and also to compartmentalize and insulate on board energetic systems as auxiliary power system, fuel cells, kerosene reforming, O_2 production devices, etc.. In term of fire safety, these composites must ensure at least an equivalent level of safety as those of the former materials by acting as an efficient barrier to prevent external flame penetration into the cabin to protect passengers, crew and flight equipments [1,2].

The work whose results are presented here had several objectives: to design and realize an original setup allowing testing the composite materials in thermal conditions representative of fire standard tests (in-flight, engine or post-crash fires) at a laboratory scale. The goal was then to reach the major flammability and burning properties of the material investigated. Accordingly aeronautical thermoset and thermoplastic composites were examined, and their fire behaviours and fire resistance were characterized, in such a way that a material ranking based on the FIGRA parameter could be determined.

THE ORIGINAL TEST DEVICE

The device that we developed consists of a generator of a jet of hot combustion products (propane - propylene/air flame) impinging on the surface of the studied material in representative fire conditions defined by the FAA standard burnthrough tests (AC 20-135 and AC 20-107B specifications) for global heat fluxes and gas temperature at the external material side [3, 4, 5, 6, 7, 8, 9, 10, 11].

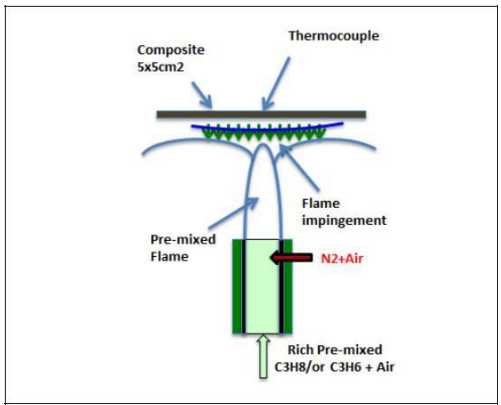

Figure 1: Schematic of lab-scale burnthrough test facility

To go further than standard passed-failed tests [5], a reduced material size (0.05x0.05 m^2) was used to decrease the trial cost, to multiply the test number and to have access to the flammability and burning properties by using more diagnostics.

The test parameters, the evolution of the surface temperature at the material surfaces and of the sample mass loss (ML) were measured. For various incident heat fluxes (75 to 202kW/m^2) and temperature (830 to 1160°C), a signal data processing allowed the determination of the Burnthrough Time (BTT corresponding to the time for the flame to drill a given thickness of material), *the material Mass Loss Rate* (MLR) – *time derivative of the ML* or burning rate - which is proportional to the Heat Release Rate (HRR), the pyrolysis and ignition t_{ign} times, the off-gassing time -*time for degrading the sample backside*-, the Peak of MLR (PMLR), the total Burning time, the mean burning time. These data determine the dimensional Fire Growth Rate parameter (FIGRA).

THE STUDIED COMPOSITES

The composites are made of a polymer matrix reinforced with fibres (FRP). In aircraft (A350 and B787 plane families), the structure is made with a *carbon-fibre-reinforced polymer*. In the case of thermosets, the polymer is an epoxy resin, the raw uncured resin molecules (macro-molecules) are crossed linked through a catalytic chemical reaction which creates extremely strong bonds with one another, by changing state from a liquid to a solid. Then, they cannot be reversed or reformed and their recycling is extremely difficult. On the other hand, for thermoplastic, the matrix is composed by semi-crystalline PEEK (PolyEtherEtherKetone) known for having high heat, chemical and mechanical resistances. The thermoplastics are formatting in liquid phase (viscous) at a temperature over their melting temperature. The molecules are long, linear or branched, but chemically separated. When heat and pressure impregnate the reinforcing fibres, it is a physical change which occurs, not a chemical reaction as with thermosets. This allows thermoplastic composites to be reformed and reshaped. This also allows, at least theoretically, their recycling at end of life.

The characteristics of the tested materials are listed on Table 1.

	Thermosets				Thermoplasts	
	AcF1	AcF2	AcF3	AcF9-1	AcF5	AcF6
Fibre	Carbon	Carbon	Carbon	Glass	Carbon	Carbon
Matrix	Epoxy	Epoxy	Epoxy	Phenolic	PEEK	PEEK
Fire barrier	Single laminate	Woven laminate	Single laminate	Woven laminate	Single laminate	Woven laminate
Layup	Carbon/ Epoxy	[90/0] Carbon/ Epoxy	Epoxy	[90 °/0 °] Glass/ Phenolic	+45/90/-45/0 Carbon/PEEK	90/45/0 Carbon/PEEK

Table 1 : Tested composite materials

THE MAIN RESULTS

Standard mass loss rate evolutions
For q=220 kW/m^2,
The following results were observed :

- The material is never burnthrough before a period of 15 minutes (the aluminium BTT is around 50s for 2 mm thick plate);
- There exists one peak of MLR;
- an increase of MLR up to the time of PMLR (t_{pMLR}): the composite degradation kinetic is controlled by the available heat flux (q_{net}) and the pyrolysis law (relationship between surface temperature and mass flow rate of the degradation products);
- a decrease of PMLR: the composite degradation kinetic is controlled by the availability of resin to be degraded;
- It is noted that the time of heat penetration $t_{penetration}$ in the composite (beginning of the backside temperature t_b rise) is 2,4 s after the front face heating;
- The pyrolysis time $t_{pyrolysis}$, (starting of the composite degradation);
- The ignition time t_{ig} (time from the beginning of the degradation and PMLR);

The burning time $t_{burning} = t_{end\ of\ burning} - t_{pyrolysis}$.
Figure 2 reports a generic evolution of the MLR for AcF2 when submitted to the flame.

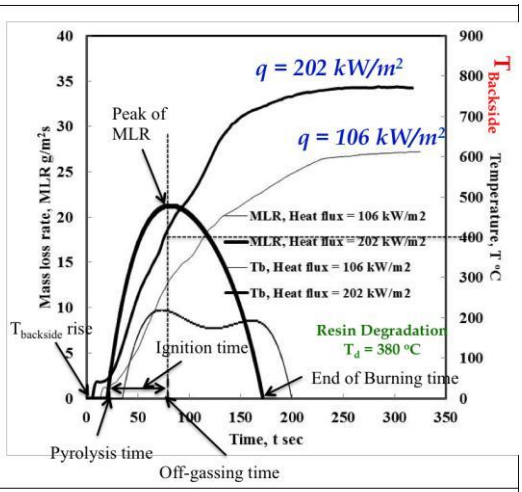

Figure 2 : Generic evolution of the MLR of the ACF2 thermoset sample

The incident heat flux preheats the solid and the pyrolysis law controls the degradation product emission on the exposed front side, up to PMLR. In all conditions, it was observed that the time of PMLR always coincides with the time where T_b (sample backside temperature) reaches the degradation temperature T_d of the resin i.e. 350-380°C for epoxy resin. The backside surface of the material becomes porous to degradation products and a black smoke is emitted. It is then considered that a major amount of degradation products is preferentially emitted from this side, and controlled by the resin availability. MLR decreases with the degradation of the residual resin (off-gassing with a beginning of emission of flammable gases in the cabin).

For q=106 kW/m^2 , The following was observed:

For heat fluxes of 75 and 106 kW/m^2, the MLR evolution first increases (the burning rate is controlled by the incident heat flux and as well as the pyrolysis law) and then decays before increasing again. This is attributed to the formation of a char protective layer during the resin degradation (first rise of MLR), the char is heated over the resin degradation temperature and re-radiates an important part of the incident heat flux: the net heat flux q_{net} to the solid is decreasing down to zero (no heat flux penetrates the solid). Then, carbon fibres are roughly depleted off by further exposure to heat with residual resin burning (second rise of MLR).

This interpretation, previously developed for wood or PMMA, is extrapolated here considering that it is not a char re-radiation, but the carbon fibres re-radiation [11] that decreases q_{net}.

- The 1st peak time corresponds to $t_b=t_{ignition}$;
- MLR decreases (char formation), then increases (char oxidation) up to the second MLR peak;
- After the second PMLR, the availability of resin controls MLR.
- All the other phenomena are similar to the ones observed in the case **q=220 kW/m^2** exposed in the previous paragraph

Synthesis of the results

From a processing of the Mass Loss (ML) and temperature signal evolutions, the following features were determined: the influence of the thermal impact, the sample thickness, the carbon fibre arrangement and percentage, the resin type (epoxy or PEEK), etc.. on the main flammability and burning properties of the materials such as the Ignition delay $t_{ignition}$, BTT, MLR, the degradation temperatures, PMLR corresponding to the beginning of off-gasing through the sample back side (synonym of toxicity for passengers and crew), the total burning rate, and more minor properties.

For all thermal conditions and all tested composites, BBT is always greater than the one for aluminium BBT (BBT>15min) and standard safety levels: all BT tests pass. For both material types, the behaviour of the fibres are similar.

Moreover, the results show (Figure 3) that thermoplasts present a better fire resistance to a thermal stress than thermosets. Two main reasons can be identified: a lower density for thermoplasts and a better fire resistance of PEEK resin attributed to its activation energy and degradation chemistry. Then, the resin burning is never complete, as confirmed by the measurement of the mass loss after the test, polymer staying still anchored to the fibres. This property is probably inherent to its manufacturing under pressure at a temperature level over the melting temperature of the resin.

The excellent fire resistance of composites to burnthrouh can be attributed to the fibres re-radiation of a part of the incident heat flux, limiting the heat flux transfer into the material, acting as a carbon curtain after the pyrolyse. The resin degradation temperature is about 380°C for thermosets while the fibre temperature, after the resin degradation, can reach the gas temperature (around 1200°C). The fibres are slowly oxidized and burnthrough can occur later. The fibre radiation, proportional to T^4_{fibres}, becomes important and the net heat flux q_{net} transmitted to the composite balances the heat loss by the solid to the environment. A thermal equilibrium is reached. In these conditions, the composites are a better fire barrier than a metallic skin as soon as the metal melting temperature is lower than the temperature at the impinging plane.

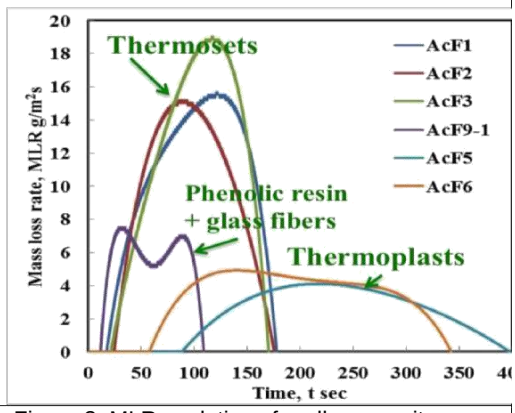

Figure 3: MLR evolutions for all composites - Heat flux, *q=155 kw/m^2* ; Strain rate, *τ=430s^{-1}* ; Sample thickness 2 *mm*

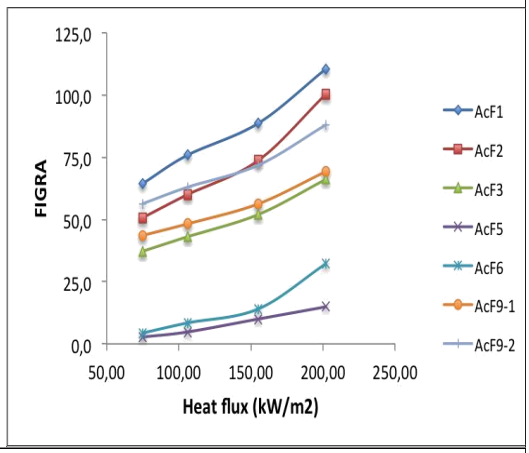

Figure 4: Variation of the FIGRA number with the incident heat flux for each composite

The measured flammability and burning properties allow the determination of the values for a dimensionless number FIGRA (FIre Growth RAte) that characterizes the ranking of the materials in term of safety (Figure 4). FIGRA is defined by [12]:

$$FIGRA = \left(\frac{\dot{Q}_{max}}{t_{max}}\right)_{SBI} \propto \frac{PHRR^2}{t_{ign}}$$

where *PHRR= Hc * PMLR* and Hc is the heat of combustion measured by a Cone Calorimeter (Hc 17-22 kJ/g).

This ranking (Figure 4) confirms that thermoplasts present a better fire resistance to a fire stress than phenolic resin/glass fibre thermosets, and finally than epoxy resin/carbon fibre thermosets.

Off-gasing time of the composites

Figure 5 reports the time when the Peak of MLR happens the same as the time when the degradation front reaches the backside of the sample (off-gasing time). At this instant, toxic gases are emitted on the internal side of the panel risking to poison passengers and crew. Although the BBT is much longer than the aluminium BBT, the order of magnitude off-gasing time is similar to this last one for equivalent sample thickness. Again, the off-gasing times for thermoplastics are better in terms of passengers and crew survivability.

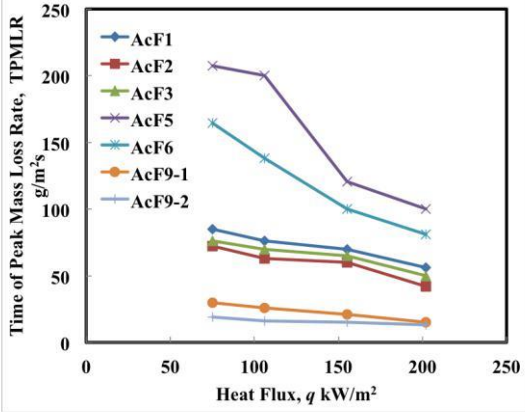

Figure 5 : Time of peak Mass Loss Rate for all composites versus the incident heat flux

CONCLUSION

An original experimental apparatus was designed to determine the fire resistance of composites under thermal stress conditions representative of standard aviation fire scenarios.

The Burnthrough times for all thermoplasts and thermosets were found to be always larger than for aluminium giving to the FRP a better fire resistance. This results can be attributed to an excellent fire resistance of resin to a high thermal stress and the benefit effect of the carbon fibres which allow a re-emission of the incident heat flux, then acting as a protective screen.

A composite ranking, based on the MLR evolution and the FIGRA parameter, shows that all material types are never burnthrough (4mm thick plate) in less than 15 minutes (the BT of aluminium is around 50s), then they satisfy the standard tests, showing a very good resistance to fire.

Moreover, thermoplasts are lighter than thermosets with a density of 0.95 instead of 1.2 (respectively 40% and 30% lighter than aluminium) and are potentially recyclable. These conclusions seem to indicate than thermoplastics present larger advantages for the future aircraft generation. But, thermoplastic resin being naturally in a solid state, it is much more difficult to impersonate reinforcing fibres. The resin must be heated to its melting point, and pressure is required to impregnate fibres. The composite must then be cooled under this pressure. This is complex and far different from traditional thermoset composite manufacturing. Special tooling, technique, and equipment must be used, many of which are expensive. This is, as well as the additional cost, the major disadvantages of thermoplastic composites.

About the safety point, the off-gasing of the composite degradation products must be considered in a global approach.

ACKNOWLEDGMENTS

This work is a part of the Project AircraftFire (contract 265612) funded under the European Union Framework 7 Transport initiative. The authors acknowledge the co-operation of their project partners in undertaking this work and in allowing the project findings to be published.

REFERENCES

1. Cherry, R., and K. Warren. 1999. Fuselage burnthrough protection for increased post-crash occupant survivability: safety benefits analysis based on past accidents. FAA Office of Aviation Research. Washington DC. DOT/FAA/AR-99/57.

2. Cherry, R. 2009. Burnthrough resistance of fuselage. EASA service contract number EASA 2008.C19. Prepared for: European Aviation Safety Agency.

3. Dodd, D.C., C.R. Jenkins, M A. Snell.1996. Burnthrough assessment study. CAA Paper 96002 Civil Aviation Authority. London.

4. Dodd, D.C., C.T.M. Hall, J. Pollard, M.A. Snell. 1994. Burnthrough resistance of fuselages: Initial findings. CAA paper 94002. London

5. Marker, T.R. 1999. Full-scale test evaluation of aircraft fuel fire burnthrough resistance improvements. FAA Office of Aviation Research. DOT/FAA/AR-98/52.

6. Marker, T.R. 2000. Development of improved flammability criteria for aircraft thermal acoustic insulation. Document Fire Safety Section AAR-422. FAA Office of Aviation Research. Washington DC.

7. Cahill, P. 1986. An investigation of the FAA vertical Bunsen burner flammability test method. FAA Office of Aviation Research. Washington DC. DOT/FAA/CT-8/22.

8. Lyon, R.E. 1997. Fire-resistant materials: research overview. FAA Office of Aviation Research. Washington DC. DOT/FAA/AR-97/99.

9, Horner, A. 2000. *Aircraft materials fire test handbook.* FAA Office of Aviation Research. Washington DC. DOT/FAA/AR-00/12.

10. Le Neve, S. 2010. Fire Behaviour of structural composite materials. In: *Proceedings of the* International Aircraft Fire and Cabin Safety Research.

11. Webster, H. 1994. Fuselage burnthrough from large exterior fuel fires. FAA Office of Aviation Research. Washington DC. DOT/FAA/CT-90/10.

12. B. Sundström Development of a European Fire Classification System for Building Products, Phd Thesis, Lund, 2007.

International Symposium on Sustainable Aviation 2018
4 – 6 June 2018
Rome, Italy

P3T3 NOX MODEL OF TURBOFAN ENGINE

Kateryna Synylo[1], Nicolas Duchene[2]
[1] Institute of Environmental Safety, National Aviation University, Kiev, Ukranie [2] VERIFAVIA, Paris, France
*Corresponding author e-mail: synyka@gmail.com

SUMMARY

Aircraft emissions are of concern due to the expansion of air traffic over the years (a mean annual rate of 5 to 7%) and their potential impact on air quality in local, regional and global scalses .

The airc raft emission inventory is usually calculated on the basis of certif icated engine emission indices, which are provided by the engine manufacturers and reported in ICAO engine emission database. Under real circumstances, however, these conditions may vary and deviations from the certificated emission indices may occur due t o impact such factors, as: the life expectancy (age) of an aircraft; the type of an engine installed on an aircraft; meteorological conditions .

The tasks reported in this paper consist in the validation and sensitivity analysis of the TURBOGAS advanced emission model to define some key parameters for the estimation of aircraft emission indexes under real operation conditions and to provide precise aircraft emissions inventories

Keywords: Aircraft, turbofan engine, thermodynamic analysis, efficiency, emission.

INTRODUCTION

Aircraft emissions are of concern due to the expansion of air traffic over the years (a mean annual rate of 5 to 7%) and their potential impact on air quality in local, regional and global environments (ICAO Environmental Report 2013; Enviro.2011]. Keeping in mind that some of the European hubs operate close to their maximal capacity (never mind operational or environmental), the transfer of the air traffic to other airports, with less intensive traffic, but usually closer to habitation areas, is likely to provoke a rise of concerns about their LAQ impact.

The analysis of emission inventories at major European (Frankfurt am Main, Heathrow, Zurich and etc.) and Ukrainian airports highlighted that aircraft are the dominant source of air pollution in most cases, with contributions to inventories higher than 50% of their total values in most of the airports [Fraport Environmental Statement 2014; Zaporozhets O., 1997].

The aircraft emission inventory is usually calculated on the basis of certificated engine emission (EE) indices, which are provided by the engine manufacturers and reported in ICAO EE database [ICAO. Doc. 9646, 1995].

The emission indices rely on well-defined measurement procedure and conditions during aircraft engine certification. Under real circumstances, however, these conditions may vary and deviations from the certificated emission indices may occur due to impact such factors, as:

- the life expectancy (age) of an aircraft – emission of an aircraft engine might vary significantly over the years (the average period – 30 years), usually aging aircraft/engine provides higher emission indices in comparison with same type compared to new ones;
- the type of an engine (or its specific modification, for example with different combustion chambers) installed on an aircraft, which can be different from an engine operated in an engine test bed (during certification);
- meteorological conditions – temperature, humidity and pressure of ambient air, which can be different for certification conditions.

The impacts of aviation emissions of NOx, PM, and other gaseous emissions need to be further assessed and understood [ICAO Environmental Report 2013]. In respect to this an assessment of aircraft emission indices under operating conditions, also including from measurements, is an actual task, which must provide more accurate emission inventory and to improve total LAQ modeling systems.

Analysis of emission measurement data for aircraft engine concluded that method, which takes into account the influence of the real operational (fuel flow rate, operation period of engine/age and its maintenance) and ambient temperature on emission indices, allows to get more precisely the results of emission inventory of the aircraft, their contribution to total inventory and local air quality analysis in airports.

The advanced emission model of turbofan engine (TURBOGAS emission model) was developed for estimating aircraft engine emissions taking into account the influence of operational factors and meteorological conditions to calculate aircraft emission inventories more robustly. Sensitivity analyses of the TURBOGAS advanced emission model were performed in order to identify the key parameters for the estimation of aircraft emission indexes under real operation conditions in an effort to improve aircraft emission inventories.

AIRCRAFT EMISSIONS METHODOLOGIES

Aircraft main engines have received a lot of attention in sector of aviation emissions as they are the dominant airport-related source [O.Zaporozhets, K.Sinilo, 2005].

There are various methodologies, to quantify aircraft emissions – each with a degree of accuracy and an inverse degree of uncertainty.

The purpose and need for quantifying aircraft emissions drive the level of accuracy needed in an inventory, which in turn, determines the appropriate approach. A secondary factor is data availability [ICAO. Doc. 9889, 2011].

Aircraft emission is function of following parameters [ICAO. Doc. 9889, 2011; SAE AIR 5715, 2009]:

$$Q = FF \quad EI \quad T \quad n, \qquad (1)$$

where *FF* – fuel flow rate, kg/s;
EI – emission index, g/kg;
T – time in mode, s;
n – number of aircraft engines.

Basic methodologies (ICAO. Doc. 9889, 2011; SAE AIR 5715, 2009) are used to find the two most parameters: the fuel flow rate and the emission factor or index (Tier 1 and Tier 2).

For presenting available methods to compute aircraft emissions of different pollutants, the Intergovernmental panel on Climate Change (IPCC) (SAE AIR 5715, 2009) used a tired approach based on level of accuracy and complexity, Tab.1.

Table 1

IPCC tier categorization

IPCC Tiers	Level of complexity	Level of accuracy	Example of this method
Tier 1	Low	Empirical	**ICAO**
Tier 2	Medium to High	Empirical	**BFFM2**
Tier 3	High	Modeled or measurement based	**P3T3**

The final tier (Tier 3), to which TURBOGAS belongs, represents the highest level of complexity. The results generated by this method are considered to be the “most accurate” (SAE AIR 5715, 2009). The drawback comes from the amount of data required, some of which are not in the public domain or are difficult to obtain, as it will be shown in a later section. The computational procedure is also more intensive, so it will take longer to generate the results as compared to the other two methods. An example of this tier is the P3T3 method.

Both BFFM2 and P3T3 methods have been implemented in the TURBOGAS emission model [S. Aloysius, L. Wrobel, 2010; Synylo, K., Duchene, N., 2014].

The model estimates values for P3, T3 and FAR before completing the P3T3 model and providing an estimate for NOx emissions.

A NOx emissions rate is calculated based on the standard P3T3 formula presented in SAE AIR 5715. This emissions index is then converted into an emissions value by multiplying the g/kg value by the fuel flow (kg/s) for each segment.

One of the requirements of the P3T3 is the fuel-air-ratio. Establishing this ratio is in most models calculated by attempting an energy balance across the burner. However, because fuel flow is an explicit input for the TURBOGASTURBOGAS tool, this can be completed by establishing the mass of air required to achieve stoichiometric combustion. During optimum flight conditions, this is a reasonable assumption. Assuming a mean fuel composition of 13.84% hydrogen by mass, this results in an emission index of 3.15 for CO_2 and 1.25 for H_2O (which is the value implemented in the EU Emission Trade System for aviation). Subsequently, each 1 unit of fuel requires 3.4 units of oxygen for complete combustion.

SENSITIVITY STUDIES FOR ENGINE FJ44-3A

Sensitivity analyses were performed for TURBOGAS model for engine FJ44-3A on the ground of ANP flight profile for a Citation 3 for following two points:

- **Point №1**:
  - Fuel flow, FF = 0.153573523 kg/s;
  - Altitude, m = 457.2
  - Mach number = 0.23044085
  - Thrust, kN = 8.8442306
  - Air temperature, T_A = 284.19K;
  - Air humidity, H = 60%;
  - Atmospheric Pressure, Pa = 942.1mbar
- **Point №2:**
  - Fuel flow, FF = 0.1272584 kg/s;
  - Altitude, m =3048.00
  - Mach number = 0.44015261
  - Thrust, kN = 7.63414211
  - Air temperature, T_A = 268.34K;
  - Air humidity, H = 60%;
  - Atmospheric Pressure, Pa = 696.80mbar

The aim of sensitivity studies was to investigate the changes in output (EINOx) caused by variation of input data. The following parameters are studied, with step-wise variations of 2, 5 and 10%: fuel flow,

temperature, pressure, Mach number and thrust.

Obtained results of the sensitivity tests are collected in following tables correspondingly for Point 1 and Point 2.

Table 2

Results from sensitivity studies for the FJ44-3A (point 1)

Parameter	Range of parameter	Range of NOx (+/-% mean)
Ambient temperature	11.2ºC to 39.6ºC	30.70%
Ambient pressure	942.1 mbar to 1036.3	4.84%
Ambient relative humidity	60.0% to 66%	1%

Table 3:

Results from sensitivity studies for the FJ44-3A (point2)

Parameter	Range of parameter	Range of NOx (+/-% mean)
Ambient temperature	-4.7ºC to 22.17ºC	12.70%
Ambient pressure	696.80 mbar to 766.48	4.30%
Ambient relative humidity	60.0% to 66%	0.5%

The results of TURBOGAS model sensitivity and found dependence of EI NOx on ambient conditions (temperature, humidity and pressure) is represented on the plot 1 for cases taken into consideration.

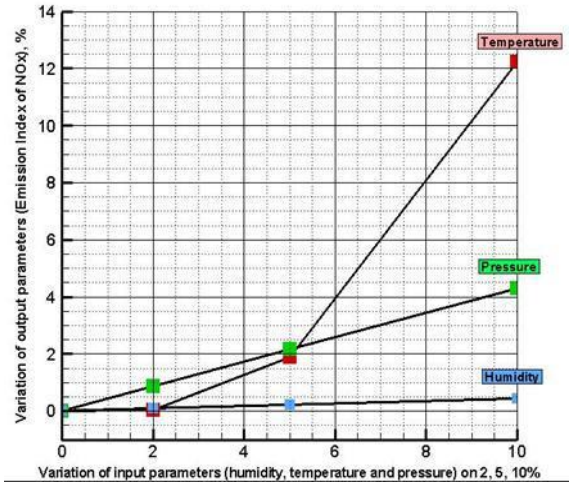

a)

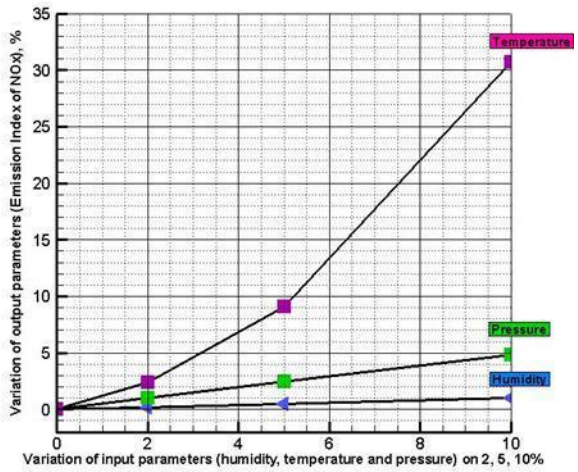

b)

Figure1. EINOX variability vs input parameters for FJ44-3A (a-point №1, b-point №2)

On the ground of the results obtained for two points and of the comparison of the resulting differences it can be concluded that the TURBOGAS model (P3T3 method) is not highly sensitive to air pressure and humidity. That is because the changes of these parameters input by 2% lead to variations of calculated EI NOX lower than 2%. Likewise, the changes of input parameters by 5% implied variations lower than 5%.

The analysis of the implemented tests showed, that the TURBOGAS model is sensitive to ambient temperature. Based on obtained results, it was found a dependence of a sensitivity level of model on altitude. As, it was observed, on altitude 457.2 m (first point, figure1/a) ambient temperature change on 10% leads to an increase in EI NOX of 12%, while on altitude 3048.0 m (second point, figure2/b) – 30.7%.

In addition, on the ground of investigation was found, that the TURBOGAS model (P3T3 method) is not sensitive to operational conditions at all: fuel flow, Mach number and thrust.

Coclusions

Sensitivity analyses were performed for TURBOGAS model for engine FJ44-3A on the ground of ANP flight profile for two points.

According to calculation results by Turbogas model, the ambient atmosphere conditions (air temperature, pressure and humidity) have a an impact on the $EINO_X$. In particular the sensitivity analysis showed that the model is highly sensitive to ambient temperature (1.5 to 2% increase in $EINO_X$ per 1 degree C), which was in accordance with literature on the topic.

In addition, on the ground of investigation was found, that the TURBOGAS model (P3T3

method) is not sensitive to operational conditions at all: fuel flow, Mach number and thrust.

References

1. ICAO Environmental Report 2013. Aviation and Climate Change. – 2012 p. // http://cfapp.icao.int/Environmental-Report-2013.
2. Enviro.2011 [online] http://www.enviro.aero/Content/Upload/File/BeginnersGuide_Biofuels_Web>.
3. Fraport Environmental Statement 2014 Including the Environmental Program until 2017. – Fraport AG, 2015. – 24–30 p.
4. Zaporozhets O., Strakholes V., Tokarev V.I. Estimation of emissions and concentration of air pollutants inside the airport // State and perspective of activities on environment protection in civil aviation – Moscow: GosNIGA, 1991. – P. 18–20 (in Russian).
5. ICAO data bank of aircraft engine emissions. – Montreal: ICAO. Doc. 9646 - AN/943, 1995. – 152 p.
6. Synylo K. Aircraft emission estimation under operational conditions in the airport area // Proceedings of the NAU, vol. 62, No 1, 2015 – P. 70-79.
7. Airport Air Quality Guidance Manual. – Montreal: ICAO. Doc. 9889, 201107. – 114 pg.
8. SAE, Procedure for the Calculation of Aircraft Emissions. SAE Committee A-21, Report SAE AIR 5715, 2009
9. S. Aloysius, L. Wrobel, Deliverable D2 – Definition and Justification Document, CS-GA-2009-255674-TURBOGAS – TURBOGAS, 2010.
10. Synylo, K., Duchene, N., 2014 NOx emission model of turbofan engine, International Journal of Sustainable Aviation, Vol.1. – P. 72–84

International Symposium on Sustainable Aviation 2018
9 – 11 July 2018
Rome, Italy

ISSA-2018-032

A COMPARATIVE CFD STUDY OF CENTRIFUGAL PUMP WITH COMMERCIAL AND OPEN-SOURCE FLOW SOLVERS

Osman Babayigit[1], Saim Kocak[2], Kursad Melih Guleren[3] [1]Selcuk University, Hadim Vocational School, TURKEY, sbabayigit@selcuk.edu.tr [2]Selcuk University, Faculty of Engineering, TURKEY, skocak@selcuk.edu.tr [3]Anadolu University, Faculty of Aeronautics and Astronautics, TURKEY, kmguleren@anadolu.edu.tr

SUMMARY

In the present study, numerical results of a multi -stage c entrifugal pump are compared with the experimental ones using commercial ANSYS/Fluent and open source OpenFOAM flow solvers .
ANSYS/Fluent and CFX software will be used as commercial flow solvers and OpenFOAM for the open source solver. For the closure of the governing equations, k -w SST and DES turbulence model will be used with employing sliding mesh technique. It is expected that the prediction performance and computer cost of these two solvers will be reve aled.

Keywords: Centrifugal Pump, Numerical Analysis, Fluent, OpenFOAM

INTRODUCTION

Pumping systems are widely used in many industrial areas. It is of great importance to increase the efficiency of pumping systems where approximately 20% of the world's electricity consumption is occurred (Kaya et al. (2008)). Centrifugal pumps constitute a significant part of the pumping systems. In order to provide the efficiency of the centrifugal pumps at the highest possible level, the flow in the pumps should be solved numerically and thereafter new designs, where the abnormal flow structures are eliminated, can be offered.

There are many options to solve the flow in the centrifugal pumps, including commercial programs or open source codes. It is deduced from the literature that ANSYS/Fluent and CFX are mostly used as commercial software. Nevertheless, in recent years, the use of open source codes has accelerated significantly. Because of the cost of commercial software in particular, the use of open source flow solvers is of great importance in these days.

PROBLEM STATEMENT

In the present study, numerical results of a multi-stage centrifugal pump are compared with the experimental ones using commercial and open source flow solvers. One of the important parameters that affects the efficiency of multi-stage pumps is the volumetric efficiency. To minimize the losses due to the internal leakage, the pump must be designed so that the clearance between the pump elements is minimum during assembly installation. CFD validation in this context requires the inclusion of leakage losses in the numerical analysis (Stel et al., 2015, Ayad et al. ,2015). To decrease the axial loads on bearings, balancing holes are applied on the impeller. This increase the leakage losses and adversely affects the total efficiency. The pump geometry becomes more complex with these balancing holes and the creation of the computational mesh is getting very difficult and tedious. A demounted view of the solid model and the clearances on a partial cross section of one stage of the pump are seen in Figure 1.

Both the inclusion of leakage-losses and balancing holes in the numerical analysis with the use of open source flow solver is the focus of this study. Additionally, long term plans on the sensibility features of the codes will be made.

METHODOLOGY

Numerical analyses in this study are performed via a workstation of two Intel Xeon X5650 of 6 cores each, 2.66 GHz speed, 12 MB Cache. It has 96 GB memory of 1333 MHz DDR3 RAM and 2 GB GDDR5 GPU NVIDIA Quadro 4000.

An example of mesh structure used for the solution of flow problems are seen in Figure 2. The mesh has approximately 17 million computational cells with a maximum skewness factor of 0.92.

ANSYS/Fluent and CFX software will be used as commercial flow solvers and OpenFOAM for the open source solver. For the closure of the governing equations, k-w SST and DES turbulence model will be used with employing sliding mesh technique. These predictions will be compared to the ones of the standard k-e turbulence model with frozen mesh technique (Babayigit et al., 2017). Boundary conditions are reported in Table 1.

RESULTS

The total efficiency at design mass flow rate is found as 51.98 % and 51.02 % for ANSYS/Fluent and CFX. The experimental data indicates 51.42 % efficiency. Therefore, CFD analyses with including of balancing holes improves the efficiency prediction quite significantly (Babayigit, 2017)).

Relative velocity vectors and contours are seen on a cross-sectional view of the two-stage centrifugal pump with balancing holes are seen in Figure 3. The flow inside the balancing holes and gaps are captured in detail.

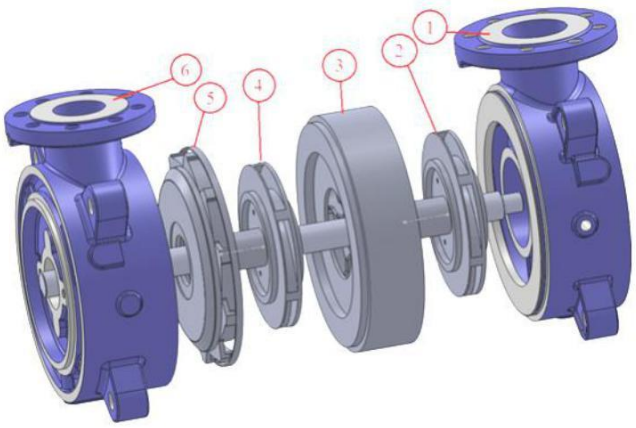

1- suction side 2- first impeller 3- first diffuser
4- second impeller 5- second diffuser 6- discharge side
(a)

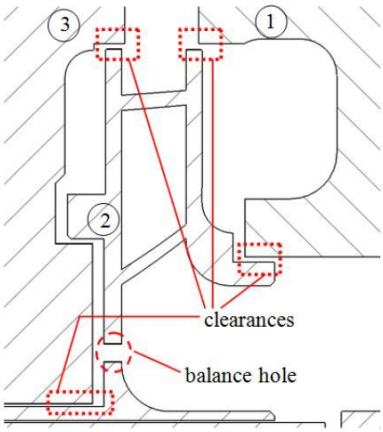

1-suction side 2-impeller 3- diffuser
(b)

Figure 1: Demounted solid model of the pump and clearances on a partial cross section view of one stage of the pump

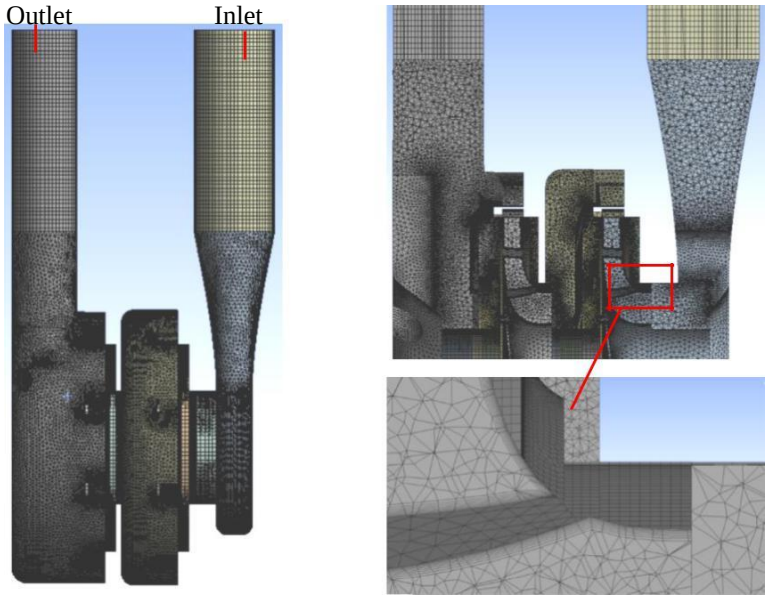

Figure 2: An example mesh structures of the fluid domain of the pump

Table 1: Boundary conditions used for CFD analyses

Boundary Type	Inlet	Outlet	Blades, hub and shroud	Impeller walls	Other walls
Constant mass flow rate (kg/s)	4.51/24.05	-	-	-	-
Turbulent Intensity (%)	3.5	5	-	-	-
Hydraulic diameter (mm)	80	65	-	-	-
Static Pressure (kPa)	-	700/1000	-	-	-
Surface Roughness (mm)	-	-	0.035	0.035	0.035
Roughness Constant	-	-	0.5	0.5	0.5
Rotational speed (rpm)	-	-	0	2950	-

REFERENCES

Ayad, F., Abdalla, H.M., Abou El-Azm Aly A., 2015, Effect of semi-open impeller side clearance on the centrifugal pump performance using CFD, Aerosp. Sci. Technol., 47, 247–255.

Babayigit, O., Ozgoren, M., Aksoy, M. H. ve Kocaaslan, O., 2017, Experimental and CFD investigation of a multistage centrifugal pump including leakages and balance holes, Desalination and Water Treatment, 67 28-40.

Babayigit O., 2017, Investigation of the performance effect of multiple impeller parameters of a centrifugal pump, PhD Thesis, Selcuk University Institute of Science and Technology, In Turkish

Kaya, D., Yagmur, E. A. , Yigit, K. S., Kilic, F. C. , Eren A. S. and Celik, C., 2008, Energy efficiency in pumps, Energ. Convers. Manage., 49, 1662–1673.

Stel, H., Sirino, T., Ponce, F.J. , Chiva, S. , Morales, R.E.M., 2015, Numerical investigation of the flow in a multistage electric submersible pump, J. Pet. Sci. Eng., 136, 41–54.

International Symposium on Sustainable Aviation 2018
9 – 11 July 2019
Rome, Italy

ISSA-2018-034

VISUAL DETECTABILITY STUDY OVER DIFFERENT LOW ALTITUDE UAV TYPES, ORNICAMOUFLAGE ON AIR

Emre ÖZBEK[1], Yasin ŞÖHRET[2], T. Hikmet KARAKOÇ[3]

[1] Eskisehir Technical University, Graduate School of Sciences, Eskisehir, Turkey, [2] Suleyman Demirel University, School of Civil Aviation, Isparta, Turkey

[3] Eskisehir Technical University, Faculty of Aeronautics and Astronautics, Eskisehir, Turkey

[1]emreozbek@eskisehir.edu.tr, [2]yasinsohret@sdu.edu.tr, [3]hkarakoc@eskisehir.edu.tr

SUMMARY

Unmanned aerial vehicles are a research field that is currently being worked on for both civilian and military applications . Anti -UAV systems are also an emerging field of research as a m easure of unwanted UAV activity . Low altitude surveillance mission UAV's and low altitude special operation UAV's are the most endangered UAV types against the Anti -UAV weapons . The usage of man held anti UAV weapons depend on UAV detecting with an eye. In this study, different low altitude UAV types from the literature are examined on their detectability characteristics with a bird spotting approach. Visual detectability and noise detectability are examined separately . Unmanned aerial vehicles with station ary wings and rotating wings have their own detectability characteristics . In this paper, an unusual unmanned aerial vehicle type that can fly by flapping motion is also examined by noise and visual detectability . Also, a proposal and mission model were ma de on ornithopter usage for low altitude surveillance and special operations .

Keywords: UAV, Ornithopter, Visibility, Detection, Anti-UAV

INTRODUCTION

Unmanned aerial vehicles are a research field that is currently being worked on for both civilian and military applications. Anti-UAV systems are also an emerging field of research as a measure of unwanted UAV activity. Low altitude surveillance mission UAV's and low altitude special operation UAV's are the most endangered UAV types against the Anti-UAV weapons. The usage of man held anti UAV weapons depend on UAV detecting with an eye. In this study, different low altitude.

UAV with rotary wings tend to have little wind tendency, thus they fly in low altitude on almost every flight mission. Rotary wing UAV's have many types vary on the number of motors. Bicopter with two motors, tricopter with three motors, X4 with four arms and four motors, X8 with four arms and eight motors, hexacopter with six motors and octocopter with eight motors, all these types have one thing similar, noise and easy detectability. The noise from rotary wing UAVs is a result of multi propeller usage.

UAV with fixed wings also have many types vary on shape, weight, altitude, endurance and engine type. As for shape, there are tailless delta UAVs, conventional UAVs, biplane UAVs and canard UAVs. All these types have one thing in common, fixed wings. Fixed wings are easy to detect visually during flight missions on low altitude. Engine type is another matter of classification. There are electric engines, piston engines, gas turbine engines and ducted fan engines. All of these types have a thing in common, they rotate a shaft. It is propeller shaft for electric engines, piston engines and ducted fans, compressor shaft for gas turbine engine. The three with propellers cause noise due to RPM of propellers and propelled air. The UAV with gas turbines also causes immense noise due to acoustic resonance, vibration resonance and turbulence due to poor exhaust circuit design. Thus, all types of fixed wings are easy to detect due to noise their propulsion systems and fixed wings.

UAV with an inflatable body has been used for almost 140 years since the balloon strike on Venice is considered as first UAV operation in history. Airships are a type of aircraft which flies with both aerostatic and aerodynamic principles. Although they manage to fly silently, they are very easy to detect by any means of visual detection.

ORNITHOPTERS AND MEANING OF ORNICAMOUFLAGE

Ornithopter defines an aircraft with the ability of active articulating, the ability to flap wings. The first examples of such aircraft date back to notes of great Renaissance artist and engineer Leonardo da Vinci (Figure 1). Although his design was a manned ornithopter, manned ornithopters are not a feasible study in these days. On the other hand, unmanned ornithopters are a trending research area. Flying both by wing flapping and gliding is a very resourceful type of flight operation. Flapping wings grant high maneuverability and gliding flight makes the flight efficient in terms of energy.

Fig. 1. Manned ornithopter of Leonardo da Vinci

Ornithopter design studies are divided into two sub research areas. These areas are ornithopters with bird inspired designs and ornithopters with fly or bug inspired designs. The increase in research and development in micro electrical mechanical systems have made bug inspired designs viable. Micro-sized controllers, servos and motors are feasible for research studies (Figure 2). The increase of developments in micro electrical mechanical systems decrease the component weights. Bug-fly inspired ornithopter design will be a trend research topic for some years due to development in these areas.

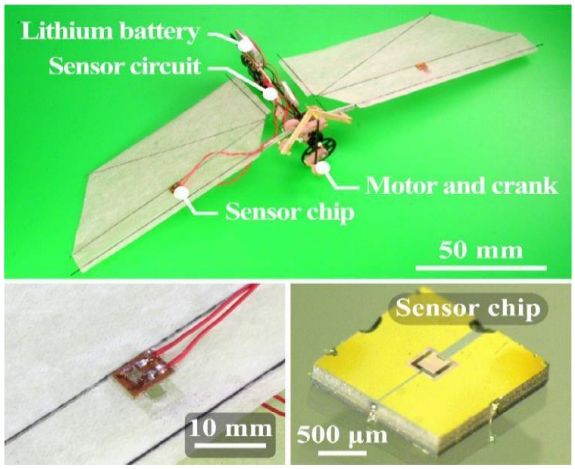

Fig. 2. MEMS on a bug inspired ornithopter

(ioppublishing, 2018)

The bug-fly inspired ornithopters are very small in size and have membrane wings such as the animals which were their design starting point (Figure 3). Although they are not as small as the real ones. Their sizes are on a decreasing trend. These technologies are meant to be used in spying missions and search and rescue missions particularly. Their little size provides a difficulty on eye detection. The noise detection is also difficult in open areas. However there bug-fly inspired ornithopters have problems with outdoor flight. Their speed is very low and they are hard to control at even very little wind speeds such as 3 m/s. This feature restricts their field of usage with indoor operations.

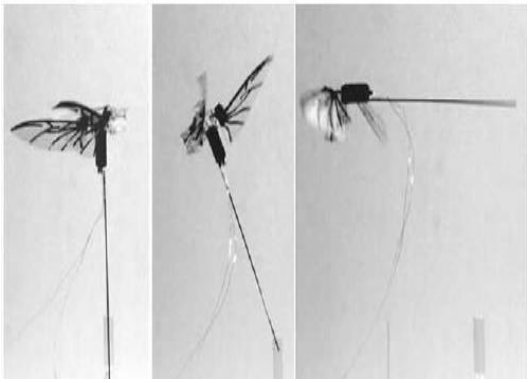

Fig. 3. Beetle inspired Ornithopter (Phan, H. V. et al., 2012)

It is also important to note that ornithopter also has the advantage of vertical take-off and landing. All the nature's avians have this trait and they manage to take off vertically with flapping their wings. Since the UAVs with vertical take-off landing (VTOL) is a trend research topic, it is favorable to note that this feature is available for flapping flight.

The bird inspired ornithopter design is the second sub research area of ornithopter design. The source of inspiration is a bird rather than a fly or bug in these researches. In these designs, the bio-inspired ornithopter sizes are almost equal to real birds.

There are 10404 known bird species living on earth. Which means there is a lot of source for bio-inspired ornithopter designs out there. Since there is no common way to design a bio-inspired ornithopter, the similarity between the bird and the ornithopter is a choice of designer to make. Bird species even vary in weight, wingspan and length in same species due to their breeding or gender.

Bats are also a trending topic for avian flight and bio-inspired ornithopter design. Bat-bot is a successful example of such designs (Figure 4). Although they are mammals, their flight characteristics are as successful as birds. Bats' have membrane wings rather than bird wings with feathers which are easier to imitate.

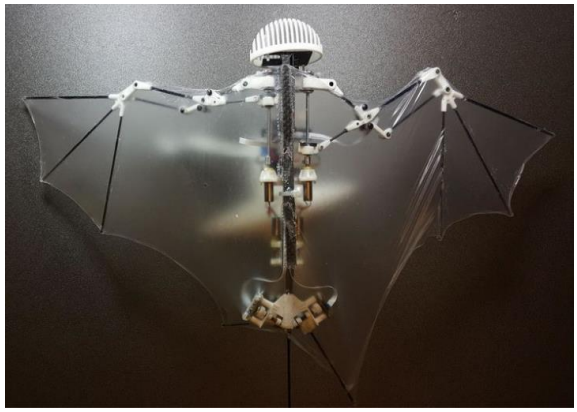

Fig. 4**.** Bat-Bot – Bat inspired ornithopter (Ramezani et al 2017)

As for the size, the ability to glide is another difference between two sub research areas. Gliding requires a rigid wing with the ability to lock at glide position. Birds can glide, and their gliding method studied using wind tunnels (Figure 5). Gliding is an effortless type of flight. Birds of prey glide while they search the area for their prey. Gliding decreases the birds' energy consumption in overall flight and increases its endurance. The same feature and results are also viable for bird inspired ornithopter designs.

Fig. 5. Jackdaw in a windtunnel (Lund University)

Bird inspired ornithopters share the size, gliding method and articulation with their inspiration source, real birds. The only difference is the aesthetics they have. Feathers of birds have not been successfully imitated yet. But the ornithopter wings could be painted such as the real ones. Fuselage shapes are also easy to imitate with additive manufacturing techniques available and feasible for some years.

With researches on this topic, the flight kinematics will be able to imitate bird articulation successfully. Composite technology is also a developing field of research. With composites, it is feasible to build stiff and light structures which are being used as ornithopter body frames (Figure 6). Additive manufacturing is also an important production method which eases the prototyping time and expenditure.

Fig. 6. Aerotrix (NSSCI)

The developments in MEMS technology is also beneficial for bird inspired ornithopter designs. The size of batteries, electronic speed controllers, receivers, flight cameras, servos and datalink transmitters provide great an amount of lightning. In a platform works against gravitational force, lightening means less effort to stay airborne. Thus, these developments in MEMS, increases flight performance, flight endurance and payload capacity.

Ornicamouflage is a term defines the camouflage attribute of ornithopters. Common bird spotting methods include watching the birds flying characteristics and listening to their singing and there are many books and guides written in this issue. Common bird spotting methods include watching the birds flying characteristics and listening to their singing. There are many published books and guides written on this issue. Therefore, the look, articulation and noise are very important on spotting (Figure 7).

Fig. 7. African eagle spotting guide

The look similarity is a matter of paint job and aesthetics. Could be improved in quality with improving additive manufacturing techniques. Articulation is related with studies over bird flight kinematics. Noise during flapping flight is at normal bird levels since bird inspired ornithopters are outdoor UAVs. The use of image processing on UAV detection is a trending topic due to research on anti UAV measures. The common image processing algorithm depends on a database of UAVs and airplanes. These pictures archives usually contain multirotor rotary wing UAVs and fixed-wing UAVs with different types. As an addition to visual detection, the detection methods with image processing are also not very useful for detecting ornithopters. Thus, Ornicamouflage term includes, visual detection, noise detection and detection with image processing.

CONCLUSIONS

Ornithopters with bird inspired designs have great advantages over traditional UAV types such as Fixed Wing UAVs and Rotary Wing Multirotor UAVs. Bird inspired designs to have advantages of high maneuverability and ability to perform gliding flight. They also have the advantage of Ornicamouflage. Bird inspired ornithopter UAV designs are harder to detect since they can articulate like a bird, painted like a bird and fly super silent. The ornithopter related researches will increase with the developments in micro electrical mechanical structures, additive manufacturing and composite technologies. It is expected to see many products for both civilian and military applications of

bio-inspired ornithopters in both fly and bird categories.

REFERENCES

H. V. Phan, Q. V. Nguyen, Q. T. Truong, T. V. Truong, H. C. Park, N. S. Goo, D. Byun, M. J. Kim, ''Stable Vertical Takeoff of an Insect-Mimicking Flapping-Wing System Without Guide Implementing Inherent Pitching Stability'', Journal of Bionic Engineering, Volume 9, Issue 4, 2012, Pages 391-401

A. Ramezani, S. Chung and S. Hutchinson, ''A biomimetic robotic platform to study flight specializations of bats'', Science Robotics 01 Feb 2017: Vol. 2, Issue 3, eaal2505

Lund University, Animal Flight Lab, https://www.biology.lu.se/research/research-groups/animal-flight-lab/research/gliding-flight-in-birds

IOP Asia-Pacific - Institute of Physics

NSSC – Aerotrix – Workshops - http://2016.nssc.in/Workshops/ accessed on 12.06.2018

In Depth Tutorials - http://what-when-how.com/birds/african-fish-eagle-birds/ accessed on 14.06.2018

Cornell University – Clement's List - http://www.birds.cornell.edu/clementschecklist/2014-overview/ accessed on 10.06.2018

Aeroecoustics, https://aercoustics.com/noise-vibration-gas-turbine-cogeneration-power-plants/ accessed on 9.06.2018

ISSA-2018-035

EFFECTS OF ADDITIVE MANUFACTURING METHODS ON BIO-INSPIRED UAV STRUCTURES

Emre ÖZBEK[1], Yasin ŞÖHRET[2], I. Yavuz DAL[3], T. Hikmet KARAKOÇ[4]
[1,3] Eskisehir Technical University, Graduate School of Sciences, Eskisehir, Turkey,
[2] Suleyman Demirel University, School of Civil Aviation, Isparta, Turkey
[4] Eskisehir Technical University, Faculty of Aeronautics and Astronautics, Eskisehir, Turkey
[1]emreozbek@eskisehir.edu.tr, [2]yasinsohret@sdu.edu.tr, [3]ydal@eskisehir.edu.tr, [4]hkarakoc@eskisehir.edu.tr

SUMMARY

UAV's are a trending field that is currently being researched throughout the world. Mini and micro type UAV's are the most feasible research platforms due to their size and ease of the feasibility of their components . Bio - inspired design techniques such as scaling and full simulation are easy to apply on mini UAVs due to their size similarity between the real birds . Especially the daytime predators such as eagles, buzzards and falcons are suitable because of their sta ll and cruise speed, glide performance, payload capacity and weight . In this study, the key metrics of airfoil determination for bio -inspired mini UAV designs were studied. Wing sections from different birds were also inv estigated. Airfoil recommendations for bio -inspired the mini UAV design projects were presented with an analysis applied on airfoils which comply with design requirements . Selig - Donovan's S1223 airfoil was proposed for applications with the high lift requirement . In applications which deman d an ease of manufacture, Eppler's E423 airfoil was proposed. Royal Airforce's RAF 19 airfoil was also recommended for the mini UAV's designs which require ease in control . This study defines airfoil requirements for mini UAV airfoil selection process and will provide useful information for UAV designers for their conceptual design phase.

Keywords: Bio- UAV, Design Inspiration, Airfoil, Mini UAV

INTRODUCTION

Unmanned Aircraft Systems are a trending research area throughout the world since last twenty years. Evolving technology has made it possible to make electronic systems smaller, lighter and cheaper. These developments boosted mini and micro-sized UAV designs and applications. Mini and micro-sized UAV's are easy to relate to a real bird or fly.

Thus, increasing involvement in mini and micro-sized UAV's also increased interest in the Bio-Inspired design area. Bio-Inspired structures are not easy to grasp and also hard to produce with all the details. The composite technology can't offer these details even with a high-quality mold in mini and micro UAV scale. Another technology can produce these structures with all details is Additive manufacturing. Additive manufacturing is a general term to refer to technologies include layer by layer method. Additive manufacturing method produces structures layer by layer by joining of liquid, powder or sheet materials as opposed to traditional like milling which are subtractive.

ADDITIVE MANUFACTURING AND 3D PRINTERS

Additive manufacturing method is a method uses molten thermoplastics to form an object throughout a predefined gcode. A gcode is a code that implies the machine's step motors the coordinates of nozzle. The nozzle is where the thermoplastic filament melted and poured onto heatbed.

Heatbeds are used to make sure the first layers of 3D printed object are stay immobile during the addition of upper layers. If the first layer moves during the print process, the printed object won't be same with the solid model.

The additive manufacture method requires both support and material filaments. Although support filament could be same with the material filament, the support layers usually have a grid zig-zac structure to be cleared easily. Support structure is essential for 3D printing due to gaps in X,Y or Z coordinates. Support structure fills these gaps to ensure upper layers won't fall apart (Figure 1).

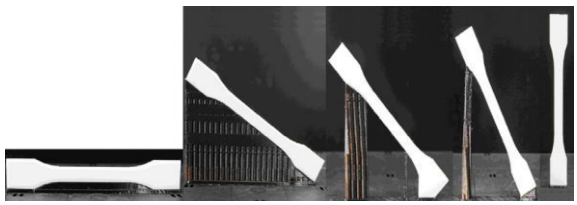

Fig.1. Support structure (Zou et al., 2016).

Materials of 3D printers are an emerging field of study. ABS Polymer is one of the prior materials. It has 40 Mpa ultimate strength, 98°C operational temperature and 1.04 g/cm³ density. ABS polymer is a stiff material but also a dense one. The UAV parts printed with ABS polymer tend to be heavy which makes it only a good choice for joints and other apparatus.

PLA is the material which is easiest to print. Civil and hobby use printers usually print with PLA. PLA has very low durability and maximum service temperature which is 52 °C. PLA has 1.24 g/cm³ density which is higher than the ABS polymer.

Nylon and PetG materials are very durable materials. They are easy to print but pricier than PLA and ABS. Their maximum operating temperature is over 70 °C. The flexible material is also a viable option when it comes to UAV structures. Although it is not very feasible or easy to print, it has very high durability.

There are many other 3D printer material filament options such as Carbon Fiber Filled, ASA,

Polycarbonate, Polypropylene, Metal Filled and Wood Filled. But these options are not very feasible because some of them require special printers and the others are very expensive.

Printing options are also important in the matter of print quality. These options are defined during the procedure of transforming the solid model into gcode. A freeware called as Cura, performs this job very efficiently. Infill density is by far the most important selection during the UAV part printing. Infill density is a parameter change 0 to 100. It defines the amount of material inside printing object walls. A low selection of infill density such as 10% will result with a light but fragile object. A higher selection such as %80 will result with a stiff but heavy object. Figure 3 shows the effect of infill density.

Fig. 2. Filament types

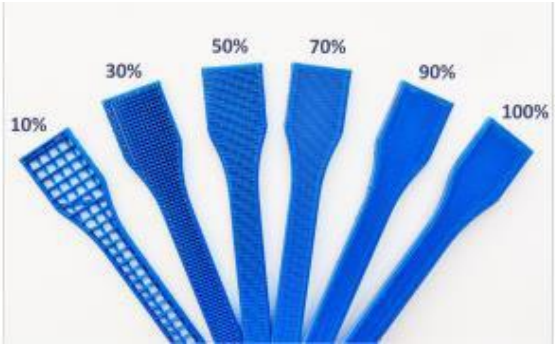

Fig. 3 Effects of infill density

3D printers also vary as machines. There are home use printers which are feasible for hobbyists and there are bigger classes which are more professional. These classes are called prototype class and production class.

The hobbyist printers are cheap, open bed, open filament and usually has SD card sockets for importing gcodes. These printers are faulty. The fault reasons could be step motors, heatbed, sensors or extrusion mechanism. Requires user attention and repairing from time to time.

Prototype class printers usually have double extruders and model material and support material separated. These printers have closed production area, closed filament, can clear its nozzle autonomously and connect wifi for importing gcode. These printers require less attention and can print very detailed objects with very high precision.

Production type printers are designed to print objects with high precision in production lines. Such as car parts, aircraft parts, UAV parts. These printers have the most advanced extrusion systems.

ADDITIVE MANUFACTURING ON UAV APPLICATIONS

UAV technology is an emerging field of science. UAV design and production are a low resource demanding area of work. Thus, many scientists from all around the globe studies UAV related topics. Unmanned Aerial Systems has many subtopics such as rotary wing multirotor UAVs, fixed-wing UAVs, lighter than air inflatable UAVs and bio-inspired ornithopter UAVs.

Mini and micro class UAVs weigh around 500 g to 2500 g. These little sizes require special structural concepts. Structural concepts such as modular designs, special joints and assembly apparatus. These kinds of mini structures require special construction methods. Additive manufacturing brings great improvement in the production of both structural components (figure 4).and joints (figure 5).

Fig. 4. Drone with 3d printed structure

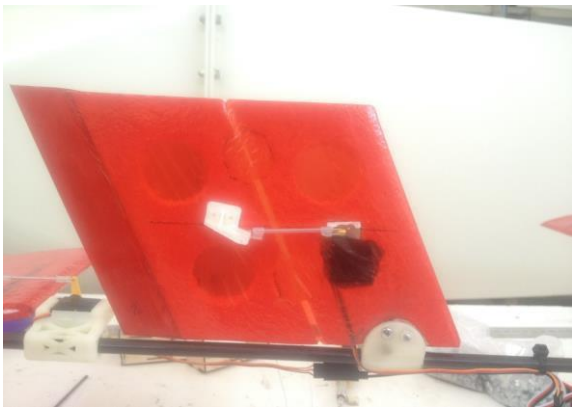

Fig. 5. 3D Printed joints and apparatus

In the production of complex structures such as motor mounts, drone arms and drone landing pods 3D printers offer rapid production and precision. Also, in fixed-wing UAV production, complex

structures need precision such as tail assembly mounts, wing assembly mounts could be produced with design incidence angle.

BIO-INSPIRED DESIGNS AND ADDITIVE MANUFACTURING

The bio-inspired designs are trending due to wing flapping mechanisms and air camouflage. Flapping flight results in high maneuverability and silent flight. Noise emission has been a big problem for aircrafts. Flapping flight induces little noise due to gear mechanisms which are adequate for outdoor flight.

Bio-inspired structures are complex, hard to design and even harder to produce. A bird body inspired fuselage design is time-consuming and hard to construct due to its complex slopes.

Traditional prototyping methods such as laser cutting and hot wire can't keep up with these details. The composite technology can be applied in such structures but the mold making is a costly and time-consuming process.

Additive manufacturing technique solves the problem by high precision layer by layer production. Detailed parts like bird body shaped fuselages (Figure 6), feathers (Figure 7) and beaks could be printed with 3D Printers.

Fig. 6. 3D printed bird body

Fig. 7. 3D printed bird feathers

Drive systems between the electric motor and wing spars are also a very crucial system for bio-inspired ornithopters. The drive system components should be light and precise. Additive manufacturing technology offers rapid and feasible construction of these components (Figure 8).

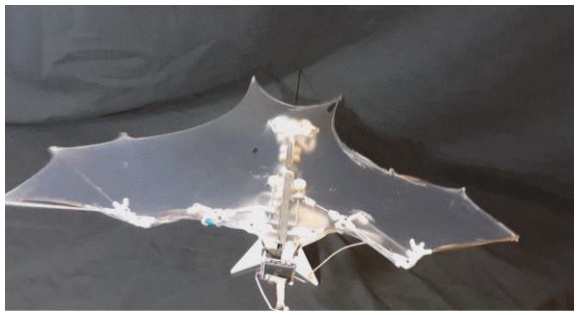

Fig. 8. 3d printed bat joints

CONCLUSIONS

Addictive manufacturing technologies offer great momentum on the development of bio inspired ornithopters and other bio inspired unmanned aerial vehicles. Addictive manufacturing provides rapid prototyping, precise structures and a plenty of material to choose from. Since each material has their own characteristic parameters, the material selection of 3D printed parts should be added to the UAV design system engineering chart. The usage of additive manufacturing techniques in the design of bio-inspired UAV projects may ease the process and provide more successful systems. UAV and additive manufacturing technologies are both emerging and will provide mutual benefits during their development.

REFERENCES

Z. Rui, X. Yang, L. Shiyi, P. Hu, W. Hou, Q. Hu, C. Shan, ''Isotropic and anisotropic elasticity and yielding of 3D printed material'', June 2016Composites Part B Engineering 99

https://3dprinting-blog.com/tag/3d-printer-materials/ accessed on 12.5.2018.

G.D. Goh, S. Agarwala, G.L. Goh, V. Dikshit, S.L. Sing, W.Y. Yeong, ''Additive manufacturing in unmanned aerial vehicles (UAVs): Challenges and potential'', Aerospace Science and Technology, Volume 63, 2017, 140-151

http://my3dmatter.com/influence-infill-layer-height-pattern/ accessed on 5.5.2018.

https://colorfabb.com/media/wysiwyg/colorfabb_catalogue/files/assets/common/downloads/final_export_digitaal_3.pdf accessed on 12.5.2018.

Kimerius, Airplane Turbofan Engine A. Ramezani, S. Chung and S. Hutchinson, ''A biomimetic robotic platform to study flight specializations of bats'', Science Robotics 01 Feb 2017: Vol. 2, Issue 3, eaal2505

http://www.ipfl.co.uk/icarus-had-a-sister/ accessed on 15.5.2018

A. Brentjes and H. Hoeijmakers. "Experimental Investigation into Wake Flapping Wing Robotic Bird", 35th AIAA Applied Aerodynamics Conference, AIAA AVIATION Forum, (AIAA 2017-3409)

International Symposium on Sustainable Aviation 2018
9 – 11 July 2018
Rome, Italy

ISSA-2018-036

COMPARATIVE LIFE CYCLE ASSESSMENTS OF AIRBUS A330 AND A350 TO ASSESS ENVIRONMENTAL IMPACTS AND SUGGEST OPTIONS FOR IMPROVEMENT

Asad Parkar and Gera Troisi
Department of Mechanical and Aerospace Engineering, College of Engineering, Design & Physical Sciences,
Brunel University London, Kingston Lane, Uxbridge, London, UB8 3PH
Email: 1443085@brunel.ac.uk & gera.troisi@brunel.ac.uk

SUMMARY

Life cycle assessment is used to assess the environmental impact of using Carbon Fibre Reinforced Polymers (CFRP) for aircraft manufacture and to identify options for improving sustainability of aircraft . Complete Life Cycle Assessments (LCA) were undertak en for Airbus A330 and A350 and results showed that CFRP has a much greater environmental impact than previously recognised. P ast comparable previous LCA studies of aircraft typically excluded the aircraft interior and certain life cycle stages in their assessments . Regulatory drivers to reduce greenhouse gas (GHG) emissions and to reach government set targets, especially for Carbon Dioxide (CO_2) emissions, since aircraft are now included in the European Union Emissions Trading Scheme (EU ETS), are driving manufacturers to focus on the use phase of aircraft life cycles, instead of looking at the whole picture from cradle to grave.

Keywords: CFRP, EU ETS, GHG, LCA, Sustainability.

INTRODUCTION

There are various environmental issues in today's world ranging from greenhouse gas emissions, global warming to climate change and sustainability. In the 21st century, aviation is one of the fastest growing sources of GHG emissions. It is the most climate intensive form of transport (Transport Environment, 2017).

The biggest challenge is reducing the greenhouse gas emissions resulting from the aviation industry. It accounts for around ~3% of the EU's total emissions and ~2% of global emissions (European Commission, 2017). They have grown by around 75% between 1990 and 2012. Furthermore, the ICAO predicts that global aviation emissions will be approximately 70% higher by 2020 and roughly 300-700% higher by 2050 compared to 2005 (European Commission, 2017).

The aviation sector is taking part in reducing emissions through the EU ETS. The CO_2 and non-CO_2 impacts are jointly responsible for approximately 4.9% of the world's man-made global warming (Transport Environment, 2017). So far, through the EU ETS, the aviation sector has been able to reduce the carbon footprint (CFP) of the industry by more than 17 million tonnes per year but there is still a long way to go (European Commission, 2017). Modern operational measures such as improvement in air traffic technology etc. are playing a key role in the journey to reducing emissions.

Environmental awareness is a matter of increasing importance in the last decade throughout many industries. With further regulation and penalties, it becomes imperative to fully acknowledge the environmental impacts of different products and services. The aviation sector in particular is of great importance and therefore it is vital that the environmental impacts of aircraft be assessed. LCA emerges as an excellent choice, providing the assessment of the product during its whole life cycle, and allowing an insight into the contribution of each process.

An LCA evaluates all stages of a product's life from an interdependent perspective. LCAs enable the estimation of environmental impacts from all stages involved including stages that are normally ignored in more traditional analyses (EPA, 2006). LCAs are being used more and more by scientists and engineers to discover opportunities to reduce environmental impacts across an entire product's life cycle. Leading academics around the world are working to make LCAs more relevant to GHG emissions and its reduction policies. By focusing the method on the manufacturing or purchase of products within a specific region, opportunities to reduce greenhouse emissions and save energy can be identified for that particular region.

LCA's are extensively used in different industry sectors, such as LCA of lightweight vehicles manufactured with CFRP in place of steel. This is particularly common in the automotive industry. CFRP has been successfully used in various aerospace applications due to their lighter weight, higher strength and rigidity. Recent examples include the Boeing 787, Airbus 380 and the Airbus 350. However, at the End of Life (EOL) there is a high price both in terms of cost and the difficulty in recycling or reusing CFRP. However, there have been recent advances in reducing this.

LCA's have been used to determine the changes in environmental impact as a result of substituting traditional metals with CFRPs. As a result of this and other similar studies, CFRP is now widely preferred for vehicle and aircraft manufacture to save on fuel consumption, which saves on costs over the use phase of the life cycle without compromising on mechanical strength. However, it has to be noted that some of these studies did not include the entire life cycle and key areas such as product interiors or appropriate disposal scenarios were neglected. Despite this, when taking the whole life cycle in to consideration, the significantly adverse impacts at

EOL need to be addressed such as the difficulties in recycling and reusing CFRP composites after the product is dismantled.

The materials most heavily used in current aircraft manufacturing include Aluminium (Al) and CFRP. The published literature portrays CFRP composites as ideal materials for aircraft manufacture based on the fact they are light-weight and strong, maximise fuel efficiency and hence reduce GHG emissions over the use phase of the aircraft life cycle. These studies are misleading as the environmental benefit is restricted to the use phase only. To determine the total environmental impact of CFRP use in aircraft manufacture, the whole life must be taken in to consideration.

Furthermore, previous LCA of aircraft do not assess the interior which covers the cabin interiors, seating, galley equipment etc. This further compounds the issue since the interior of an aircraft can be changed several times over its lifetime and this must be reflected in the functional unit used for the LCA to ensure a complete assessment of the whole aircraft per unit distance travelled. Material choices made to reduce emissions over the use phase may inadvertently increase net environmental damage over whole life cycle.

A comparative LCA was taken to investigate the environmental impact of the Airbus A330 and the A350 aircraft over the whole life cycle, from extraction, manufacturing, operation and disposal. LCA is an ideal tool to audit environmental impacts at each life cycle stage and to identify opportunities where changes can be made to improve the sustainability of an aircraft.

METHODOLOGY

LCAs of aircraft were conducted in this study from cradle to grave and included the interior (in addition to the fuselage and other major structural components) for a complete understanding of impacts over the whole life cycle. LCAs were carried out in accordance with ISO 14040. The LCA was executed with SimaPro 8, the most widely used tool in industry. This ensures that the results of this study are comparable with previously published literature. Within SimaPro 8, Eco Invent 3 Recycled Content database was used for the Inventory Analysis.

Goal Definition

The aim of this report is to carry out an environmental impact assessment using LCA as a tool of two aircraft the A330 and A350. Furthermore, it provides a basis for possible improvement options at various stages of the life cycle. The products to be studied are the two aircraft, the A330 and the A350.

System Boundary

In the LCA, the whole life cycle will be considered. This includes manufacturing of components, the operational life of the aircraft and end of life (disposal, incineration, recycling etc). For the operations phase, the average life of the aircraft was considered to be 25 years. Transportation of assemblies during manufacture was considered and data that is available in SimaPro was used. This was the same for the production of the aircraft.

Type of Assessment Performed

The ReCiPe Endpoint (H), Europe (H/A) method was used to perform the assessment. It is a Hierarchist method and balances between short term and long term impacts.

Assumptions and Limitations

When carrying out an LCA, ideally all material and energy fluxes need to be quantified. However, there are time, resource and data limitations which can affect this process. Therefore, one should make reasonable decisions as to what should be included and what should be excluded. It should also be noted that the system boundaries will depend on data availability and any omissions should be made clear and appropriately referenced and justified. Furthermore, the interior of both aircraft was considered in this study, but it was assumed that the major material used is CFRP as shown from previous studies (Albrecht et al., 2011).

Functional Unit

The functional unit was defined as passenger.km, over which it was assumed that the interior was replaced 5 times.

Life Cycle Inventory

The A330 and A350 both use different kinds of composite materials to save weight. This makes it more fuel efficient thus reducing emissions. The material weight and contribution of both aircraft is shown in Tables 1 and 2.

Table 1. Material Weight and Contribution in A330

Material	Weight (kg)	Contribution (%)
Aluminium	62,056	58.3
Steel	20,388	19.2
CFRP	9,743	9.2
Titanium	8,161	7.7
Nickel	2,948	2.8
Miscellaneous	2,015	1.9
GFRP	1,059	1.0
TOTAL	**106,218**	**100**

Table 2. Material Weight and Contribution in A350

Material	Weight (kg)	Contribution (%)
CFRP	63,635	55.0
Aluminium	24,297	21.0
Titanium	18,512	16.0
Steel	9,256	8.0
TOTAL	**115,700**	**100**

For both tables, the total weight does not include components and systems such as; the navigation system, hydraulic fluid, electronics etc. As for the interior, it is assumed that it is made of CFRP for the majority and replaced 5 times over the lifespan of the aircraft. Also, as it is not known what miscellaneous includes, its total weight is split equally amongst the other materials to prevent omission of data.

RESULTS AND DISCUSSION

The results section will look at the environmental impacts of manufacturing CFRP and across the life cycles of both aircraft.

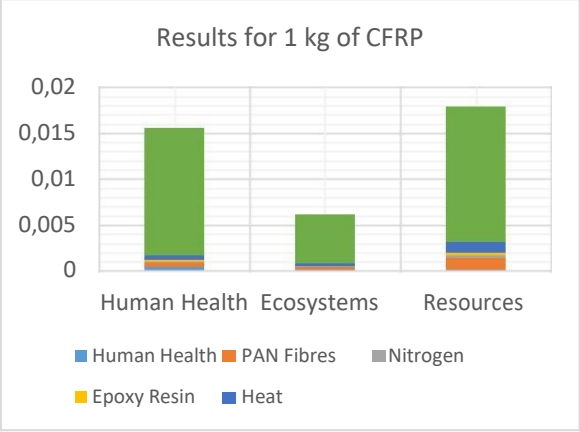

Fig. 2. Impact Results for 1 kg of CFRP

It can be clearly seen in Fig. 2. that CFRP has a big impact on resources and human health. This is due to the high levels of energy required electricity to manufacture CFRP. Significant amounts of electricity are required, and this is produced through fossil fuels. This would put a strain on resources. Furthermore, fossil fuels release unwanted GHG emissions and pollutants which exaggerate climate change. It is very clear that for every kilogram of CFRP produced, the greatest impact is on climate change – human health and fossil depletion.

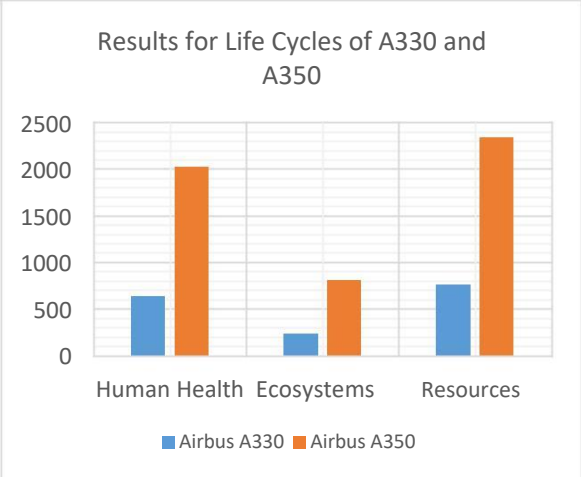

Fig.3. Impact Results for both aircraft

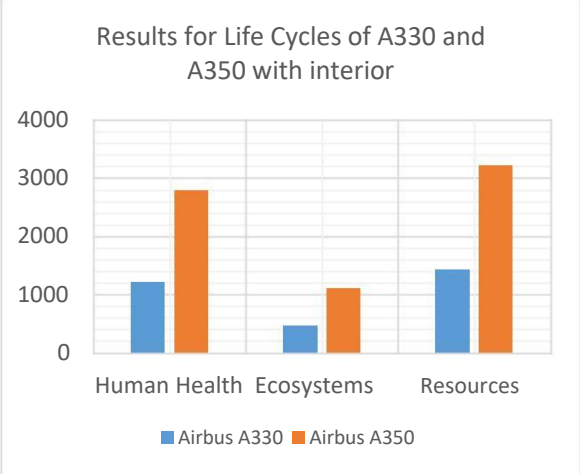

Fig. 4. Impact Results for both aircraft with interior

From Fig. 3. and 4. above, it can be clearly seen that the A350 has a much greater environmental impact than the A330. This is predominately due to the heavy use of CFRP in the A350. It has a very high impact score on human health, resources and ecosystems. Furthermore, it has to be noted that the operation phase was the most environmentally damaging in the life cycle as it uses a lot of fuel which leads to fossil depletion as jet fuel is processed from crude oil. Large amounts of fuel burn also lead to damage on human health due to the release of various GHG emission such as CO_2, NO_X etc. These in turn lead to an increase in the climate change effect. The disposal scenario for aluminium adds a small positive value to the life cycle as it is mostly recycled along with steel. However, the difficulty in recycling CFRP means it is mostly either incinerated or sent to landfill.

CFRP manufacture is a heavily energy intensive process. It is estimated that during production, roughly 30% of carbon fibre ends up as waste (Composites World, 2016). In addition, the process is 14 times more energy intensive than producing steel and significant amount of GHG emissions are emitted during the process,

making it very environmentally unfriendly (Recycle Nation, 2015). Unlike its metal counterparts, CFRP cannot be recycled easily. As CFRP is cured at high temperatures and pressures, the only way to reclaim the fibres is to incinerate or chemically burn off all the resin and polymer to leave the carbon fibres behind. But the result is shorter, irregular fibres that have a much lower ability to bear heavy loads. So, it ends up in products where light weight is more important than strength such as tennis rackets etc (Guardian, 2017).

Incineration based processes mostly involve pyrolysis. This is where CFRP is heated to around 400-650 C under high pressure with very little oxygen present. This burns off the epoxy matrix and any harmful fumes released are separated off and incinerated in accordance to relevant environmental standards (Material for Engineering, 2017). The process produces cotton wool like fibres which have 90-95% of their original mechanical properties. However, this is not a replacement for virgin carbon fibre, as is required in heavy applications such as aerospace and automotive. Other methods include milling or shredding but this produces shorter fibres as mentioned before with lower mechanical properties (Recycle Nation, 2015).

A new process however, looks at removing the epoxy matrix through using supercritical fluids which dissolve the epoxy while leaving the fibres intact in almost their virgin state. This leaves the fibres clean and unbroken and, in some cases, had almost 99% of their original mechanical properties when tested. But it cannot be said for certain that this process will be commercially and economically viable on an industrially large scale. Recycled fibres can be 30-40% (Composites World, 2014) cheaper than virgin fibre which can cost up to £10,000 per tonne (Materials Today, 2009).

The results showed that CFRP causes much more damage to the environment than previously thought. This is due to the energy intensive manufacturing process which cannot be offset by recycling or reuse during end of life. Environmental impact is further increased when aircraft interiors are included in the LCA as these are replaced several times over the lifespan of an aircraft. Furthermore, other materials are far easier to repair during maintenance and overhaul than CFRP which requires expensive, time consuming repairs which would further increase environmental impacts if considered in the LCA. In comparison, repair of Al panels is less costly and time consuming, while achieving the same integrity and quality required for airworthiness.

CONCLUSIONS

Overall, CFRP was discovered to have a greater environmental impact than other materials. The use of CFRP has become more common with today's aircraft being composed of up to 50% CFRP. The industry needs to work together in finding new environmentally friendly ways of disposing CFRP or energy efficient means of recycling it and finding markets/applications for recyclates that are not fit for re-use in aircraft. Clearly, recycling of the interior or replacement of the interior with recycled CFRP would be an area of development to improve sustainability, in addition to reducing CFRP dependence. Various companies have developed cost effective solutions for composites, but they all now need to work together to ensure that recycling of CFRP becomes a vital part of the composites market globally.

REFERENCES

Albrecht S., Linder J.P. and Michelis B., (2011). *Life Cycle Assessment of an aircraft cabin element.* German Federal Ministry of Economics and Technology (BMWi).

Composites World, (2014). *Recycle Carbon fibre: Comparing cost and properties.* [Online] Available from: https://www.compositesworld.com/articles/recycled-carbon-fiber-comparing-cost-and-properties [Accessed 12th April 2018].

Composites World, (2016). *Recycled carbon fibre: its time has come.* [Online] Available *from:* https://www.compositesworld.com/columns/recycled-carbon-fiber-its-time-has-come- [Accessed 7th April 2018].

Environmental Protection Agency (EPA), (2006). *Life Cycle Assessment: Principles and Practice.* National Risk Management Research Laboratory. EPA/600/R-06/060.

European Commission, (2017). *Reducing emissions from aviation.* [Online] Available from: https://ec.europa.eu/clima/policies/transport/aviation_en [Accessed 21st November 2017].

Guardian, (2017). *Carbon fibre: the wonder material with a dirty secret.* [Online] Available from: https://www.theguardian.com/sustainable - business/2017/mar/22/carbon-fibre-wonder-material-dirty-secret [Accessed 12th April 2018].

Materials for Engineering, (2017). *Recycling carbon fibre.* [Online] Available from: http://www.materialsforengineering.co. uk/engineering - materials-features/recycling-carbon-fibre/160324/ [Accessed 12th April 2018].

Materials Today, (2009). *Recycling carbon fibre composites.* [Online] Available from: https://www.materialstoday.com/carbon - fiber/features/recycling-carbon-fibre-composites/ [Accessed 12th April 2018].

Recycle Nation, (2015). Is *carbon fibre better for the environment than steel?* [Online] Available from: https://recyclenation.com/2015/10/is -carbon-fiber-better-for-environment-than-steel/ [Accessed 12th April 2018].

Transport Environment, (2018). *Aviation 2030*. [Online] Available from: https://www.transportenvironment.org/sites/te/files/publications/Aviation%202030%20briefing.pdf [Accessed 10th April 2018].

International Symposium on Sustainable Aviation 2018

ISSA 2018

9 - 11 July 2018 Rome, Italy

Official Airlines

TURKISH AIRLINES

A STAR ALLIANCE MEMBER

Sponsors

ENAC

ENTE NAZIONALE PER L'AVIAZIONE CIVILE

Heli PLAT

my TECHNIC

AIRCRAFT MRO SERVICES

TAV Airports

Ecoengineering Associazione Culturale

ISBN

978-605-68640-2-5